# TWO-DIMENSIONAL TANDEM MASS SPECTROMETRY: INSTRUMENTATION AND APPLICATION

by

**Lucas J. Szalwinski**


**A Dissertation**

*Submitted to the Faculty of Purdue University*

*In Partial Fulfillment of the Requirements for the degree of*


**Doctor of Philosophy**



Department of Chemistry

West Lafayette, Indiana

May 2022

# THE PURDUE UNIVERSITY GRADUATE SCHOOL
## STATEMENT OF COMMITTEE APPROVAL

**Dr. R. Graham Cooks**

Department of Chemistry

**Dr. Scott A. McLuckey**

Department of Chemistry

**Dr. Hilkka I. Kenttämaa**

Department of Chemistry

**Dr. Julia Laskin**

Department of Chemistry


**Approved by:**

Dr. Christine A. Hrycyna

*To Mom and Dad*
*for always believing in me*

# ACKNOWLEDGMENTS

# TABLE OF CONTENTS

# LIST OF TABLES

# LIST OF FIGURES

17

# LIST OF SCHEMES

# ABSTRACT

Mass spectrometry has become the premium chemical identification method. The next advancement for mass spectrometry is the widespread use of mass spectrometers for on-site chemical/biological identification. Ion trap mass spectrometers have emerged as powerful on-site analytical platforms, in spite of limited mass resolution, due to their compatibility with ambient ionization methods and ready implementation of tandem mass spectrometry (MS/MS). However, conventionally operated ion traps are inefficient in accessing the entire tandem mass spectrometry dataspace. By operating the ion trap at a constant trapping voltage, more efficient tandem mass spectrometry scan modes are accessible. The most efficient is to acquire the entire tandem mass spectrometry data space and this work demonstrates three different methods of acquiring this data domain. These methods acquire the data in under a second and the best performing method was implemented in a miniature mass spectrometer without performance decrease. The impact of this device is most powerful when analysis requires the entire ionized sample be considered to determine the identity of the sample. This was shown to be useful for monitoring the lipid metabolism in a model microorganism.

# CHAPTER 1.     INTRODUCTION

## 1.1     Quadrupole Ion Traps

### 1.1.1     Structure and Ion Motion

The ability to store ions over a meaningful period of time was revolutionary tool for physical chemists to study ion chemistry and Wolfgang Paul was awarded one-fourth of the 1989 Nobel Prize in Physics for the development of the quadrupole ion trap.[1] The use of ion traps as analytical mass spectrometers wasn't widespread until the invention of mass-selective axial instability by George Stafford made commercialization of the quadrupole ion trap possible.[2] The dual use of the quadrupole ion trap as an ion reaction vessel and analytical instrument makes it an incredibly powerful device.

Ions trapped in a quadrupole field are strongly focused because the restoring force increases as the ion moves away from the center of the trap. There are many structural forms of the quadrupole ion trap, but the two main variants of interest are the 3D (Paul) trap and the linear quadrupole ion trap.[3] The 3D trap revolves the quadrupole field around a point whereas the linear quadrupole ion trap extrudes the quadrupole field from a line. This results in the linear quadrupole ion trap having considerably more ion storage capacity given the same quadrupole radius; however, this results in no axial trapping force. This downside is negated by the application of addition electric fields to trap the ions axially and nearly all modern quadrupole ion traps are linear quadrupole ion traps due to the increased ion storage capacity.

Since either the trapping or ejection of ions depends on the stability of ions, it is important to be able to mathematically describe the motion of ions in the quadrupole field. The stability of ions in the quadrupole field can be mathematically described by the solution to the second-order linear differential Mathieu equation.[4] This stability can be expressed as a force where the physical parameters such as the frequencies and voltages of applied potentials can be related to this stability by the Laplace condition.

Starting with the commonly accepted form of the Mathieu equation

$$\frac{d^2u}{d\xi^2} + (a_u - 2q_u cos2\xi)u = 0 \tag{1.1}$$

where $u$ represents the coordinate axis. The parameters $a$ and $q$ are dimensionless trapping parameters. $\xi$ is a dimensionless parameter but if chosen to be equal to $\Omega t/2$ where $\Omega$ is a frequency and t is time we can obtain the following

$$\frac{d}{dt} = \frac{d\xi}{dt}\frac{d}{d\xi} = \frac{\Omega}{2}\frac{d}{d\xi} \tag{1.2}$$

and

$$\frac{d^2}{dt^2} = \frac{d\xi}{dt}\frac{d}{d\xi}\frac{d}{dt} = \frac{\Omega^2}{4}\frac{d^2}{d\xi^2} \tag{1.3}$$

where the result from (1.3) can be substituted into (1.1) so that the following is obtained

$$m\frac{d^2u}{dt^2} = \frac{-m\Omega^2}{4}(a_u - 2q_u cos\Omega t)u \tag{1.4}$$

The resultant equation relates force, left-hand side, to parameters which describe the ion's stability, a and q. Now the force imposed on an ion in quadrupole field must be determined. To begin, the quadrupole potential, $\phi$ , is described as

$$\phi = \frac{\phi_0}{r_0{}^2}(\lambda x^2 + \sigma y^2 + \gamma z^2) \tag{1.5}$$

where $\lambda, \sigma$, and $\gamma$ are the weight constants for the three coordinate axes. The Laplace condition requires that the field in every coordinate axis is linear. This requires that the second differential of the potential is zero meaning that the sum of the weighing constants be equal to zero. This results in many different solutions but importantly for the 3D quadrupole ion traps the solution is $\lambda = \sigma = 1, \gamma = -2$ where substitution into ((1.5) yields

$$\phi_{x,y,z} = \frac{\phi_0}{r_0{}^2}(x^2 + y^2 - 2z^2) \tag{1.6}$$

whereby operating in cylindrical coordinates, where $x = rcos\theta$ , $y = rsin\theta$, z = z, and making using of the trigonometric identity, $\cos^2 + \sin^2 = 1$, the following equation is obtained.

$$\phi_{x,y,z} = \frac{\phi_0}{r_0{}^2}(r^2 - 2z^2) \tag{1.7}$$

23

The electric potential, $\phi$, can be either constant (DC) or time changing (RF) where $U$ and V represent the constant and time changing electric potential, respectively.

$$\phi_0 = U + V cos\Omega t \tag{1.8}$$

$$\frac{\partial \phi}{\partial x} = \frac{2x}{r_0{}^2}U + V cos\Omega t \tag{1.9}$$

Now the equation for the force acting on an ion can be related through the equation

$$F_x = ma = m\frac{d^2x}{dt^2} = -e\frac{\partial \phi}{\partial x} \tag{1.10}$$

Equation ((1.4) and ((1.9) can now be equated allowing for an ion's stability to be described by the applied electric field. The familiar form of the Mathieu equation is obtained.

$$q_x = \frac{8eV_{RF}}{mr^2\Omega^2} \tag{1.11}$$

$$a_x = \frac{16eU_{DC}}{mr^2\Omega^2} \tag{1.12}$$

It should be noted that the "8" and "16" in equation (1.11) and(1.12) are reduced to "4" and "8" when operating in linear quadrupole traps. Additionally, ion traps are operated with no quadrupolar DC resulting in the a parameter being zero.

Equations (1.11) and (1.12) only describe the ion's stability in the x-coordinate. For linear quadrupole ion traps, the electric potentials in x and y, $\lambda$ and $\sigma$, are opposite in sign. Now, its important to introduce a new trapping parameter, $\beta$, which is a complex function relating both a and q. There is no analytical representation of $\beta$ but various approximations exist with one of the simpler approximations being for when q < 0.4,

$$\beta \approx \sqrt{a + \frac{q^2}{2}} \tag{1.13}$$

Importantly, $\beta$, describes and ion's stability where the integers of $\beta$ are boundaries of stabilities. More specifically, when an ion's $a_x$ and $q_x$ results in $\beta_x$ being between 0 and 1 the ion is stable in the x dimension and when it is between 1 and 2 it is unstable. This periodic stability is common

feature of quadrupoles. Since ion's are independently stable in either x and y the overlap of $\beta_x$ and $\beta_y$ results in trapped ions. Figure 1.1 shows the regions of stability in x and y resulting in overlapped regions of simultaneous stability in both dimensions.
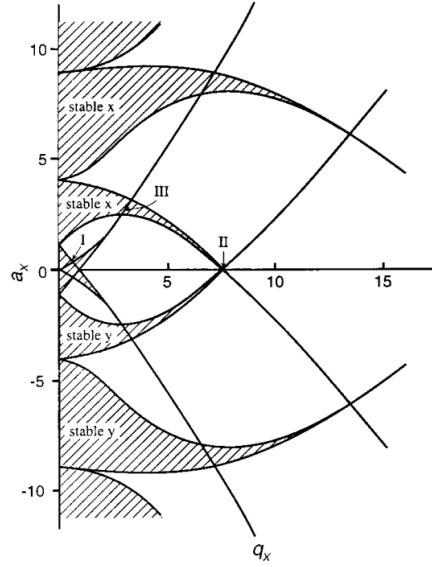


Figure 1.1 Regions where ion motion is simultaneously stable in the x and y directions, expressed in terms of $a_x$ and $q_x$. The first three are labelled I, II and III. Reproduced from Du, Z., Douglas, D.J., Konenkov, N., (1999). *Journal of Analytical Atomic Spectrometry*. 14, 1111–1119.

Although an ion's stability is essential for a quadrupole ion trap to be used as an ion storage device, the use of a quadrupole ion trap as an mass spectrometer did not become widespread until Stafford demonstrated a method to make ion mass selectively unstable.[5]

### 1.1.2   Resonant Ejection Techniques in Quadrupole Ion Traps

Stafford's method relied on a fundamental process described in the original patent[6] where ions can be perturbed when an external perturbing field frequency, $\omega_{ac}$, matches the ion's fundamental frequency of motion, $\omega_{ion}$. The fundamental frequency, commonly referred to as the secular frequency, can be determined by the equation

$$\omega_{ion} = \frac{\beta_{ion}\Omega_{RF}}{2} \tag{1.14}$$

25

For ions trapped in the first stability region in Figure 1.1 with no quadrupolar DC applied (a = 0), application of a supplemental frequency at half the trapping RF frequency would resonantly excite at $\beta = 1$. The determination of what $m/z$ value this corresponds to requires solving approximations for the q-value at $\beta = 1$. Incidentally, the q-value at $\beta = 1$ is 0.908 and is commonly known in the quadrupole ion trap; however, other $\beta$ to q-value relationships are less recognized. The method Stafford demonstrated applied a single frequency, resulting in a perturbation at a fixed $\beta$ near the $\beta = 1$ boundary (also known as the low mass cut off as ions of lower $m/z$ are unstable at $\beta > 1$). In order to obtain a mass spectrum, the voltage of the trapping RF voltage was increased resulting in the ion's q-value being increased proportionally (equation (1.11)). This RF voltage ramp brought ions of various $m/z$ values into the perturbation proportionally to their $m/z$. The ions would be resonantly excited until their oscillations exceeded the trapping field and would be ejected through slits in the trapping electrodes into an electron multiplier. This method's performance was aided by the addition of helium to dampen the oscillation of non-resonant motion.

Other methods of mass selectively ejecting ions have been demonstrated including variation in trap radii[7], scanning the quadrupolar DC,[8,9] and scanning the supplemental frequency.[10,11] The latter requiring determining the relationship between all $\beta$ to q-value which, although computationally intensive by historical standards, can be calculated easily. The relationship between $m/z$ and q-values is inversely proportional meaning that in order to eject ions of increasing $m/z$ linearly the q-value needs to be scanned inversely. This method's main advantage over the other methods is that the activation of an ion at a specific $m/z$ value will not affect ions at other $m/z$ values as the supplemental doesn't affect the main trapping potential. This advantage is the basis of activating two or more $m/z$ values independently and simultaneously allowing greater flexibility in experimental design.

## 1.2   Tandem Mass Spectrometry (MS/MS)

The quadrupole ion trap is a device which can be described as a "electric field test tube" where various chemical operations can be performed on the stored ion population. The advantage of interrogating charged molecules without the effects of solvent was the fundamental force driving early adoption of these devices. One of the simplest chemical reactions that can be monitored is the unimolecular disassociation which can be readily observed when an ion is heated in the absence of solvent by promoting collisions of neutral gas molecules to the ion through

resonant excitation. This resonant excitation is exactly the same procedure used to activate ions for ejection where an applied frequency matches the ion's secular frequency resulting in an increase in oscillation amplitude is increased. The increased oscillation amplitude promotes more collisions with neutral molecules increasing the internal energy of the ion until the ion dissociates or is ejected from the trap. The amplitude of the applied voltage when fragmentation is preferred is significantly smaller than that for ejection.

Tandem mass spectrometry (MS/MS) measures the intact precursor ion which is fragmented to generate multiple charged product ions which are also measured. The requirement for each n stage of MS/MS (or $MS^n$) is that independent measurements of precursor and product ion $m/z$ values are made and that they correlated.[12] The advantages of MS/MS are immense. Mass spectrometry is fundamentally a physical measurement ($m/z$) whereas the difference in mass between the precursor and product ion provides chemical information about the structure of the precursor ion and thus about the neutral analyte. This structural information can be used to identify previously unknown analytes. For a mixture analysis by mass spectrometry, where many unknowns are ionized and detected in the full scan mass spectrum, it would be ideal to be able to access as much structural information as possible for every ionized compound. However, conventionally operated quadrupole ion traps are inefficient at accessing the structural information (MS/MS information) compared to triple quadrupole mass spectrometers.

### 1.2.1    Scan Modes

For triple quadrupole mass spectrometers, tandem mass spectrometry is accomplished by two independent mass analyzers.[13] The first and second mass analyzer can be scanned or fixed on a specific $m/z$ value to obtain various structural (MS/MS) information. Since there are two mass analyzers which can be independently fixed or scanned, the result is that there are four common tandem mass spectrometry experiments.[14] For mixture analysis, compounds belonging to the same chemical class should contain some similar fragments. If the similar product is charged, then monitoring the $m/z$ of the charged product as various precursors are individually allowed to fragment would yield a spectrum where peaks correspond to species containing that functionality. This is the basis for a precursor ion scan. The same experiment can be done for when the shared fragment is neutral. The appropriately named neutral loss scan fixes the mass offset between the

two mass analyzers and scans them together. The individual MS/MS experiments commonly referred to as scan modes are shown in Figure 1.2.

It should be noted that the use of tandem mass spectrometry scans predated the triple quadrupole mass spectrometer and computer-controlled instrumentation. If a mass scan is obtained by varying some instrument parameter and recording the signal output, a tandem mass scan should be obtained similarly. The difficulty in a tandem mass scan is that the instrument parameter requires the combination of the two mass analyzers operating in parallel. For electromagnetic two-sector instruments, the linking between mass analyzers is not trivial.[15] For all electromagnetic tandem mass spectrometers besides the BE geometry[16] (MIKES, magnetic sector followed by an electric sector), both mass analyzers must be varied simultaneously. The growth of computer-controlled instrumentation,[17] spurred by Enke, was important to the growth of triple quadrupole mass spectrometers. Another advantage of a triple quadrupole mass spectrometer is that the two mass analyzers where the stability parameters of one do not affect the other. The combination of easily accessible tandem mass spectrometry scan modes with low-energy collision induced dissociation,[18] driven by Yost and Enke, thrusted the triple quadrupole mass spectrometer to become the standard analytical instrument for mass spectrometry based-mixture analysis.
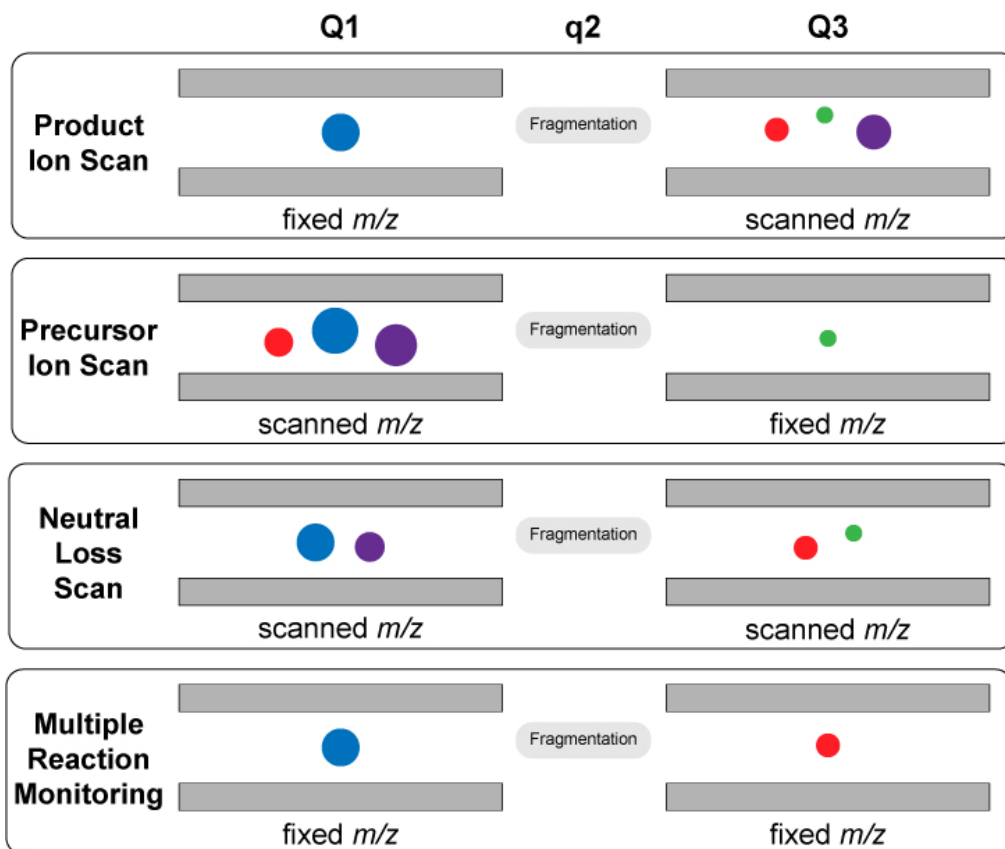
Figure 1.2. The four common scan modes in tandem mass spectrometry

In order to understand how these various scans probe the chemical information (MS/MS) data space, the common scan modes are overlain on the potential two-dimensional mass domain, a plane of data representing all of the possible fragment (product) ions for the various precursor ions (Figure 1.3). Importantly, the data collected in a MS/MS experiment commonly fall on vertical, horizontal, and diagonal lines representing the product ion, precursor ion, and neutral loss scans. These lines represent shared structural relationships between ions. The tandem mass spectrometry scan modes shown in Figure 1.2 probes only a single shared relationship between precursor and product ions. For example, the product ion scan probes the fragment ions produced by a single precursor ion species while the precursor ion scan probes a single product ion *m/z* from the ionized precursors.
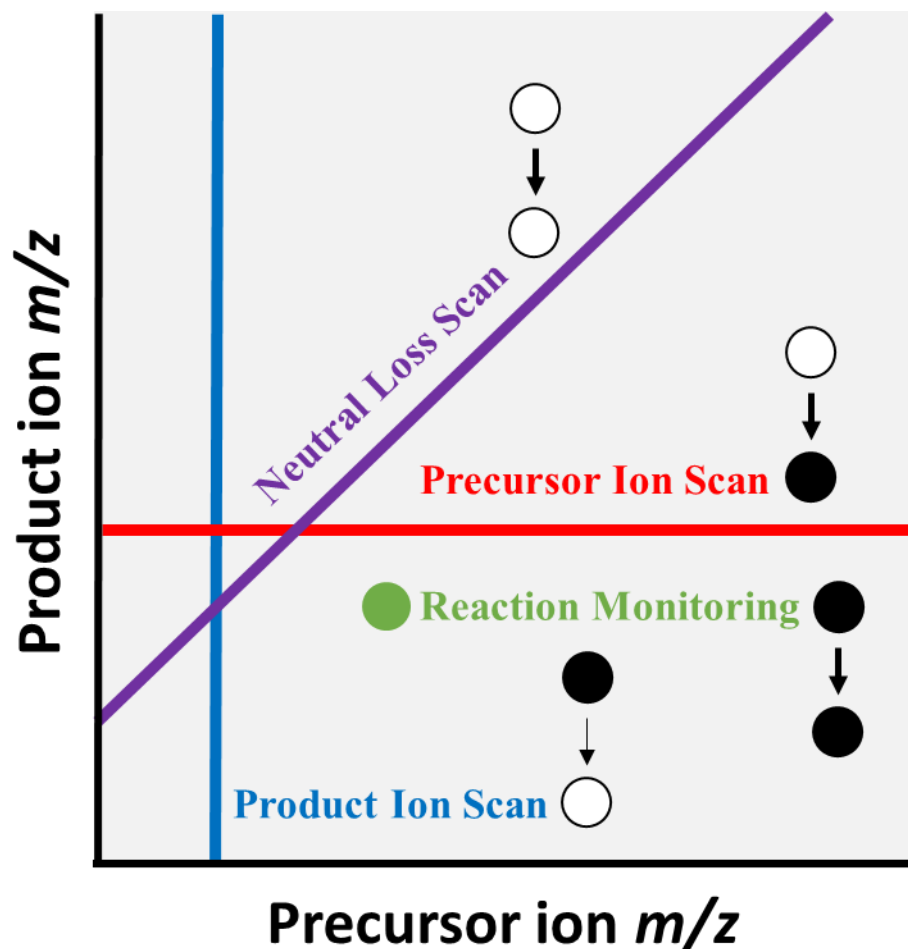
Figure 1.3. The 2D MS/MS data domain with the four common scan modes shown. The shorthand notation for the common scan modes is discussed in Schwartz, J. C., Wade, A. P., Enke, C. G., & Cooks, R. G. (1990). Systematic delineation of scan modes in multidimensional mass spectrometry. *Analytical Chemistry*, 62(17), 1809–1818.

For most quadrupole ion traps, ion isolation is needed before dissociation. This is because the dissociation product ions generated from a fragmented precursor ion would be indistinguishable from unfragmented precursor ions that happen to have the same *m/z* value of the product ions. However, when isolating a precursor ion all other precursor ion with different *m/z* values are removed and provide no information. A new ion population needs to be injected in order to obtain information for those precursor ions. This makes conventionally operated quadrupole ion traps inefficient at acquiring the precursor and neutral loss scan information. Johnson and Yost[19] demonstrated that precursor ion scans could be obtained by keeping the trapping voltage constant thereby allowing a frequency sweep to fragment precursor ions while simultaneously applying a

fixed frequency corresponding the secular frequency of the desired product ion *m/z* (calculated in equation (1.14)). This methodology was overlooked for many years. Instead, data-dependent acquisition (DDA) methods where a full scan is first performed to determine what are the most intense *m/z* values and those *m/z* values are probed using product ion scans. The DDA methodology was preferred, presumably because the instrumentation has already been well established. Another reason DDA methods have become common is that most mass spectrometers are connected to chromatography. Pre-separation of neutrals before ionization means the number of unique precursor ions introduced to the mass spectrometer is limited thereby devaluing precursor and neutral loss scans. Methods which ionize neutrals without pre-separation are most advantaged by utilizing the precursor and neutral loss scans. This is the case for ambient ionization methods where the sample is ionized as-is.

## 1.3    Miniature Mass Spectrometers

### 1.3.1    History

The most impactful place a chemical analysis can be performed is where productive actions from the result can be made; however, this is rarely where the measurements are made. As mass spectrometry started becoming routine for clinical and forensic analysis, the desire for miniature mass spectrometers has grown. The development of miniature mass spectrometers can be broken into three stages of research. The 1990s focused on miniaturizing the mass analyzer solely. The 2000s aimed ate miniaturization of the entire mass spectrometer including the vacuum system and sample introduction. The 2010s had a significant growth of ambient ionization methods and embedded data analysis methods in combination with miniature instruments.

Nearly all mass analyzers have been miniaturized in some fashion. The two notable early miniature mass spectrometers were the time-of-flight mass spectrometer (tiny-TOF) developed at Johns Hopkins[20] and the quadrupole ion traps developed at Purdue University (Figure 1.4).[21] The expectation when making any instrument more compact is that the performance is decreased. One example is that smaller mass analyzers result in lower ion storage capacity resulting in lower sensitivity. A reduction in mass resolution is also common in miniature mass spectrometers. With miniature instrumentation it is important to move away from constant comparisons to benchtop

instruments. Portable mass spectrometers only need to be adequate at performing the desired task and nothing more.
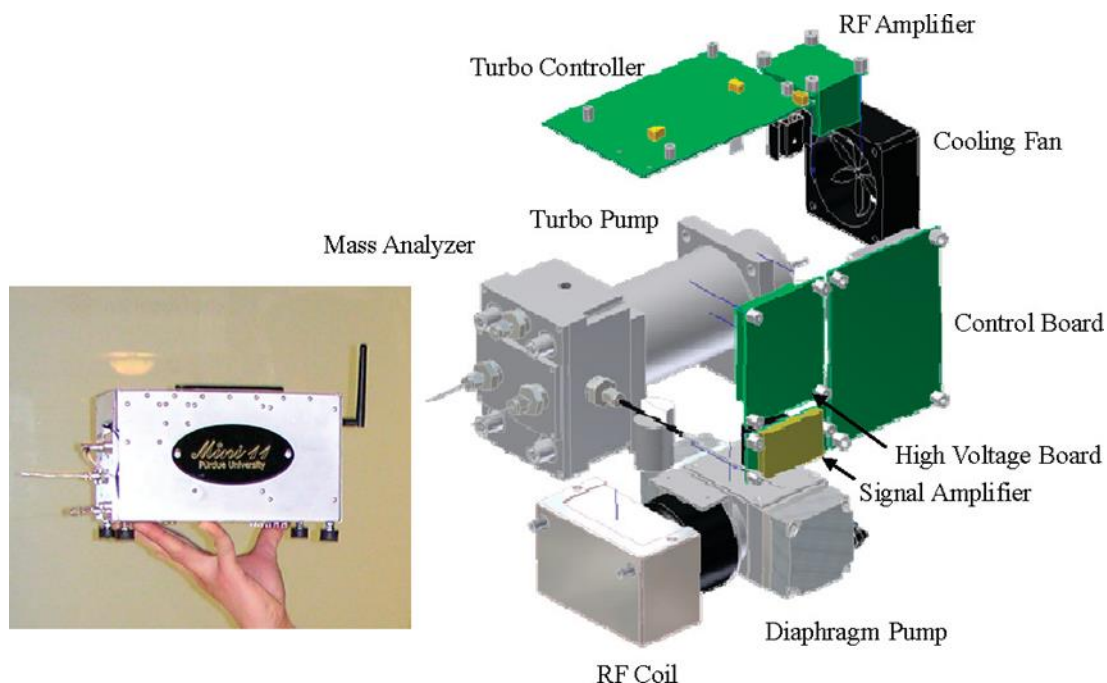


Figure 1.4. Exploded view of Mini 11 mass spectrometer and its components.

The expected performance for miniature mass spectrometers is to obtain near unit mass resolution up to *m/z* 500. This is readily accomplished for most mass analyzer even with reduced size. The most common mass analyzer for miniature mass spectrometer is the quadrupole ion trap due to its ability to perform MS/MS while requiring moderate vacuum conditions. Much of the development of miniature mass spectrometers has been centered about Purdue University where there have been three significant contributions. The first being the simplification of ion trap geometry. Early research in quadrupole ion traps demonstrated that by cutting slits in the hyperbolic surfaces for ion ejection for detection non-ideal fields were introduced to the trapping field. The field was corrected by stretching the predicted "ideal" geometry to correct for the aberrations.[22] The rectilinear ion trap utilized easily machinable flat plates with slits cut for ion ejection. Simulations were performed to determine the optimal spacing in order to approximate the "ideal" quadrupole field from a non-ideal geometry.[23] The second contribution was the invention of a discontinuous atmospheric pressure interface where the inlet of the mass spectrometer is only open for sample introduction resulting in a significant reduction in vacuum

requirements.[24] The third contribution was their part in developing ambient ionization methods. These include methods such as desorption electrospray ionization[25], paperspray ionization[26], and low-temperature plasma.[27] The ability to sample ions generated from the sample without preparation means that measurements can be obtained quickly and performed by untrained personnel.

### 1.3.2   Introducing Ions

It is important to note that gas-chromatography-mass spectrometry (GC-MS) has been a standard analytical method in forensic chemical identification. GC-MS is easily miniaturized, and the electron ionization data can be readily compared to the NIST spectral library to confidently identify unknowns. The downside of GC-MS is that it is slow, and the potential chemical space is limited by the GC. Chemicals which are non-volatile, polar, or decompose at high temperature cannot be detected without derivatization. Unfortunately, without the chromatography the identification of unknowns becomes impossible as the fragment ions produce a convoluted spectrum of all analytes. The quadrupole ion trap utilizing MS/MS does not necessarily require chromatography as long as the analytes of interest can be ionized from the sample. The first stage of mass spectrometry effectively replaces the GC thereby providing separation for each product ion spectrum allowing for the identification of unknowns.

The selection of ion sources becomes more flexible when chromatography is avoided. For surface analysis, desorption electrospray ionization (DESI)[25] or direct analysis in real time (DART)[28] allows for the analysis of polar or non-polar analysis respectively. Paperspray ionization allows for analytes present in liquids such as plasma or urine to be ionized. Importantly, these methods generate directly introduce many precursor ions to the mass analyzer where the chromatograph produces only a few precursor ions at a time. If a product ion scan of each detected precursor ion is needed, the analysis time can be quite lengthy (although still shorter than the GC timescale). This is especially true for miniature mass spectrometers utilizing a discontinuous atmospheric pressure interface (DAPI) as the re-introduction of sample is significantly longer (~500 ms) than for continuous interfaces. The diversity of precursor ions introduced miniature mass spectrometers necessitate methods which can efficiently access MS/MS information in order to shorten analysis time.

## 1.4    Introduction to This Work

The objective of this work is to increase the efficiency in which quadrupole ion traps acquire MS/MS data. The work was initially attempting to improve the methods which were newly developed which allowed quadrupole ion traps to perform the precursor ion and neutral loss scan modes.[29,30] These methods were most impactful when coupled to miniature mass spectrometers utilizing an ambient ionization source and a discontinuous atmospheric pressure interface. The first task was to combine multiple scan modes. The combination of these scan modes provided the motivation to differentiate the combined scans. Incidentally a method of identifying resonantly ejected ions was discovered while trying to identify artifactual peaks present in a different experiment. This method allowed for the combined scans to be compared where the resulting spectrum is the logical output of the combined scans.

The new method was tested to its limit where all product ions for a single precursor ion were ejected simultaneously, and the detected signal could be converted into a product ion spectrum. The result was a two-dimensional mass spectrum, two intensities of mass and one of intensity, represented as the gray plane in Figure 1.3. The two-dimensional (2D MS/MS) mass scan was initially proposed by Fred McLafferty in the early 1980's (Figure 1.5). However, the first experimental results were obtained by Pfändler using an FT-ICR.[31] The demonstration of the two-dimensional mass scan in a linear quadrupole ion trap was remarkable, even more remarkable was that the data was acquired in under a second.
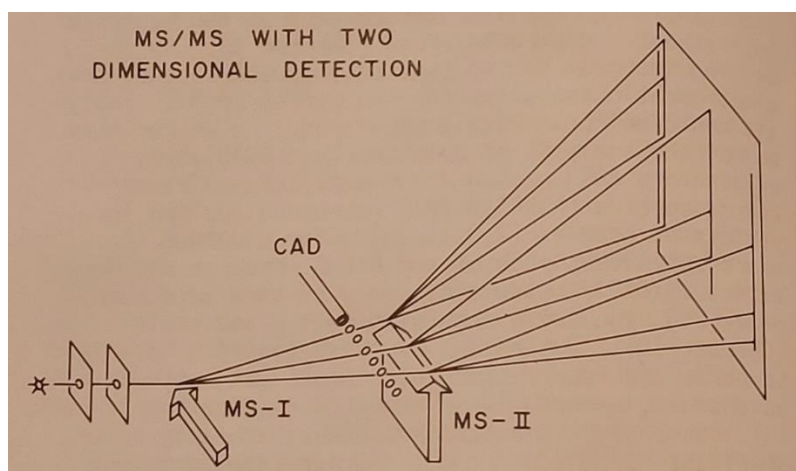


Figure 1.5. Proposed MS/MS instrument with simultaneous display of the primary spectrum and all secondary spectra. Reproduced from McLafferty, F. W. (1983). Tandem mass spectrometry.

The goal was to refine this two-dimensional mass scan to be analytically useful. A new method was developed which avoided taking a Fourier transform of the product ion signal (Chapter 6) resulting in higher mass range and improved resolution. This method was applied using a miniature mass spectrometer without a significant decrease in performance. The application of this method was demonstrated for the identification of lipids within bacteria.

## 1.5    References

(1)     Paul, W., & Steinwedel, H. (1953). Notizen: Ein neues Massenspektrometer ohne Magnetfeld. *Zeitschrift für Naturforschung A*, *8*(7), 448-450.

(2)     Stafford, G. C., Kelley, P. E., Syka, J. E. P., Reynolds, W. E., & Todd, J. F. J. (1984). Recent improvements in and analytical applications of advanced ion trap technology. *Int. J. Mass Spectrom. Ion Processes*, *60*(1), 85-98.

(3)     Schwartz, J. C., Senko, M. W., & Syka, J. E. (2002). A two-dimensional quadrupole ion trap mass spectrometer. *J. Am. Soc. Mass Spectrom.*, *13*(6), 659-669.

(4)     Mathieu, É. (1868). Mémoire sur le mouvement vibratoire d'une membrane de forme elliptique. *Journal de Mathématiques Pures et Appliquées*, *13*, 137-203.

5)     Paul, W., & Steinwedel, H. (1960). Apparatus for Separating Charged Particles of Different Specific Charges. 2939952. In: June.

(6)     Franzen, J. (1993). The non-linear ion trap. Part 4. Mass selective instability scan with multipole superposition. *Int. J. Mass Spectrom. Ion Processes*, *125*(2), 165-170.

(7)     Badman, E. R., & Cooks, R. G. (2000). Cylindrical Ion Trap Array with Mass Selection by Variation in Trap Dimensions. *Anal. Chem.*, *72*(20), 5079-5086.

(8)     Prentice, B. M., & McLuckey, S. A. (2012). Analysis of High Mass-to-Charge Ions in a Quadrupole Ion Trap Mass Spectrometer via an End-Cap Quadrupolar Direct Current Downscan. *Anal. Chem.*, *84*(17), 7562-7569.

(9)     Zhang, D., Jiang, Y., Chu, S., Dai, X., & Fang, X. (2022). Extending the mass-to-charge scannable range of a linear ion trap mass spectrometer through quadrupolar direct current scan. *Int. J. Mass spectrom.*, *471*, 116760.

(10)    Snyder, D. T., Pulliam, C. J., Wiley, J. S., Duncan, J., & Cooks, R. G. (2016). Experimental Characterization of Secular Frequency Scanning in Ion Trap Mass Spectrometers. *J. Am. Soc. Mass. Spectrom.*, *27*(7), 1243-1255.

(11)    Snyder, D. T., & Cooks, R. G. (2017). Improving mass assignments in quadrupole ion traps operated using ac scans: Theory and experimental validation. *Int. J. Mass spectrom.*, *417*, 1-7.

(12)    Louris, J. N., Brodbelt-Lustig, J. S., Graham Cooks, R., Glish, G. L., van Berkel, G. J., & McLuckey, S. A. (1990). Ion isolation and sequential stages of mass spectrometry in a quadrupole ion trap mass spectrometer. *Int. J. Mass Spectrom. Ion Processes*, *96*(2), 117-137.

(13)    Yost, R., & Enke, C. (1979). Triple quadrupole mass spectrometry for direct mixture analysis and structure elucidation. *Anal. Chem.*, *51*(12), 1251-1264.

(14)    Schwartz, J. C., Wade, A. P., Enke, C. G., & Cooks, R. G. (1990). Systematic delineation of scan modes in multidimensional mass spectrometry. *Anal. Chem.*, *62*(17), 1809-1818.

(15)    Sato, K., Asada, T., Ishihara, M., Kunihiro, F., Kammei, Y., Kubota, E., Costello, C. E., Martin, S. A., Scoble, H. A., & Biemann, K. (1987). High-performance tandem mass spectrometry: calibration and performance of linked scans of a four-sector instrument. *Anal. Chem.*, *59*(13), 1652-1659.

(16)    Beynon, J. H., Cooks, R.-G., Amy, J.-W., Baitinger, W., & Ridley, T. (1973). Design and performance of a mass-analyzed ion kinetic energy (MIKE) spectrometer. *Anal. Chem.*, *45*(12), 1023A-1031A.

(17)    Enke, C. G. (1982). Computers in Scientific Instrumentation. *Science*, *215*(4534), 785-791.

(18)    Yost, R. A., Enke, C. G., McGilvery, D. C., Smith, D., & Morrison, J. D. (1979). High efficiency collision-induced dissociation in an RF-only quadrupole. *International Journal of Mass Spectrometry and Ion Physics*, *30*(2), 127-136.

(19)    Johnson, J. V., Pedder, R. E., & Yost, R. A. (1991). MS-MS parent scans on a quadrupole ion trap mass spectrometer by simultaneous resonant excitation of multiple ions. *Int. J. Mass Spectrom. Ion Processes*, *106*, 197-212.

(20)    Cotter, R. J., Fancher, C., & Cornish, T. J. (1999). Miniaturized time-of-flight mass spectrometer for peptide and oligonucleotide analysis. *J. Mass Spectrom.*, *34*(12), 1368-1372.

(21)    Patterson, G. E., Guymon, A. J., Riter, L. S., Everly, M., Griep-Raming, J., Laughlin, B. C., Ouyang, Z., & Cooks, R. G. (2002). Miniature Cylindrical Ion Trap Mass Spectrometer. *Anal. Chem.*, *74*(24), 6145-6153.

(22)    Johnson, J. V., Peddeer, R. E., Yost, R. A., & March, R. E. (1992). The stretched quadrupole ion trap: Implications for the Mathieu au and qu parameters and experimental mapping of the stability diagram. *Rapid Commun. Mass Spectrom.*, *6*(12), 760-764.

(23)    Ouyang, Z., Wu, G., Song, Y., Li, H., Plass, W. R., & Cooks, R. G. (2004). Rectilinear Ion Trap:  Concepts, Calculations, and Analytical Performance of a New Mass Analyzer. *Anal. Chem.*, *76*(16), 4595-4605.

(24)    Gao, L., Cooks, R. G., & Ouyang, Z. (2008). Breaking the Pumping Speed Barrier in
        Mass Spectrometry: Discontinuous Atmospheric Pressure Interface. *Anal. Chem.*, *80*(11),
        4026-4032.

(25)    Cooks, R. G., Ouyang, Z., Takats, Z., & Wiseman, J. M. (2006). Ambient Mass
        Spectrometry. *Science*, *311*(5767), 1566-1570.

(26)    Liu, J., Wang, H., Manicke, N. E., Lin, J.-M., Cooks, R. G., & Ouyang, Z. (2010).
        Development, Characterization, and Application of Paper Spray Ionization. *Anal. Chem.*,
        *82*(6), 2463-2471.

(27)    Harper, J. D., Charipar, N. A., Mulligan, C. C., Zhang, X., Cooks, R. G., & Ouyang, Z.
        (2008). Low-Temperature Plasma Probe for Ambient Desorption Ionization. *Anal.
        Chem.*, *80*(23), 9097-9104.

(28)    Cody, R. B., Laramée, J. A., & Durst, H. D. (2005). Versatile New Ion Source for the
        Analysis of Materials in Open Air under Ambient Conditions. *Anal. Chem.*, *77*(8), 2297-
        2302.

(29)    Snyder, D. T., & Cooks, R. G. (2017). Single Analyzer Precursor Ion Scans in a Linear
        Quadrupole Ion Trap Using Orthogonal Double Resonance Excitation. *J. Am. Soc. Mass.
        Spectrom.*, *28*(9), 1929-1938.

(30)    Snyder, D. T., & Cooks, R. G. (2017). Single Analyzer Neutral Loss Scans in a Linear
        Quadrupole Ion Trap Using Orthogonal Double Resonance Excitation. *Anal. Chem.*,
        *89*(15), 8148-8155.

(31)    Pfändler, P., Bodenhausen, G., Rapin, J., Houriet, R., & Gäumann, T. (1987). Two-
        dimensional fourier transform ion cyclotron resonance mass spectrometry. *Chem. Phys.
        Lett.*, *138*(2), 195-200.

# CHAPTER 2.     SIMULTANEOUS AND SEQUENTIAL MS/MS SCAN COMBINATIONS AND PERMUTATIONS IN A LINEAR QUADRUPOLE ION TRAP

Portions of this work have been published in the journal *Analytical Chemistry* as the article: Snyder, D.T., L.J. Szalwinski, and R.G. Cooks. (2017). Simultaneous and Sequential MS/MS Scan Combinations and Permutations in a Linear Quadrupole Ion Trap. *Anal. Chem, 89*(20), 11053-11060.

## 2.1    Introduction

The drive to miniaturize mass spectrometers has encouraged the development of a wealth of unconventional ionization sources, atmospheric pressure interfaces, vacuum systems, and mass analyzer combinations.[1,2] Both continuous[3,4]  and discontinuous[5,6] atmospheric pressure interfaces have been developed, allowing the coupling of ambient spray and plasma ionization methods with portable systems.[7-10] The standard analyzer geometry has evolved from the 3D quadrupole ion trap (Paul trap)[11] to cylindrical,[12] rectilinear,[13] linear,[14,15] toroidal,[16-18] and halo traps,[19,20] as well as ion trap arrays,[21-24] two-plate linear ion traps,[25] wire ion traps,[26,27] and other unusual devices.

By contrast, the fundamental way in which mass analysis is performed in quadrupole ion traps has varied very little. Mass-selective instability,[28] usually with resonance ejection[12,14] either radially[14] or axially,[15,29] has remained the dominant form of mass analysis in both 2D and 3D ion traps.[30-32] Improvements in resolution, sensitivity, and space-charge tolerance can be made through nonlinear resonance ejection[33,34] and orthogonal excitation during the ejection process.[35] Ion ejection can furthermore be made unidirectional through careful selection of multipole components,[33,34] rf/ac phase relationship,[34] and ac signal components.[35]

Despite the minimal variation in ion trap mass analysis over the past three decades, three unconventional mass scanning methodologies have appeared in the ion trap literature: digital ion trap frequency scanning,[36] sinusoidal rf frequency scanning,[37] and ac frequency scanning.[38] Digital technology is promising, especially with regard to high spectral resolution, mass range, and scan speed, but it requires a complete overhaul of existing instrumentation and has a higher power consumption than for conventional methods. Rf frequency scanning can similarly improve resolution and mass range. The ac frequency scanning technique, in contrast, is not particularly

high performance yet it offers increased instrument versatility while requiring virtually no instrument modifications.[39]

Among the unique capabilities made accessible by ac frequency scanning (also known as secular frequency scanning) are data-independent single analyzer precursor ion scans and neutral loss scans.[40,41] These simple scans, of which the precursor variant was demonstrated on a 3D ion trap some 25 years ago,[42] require simultaneous orthogonal excitation of precursor and product ions for fragmentation of a particular precursor ion in concert with the ejection and detection of a particular product ion. In the case of the precursor ion scan, the product ion m/z, and hence secular frequency under constant rf conditions is fixed, whereas in the neutral loss scan the difference between precursor ion and product ion m/z is fixed, and with an added "artifact rejection" scan (to neutralize unfragmented precursor ions), this requires a triple frequency scan for implementation. In comparison, previous implementations of precursor and neutral loss "scans" have largely been data-dependent sequences[43,44] of resonance excitation[45] and resonance ejection and hence are not actually "scans", but rather are sequences of scans from which precursor and neutral loss spectra can be reconstructed.

Both the precursor ion scan and the more difficult neutral loss scan that we demonstrated[41] show relatively low conversion of precursor ions to detected product ions using conventional scan rates (thousands of Th per second). For example, in cases where each precursor ion is given ~3 ms to fragment, typical estimated conversions are 5–10%, which implies that perhaps 90% of the precursor ions are left in the ion trap after a precursor ion scan. For the neutral loss scan, this is not the case because the precursor ions must be cleared from the ion trap during the scan to prevent artifact peaks. Nonetheless, the inefficiency in fragmentation in the precursor scan allows certain MS/MS permutations to be performed. These are ordered combinations of the three main MS/MS scan types: precursor ion scans, product ion scans, and neutral loss scans. The zero-dimensional multiple reaction monitoring experiment is not a scan and is not considered further because if isolation is performed strictly, no ions will remain after this experiment, which can only be the end point of an experimental sequence. By performing multiple scans on the same ion population, the information obtained from those ions can be maximized, a particularly useful characteristic for resource-constrained ion traps with relatively low duty cycles and when sample size and/or access is highly limited. The allowed combinations of scans are multiple precursor ion scans, precursor ion scans followed by a neutral loss scan, precursor ion scans followed by product ion scans, and

segmented neutral loss scans, as well as simultaneous precursor and neutral loss scans, all of which are demonstrated here for simple mixtures of illicit drugs.

## 2.2    Experimental Section

### 2.2.1    Chemicals

Amphetamine (m/z 136), methamphetamine (m/z 150), 3,4-methylenedioxyamphetamine (m/z 180), 3,4-methylenedioxymethamphetamine (m/z 194), 3,4-methylenedioxyethylamphetamine (m/z 208), cocaine (m/z 304), noroxycodone (m/z 302), oxycodone (m/z 316), buphedrone HCl (m/z 178), N-ethylcathinone (m/z 178), morphine (m/z 286), codeine (m/z 300), and 6-monoacetylmorphine (m/z 328) were purchased from Cerilliant (Round Rock, TX, U.S.A.). HPLC grade methanol was purchased from Fisher Scientific (Hampton, NH, U.S.A.). All analytes were detected in the protonated form in the positive ion mode. Oral fluid samples were spiked with amphetamine standards and subsequently diluted 10-fold in 95:4.9:0.1 acetonitrile/water/formic acid.

### 2.2.2    Ionization

Nanoelectrospray ionization using a 1.5 kV potential was utilized for all experiments. Borosilicate glass capillaries (1.5 mm O.D., 0.86 mm I.D.) from Sutter Instrument Co. (Novato, CA, U.S.A.) were pulled to 2 μm tip diameters using a Flaming/Brown micropipette puller (model P-97, Sutter Instrument Co.). The nanospray electrode holder (glass size 1.5 mm) was purchased from Warner Instruments (Hamden, CT, U.S.A.) and was fitted with 0.127 mm diameter silver wire, part number 00303 (Alfa Aesar, Ward Hill, MA), as the electrode.

### 2.2.3    Instrumentation

All scans were performed using a Finnigan LTQ linear ion trap mass spectrometer (San Jose, CA, U.S.A.) modified previously to perform orthogonal excitation. The ion trap has dimensions $x0 = 4.75$ mm, $y0 = 4$ mm, and three axial sections of lengths 12, 37, and 12 mm. The rf frequency was tuned to 1.166 MHz. The rf amplitude was held constant throughout ionization, ion cooling, and mass scan segments by substituting the rf modulation signal between the rf detector board and rf amplifier with a low voltage DC pulse (~190 mV, ~700 ms period, 90%

duty cycle) from an external function generator. All ac waveforms were generated by using two Keysight 33612A (Chicago, IL, U.S.A.) arbitrary waveform generators. Inverse Mathieu q scans were calculated in Matlab, exported as .csv files, and imported to the waveform generators. The inverse Mathieu q scan is a nonlinear sweep of the low voltage ac frequency (performed at constant rf voltage) that linearizes the mass scale in contrast to the result of linear frequency sweeping. Scan rates were in the range 200–500 Th/s and the lower-mass cutoff was usually set at 90 Th.

Precursor ion scans were performed by applying to the y electrodes of the linear ion trap a low voltage (~200 mVpp) swept frequency (an inverse Mathieu q scan) for precursor ion excitation while simultaneously applying a higher voltage (~600 mVpp) fixed frequency to the x electrodes at a particular product ion's secular frequency.

Similarly, neutral loss scans required three identical inverse Mathieu q scans with appropriate trigger delays. (55) A first frequency scan (~200 mVpp) was used for precursor ion excitation, a second frequency scan (~600 mVpp) with trigger delay was applied to reject into the y electrodes remaining precursor ions subsequent to their excitation, and finally, a third frequency sweep (~600 mVpp) with a trigger delay larger than the artifact delay was used for product ion ejection. The fixed neutral loss selected was directly proportional to the time delay between the excitation and ejection sweeps. Each scan was calibrated separately using a linear fit of m/z vs time.

Permutation scans were performed by applying the appropriate waveforms back-to-back or simultaneously. For sequential precursor ion scans, the excitation frequency sweep was applied twice in sequence. During the first sweep a first product ion ejection frequency was applied to target a first product ion, and during the second sweep a different frequency was applied to target a different product ion m/z. For the double (simultaneous) precursor ion scan, a single inverse Mathieu q scan was applied to the y electrodes for ion excitation while a dual frequency sine wave was applied to the x electrodes to target two product ions for ejection. To perform a precursor scan and neutral loss scan sequentially, an inverse Mathieu q scan was applied twice in sequence for ion excitation. During the first sweep a single frequency was applied to the x electrodes to target ions of a fixed m/z for ejection, and during the second sweep two trigger-delayed frequency sweeps (artifact rejection and product ion ejection) were applied to complete the neutral loss scan. For simultaneous precursor and neutral loss scans the waveforms required for each scan were summed and applied to the appropriate electrodes simultaneously. Hence, an excitation scan and artifact

rejection scan were applied to the y electrodes while a fixed frequency and time-delayed frequency scan were summed and applied to the x electrodes. For the precursor ion scan followed by the product ion scan, a precursor ion scan was performed first, after which a selected precursor ion (not isolated) was excited at its secular frequency. A full ac frequency sweep then gave the product ion mass spectrum. Segmented neutral loss scans were simply back-to-back neutral loss scans (targeting different neutral losses) at different rf amplitudes. Simultaneous neutral loss scans were performed by using two single frequency sweeps on the y electrodes for ion excitation and artifact rejection while simultaneously applying two frequency sweeps on the x electrodes, one for each neutral loss. Only one ion injection event was used for each permutation, and automatic gain control was turned off. Injection time was varied from 5 to 25 ms, depending on sample concentration (generally 1–10 ppm, viz. g/L). Each mass spectrum shown here is the average of 10 scans.

## 2.3    Results and Discussion

Precursor ion scans and neutral loss scans are possible in single quadrupole ion traps using double resonance excitation, that is, by simultaneously exciting a precursor ion and ejecting a particular product ion so that the detection of that product ion occurs at the unique time during which its precursor fragments. Unlike CID in beam-type instruments (e.g., sectors and triple quadrupoles), CID in ion traps requires a relatively long time to increase internal energies because (1) helium is usually used as the collision partner and (2) collision energies are quite small. Hence, many collisions, and thus more time, are required for fragmentation in ion traps. For the precursor scans and neutral loss scans, the low fragmentation efficiency translates into relatively low sensitivity for conventional scan rates. However, precursor ion scans, if performed under low ac amplitude conditions, do not clear the ion trap completely, and thus, if only a small fraction of the precursor ions are converted to product ions, then the rest of the ions are left in the trap for re-examination. This characteristic makes available permutations of MS/MS scan modes.

The full range of allowed MS/MS permutations is shown in Table 2.1. Multiple precursor ion scans can be performed on the same ion population so long as the precursor ions are not ejected and fully fragmented. Precursor ion scans can also be followed by a single neutral loss scan. Because the neutral loss scan clears the ion trap with an "artifact rejection" frequency sweep, no subsequent scans are possible using a single ion injection event. Any number of product ion scans

can succeed precursor ion scans as well. Finally, although two neutral loss scans cannot interrogate the same mass range (for a single ion injection event), one ion packet can be used for a segmented neutral loss scan wherein different neutral loss scans are performed over different mass ranges. Simultaneous scans are also allowed. Multiple precursor ion scans may be performed concurrently as well as precursor scans with neutral loss scans and finally multiple simultaneous neutral loss scans. In each of the scans the AC amplitudes are optimized while constant RF amplitude is used.

Table 2.1 MS/MS permutations available to the linear ion trap

| MS/MS permutation | advantages over single stage MS/MS | example | experimental scan rate (Th/s) | experimental LMCO (Th) |
|---|---|---|---|---|
| $Pre^n$ | broad coverage of molecular functionality; increased coverage of a set of related analytes (e.g., amphetamines) | Figure 2.1 | 469 | 93 |
| $Pre^n$-NL | coverage of several classes of compounds; increasing information yield from particularly uninformative MS/MS experiments (e.g., NL of water) | Figure 2.2 | 475 | 99 |
| $Pre^n$-$Pro^n$ | extensive MS/MS domain mapping; confirmation of precursor ion identity, esp. isobars | Figure 2.3 | 226 | 85 |
| $NL^n$ (segmented) | ability to work with several classes of compounds that generally lie in different $m/z$ ranges | Figure 2.4 | 230, 415 | 91, 165 |
| simultaneous $Pre^n$ | broader analyte coverage in a single mass scan, although presents more ambiguity than discrete scans | Figure 2.5b | 240 | 93 |
| simultaneous $Pre^n$-NL | broader analyte coverage in a single mass scan, although presents more ambiguity than discrete scans | Figure 2.5d | 342 | 128 |
| simultaneous $NL^n$ | monitor multiple classes of compounds in a single scan, though there is ambiguity in precursor → product relationships | Figure 2.5f | 214 | 83 |

*Pre = precursor ion scan; NL = neutral loss scan; Pro = product ion scan. n = a positive integer. Product ion scans can also be performed earlier in the sequence provided the masses of the fragments do not fall into ranges of interest in the other scan types. Multiple reaction monitoring (MRM) experiments can also be done at the end of any permutation, but they are not considered further as they are not scans.*

### 2.3.1 Multiple Precursor Ion Scans in Sequence

Multiple precursor ion scans are allowed because each precursor ion scan (at scan rates of hundreds of Th per second) converts a small fraction of precursor ions to product ions. Permutations of precursor ion scans could be useful for scanning an analyte population for different molecular functionalities and for monitoring more than one class of molecules. An example of a double sequential precursor ion scan is shown in Figure 2.5 (compare to full scan in panel a). In this example, amphetamines are monitored using a precursor ion scan of m/z 163 and cocaine is monitored using a precursor ion scan of m/z 182. All three amphetamines in this simple mixture could be detected at ~1 ppm with no artifact peaks and about 8% conversion of precursor ions to product ions at a scan rate of ~450 Da/s. Note that MDEA was detected with S/N ~ 10 but is hard to see without an expanded intensity axis. The same precursor ion scan could, in principle, be performed multiple times, allowing for signal averaging or signal accumulation, somewhat mitigating the relatively low sensitivity of the method.
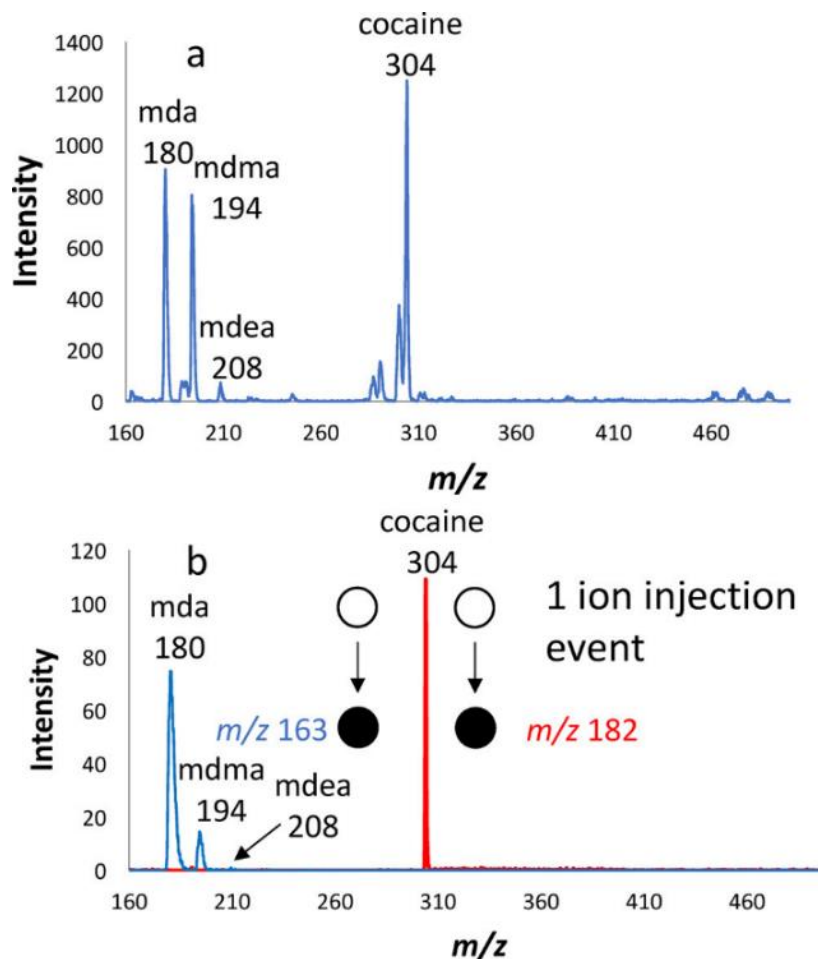
Figure 2.1. Permutations of precursor ion scans: (a) full ac scan mass spectrum of 3,4-methylenedioxyamphetamine (mda), 3,4-methylenedioxymethamphetamine (mdma), 3,4-methylenedioxyethylamphetamine (mdea), and cocaine, and (b) precursor ion scan of m/z 163 followed by precursor ion scan of m/z 182 using the same ion population.

### 2.3.2 Precursor Ion Scans Followed by a Neutral Loss Scan

Precursor ion scans can be followed by a single neutral loss scan. Because the neutral loss scan clears the trap of ions, no other scans are possible subsequently. Nonetheless, like permutations of precursor ion scans, precursor ion scans followed by a neutral loss scan may be useful for examining an ion population for different functional groups. Figure 2.2 (full scan in panel a) shows a precursor ion scan of m/z 182 (the most abundant product ion of cocaine) followed by a neutral loss scan of 18 Da, which targets opioids oxycodone and noroxycodone. In the case of the neutral loss scan, unit resolution is observed at a scan rate of 470 Da/s and at most 17% of the precursor ions are converted to detected product ions. In principle, multiple precursor

46

ion scans could be followed by a single neutral loss scan; however, the electronic constraints of our system limited the number of sequential scans we could perform.
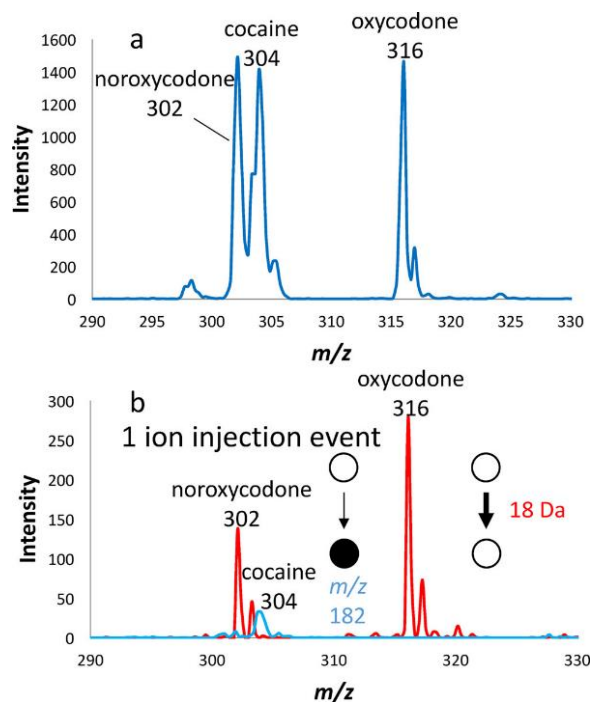


Figure 2.2. Permutation of precursor ion scans and neutral loss scans: (a) full ac scan mass spectrum of cocaine, noroxycodone, and oxycodone, and (b) precursor ion scan of m/z 182 followed by neutral loss scan of 18 Da.

### 2.3.3    Precursor Ion Scans Followed by Product Ion Scans

Product ion scans may follow precursor ion scans as well. A useful example of the utility of this scan mode is shown in Figure 2.3, where isobaric buphedrone and N-ethylcathinone were detected in the full scan in panel a, from a mixture with methamphetamine, and also in a precursor ion scan of m/z 160 (panel b, blue). A product ion scan of m/z 178 (panel b, orange) then confirms that both isobars are present since m/z 91 and 147 are unique to buphedrone and m/z 133 is unique to N-ethylcathinone. Note that no isolation was performed prior to the product ion scan (and hence methamphetamine was also detected in the final mass scan) although, in principle, it would usually precede the product ion scan.
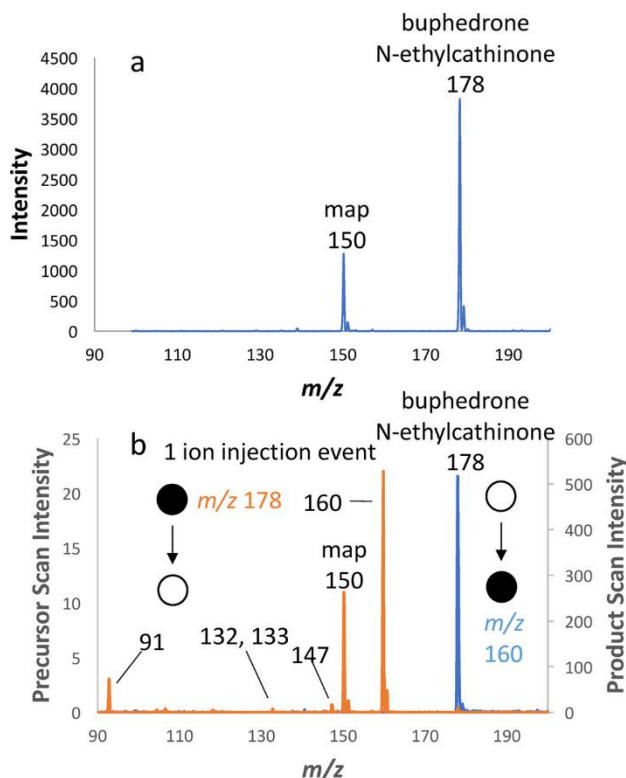
Figure 2.3. Permutation of precursor ion scan and product ion scan: (a) full rf scan mass spectrum of buphedrone, N-ethylcathinone, and methamphetamine, and (b) precursor ion scan of m/z 160 followed by product ion scan of isobars at m/z 178, confirming that both buphedrone and N-ethylcathinone are present. Note that m/z 178 was not isolated before the product ion scan, and hence, m/z 160 is present (though not fragmented) in (b).

### 2.3.4   Segmented Neutral Loss Scans

Because neutral loss scans clear the precursor ions from the ion trap via the "artifact rejection" frequency sweep, no other scan modes may follow them. Hence, although neutral loss scans may not be repeated in the same mass range, segmented neutral loss scans are still allowed. These are similar to segmented full mass scans documented previously wherein different mass ranges are interrogated at dissimilar rf amplitudes to improve resolution and mass accuracy across a portion of the mass range. Neutral loss scans can also be "segmented" so that different mass ranges can be analyzed for different neutral losses. Segmenting the neutral loss scan allows better mass spectral resolution to be obtained for higher mass ions, which have lower secular frequency dispersions compared to lower mass ions. Moreover, often different classes of molecules will occupy different mass ranges so that multiple classes of molecules could be monitored with a single ion injection event (e.g., fatty acids and complex phospholipids in tissue). Figure 2.4b shows

a segmented neutral loss scan of a mixture of methamphetamine, mdma, noroxycodone, and oxycodone (all of which were detected in the full scan in panel a). A first neutral loss scan of 31 Da was initiated at a low mass cutoff of ~91 Th, and a second neutral loss scan of 18 Da was carried out at a low mass cutoff of ~165 Th (i.e., using a higher rf amplitude). Both spectra exhibit unit resolution at a scan rate of 230 (first scan) and 415 Da/s (second scan) and with approximately 4% conversion of precursor ions to detected product ions.
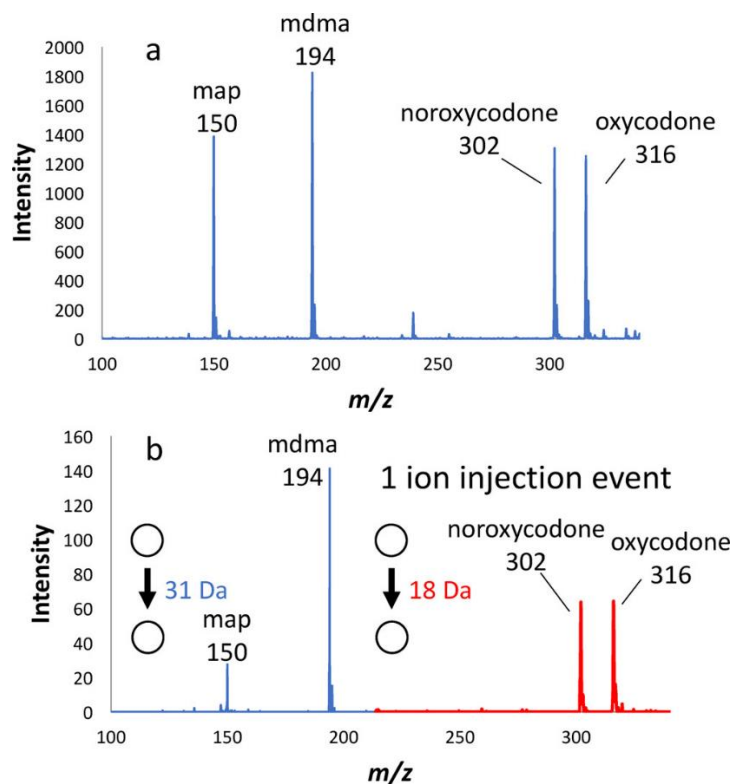


Figure 2.4. Segmented neutral loss scan: (a) full rf ramp resonance ejection mass spectrum of methamphetamine (map), 3,4-methylenedioxymethamphetamine (mdma), noroxycodone, and oxycodone, and (b) segmented neutral loss of 31 Da (at a LMCO of 91 Da) and, subsequently, 18 Da (at a LMCO of 165 Da) using a single ion injection. No signal was observed with the precursor ion excitation signal off.

### 2.3.5    Simultaneous Scans

One of the disadvantages of performing multiple discrete MS/MS scans in sequence is that an insufficient number of ions may remain after the first scan for several reasons. It is possible that most of the precursor ions are fragmented in the first scan, or if enough collision energy is imparted to the precursors then they may collide with the orthogonal electrodes (y direction, in our case) and, hence, be lost before any other scans take place. In this case, it is possible to perform simultaneous MS/MS scans. That is, one may perform multiple simultaneous precursor ion scans, simultaneous precursor and neutral loss scans, and simultaneous neutral loss scans.

Figure 2.5 gives examples of all three cases. In Figure 2.5a, a full ac frequency scan of methamphetamine, mdma, and mdea is shown. Methamphetamine fragments to m/z 119 and the latter two drug fragments to m/z 163. Hence, all three amphetamines can be targeted (Figure 2.5b) by doing a simultaneous precursor ion scan of both product ion m/z values, which is accomplished by using a dual frequency waveform (332 and 227 kHz) for product ion ejection. An important characteristic of these spectra is the resolution observed. Although unit resolution was not observed in the full scan due to space charge effects (i.e., the trap was purposely overloaded with ions), unit resolution was observed in the MS/MS scan. The cause of the resolution increase is likely the orthogonal excitation that causes the product ions to circle the bulk of the ion cloud just before ejection, and hence, better resolution is observed compared to the full scan mode, wherein the precursor ions were only excited in one dimension. This effect has been previously documented in the study of "rhombic" ion excitation.
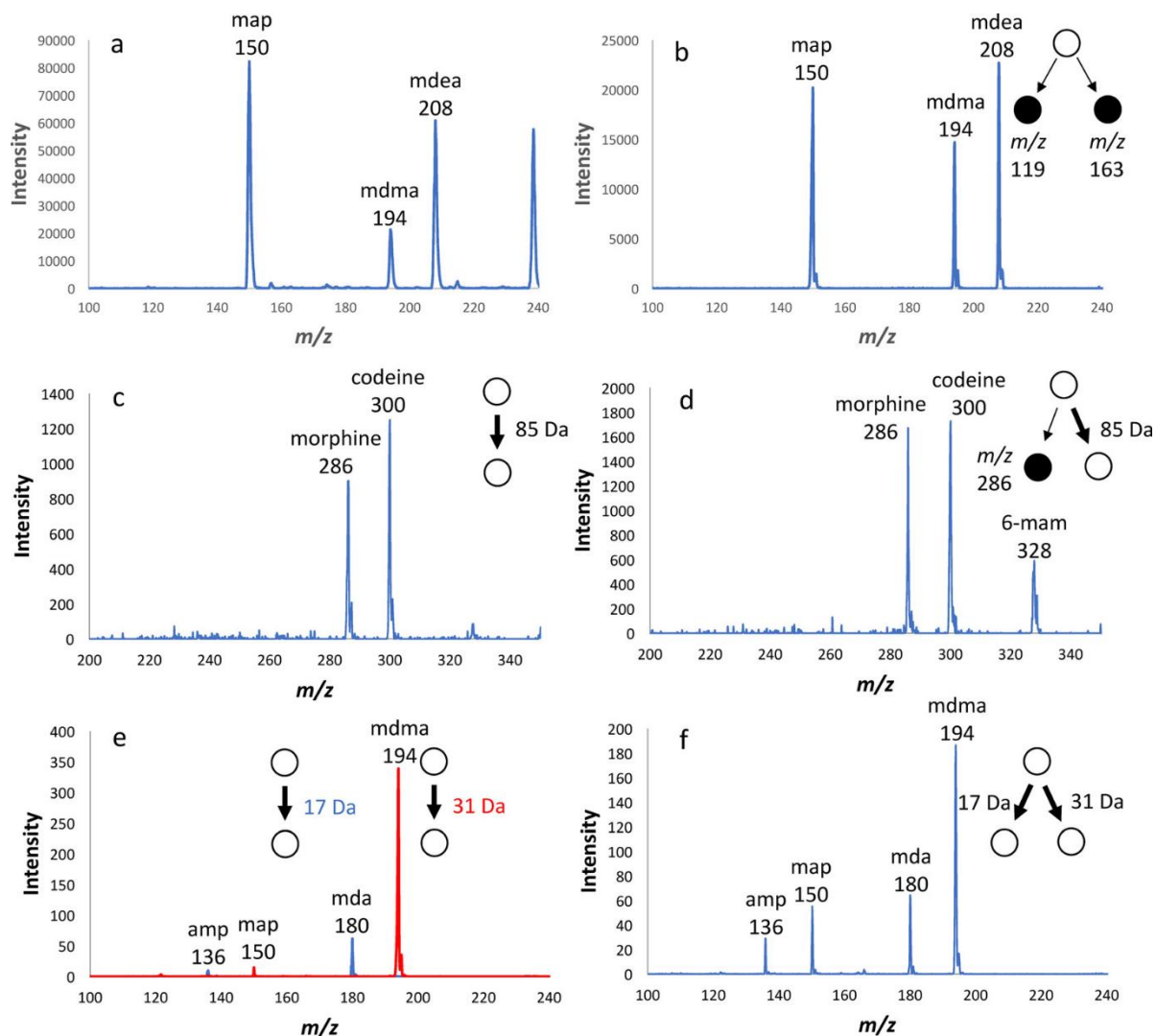
Figure 2.5. Simultaneous MS/MS scans: (a) full ac frequency scan of protonated methamphetamine, 3,4-methylenedioxymethamphetamine, and 3,4-methylenedioxyethylamphetamine, (b) simultaneous double precursor ion scan of m/z 119 and m/z 163, (c) single neutral loss scan of 85 Da of a mixture of morphine, codeine, and 6-monoacetylmorphine, (d) simultaneous precursor ion scan of m/z 286 and neutral loss scan of 85 Da, (e) separate neutral loss scans of 17 Da (blue) and 31 Da (red) performed on amphetamine, methamphetamine, 3,4-methylenedioxyamphetamine, and 3,4-methylenedioxymethamphetamine, and (f) simultaneous neutral loss scan of 17 and 31 Da performed on the four amphetamines.

A simultaneous precursor and neutral loss scan can similarly be performed by applying the following waveforms simultaneously: (1) a frequency scan in y for precursor ion activation, (2) a fixed frequency sine wave in x for product ion ejection (precursor scan), (3) a frequency scan in y for precursor ion rejection (artifact rejection) after activation, and (4) a frequency scan in x, with fixed mass offset from the excitation frequency scan, for neutral loss product ion ejection into the detectors. Figure 2.5c shows a single neutral loss scan of 85 Da on a simple solution of morphine, codeine, and 6-monoacetylmorphine, which detects the transitions m/z 286 → 201 and m/z 300 → 215. By simultaneously performing a precursor ion scan of m/z 286 (a product ion of 6-mam), 6-mam also appears in the MS/MS spectrum. Note that the ejection frequency for m/z 286 was switched on after morphine was excited to prevent ejection of the morphine precursors prior to their excitation. Of course, whether each ion is ejected by the precursor scan, or the neutral loss scan is ambiguous. Nonetheless, a simultaneous scan would still be useful, for example, in providing broad coverage of the amphetamines, which fragment either to m/z 163 or m/z 119. In this case, it is not critical to know which fragment is produced by an unknown amphetamine, but a subsequent product ion scan would make the assignment clear.

Finally, an example of a simultaneous neutral loss scan performed on a mixture of amphetamine, methamphetamine, 3,4-methylenedioxyamphetamine, and 3,4-methylenedioxymethamphetamine is shown in Figure 2.5f. The individual neutral loss scans (shown in Figure 2.5e) are loss of 17 Da and loss of 31 Da. Because each of these scans detects two of the amphetamines, all four of the amphetamines can be targeted by simultaneous neutral loss scans of 17 and 31 Da. This experiment required the following waveforms: (1) precursor ion excitation frequency sweep on the y electrodes, (2) artifact rejection sweep to eject unfragmented precursor ions into the y electrodes, (3) product ion ejection frequency sweep on the x electrodes for the 17 Da loss, and (4) product ion ejection frequency sweep on the x electrodes for the 31 Da loss.

### 2.3.6   Performance of MS/MS Scans on Oral Fluid

The final experiment performed in this work was utilization of the MS/MS scan modes in the case of a complex mixture. Oral fluid was chosen as an appropriate sample, as it has previously been examined for illicit drugs by swab touch spray tandem mass spectrometry.[46] In this work, amphetamine standards were spiked into the oral fluid at concentrations ranging from 1 to 100

ppm and subsequently the sample was diluted 10-fold in 50:4.9:0.1 acetonitrile/water/formic acid to improve nanospray performance. A full scan of the nanosprayed solution containing the drugs at 100 ppb final concentration (each is 1 ppm in oral fluid) is shown in Figure 2.6a. The four amphetamine peaks are buried in the mass spectrum. A simultaneous double precursor ion scan, Figure 2.6b, of m/z 119 and m/z 163 reveals all four amphetamines, although clearly the scan was performed near the limit of detection. The same scan with 5× higher concentration of amphetamines is shown in panel c. Both spectra are remarkably clean and free from artifacts.
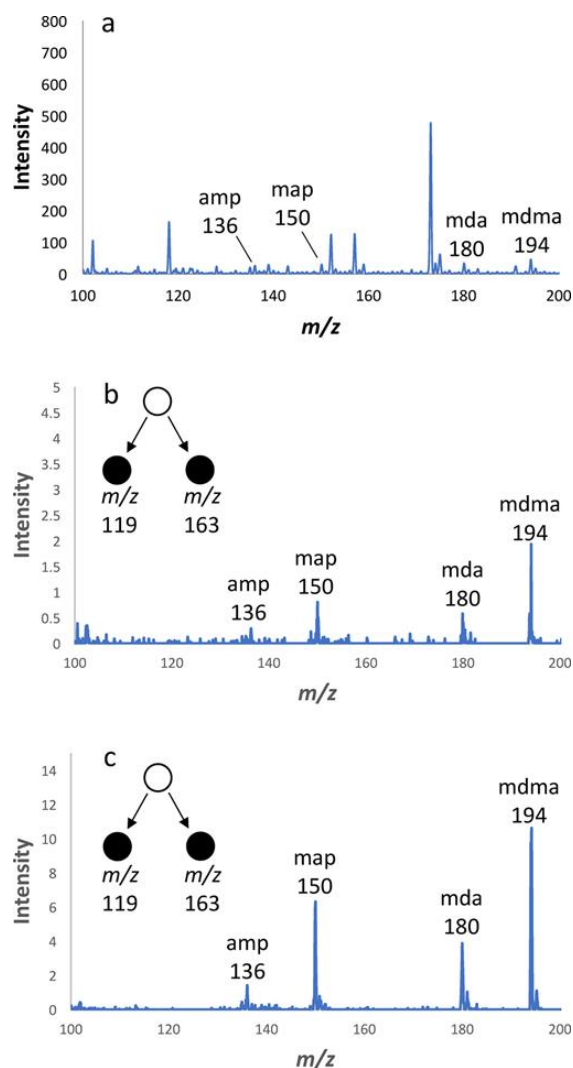


Figure 2.6. Simultaneous double precursor ion scan of oral fluid spiked with amphetamines: (a) full scan of 10% oral fluid with final concentration 100 ppb amp, map, mda, and mdma (1 ppm in oral fluid), (b) simultaneous double precursor ion scan of m/z 119 and 163, and (c) the same experiment at 500 ppb final concentration of amphetamines.

### 2.3.7   Duty Cycle and Sensitivity

The scans demonstrated here on a commercial benchtop instrument are quite slow ($10^2$ Th/s) compared to data-dependent scans ($10^4$ Th/s for each scan in the sequence). However, when translated to miniature instruments that use discontinuous interfaces, these data-independent scans will be more practical. For example, the Mini 12[47] takes $\sim$700 ms to pump down after ion injection (when the DAPI valve is opened briefly) and uses an approximately 300 ms mass scan in the resonance ejection mode. Operating this system in a data-dependent mode would hence require several ion injection and cooling events, thereby using tens of seconds of instrument runtime, not including signal averaging. In comparison, a sequential or simultaneous MS/MS permutation scan would require $\sim$1 s total and would therefore be faster than the data-dependent mode while still retaining selectivity and increase in signal-to-noise from MS/MS transitions. Lastly, in comparison to the product ion scan mode, precursor and neutral loss scans in ion traps are considerably less sensitive, perhaps 2 orders of magnitude. Some of the loss of sensitivity may be compensated for by using air as cooling and collision gas, which is common on miniature instruments. Work is currently underway to implement the full MS/MS suite on a miniature system and will be the subject of a future report.

### 2.4   Conclusion

Permutations of MS/MS scan modes have been demonstrated on a single linear ion trap. Using one ion injection event, the information obtained from the injected ions can be maximized by performing particular ordered combinations of precursor ion scans, product ion scans, and neutral loss scans. Simultaneous precursor ion scans or precursor and neutral loss scans are also possible, expanding the range of analytes that can be detected with a single MS/MS scan. These scan modes are particularly important for resource-constrained instruments with limited instrument volume, power, or samples such as those examined using an ion trap for Mars origin of life studies or a portable instrument for forensic analyses in the field.

### 2.5   References

(1)     Ouyang, Z., & Cooks, R. G. (2009). Miniature Mass Spectrometers. Annual Review of Analytical Chemistry, 2(1), 187-214.

(2)     Snyder, D. T., Pulliam, C. J., Ouyang, Z., & Cooks, R. G. (2016). Miniature and Fieldable Mass Spectrometers: Recent Advances. Anal. Chem., 88(1), 2-29.

(3)     Zhai, Y., Feng, Y., Wei, Y., Wang, Y., & Xu, W. (2015). Development of a miniature mass spectrometer with continuous atmospheric pressure interface. Analyst, 140(10), 3406-3414.

(4)     Zhai, Y., Jiang, T., Huang, G., Wei, Y., & Xu, W. (2016). An aerodynamic assisted miniature mass spectrometer for enhanced volatile sample analysis. Analyst, 141(18), 5404-5411.

(5)     Gao, L., Cooks, R. G., & Ouyang, Z. (2008). Breaking the Pumping Speed Barrier in Mass Spectrometry: Discontinuous Atmospheric Pressure Interface. Anal. Chem., 80(11), 4026-4032.

(6)     Wei, Y., Bian, C., Ouyang, Z., & Xu, W. (2015). A pulsed pinhole atmospheric pressure interface for simplified mass spectrometry instrumentation with enhanced sensitivity. Rapid Commun. Mass Spectrom., 29(8), 701-706.

(7)     Venter, A., Nefliu, M., & Graham Cooks, R. (2008). Ambient desorption ionization mass spectrometry. TrAC, Trends Anal. Chem., 27(4), 284-290.

(8)     Hou, K., Xu, W., Xu, J., Cooks, R. G., & Ouyang, Z. (2011). Sampling Wand for an Ion Trap Mass Spectrometer. Anal. Chem., 83(5), 1857-1861.

(9)     Harper, J. D., Charipar, N. A., Mulligan, C. C., Zhang, X., Cooks, R. G., & Ouyang, Z. (2008). Low-Temperature Plasma Probe for Ambient Desorption Ionization. Anal. Chem., 80(23), 9097-9104.

(10)    Lawton, Z. E., Traub, A., Fatigante, W. L., Mancias, J., O'Leary, A. E., Hall, S. E., Wieland, J. R., Oberacher, H., Gizzi, M. C., & Mulligan, C. C. (2017). Analytical Validation of a Portable Mass Spectrometer Featuring Interchangeable, Ambient Ionization Sources for High Throughput Forensic Evidence Screening. J. Am. Soc. Mass. Spectrom., 28(6), 1048-1059.

(11)    Paul, W., & Steinwedel, H. (1953). Notizen: Ein neues Massenspektrometer ohne Magnetfeld. Zeitschrift für Naturforschung A, 8(7), 448-450.

(12)    Fulford, J. E., Nhu-Hoa, D., Hughes, R. J., March, R. E., Bonner, R. F., & Wong, G. J. (1980). Radio-frequency mass selective excitation and resonant ejection of ions in a three-dimensional quadrupole ion trap. Journal of Vacuum Science and Technology, 17(4), 829-835.

(13)    Ouyang, Z., Wu, G., Song, Y., Li, H., Plass, W. R., & Cooks, R. G. (2004). Rectilinear Ion Trap: Concepts, Calculations, and Analytical Performance of a New Mass Analyzer. Anal. Chem., 76(16), 4595-4605.

(14)     Schwartz, J. C., Senko, M. W., & Syka, J. E. P. (2002). A two-dimensional quadrupole ion trap mass spectrometer. J. Am. Soc. Mass. Spectrom., 13(6), 659-669.

(15)     Hager, J. W. (2002). A new linear ion trap mass spectrometer. Rapid Commun. Mass Spectrom., 16(6), 512-526.

(16)     Lammert, S. A., Plass, W. R., Thompson, C. V., & Wise, M. B. (2001). Design, optimization and initial performance of a toroidal rf ion trap mass spectrometer. Int. J. Mass spectrom., 212(1), 25-40.

(17)     Lammert, S. A., Rockwood, A. A., Wang, M., Lee, M. L., Lee, E. D., Tolley, S. E., Oliphant, J. R., Jones, J. L., & Waite, R. W. (2006). Miniature toroidal radio frequency ion trap mass analyzer. J. Am. Soc. Mass. Spectrom., 17(7), 916-922.

(18)     Contreras, J. A., Murray, J. A., Tolley, S. E., Oliphant, J. L., Tolley, H. D., Lammert, S. A., Lee, E. D., Later, D. W., & Lee, M. L. (2008). Hand-portable gas chromatograph-toroidal ion trap mass spectrometer (GC-TMS) for detection of hazardous compounds. J. Am. Soc. Mass. Spectrom., 19(10), 1425-1434.

(19)     Austin, D. E., Wang, M., Tolley, S. E., Maas, J. D., Hawkins, A. R., Rockwood, A. L., Tolley, H. D., Lee, E. D., & Lee, M. L. (2007). Halo Ion Trap Mass Spectrometer. Anal. Chem., 79(7), 2927-2932.

(20)     Peng, Y., Hansen, B. J., Quist, H., Zhang, Z., Wang, M., Hawkins, A. R., & Austin, D. E. (2011). Coaxial Ion Trap Mass Spectrometer: Concentric Toroidal and Quadrupolar Trapping Regions. Anal. Chem., 83(14), 5578-5584.

(21)     Tabert, A. M., Griep-Raming, J., Guymon, A. J., & Cooks, R. G. (2003). High-Throughput Miniature Cylindrical Ion Trap Array Mass Spectrometer. Anal. Chem., 75(21), 5656-5664.

(22)     Chaudhary, A., Amerom, F. H. W. v., & Short, R. T. (2009). Development of Microfabricated Cylindrical Ion Trap Mass Spectrometer Arrays. Journal of Microelectromechanical Systems, 18(2), 442-448.

(23)     Xu, W., Li, L., Zhou, X., & Ouyang, Z. (2014). Ion Sponge: A 3-Dimentional Array of Quadrupole Ion Traps for Trapping and Mass-Selectively Processing Ions in Gas Phase. Anal. Chem., 86(9), 4102-4109.

(24)     Kornienko, O., Reilly, P. T. A., Whitten, W. B., & Ramsey, J. M. (1999). Micro ion trap mass spectrometry. Rapid Commun. Mass Spectrom., 13(1), 50-53.

(25)     Austin, D. E., Peng, Y., Hansen, B. J., Miller, I. W., Rockwood, A. L., Hawkins, A. R., & Tolley, S. E. (2008). Novel ion traps using planar resistive electrodes: Implications for miniaturized mass analyzers. J. Am. Soc. Mass. Spectrom., 19(10), 1435-1441.

(26)     Wu, Q., Li, A., Tian, Y., Zare, R. N., & Austin, D. E. (2016). Miniaturized Linear Wire Ion Trap Mass Analyzer. Anal. Chem., 88(15), 7800-7806.

(27)    Wu, Q., Tian, Y., Li, A., Andrews, D., Hawkins, A. R., & Austin, D. E. (2017). A Miniaturized Linear Wire Ion Trap with Electron Ionization and Single Photon Ionization Sources. J. Am. Soc. Mass. Spectrom., 28(5), 859-865.

(28)    Stafford, G. C., Kelley, P. E., Syka, J. E. P., Reynolds, W. E., & Todd, J. F. J. (1984). Recent improvements in and analytical applications of advanced ion trap technology. Int. J. Mass Spectrom. Ion Processes, 60(1), 85-98.

(29)    Londry, F. A., & Hager, J. W. (2003). Mass selective axial ion ejection from a linear quadrupole ion trap. J. Am. Soc. Mass. Spectrom., 14(10), 1130-1147.

(30)    Dawson, P. H. (2013). Quadrupole Mass Spectrometry and Its Applications.

(31)    March, R. E. (2009). Quadrupole ion traps. Mass Spectrom. Rev., 28(6), 961-989.

(32)    March, R. E., & Todd, J. F. J. (2010). Practical Aspects of Trapped Ion Mass Spectrometry (Vol. IV).

(33)    Franzen, J. (1993). The non-linear ion trap. Part 4. Mass selective instability scan with multipole superposition. Int. J. Mass Spectrom. Ion Processes, 125(2), 165-170.

(34)    Splendore, M., Marquette, E., Oppenheimer, J., Huston, C., & Wells, G. (1999). A new ion ejection method employing an asymmetric trapping field to improve the mass scanning performance of an electrodynamic ion trap11Dedicated to J.F.J. Todd and R.E. March in recognition of their original contributions to quadrupole ion trap mass spectrometry. Int. J. Mass spectrom., 190-191, 129-143.

(35)    Kotana, A. N., & Mohanty, A. K. (2015). A modified auxiliary excitation signal for achieving unidirectional ion ejection in quadrupole ion trap mass spectrometers operating in the resonance ejection mode. Int. J. Mass spectrom., 386, 15-23.

(36)    Ding, L., Sudakov, M., Brancia, F. L., Giles, R., & Kumashiro, S. (2004). A digital ion trap mass spectrometer coupled with atmospheric pressure ion sources. J. Mass Spectrom., 39(5), 471-484.

(37)    Jiang, T., Zhang, H., Tang, Y., Zhai, Y., Xu, W., Xu, H., Zhao, X., Li, D., & Xu, W. (2017). A "Brick Mass Spectrometer" Driven by a Sinusoidal Frequency Scanning Technique. Anal. Chem., 89(10), 5578-5584.

(38)    Snyder, D. T., & Cooks, R. G. (2017). Improving mass assignments in quadrupole ion traps operated using ac scans: Theory and experimental validation. Int. J. Mass spectrom., 417, 1-7.

(39)    Snyder, D. T., Kaplan, D. A., Danell, R. M., van Amerom, F. H. W., Pinnick, V. T., Brinckerhoff, W. B., Mahaffy, P. R., & Cooks, R. G. (2017). Unique capabilities of AC frequency scanning and its implementation on a Mars Organic Molecule Analyzer linear ion trap [10.1039/C7AN00664K]. Analyst, 142(12), 2109-2117.

(40)     Snyder, D. T., & Cooks, R. G. (2017). Single Analyzer Precursor Ion Scans in a Linear Quadrupole Ion Trap Using Orthogonal Double Resonance Excitation. J. Am. Soc. Mass. Spectrom., 28(9), 1929-1938.

(41)     Snyder, D. T., & Cooks, R. G. (2017). Single Analyzer Neutral Loss Scans in a Linear Quadrupole Ion Trap Using Orthogonal Double Resonance Excitation. Anal. Chem., 89(15), 8148-8155.

(42)     Johnson, J. V., Pedder, R. E., & Yost, R. A. (1991). MS-MS parent scans on a quadrupole ion trap mass spectrometer by simultaneous resonant excitation of multiple ions. Int. J. Mass Spectrom. Ion Processes, 106, 197-212.

(43)     McClellan, J. E., Quarmby, S. T., & Yost, R. A. (2002). Parent and Neutral Loss Monitoring on a Quadrupole Ion Trap Mass Spectrometer:  Screening of Acylcarnitines in Complex Mixtures. Anal. Chem., 74(22), 5799-5806.

(44)     Schroeder, M. J., Shabanowitz, J., Schwartz, J. C., Hunt, D. F., & Coon, J. J. (2004). A Neutral Loss Activation Method for Improved Phosphopeptide Sequence Analysis by Quadrupole Ion Trap Mass Spectrometry. Anal. Chem., 76(13), 3590-3598.

(45)     Louris, J. N., Cooks, R. G., Syka, J. E. P., Kelley, P. E., Stafford, G. C., & Todd, J. F. J. (1987). Instrumentation, applications, and energy deposition in quadrupole ion-trap tandem mass spectrometry. Anal. Chem., 59(13), 1677-1685.

(46)     Pirro, V., Jarmusch, A. K., Vincenti, M., & Cooks, R. G. (2015). Direct drug analysis from oral fluid using medical swab touch spray mass spectrometry. Anal. Chim. Acta, 861, 47-54.

(47)     Li, L., Chen, T.-C., Ren, Y., Hendricks, P. I., Cooks, R. G., & Ouyang, Z. (2014). Mini 12, Miniature Mass Spectrometer for Clinical and Other Applications—Introduction and Characterization. Anal. Chem., 86(6), 2909-2916.

# CHAPTER 3.    TRIPLE RESONANCE METHODS TO IMPROVE PERFORMANCE OF ION TRAP PRECURSOR AND NEUTRAL LOSS SCANS

Portions of this work have been published in the *Journal of the American Society for Mass Spectrometry* as the article: Szalwinski, L. J., Snyder, D. T., Wells, J. M., & Cooks, R. G. (2020). Triple Resonance Methods to Improve Performance of Ion Trap Precursor and Neutral Loss Scans. *Journal of the American Society for Mass Spectrometry*, 31(5), 1123–1131.

## 3.1    Introduction

Data independent scan modes, such as the precursor and neutral loss scans, enable the user to quickly identify compounds containing particular functional groups. However, precursor ions do not always fragment directly to product ions that are diagnostic of the chosen functionality.[1]  In such cases, further fragmentation of the primary product ion might yield the desired diagnostic information.  This is a motivation for using high energy photons to increase the possible product ions generated.[2,3] Such techniques typically require significant activation time for sufficient fragmentation, making them difficult to couple to data independent scan modes.[4] The combination of improved fragmentation methods coupled to data independent analysis is highly desirable as data independent scan modes decrease the number of scans required to answer questions in chemical analysis.  However, the structural analysis performed is completely dependent on the degree and efficiency of fragmentation.  The capability to conduct data-independent analysis would be particularly valuable in miniature mass spectrometers where a discontinuous atmospheric pressure interface (DAPI) decreases instrument size at the cost of reduced duty cycle[5]. Improvements in MS/MS capabilities would then mirror recent improvements in mass range[6], instrument size and power[7], and resolution[8] which have made miniature ion trap mass spectrometers attractive as on-site chemical sensors.

Precursor ions can sometimes fragment to product ions with the same *m/z* value as the diagnostic product ion, but with a different structure.  In this case, the isobaric product ions can be fragmented again, and a diagnostic secondary product ion can be detected to confirm the primary product ion's structure.  This can readily be accomplished by performing another stage of mass analysis (MS[3]).[9] However, triple quadrupole mass spectrometers, which are the most common mass spectrometers that allow data independent analysis, do not have the capability of performing

a third stage of mass analysis. Ion traps can easily obtain $MS^3$ product ion information by using multiple stages of isolation/fragmentation in time.[10] However, ion isolation restricts the capability to perform data independent scan modes.[11] During isolation, all other precursor ions are removed from the trapped ion population. The ion trap must be repopulated to interrogate another precursor ion. If one mass selectively activates but does not remove precursor ions, one can avoid isolation thereby allowing data independent scan modes.

In previous work, we implemented $MS^2$ scans using a single quadrupole ion trap instrument.[12,13] In particular, we showed that it was possible to implement precursor and neutral loss scans by using a fixed trapping rf and applying orthogonal double resonance frequencies for ion excitation and ejection. These individual $MS^2$ scans could then be combined sequentially or simultaneously to perform experiments in which more MS/MS data is acquired per injected ion population.[14] In the present study, ions are resonantly excited at their secular frequency using a swept ac signal while a frequency in resonance with that of a single first-generation product ion is constantly applied so that a set of precursor ions and a first-generation product ion are both excited simultaneously, for dissociation and ejection, respectively. In other words, a double resonance condition is met by simultaneously and orthogonally exciting precursor and first-generation product ions. A fixed third frequency can also be applied to eject a particular second-generation fragment ion. This experiment is termed a sequential precursor ion scan in the original nomenclature for $MS^n$ spectra[15,16]; in the ion trap case it represents a *triple resonance* experiment because a precursor ion and two generations of product ions are irradiated simultaneously. The output of this particular $MS^3$ experiment has one dimension of mass plus a dimension of intensity. In the nomenclature of $MS^n$ scans, showing variable (O) and fixed (●) mass/charge values, the scan is written O→ ● → ● ; as such it is clear that it is a more selective version of a precursor ion scan O→ ●. Another feature of the experiment is that the third frequency can be used to create a beat frequency in the ejection waveform, modulating the trajectories of resonantly ejected ions but not the trajectories of product ions whose working points fall outside the stable region of the Mathieu stability diagram. The consequence of the beat frequency is that artifact peaks in precursor and neutral loss spectra are readily identified by peak shape.

## 3.2    Experimental

### 3.2.1    Chemicals

All amphetamines, pheniramines, and phosphonates were purchased from Sigma-Aldrich (St. Louis, MO,U.S.A.).   These compounds were diluted in 50:50 methanol/water with 0.1% formic acid to a concentration of 1 ppm.   HPLC grade methanol was purchased from Fisher Scientific (Hampton, NH, U.S.A.).

### 3.2.2    Instrumentation

All experiments were performed using a Finnigan LTQ linear ion trap mass spectrometer (San Jose, CA, U.S.A.) previously modified to perform orthogonal excitation using low voltage ac waveforms supplied by external function generators.[13]   A constant amplitude rf voltage was maintained by supplying a DC pulse (160 mV, 700 ms period, 90% duty cycle) to the rf detector board. This signal is substituted for the instrument's original rf modulation signal so that the rf voltage can be controlled externally. One consequence of this implementation is that the rf voltage drifts slightly from scan to scan, which slightly degrades mass accuracy and resolution but otherwise has minimal effects on the spectra. The linear ion trap has dimensions $x_0 = 4.75$ mm, $y_0 = 4$ mm, and three axial sections of lengths 12, 37, and 12 mm.   The rf frequency was kept at 1.166 MHz. Nitrogen (ion gauge reading $1.4 \times 10^{-5}$ torr) was used as bath gas instead of helium to improve sensitivity.

AC waveforms were supplied by two Keysight 33612A arbitrary waveform generators (Newark element14, Chicago, IL, USA).   An inverse Mathieu q scan was calculated in Matlab in a manner which allowed the mass scale to be linearized with time.[17]   A linear relationship between *m/z* and time is obtained from the linear relationship between $1/q$ and *m/z*.   The frequencies were calculated from the q-values in order to obtain the final waveform. All inverse Mathieu *q* scans were 600 ms in length from Mathieu $q = 0.908$ to $q = 0.15$ and had a constant peak voltage. For ion excitation, 150 $mV_{pp}$ signals were used, whereas 500 $mV_{pp}$ signals were used for ejection. The low mass cut off (LMCO) in these experiments was set at 80 Th.   Once the LMCO is calibrated by varying the external rf modulation voltage, all resonant frequencies can then be predicted from the Mathieu equation.   The components of the secular frequency in the x and y directions are assumed to be equal for a given ion.

Precursor ion scans were performed using an inverse Mathieu q scan to excite ions in the y-dimension while simultaneously applying a single frequency matching the secular frequency of a particular product ion in the x-dimension for ejection. Triple resonance excitation was conducted by supplying a third frequency in the x- dimension corresponding to the secular frequency of a particular $MS^2$ product ion. Note that in the case of the triple resonance scan, the product ion ejection signal, applied on the x electrodes, targets an $MS^3$ ion rather than an $MS^2$ ion. The frequency sweep waveform used to fragment precursor ions and the static frequency to fragment $MS^2$ product ions were summed within the waveform generator before being inductively coupled to the y-rod pair. Neutral loss scans were performed by applying two inverse Mathieu q scans on orthogonal electrodes (fragmentation of precursors in y, ejection of product ions in x). One scan had a fixed time offset from the other which was proportional to the neutral loss mass [13]. A third inverse Mathieu q scan applied to the y electrodes was used for ejection of unfragmented precursor ions to prevent their ejection (and detection) by the product ion ejection frequency sweep.

Beat frequencies were generated for precursor ion scans by summing two sine waves with a small (~1 kHz) frequency difference and applying this dipolar ejection signal to the x electrodes. A first sine wave matched the product ion's secular frequency and a second was offset from the first in order to generate the beat frequency. These two sine waveforms were summed within the waveform generator. The amplitudes of the sine waves were identical. In the neutral loss scan mode, beat frequencies were generated by summing two inverse Mathieu q scans with one of the scans having a constant frequency offset from the other, corresponding to the desired beat frequency. The two inverse Mathieu q scans were summed after each was calculated in Matlab and the summed output waveform was then imported into the arbitrary waveform generator.

## 3.3    Results and Discussion

### 3.3.1    Triple Resonance Excitation

Triple resonance excitation is a term covering several $MS^3$ experiments of which just one is discussed in this chapter. These experiments require application of a third ac frequency to an existing ion trap equipped with two frequency generators. The experiment discussed here increases the selectivity and sensitivity of the ion trap precursor ion scan performed by double resonance. The existing double resonance ion trap precursor scan uses two frequencies to excite and eject ions.

The first waveform is swept non-linearly in frequency so that all precursor ions are excited and fragmented in order of increasing *m/z* (Figure 3.1). A second ac signal of constant frequency is applied and corresponds to a product ion of particular *m/z* so that a specific molecular functionality can be monitored in the second-generation fragment ions. This allows species that generate product ions with the same *m/z*, but not the same functional structure, to be discriminated through a second stage of fragmentation. To achieve this, a third resonance is applied so that specific second-generation product ions are ejected and detected.
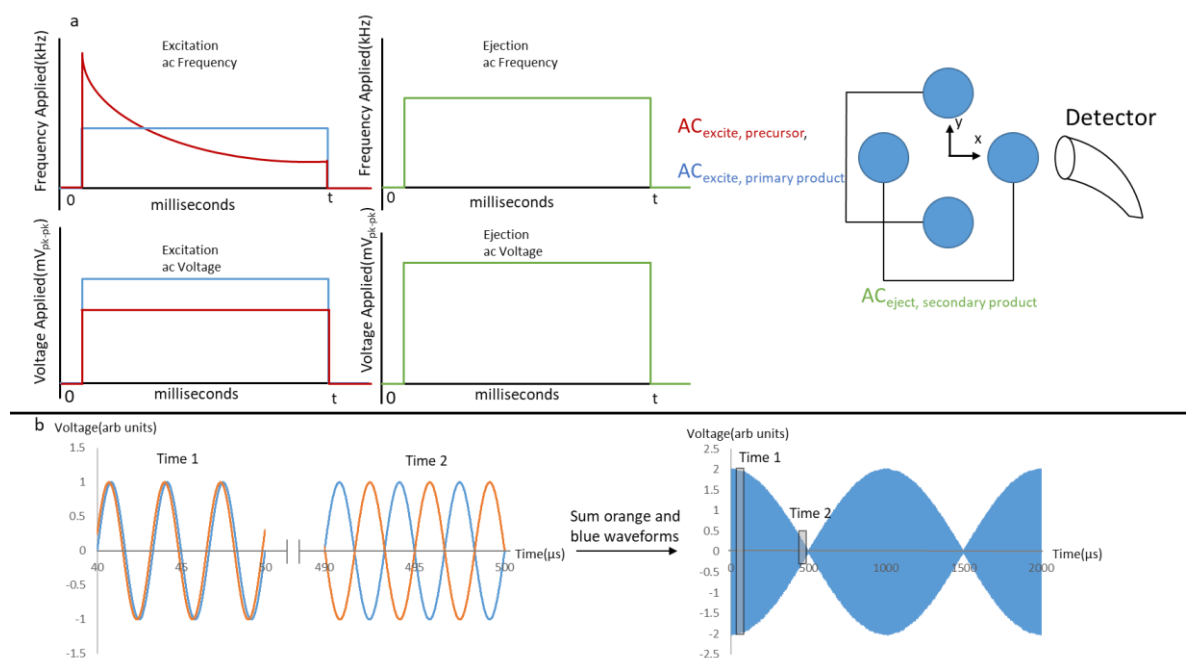


Figure 3.1. Scan methodology for the various experiments. a.) Illustration of a triple resonance precursor ion scan in which two frequencies are applied to the y-electrodes, one of which scans across the frequency range to fragment precursor ions while a second fixed frequency held on a constant product ion secular frequency (an $MS^2$ ion). A third frequency can be applied to the x-electrodes at a frequency chosen to eject the desired $MS^3$ product ion into the detector. Voltages of each of the frequencies are shown as well. b.) Example of how beat frequencies were generated. The two waveforms (orange and blue, 300 and 301 kHz) have a small frequency difference between them. If these two frequencies are summed the resultant (dark blue) waveform has characteristics of the beat frequency (1 kHz) and the original frequencies (300 and 301 kHz).

Experimentally, triple resonance excitation is accomplished by applying the sum of two sinusoidal waveforms on the y-electrodes, one of which is a non-linear frequency sweep used to

excite precursor ions and the other which is a fixed frequency associated with fragmentation of a selected $MS^2$ product ion (Figure 3.1). This combination of waveforms allows for detection of product ions not normally very abundant – or absent altogether - in an $MS^2$ experiment, but detectable in an $MS^3$ experiment. The excitation of precursor ions and first-generation product ions, as well as the ejection of the second-generation product ions, occurs simultaneously to preserve the *m/z* of the precursor ions, which is proportional to time. Such a scan can be used to improve 1) sensitivity, 2) selectivity, and 3) molecular coverage in the cases presented.

### 3.3.2   Triple Resonance Excitation for Increased Sensitivity

Increased sensitivity in ion trap precursor ion scans using triple resonance excitation can be observed if there are shared products between $MS^2$ and $MS^3$ spectra, that is, if first generation product ions fragment further to give other ions observed in $MS^2$ scans. For example, increased sensitivity can be observed when performing a precursor ion scan of chemical warfare agent simulants cyclohexyl methylphosphonate and pinacolyl methylphosphonate, *m/z* 177 and 179 respectively, both (M - H)⁻ (Figure 3.2a). When performing an individual precursor scan for either (Figure 3.2a, brown) *m/z* 95 (methylphosphonate) or (Figure 3.2a, orange) *m/z* 79, the signal intensity is less than when a triple resonance precursor scan is performed to simultaneously excite in the y dimension precursor ions along with $MS^2$ ion *m/z* 95 (using a fixed frequency sine wave) and to eject the $MS^2$ →$MS^3$ ion *m/z* 79 in the x dimension using a second fixed frequency sine wave. Increased sensitivity in the triple resonance scan is observed (Figure 3.2b) because *m/z* 95 fragments to *m/z* 79 so that simultaneous fragmentation of the precursors *m/z* 177 and 179 as well as $MS^2$ ion *m/z* 95 collapses the product ions into a single channel (*m/z* 79), therefore resulting in higher ion abundance at the detector. It should be noted that in the triple resonance method there is a loss in selectivity for either *m/z* 95 or 79 product ion compared to each individual double resonance scan as the product ions cannot be differentiated in the triple resonance scan, but the selectivity for the precursor ions containing methylphosphonate is increased by including both product ions.
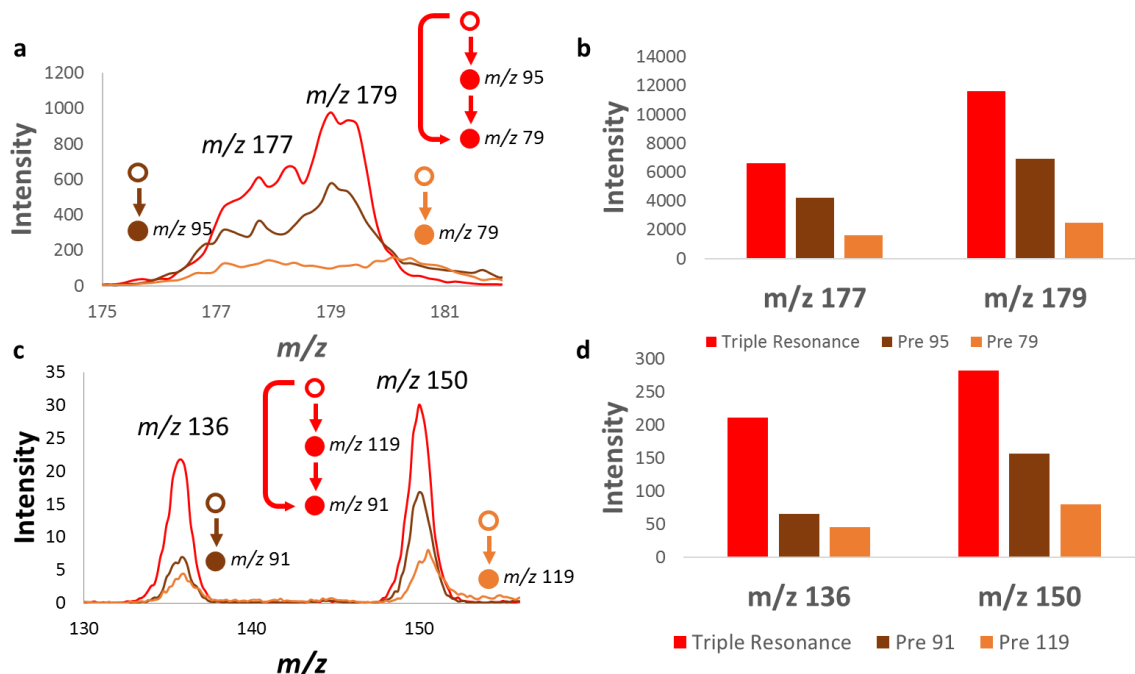
Figure 3.2. Triple resonance for increased sensitivity in the precursor ion scan mode. Analytes were chemical warfare agent simulants examined in negative ion mode (cyclohexyl methylphosphonate and pinacolyl methylphosphonate, $(M - H)^-$, $m/z$ 177 and 179, respectively) and amphetamines in positive ion mode (amphetamine and methamphetamine $(M+H)^+$ $m/z$ 136 and 150, respectively). (a) Overlaid mass spectra of precursor ion scan of $m/z$ 95 (brown), precursor ion scan of $m/z$ 79 (orange), and triple resonance precursor scan of $m/z$ 79 with a y-dimension resonance at the frequency corresponding to $m/z$ 95 (red) and an x-dimension resonance at $m/z$ 79, b) showing integrated signal intensities of $m/z$ 177 and 179 in each case, (c) overlaid mass spectra of precursor ion scan of $m/z$ 91 (brown), precursor ion scan of $m/z$ 119 (orange), and triple resonance precursor scan of $m/z$ 91 with a second resonance at the frequency corresponding to m/z 119 (red), and (d) integrated signal intensity of $m/z$ 136 and 150 in each case.

A second case of increased sensitivity is shown in Figure 3.2c for two structurally similar central nervous system stimulants, amphetamine ($m/z$ 136, $[M+H]^+$) and methamphetamine ($m/z$ 150, $[M+H]^+$). The signal intensity of the precursor ion scan of $m/z$ 91 increases when an additional frequency corresponding to $m/z$ 119 is applied to the y-electrode. This increased sensitivity can be attributed to the reduction in available states the product ions could reside in, that is, $MS^2$ ion $m/z$ 91 is conveniently an $MS^3$ product ion of $m/z$ 119. Of course, the triple resonance experiment can result in additional peaks in the mass spectrum because it occurs concurrently with the corresponding double resonance scan (i.e. the triple resonance scan for $m/z$ 91 occurs concurrently with the double resonance scan of $m/z$ 91), and it is ambiguous which peaks and how much signal

intensity result from the double resonance scan compared to the triple resonance scan. It could be anticipated that the signal of the triple resonance scan would be the summation of the two individual double resonance scans (the combination of individual precursor ion scans of *m/z* 119 and 91 is equal to the sequential precursor ion scan of 119 to 91). However, the difference could be attributed to different fragmentation pathways. Specifically, the secondary product ion distribution from the primary product ion, *m/z* 119, is different when it is resonantly activated for fragmentation than when the fragmentation is caused by residual energy from the first fragmentation event. In either case, the percentage of precursor ions that are successfully converted to detected product ions can be quite low (< 1% on the LTQ) on an ion trap operated in the precursor scan mode (see 'detection efficiency')[18], so any increase in signal intensity can be beneficial so long as selectivity is not compromised. This sensitivity improvement is dependent on the fragmentation pathway of the particular functional group being interrogated. It is expected that for small molecules fragmentation is often sequential and limited to a few product ions.

### 3.3.3  Triple Resonance Excitation for Increased Selectivity

A challenge with ion trap precursor and neutral loss scans is obtaining unit resolution for both precursor ions and product ions. As currently implemented, precursor ions and product ions all reside at different Mathieu q values and hence have different secular frequency dispersions as a function of *m/z*. The higher in Mathieu q position at which an ion resides, the better the mass selectivity that is obtained because the frequency dispersion is greater. One method of increasing selectivity in ion trap precursor and neutral loss scans is by using triple resonance excitation. Higher selectivity will necessarily be obtained because the detected ions must satisfy *both* the MS$^1$->MS$^2$ relationship as well as the targeted MS$^2$->MS$^3$ relationship. Furthermore, the MS$^2$ product ions and precursor ions must be labile enough to fragment *successively* in the short time available in the ion trap scan. Moreover, the MS$^3$ ion will reside at a higher Mathieu q value than its MS$^2$ precursor, which is also beneficial for mass resolution.

To demonstrate this, a five-component mixture with analytes that produce fragments within 6 Th of *m/z* 182 was subjected to a precursor ion scan of *m/z* 182 (Figure 3.3, red). As shown, not only is cocaine detected (*m/z* 304->*m/z* 182->*m/z* 150), but so too are hydromorphone (*m/z* 286->*m/z* 185->*m/z* 157), cocaine-d3 (*m/z* 307->*m/z* 185->*m/z* 153, 151), acetyl fentanyl (*m/z* 323->*m/z* 188->*m/z* 146, 105), and butyryl fentanyl (*m/z* 351->*m/z* 188->*m/z* 146, 105) because their MS$^2$

66

ions have secular frequencies within 10 kHz of *m/z* 182. A triple resonance precursor ion scan of *m/z* 150 (Figure 3.3, blue) was then used to improve the selectivity of the scan for cocaine compared to the double resonance case. This was accomplished by applying a fixed frequency corresponding to *m/z* 182 to the y-electrodes during a precursor ion scan of *m/z* 150. In this case the decrease in relative intensity of the fentanyls relative to cocaine can be attributed to a stable $MS^2$ product ion (*m/z* 188) which further fragments largely to *m/z* 105 (*m/z* 146 is a minor product), but not on the short time scale (a few ms) of the excitation and detection in this scan. Deuterated cocaine and hydromorphone are still present because their $MS^2$ ions are more labile. Both deuterated cocaine and hydromorphone produce secondary product ions (*m/z* 153 and 157, respectively) within the resonant bandwidth of the ejection mass, *m/z* 150, thus both product ions are detected in the triple resonance scan. However, the decrease in signal of deuterated cocaine is greater because the primary fragment ion, m*/z* 185, fragments to many other product ions besides 153 whereas the primary product ion from hydromorphone, also *m/z* 185, primarily produces *m/z* 157. One would also expect increased *mass selectivity* by targeting a particular $MS^3$ ion (*m/z* 150, q = 0.463) that resides at a higher Mathieu q value than the $MS^2$ ions (*m/z* 182, q = 0.381). This is because the *m/z* window affected by the 10 kHz activation/ejection window is smaller with decreasing mass. For example, a 10 kHz bandwidth centered at m/z 90, 150, and 210 correlate with 1.2, 6.5, and 13.5 Th bandwidths, respectively. While the presence of hydromorphone and cocaine-d3 are evident even at q = 0.463, the mass selectivity is not close to unit (which we will show later). Although selectivity is increased, signal intensity decreased from 174 counts in the double resonance scan to 35 counts in the triple resonance scan, so clearly an increase in selectivity is accompanied by a decrease in sensitivity. Note that this $MS^3$ experiment is the sequential precursor ion scan, viz. ○→ ● → ●, per the original $MS^n$ nomenclature [15].
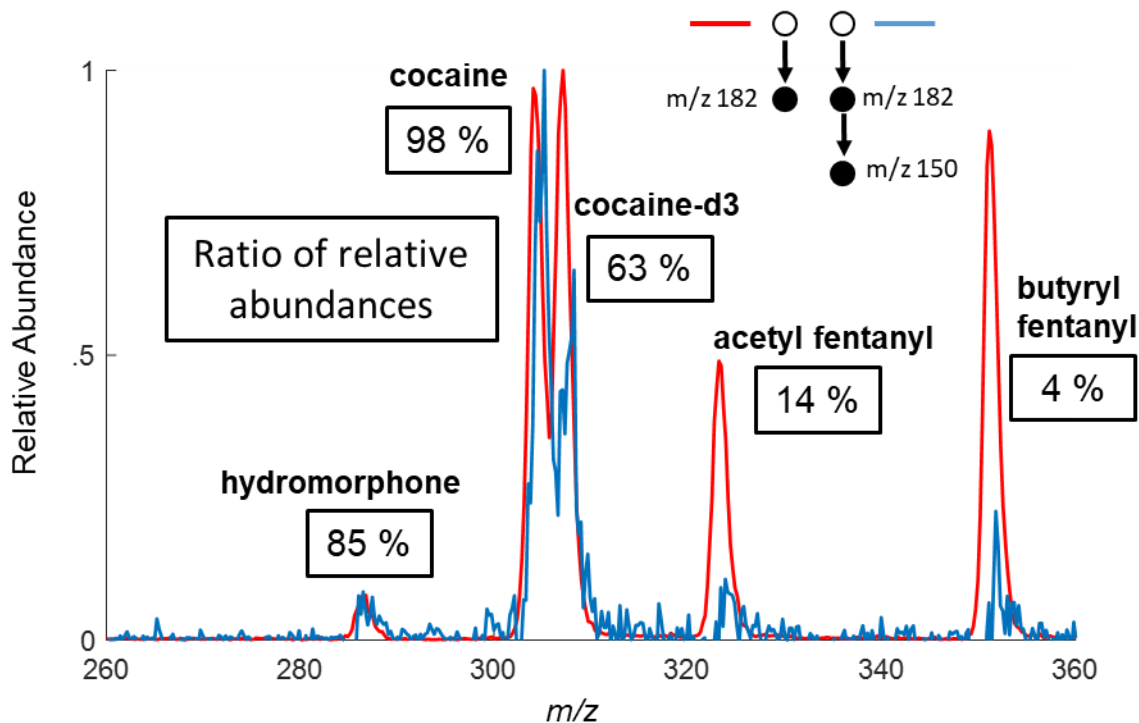
Figure 3.3. Increased selectivity in the detection of various opioids using triple resonance excitation. Hydromorphone (*m/z* 286, MS$^2$ *m/z* 185, MS$^3$ *m/z* 157), cocaine (*m/z* 304, MS$^2$ *m/z* 182, MS$^3$ *m/z* 150), cocaine-d3 (*m/z* 307, MS$^2$ *m/z* 185, MS$^3$ *m/z* 153, 151), acetyl fentanyl (*m/z* 323, MS$^2$ *m/z* 188, MS$^3$ *m/z* 146, 105)), and butyryl fentanyl (*m/z* 351, MS$^2$ *m/z* 188, MS$^3$ *m/z* 146, 105)) were subjected to both precursor ion scan of *m/z* 182 (red) and triple resonance precursor ion scan of *m/z* 150 in which *m/z* 182 (blue) was fragmented in the y dimension during the scan.  Each percentage describes the ratio of relative intensity of the triple resonance scan compared to the double resonance scan**.**

### 3.3.4   Triple Resonance Excitation for Increased Molecular Coverage

Per-scan molecular coverage can be increased using triple resonance precursor ion scans because this reduces the number of individual scans required to detect the same number of targets of a molecular class. Specifically, even precursor ions that have similar molecular structures may not all fragment to the same MS$^2$ products, but they may share product ions if we are also able to access MS$^3$ ions. This reduction of scans is demonstrated with pheniramines, which are antihistamines that produce three different major product ions but share ions between the MS$^2$ and

MS$^3$ data spaces. Figure 3.4, red, shows a precursor ion scan of *m/z* 196 used to detect pheniramine, Figure 3.4, purple, shows a precursor ion scan of *m/z* 167 used to detect diphenhydramine, and Figure 3.4, blue, shows a precursor ion scan of *m/z* 246, the dominant product ion of chlorpheniramine. Conveniently, when *m/z* 196 and *m/z* 246 are fragmented they generate product ions at *m/z* 167 and *m/z* 168. A *double triple* resonance precursor ion scan, i.e. fragmenting the precursor ions and simultaneously fragmenting *m/z* 196 and *m/z* 246 while ejecting *m/z* 167/168, is then shown in green. This experiment detects all three pheniramines in a single scan. Note that the LMCO in this experiment was 120 Th, compared to 80 Th in the other triple resonance experiments.
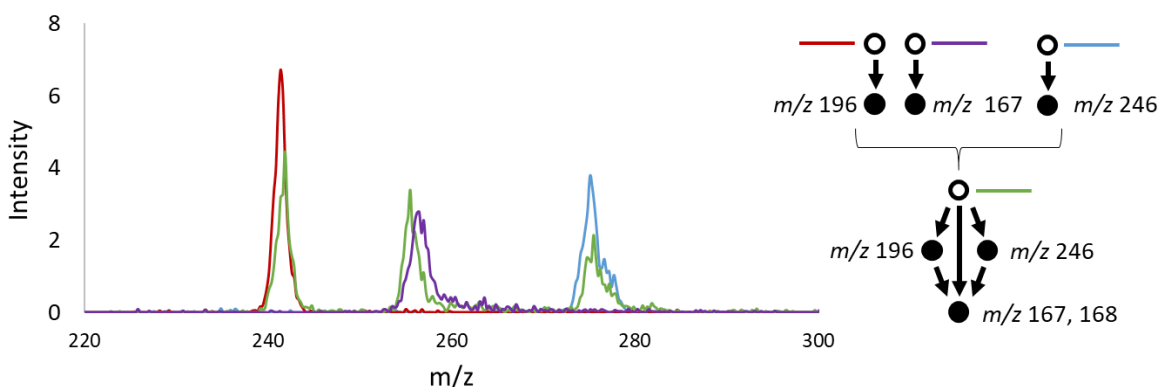


Figure 3.4. Increased molecular coverage using triple resonance excitation. Overlaid spectra of various precursor ion scans of a mixture containing pheniramine (*m/z* 241), diphenhydramine (*m/z* 256), and chlorpheniramine (*m/z* 275), all [M+H]$^+$. Precursor ion scans of *m/z* 196, 167, and 246 are shown as red, purple, and blue traces, respectively. A triple resonance precursor ion scan shown in green applies two fixed frequencies corresponding to *m/z* 196 and 246 for further fragmentation in the y dimension while a fixed frequency associated with *m/z* 167 is used to eject product ions of *m/z* 167/168 in the x dimension. The LMCO in this experiment was 120 Th.

### 3.3.5 Frequency Tagging for Identification of Artifact Peaks in Precursor and Neutral Loss Scans

A shortcoming of using a single quadrupole ion trap for simultaneous fragmentation and detection is that product ions generated from trapped precursor ions whose trajectories are unstable (q > 0.908) will be immediately ejected from the trap. This presents a challenge because product ions whose *m/z* values are below the low mass cutoff are detected in the same manner as resonantly ejected ions, which creates 'artifact' peaks in the mass spectrum, i.e. false positives. These artifact peaks have similar profiles as the resonantly ejected peaks due to the detected peak shapes being

determined by the precursor fragmentation profile.  The ejection of product ions, whether it be due to instability or resonant ejection, will happen much faster (10s to 100s of microseconds) than the time required for precursor ions of a single m/z to be fragmented (1 – 3 milliseconds).   The intensity of these boundary peaks is much lower than the resonant peaks due to their ejection being unspecific to radial dimension.  This is demonstrated in Figure 3.5a and 5b where the difference between the two spectra is the result of the addition of a resonant frequency to eject product ions. Artifact peaks can be considered background and can be subtracted from the precursor or neutral loss scan spectra after recording an 'artifact scan', that is by scanning without the ejection waveform and determining which peaks remain. These peaks are produced solely by ejection of unstable product ions. This solution, however, is not ideal because the background artifact scan must be obtained *for each sample*, thereby doubling analysis time and instrument power consumed, which for portable ion traps (where precursor and neutral loss scans are particularly useful) is especially inconvenient [18].

An alternative solution that does not require additional scans is to detect the secular frequency of the ions at the detector.   Ions which are excited at their secular frequency will oscillate with that same frequency (and related higher-order frequencies) and will be ejected in 'packets'. The rate of observation of those packets at the detector will correspond approximately to the ion secular frequency. The packets are not observed in conventional ion trap mass spectra because the detector typically has a much lower frequency bandwidth $10^3$-$10^4$ Hz compared to the ions' secular frequency, typically between 10-550 kHz for a 1.1 MHz trapping field.  This produces spectra with a deceptively (and erroneously) continuous ion current [19]. This solution is not demonstrated here, but a third alternative which is compatible with slower detection electronics is proposed.
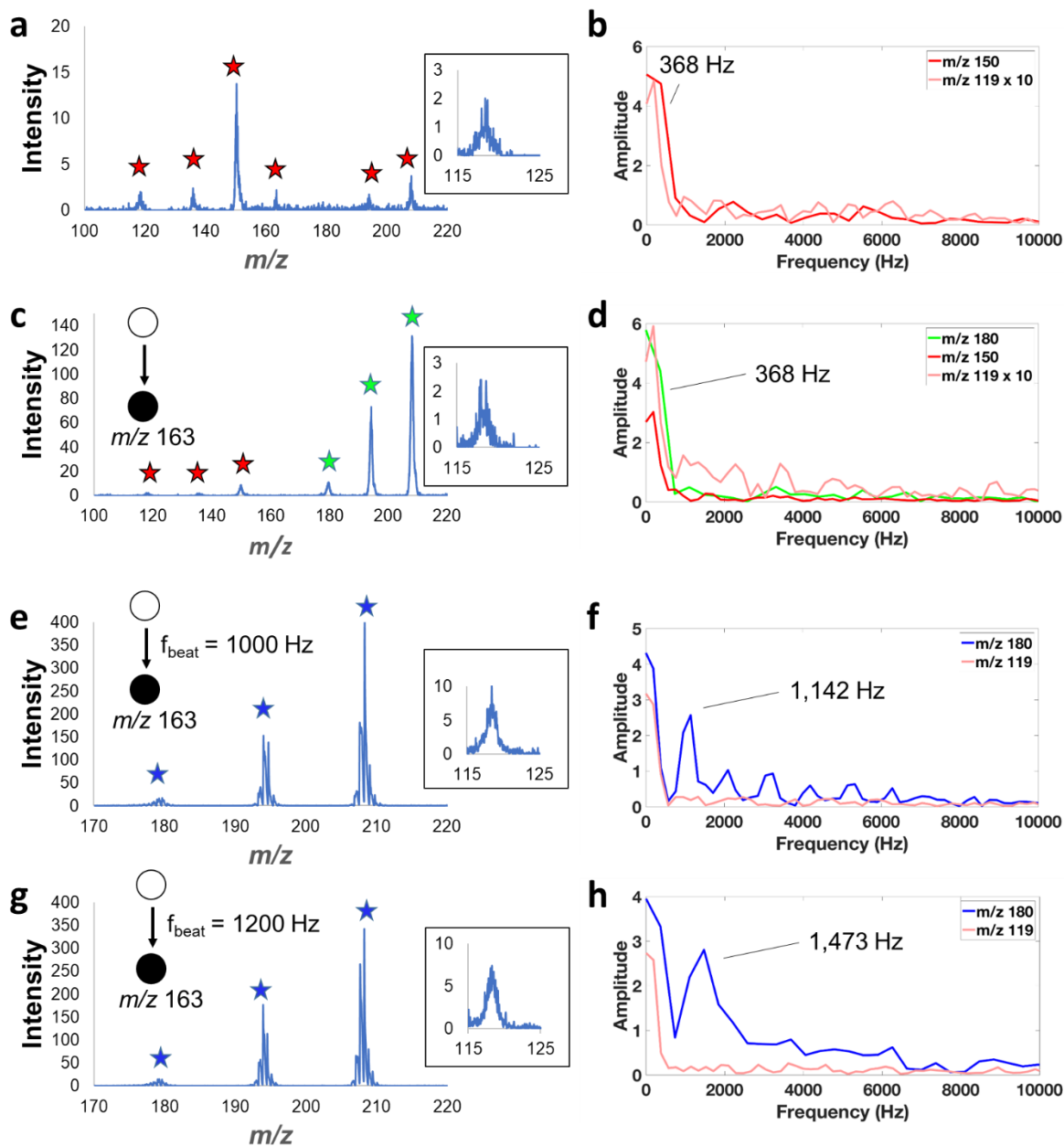
Figure 3.5. Frequency tagging for discrimination of artifact peaks in ion trap precursor scans. (a) 'Artifact scan' of five amphetamines (*m/z* 136, 150, 180, 194, and 208) at a LMCO of 92 Th, (b) FFTs of peaks at *m/z* 150 and 119 (both artifacts), (c) precursor ion scan of *m/z* 163 without using frequency tagging, (d) FFTs of peaks at *m/z* 180 and 150 (resonance ejection peaks) and 119 (an artifact, magnified by 10), (e) precursor ion scan of *m/z* 163 using a beat frequency of 1,000 Hz, (f) FFTs of peaks at *m/z* 180 and *m/z* 119 (the artifact), (g) same as (e) but with beat frequency 1,200 Hz, and (g) resulting FFTs. Green peaks are from resonance ejection, blue peaks are from frequency tagging resonance ejection, and red peaks are solely artifacts from boundary ejection of unstable product ions.

The third solution is to mass-selectively 'tag' resonantly ejected ions with a secondary frequency that can be observed at the detector. This 'frequency tagging' method can be accomplished by creating a 'beat' in the ac frequency used to manipulate (either excite or eject) the ions. As we have shown before [20,21], ejecting ions with the sum of two closely spaced frequencies, one which corresponds to the ion's secular frequency and one which is used to produce a particular beat frequency, shapes mass spectral peaks according to the beat frequency. For example, the summation of two sine waves with a frequency of 250 kHz and 251 kHz would produce a beat of 1 kHz, and as we will show here the mass spectral peaks corresponding to this resonance frequency are modulated by this beat.

Figure 3.5 and 6 demonstrate frequency tagging for identifying artifact peaks. Five amphetamines were trapped in the LTQ at a LMCO of 92 Th. Amphetamine and methamphetamine produce a fragment ion (*m/z* 91) below this LMCO, even when no ejection frequency is applied and hence show up as artifacts in both precursor ion scans and neutral loss scans (Figure 3.5a**,** artifact scan). Here we mark all artifacts with red stars for convenience. A fast Fourier transform (FFT) of one of these peaks generates a frequency spectrum in which a single peak below 400 Hz is observed (Figure 3.5b). This low frequency signal can be attributed to the width of the mass peak, viz. it depends on the mass spectral resolution. When an ejection frequency is then applied to eject product ions, *m/z* 163 in this case, with a known secular frequency (Figure 3.5c), multiple higher intensity peaks appear. As before, the peaks marked in red are solely artifacts, whereas peaks marked with green stars are due to resonance ejection of *m/z* 163. A FFT of each of these peaks generates 3 indistinguishable spectra with a single peak below 400 Hz (Figure 3.5d). That is, boundary (red) and resonance ejection (green) peaks cannot be differentiated in this scan, resulting in false positives.

However, when the product ion's secular frequency is applied with a beat frequency, either 1 kHz or 1.2 kHz, this beat is observed in the mass spectrum (Figure 3.5e and g) *only for the resonantly ejected ions*, not for the boundary ejected ions (*m/z* 119, inset). The peak shape changes drastically (frequency tagged ions are marked with blue stars) and performing an FFT of the mass spectral peaks allows for the beat frequency to be recovered (Figure 3.5f and h). The FFT results in a peak with a frequency slightly greater than the applied beat frequency because there are not very many points in the mass spectral peaks and hence few points in the FFTs (giving low frequency resolution). Harmonics can also be seen in the FFT, though we will not comment on

them further. As shown in the insets in Figure 3.5, which display *m/z* 119 (an artifact in all spectra), artifacts are not modulated according to the applied beat frequency, thus allowing their identification.

As mentioned previously, frequency tagging is not unique to precursor ion scans. Neutral loss scans, in which the product ion is a constant *m/z* lower than the precursor ion *m/z*, can also be recorded when applying a beat frequency by summing two frequency sweeps with a constant frequency offset and using the combined waveform for ejection in the x dimension. This resultant waveform is applied with a time offset from the excitation frequency sweep to realize a constant mass offset throughout the scan. Figure 3.6 shows two neutral loss spectra for amphetamine ions. Figure 3.6a presents a case in which the ejection for a particular ion is not wholly attributed to one method. Fragmentation of *m/z* 150 creates product ions (*m/z* 91) below the LMCO (92 Th) and a product ion *m/z* 119, a neutral loss of 31 Da. The peak at *m/z* 150 is hence marked with a purple star to indicate that it has contributions from frequency tagging (resonance ejection) and boundary ejection. As shown in the FFT of *m/z* 150 in Figure 3.6b, even though the peak is in part artifactual, it is clear that *m/z* 150 also generates a neutral loss of 31 Da, indicated by the peak at ~1 kHz. A neutral loss scan of 17 Da performed on the same analytes (Figure 3.6c) will identify both ions that lose 17 Da as well as ions that generate product ions below the LMCO (e.g. *m/z* 150). In this case, *m/z* 150 is clearly only an artifact because its frequency spectrum does not have a peak at 1 kHz, whereas *m/z* 136 and 180 are both frequency tagged.
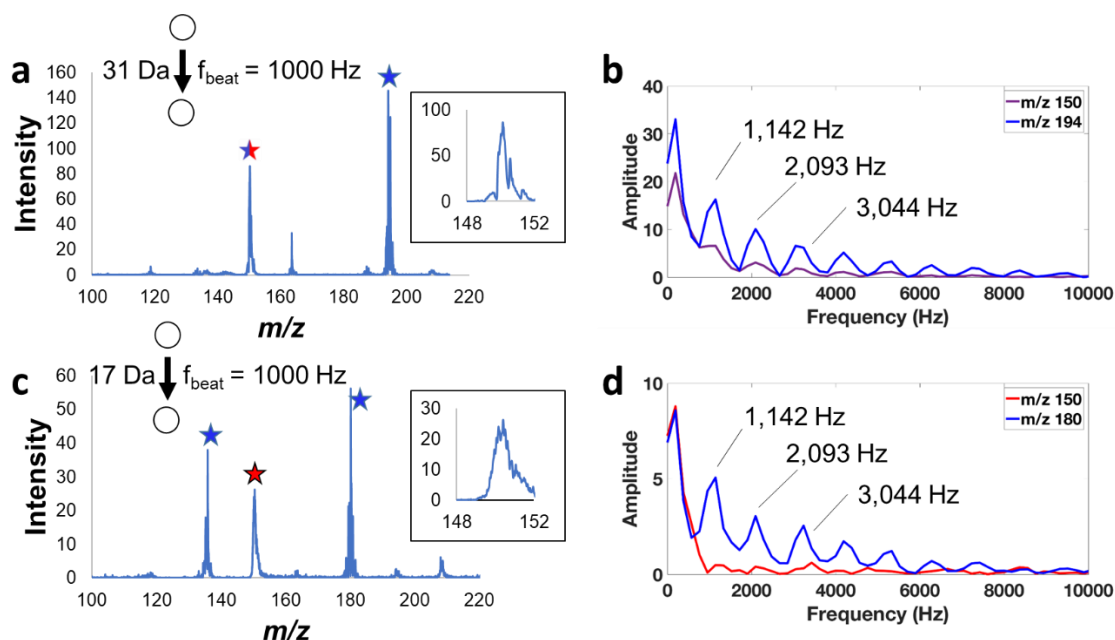
Figure 3.6. Frequency tagging for discrimination of artifact peaks in neutral loss scans. Amphetamine analytes were used for this experiment. (a) Neutral loss scan of 31 Da at constant beat frequency of 1,000 Hz and (b) peak FFTs, and (c,d) the same for a neutral loss scan of 17 Da. In (a) m/z 150 is part artifactual and so is modulated by the beat frequency but in (c) it is entirely an artifact and hence not modulated. Blue peaks are from resonance ejection using frequency tagging, red peaks are solely artifacts from boundary ejection of unstable product ions, and purple peaks have contributions from frequency tagging resonance ejection and boundary ejection (i.e. they are only part artifactual).

The selection of which frequency to "tag" to discriminate artifact peaks from boundary ejected peaks is dependent on a few parameters. The low frequency limit is determined by the time required to fragment a single precursor *m/z*. This period corresponds to the frequency detected below 1 kHz in Figure 3.5 and 6. This period is fairly consistent across the precursor mass range, so for 1 kHz tag there will always be three to five ejection events, which is sufficient to separate the tag from the lower frequency peak. It would be expected that higher resolution would be obtained by using a higher frequency tag as you would measure more ejection events in a given time. However, creating a high beat frequency by this method would require separating the frequencies further. This causes a decrease in product ion selection as the applied waveform covers a wider range of frequencies. If this decrease in selectivity were acceptable, the next limitation would be based on the detection circuitry bandwidth, which for most commercial ion trap systems is about $10^4$ Hz. Product ion selectivity was prioritized in these experiments since the detection of any frequency above 1 kHz indicates at least partial resonance ejection. If a higher

frequency resolution is required, possibly to differentiate between different resonance ejection events, then higher harmonics could be utilized to improve frequency resolution. The ideal frequency to measure to differentiate between resonant ejection processes is the ion's secular frequency. However, this requires sensitivity in detection circuitry with high frequency bandwidth not typically found in commercial ion trap systems.

One of the motivations for identifying artifacts peaks in the same MS/MS scan is that it allows for the trapping rf voltage to be increased during the scan, thus placing ions at higher q values to obtain higher mass selectivity but also producing more artifacts because the LMCO is higher. However, if artifacts can easily be identified, then they are less problematic. For example, a precursor ion scan for *m/z* 163 was used to identify the *m/z* range of the ejected product ions as a function of the LMCO (Figure 3.7), which we have previously defined as the *product ion selection window* [18]. All ions within the selection window will be ejected even if they are excited off-resonance. Clearly the selection window and hence mass selectivity for the product ion is greater at high q, giving selection windows of approximately 2 Th when the LMCO is 153 Th and 159 Th, respectively, a notable improvement over the ~7 Th window when the LMCO is 77 Th. Interestingly, points where the product ion *m/z* 163 had its working point on a non-linear resonance line were observed in the data and can be identified as $\beta = 2/3$ and $\beta = 0.586$ [22–24]. On these lines a decrease in mass selectivity was observed.
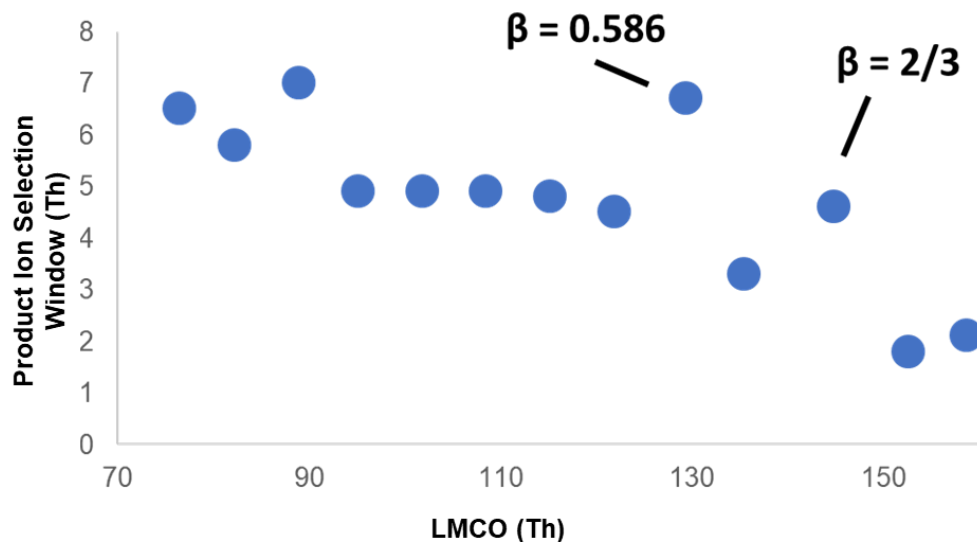
Figure 3.7. Product ion selection window (full width at half maximum) of the precursor ion scan of $m/z$ 163 as a function of LMCO (proportional to the rf voltage). Labels correspond to scans in which $m/z$ 163's working point was on or near a nonlinear resonance line.

## 3.4 Conclusions

Triple resonance precursor ion scans provide increased sensitivity for cases where a precursor ion fragments to two product ions, one of which fragments to the other in a second MS/MS stage. They can also be used to increase selectivity and to increase molecular coverage by fragmenting various structurally similar precursor ions to shared $MS^2$ and $MS^3$ ions. A 'frequency tagging' method can also be applied to determine how the product ion was ejected. Because frequency tagging can encode product ion $m/z$ values in a secondary induced frequency, it may be useful for MS/MS multiplexing, which will be the subject of a future report.

## 3.5 References

(1)   Liu, C., Topchiy, E., Lehmann, T., and Basile, F. Characterization of the dehydration products due to thermal decomposition of peptides by liquid chromatography-tandem mass spectrometry, J. Mass Spectrom., 50, 625–632. (2015)

(2)   Shaw J. B., Robinson, E. W., Paša-Tolić, L. Vacuum Ultraviolet Photodissociation and Fourier Transform–Ion Cyclotron Resonance (FT-ICR) Mass Spectrometry: Revisited. Analytical Chemistry. 88, (6), 3019-3023 (2016)

(3) Holden, D. D., Pruet, J. M., Brodbelt, J. S. Ultraviolet photodissociation of protonated, fixed charge, and charge-reduced peptides. Int. J. Mass Spectrom. 390, 81-90. (2015)

(4) Cleland, T. P., DeHart, C. J., Fellers, R. T., VanNipsen, A. J., Greer, J. B., LeDuc, R. D., Parker, R. W., Thomas, P. M., Kelleher, N. L., Brodbelt, J. S. High-Throughput Analysis of Intact Human Proteins Using UVPD and HCD on an Orbitrap Mass Spectrometer. Journal of Proteome Research. 16, 5, 2072-2079 (2017)

(5) Guo, Q., Gao, L., Zhai, Y., Xu, W.: Recent developments of miniature ion trap mass spectrometers. Chin. Chem. Lett. 29, 1578–1584 (2018)

(6) Zheng, Y., Decker, T.K., Wang, X., Lammert, S.A., Hawkins, A.R., Austin, D.E.: Extended mass range detection with a microscale planar linear ion trap mass spectrometer. Int. J. Mass Spectrom. 440, 1–3 (2019)

(7) Decker, T.K., Zheng, Y., Ruben, A.J., Wang, X., Lammert, S.A., Austin, D.E., Hawkins, A.R.: A Microscale Planar Linear Ion Trap Mass Spectrometer. J. Am. Soc. Mass Spectrom. 30, 482–488 (2019)

(8) Jiang, T., Xu, Q., Zhang, H., Li, D., Xu, W.: Improving the Performances of a "Brick Mass Spectrometer" by Quadrupole Enhanced Dipolar Resonance Ejection from the Linear Ion Trap. Anal. Chem. 90, 11671–11679 (2018).

(9) Eberlin, M.N.: Triple-stage pentaquadrupole (QqQqQ) mass spectrometry and ion/molecule reactions. Mass Spectrom. Rev. 16, 113–144 (1997)

(10) Solouki, T., Paša-Tolić L., Jackson, G. S., Guan, S., Marshall, A. G. High-Resolution Multistage MS, MS2, and MS3 Matrix-Assisted Laser Desorption/Ionization FT-ICR Mass Spectra of Peptides from a Single Laser Shot. Anal. Chem. 68, 21, 3718-3725 (1996)

(11) March, R.E.: An Introduction to Quadrupole Ion Trap Mass Spectrometry. J. Mass Spectrom. 32, 351–369 (1997)

(12) Snyder, D.T., Pulliam, C.J., Cooks, R.G.: Single analyzer precursor scans using an ion trap. Rapid Commun. Mass Spectrom. 30, 800–804 (2016)

(13) Snyder, D.T., Cooks, R.G.: Single Analyzer Neutral Loss Scans in a Linear Quadrupole Ion Trap Using Orthogonal Double Resonance Excitation. Anal. Chem. 89, 8148–8155 (2017)

(14) Snyder, D.T., Szalwinski, L.J., Cooks, R.G.: Simultaneous and Sequential MS/MS Scan Combinations and Permutations in a Linear Quadrupole Ion Trap. Anal. Chem. 89, 11053–11060 (2017)

(15) Schwartz, J.C., Wade, A.P., Enke, C.G., Cooks, R.G.: Systematic delineation of scan modes in multidimensional mass spectrometry. Anal. Chem. 62, 1809–1818 (1990)

(16)   Yost, R. A.; Enke, C. G. Selected Ion Fragmentation with a Tandem Quadrupole Mass Spectrometer. J. Am. Chem. Soc. 1978, 100 (7), 2274–2275. https://doi.org/10.1021/ja00475a072.

(17)   Snyder, D.T., Pulliam, C.J., Cooks, R.G.: Calibration procedure for secular frequency scanning in ion trap mass spectrometers. Rapid Commun. Mass Spectrom. 30, 1190–1196 (2016)

(18)   Snyder, D.T., Szalwinski, L.J., Hilger, R., Cooks, R.G.: Implementation of Precursor and Neutral Loss Scans on a Miniature Ion Trap Mass Spectrometer and Performance Comparison to a Benchtop Linear Ion Trap. J. Am. Soc. Mass Spectrom. 1–10 (2018)

(19)   Remes, P.M., Syka, J.E.P., Kovtoun, V.V., Schwartz, J.C.: Insight into the resonance ejection process during mass analysis through simulations for improved linear quadrupole ion trap mass spectrometer performance. Int. J. Mass Spectrom. 370, 44–57 (2014)

(20)   Snyder, D.T., Cooks, R.G.: Successive Resonances for Ion Ejection at Arbitrary Frequencies in an Ion Trap. J. Am. Soc. Mass Spectrom. 27, 1922–1928 (2016)

(21)   Xu Chongsheng, Xu Fuxing, Konenkov N. V., Ding Chuan-Fan: Simulation of the simultaneous dual-frequency resonance excitation of ions in a linear ion trap. J. Mass Spectrom. 53, 109–114 (2017)

(22)   Alheit, R., Gudjons, Th., Kleineidam, S., Werth, G.: Some Observations on Higher-order Non-linear Resonances in a Paul Trap. Rapid Commun. Mass Spectrom. 10, 583–590 (1996)

(23)   Franzen, J.: The non-linear ion trap. Part 4. Mass selective instability scan with multipole superposition. Int. J. Mass Spectrom. Ion Process. 125, 165–170 (1993).

(24)   Franzen, J.: The non-linear ion trap. Part 5. Nature of non-linear resonances and resonant ion ejection. Int. J. Mass Spectrom. Ion Process. 130, 15–40 (1994)

# CHAPTER 4.  LOGICAL MS/MS SCANS: A NEW SET OF OPERATIONS FOR TANDEM MASS SPECTROMETRY

Portions of this work have been published in the journal *Analyst* as the article: Snyder, D. T., Szalwinski, L. J., Wells, J. M., & Cooks, R. G.. (2018). Logical MS/MS scans: a new set of operations for tandem mass spectrometry. *Analyst*, 143(22), 5438–5452.

## 4.1   Introduction

Wolfgang Paul and colleagues obtained a patent for the first quadrupole devices, the mass filter and the 3D ion trap (QIT), in the early 1950s.[1–5] Paul shared the Nobel Prize in Physics in 1989 with Hans Dehmelt, who was the first to trap a subatomic particle (an electron).[6,7] Fulford and March first demonstrated that ions could be mass-selectively stored in what was then called the QUadrupole Ion STORage (QUISTOR) device operated in mass-selective stability (rf/dc) mode,[8] and nearly three decades after the invention of the ion trap, Stafford et al. introduced the more convenient mass-selective instability scan, a linear ramp of the trapping radiofrequency (rf) signal which is used to eject ions in order of their mass-to-charge ratio (m/z).[9] Resonance ejection was subsequently developed and is now the predominant technique for mass analysis in both 2D and 3D traps,[10–13] with the notable advantages of increased resolution,[14–16] sensitivity, and mass range.[17,18] Resonance ejection is methodologically similar to mass-selective instability but ejects ions at any specified Mathieu q value by matching the ions' secular frequencies with a supplemental low-voltage ac frequency, usually at high Mathieu q, while ramping the rf voltage. Other less-used, but still notable, modes of mass analysis include rf frequency scanning[19,20] (including in the digital ion trap),[21–24] dc voltage scanning,[25] and ac frequency scanning.[26–32]

A remarkable feature of the quadrupole ion trap is the capacity to perform various tandem mass spectrometry (MS/MS or MS[n]) operations in a single device,[33] a capability that usually requires multiple mass analyzers and a separate collision cell (e.g. in hybrid instruments or in a triple quadrupole[34]). In a QIT, an ion can be excited with a low voltage ac waveform with frequency component(s) matching the ion's secular frequency or other related frequency, causing dissociation. A subsequent scan out then yields a product ion mass spectrum.[13,35] Performing multiple fragmentation steps tandem-in-time can yield higher order MS[n] spectra as well,[36] increasing analytical selectivity while also improving signal-to-noise.

Although not widely used as such, ion traps can also conduct precursor ion scans[37–39] and neutral loss scans,[40,41] modes that usually depend on multiple mass analyzers for simultaneous mass selection of precursor and product ions. To implement these capabilities, multiple simultaneous resonance frequencies are used to mass-select (and fragment) a precursor ion while also ejecting one or more selected product ions with a second ac frequency, which can correspond to a fixed product m/z or a fixed neutral loss. The more common scanning methodology is to acquire sets of data-dependent product ion scans from which precursor or neutral loss spectra can be reconstructed,[42] a method which takes advantage of the increasingly rapid scanning capabilities of modern ion trap systems[43] but also acquires superfluous data.

The beginnings of tandem mass spectrometry as an analytical technique date back to the first mass-analyzed ion kinetic energy spectrometer (MIKES) developed by Beynon and Cooks at Purdue University.[44,45] Since then, MS/MS techniques have been developed for hybrid instruments[46–49] and Fourier transform ion cyclotron resonance traps,[50]time-of-flight instruments, and quadrupole ion traps. In almost every MS/MS scan developed to date,[51] either the precursor ion m/z is fixed and the product ion m/z is varied (closed circle with arrow pointing to open circle), the product ion m/z is fixed while the precursor m/z is scanned (open circle with arrow pointing to closed circle), or a selected neutral loss relationship is fixed (two open circles with a bold arrow between them).[51] The neutral loss scan is a subset of the functional relationship scans, in which there is a specified mathematical relationship between precursor ions and product ions.[52] In a plot of precursor m/z vs. product m/z, the product ion scan is illustrated by a horizontal line, the precursor ion scan is a vertical line, and the neutral loss scan is a diagonal. Higher order $MS^3$ scans expand the working space to three dimensions, and so on.

Multiplexed versions of the full scan and of the MS/MS scans also exist on various analyzers. Two examples of multiplexed full scan experiments take the form of the compressive mass analysis scan on quadrupole ion traps[53] and Hadamard time-of-flight mass spectrometry.[54,55] A popular recent development in MS/MS capabilities on qTOF systems is SWATH,[56,57] wherein product ion scans are collected sequentially on wide (~25 Da width) mass windows, i.e. sequential multiplexed product ion scans. In this case, precursors and products can be correlated through the precursor neutral retention time on the chromatography column. Wilson and Vachet[58] performed multiplexed MS/MS using the QIT's low-mass cutoff to encode the relationship between simultaneously isolated precursor ions (up to 5 was demonstrated) and their simultaneously

generated product ions, thus multiplexing product ion scans. Two-dimensional MS/MS is possible in FT-ICR mass spectrometers, as first demonstrated by Pfändler et al.[59,60] and more recently advanced by O'Connor's group.[61–66] This technique allows the correlation of precursor and product ions without precursor isolation but also requires lengthy analysis times. So far, no such method has been published for the quadrupole ion trap, although recent simulations have indicated that this 2D MS/MS technique can equally be applied to a linear quadrupole ion trap.[67]

In this work we describe a set of multiplexed scan modes for quadrupole ion trap tandem mass spectrometry – termed 'logical MS/MS scans' – which are complementary to the existing set of three main MS/MS scan modes (namely product ion scans, precursor ion scans, and neutral loss scans). Logical MS/MS scans use logical operations to categorize compounds in mixtures based on characteristic structural features as revealed by MS/MS behavior along multiple fragmentation pathways. An example is a NOT operation, which detects precursor ions that do not fragment to a selected product m/z (or, alternatively, do not undergo a selected neutral loss). The NOT operation is exactly complementary to either a precursor ion scan or neutral loss scan. These scans can be considered multiplexed versions of the three main MS/MS experiments, and many are two-dimensional (although one dimension is sparse) and utilize double resonance techniques originally developed for ICR instruments.[68] Here we demonstrate the implementation of logical MS/MS operations on a linear ion trap. The operations explicitly demonstrated here include TRUE/FALSE, OR, XOR, AND, NOT, and NOR.

## 4.2    Experimental

### 4.2.1    Chemicals

Amphetamine (MW 135 Da), methamphetamine (MW 149 Da), 3,4-methylenedioxyamphetamine (MW 179 Da), 3,4-methylenedioxymethamphetamine (MW 193 Da), 3,4-methylenedioxyethylamphetamine (MW 207 Da), fentanyl (MW 336 Da), acetyl fentanyl (MW 322 Da), butyryl fentanyl (MW 350 Da), furanyl fentanyl (MW 374 Da), cis-3-methylfentanyl (MW 350 Da) hydrochloride, acryl fentanyl (MW 334 Da) hydrochloride, carfentanil (MW 394 Da) oxalate, norcarfentanil (MW 290 Da), remifentanil (MW 376 Da) hydrochloride, sufentanil (MW 386 Da) citrate, and alfentanil (MW 416 Da) hydrochloride were purchased from Cerilliant (Round Rock, TX, USA). Samples were diluted to total concentrations

between 1 and 10 μg/mL$^{-1}$ (mixtures with more components had lower concentrations of individual components) in 50 : 50 methanol/water with 0.1% formic acid added to improve ionization. All analytes were detected in the protonated form in the positive ion mode. HPLC grade methanol was purchased from Fisher Scientific (Hampton, NH, USA). Product ion m/z values for all compounds used in this study are shown in Table 4.1 for reference, and chemical structures with color-coded fragments are given in Scheme 4.1.
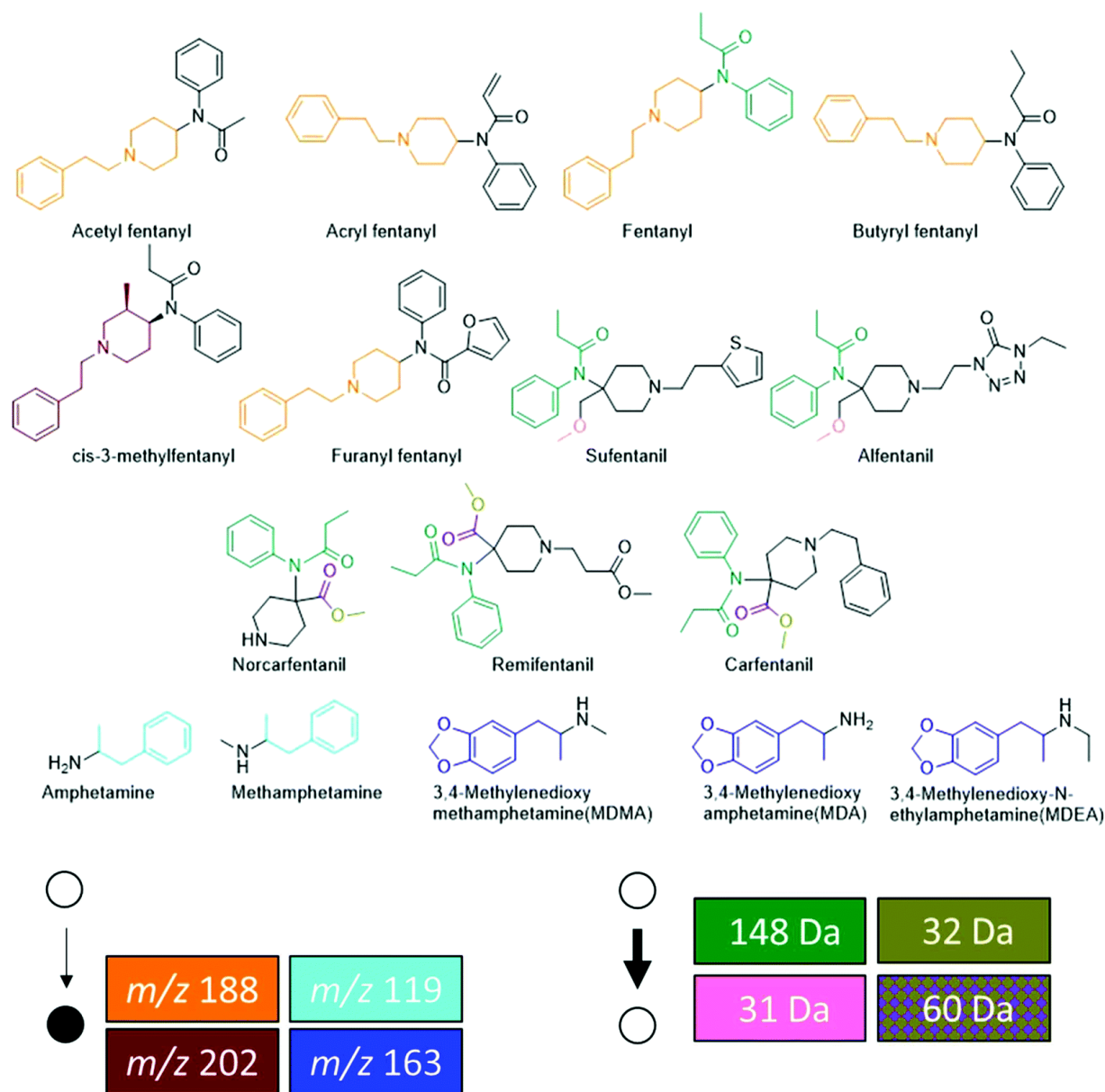


Scheme 4.1. Structures (above) and experimentally observed masses of product ions (below, left) and neutral fragments (below, right) for compounds used in this study.

Table 4.1 Fragmentation data for each compound used in this study. Helium was used as collision gas on a Thermo LTQ linear ion trap. Parameters were q = 0.25, normalized collision energy = 35, 30 ms activation time.

| Name | MW (amu) | m/z ([M + H]$^+$) | MS$^2$ m/z (RA) | NL (Da) |
|---|---|---|---|---|
| Amphetamine | 135.1 | 136.17 | 119.08 (100) | 17 |
| | | | 91.08 (1) | 45 |
| Methamphetamine | 149.1 | 150.17 | 119.08 (100) | 31 |
| | | | 91.08 (9) | 59 |
| 3,4-Methylenedioxyamphetamine | 179.1 | 180.17 | 163.08 (100) | 17 |
| 3,4-Methylenedioxymethamphetamine | 193.1 | 194.17 | 163.08 (100) | 31 |
| | | | 137.08 (0.3) | 57 |
| 3,4-Methylenedioxyethamphetamine | 207.1 | 208.17 | 163.08 (100) | 45 |
| | | | 135.08 (0.3) | 73 |
| | | | 72.08 (3) | 136 |
| Acetyl norfentanyl | 218.3 | 219.3 | 202.18 (12) | 17 |
| | | | 177.18 (6) | 42 |
| | | | 136.09 (8) | 83 |
| | | | 84.09 (100) | 135 |
| Acetyl fentanyl | 322.4 | 323.4 | 202.18 (4) | 121 |
| | | | 188.27 (100) | 135 |
| Butyryl fentanyl | 350.5 | 351.4 | 282.36 (11) | 69 |
| | | | 231.18 (4) | 120 |
| | | | 230.18 (3) | 121 |
| | | | 189.18 (100) | 162 |
| | | | 188.18 (76) | 163 |
| Furanyl fentanyl | 374.5 | 375.5 | 198.18 (100) | 177 |
| | | | 188.18 (85) | 187 |
| Fentanyl | 336.5 | 337.36 | 281.27 (8) | 56 |
| | | | 216.18 (10) | 121 |
| | | | 188.18 (100) | 149 |
| Isobutyryl fentanyl | 350.5 | 351.4 | 281.27 (5) | 70 |
| | | | 230.18 (5) | 121 |
| | | | 188.18 (100) | 163 |
| Valeryl fentanyl | 364.3 | 365.4 | 281.27 (9) | 84 |
| | | | 244.27 (4) | 121 |
| | | | 188.18 (100) | 177 |
| Acryl fentanyl | 334.5 | 335.27 | 214.18 (10) | 121 |
| | | | 188.18 (100) | 147 |

Table 4.1 continued

|  |  |  | 146.18 (3) | 189 |
|---|---|---|---|---|
|  |  |  | 105.09 (10) | 230 |
| *p*-Fluorofentanyl | 354.5 | 355.3 | 299.27 (5) | 56 |
|  |  |  | 234.18 (14) | 121 |
|  |  |  | 188.18 (100) | 167 |
|  |  |  | 150.18 (4) | 205 |
|  |  |  | 146.18 (4) | 209 |
| 4-Fluoroisobutyryl fentanyl | 368.5 | 369.3 | 299.25 (5) | 70 |
|  |  |  | 248.17 (4) | 121 |
|  |  |  | 188.17 (100) | 181 |
| *cis*-3-Methylfentanyl | 350.5 | 351.4 | 295.27 (5) | 56 |
|  |  |  | 230.27 (11) | 121 |
|  |  |  | 202.27 (100) | 149 |
| Sufentanil | 386.6 | 387.4 | 356.36 (74) | 31 |
|  |  |  | 239.18 (100) | 148 |
|  |  |  | 238.18 (68) | 149 |
| Alfentanil | 416.5 | 417.4 | 386.45 (95) | 31 |
|  |  |  | 269.27 (100) | 148 |
|  |  |  | 268.27 (68) | 149 |
|  |  |  | 237.27 (1) | 180 |
|  |  |  | 236.27 (1) | 181 |
|  |  |  | 198.18 (7) | 219 |
|  |  |  | 197.18 (8) | 220 |
|  |  |  | 171.18 (1) | 246 |
|  |  |  | 170.18 (3) | 247 |
| Remifentanil | 376.5 | 377.36 | 345.27 (100) | 32 |
|  |  |  | 317.27 (26) | 60 |
|  |  |  | 285.27 (8) | 92 |
|  |  |  | 228.18 (2) | 149 |
| Carfentanil | 394.5 | 395.36 | 363.27 (100) | 32 |
|  |  |  | 335.36 (40) | 60 |
|  |  |  | 246.27 (2) | 149 |
| Norcarfentanil | 290.4 | 291.3 | 259.27 (100) | 32 |
|  |  |  | 231.27 (4) | 60 |
|  |  |  | 186.18 (2) | 105 |
|  |  |  | 142.09 (2) | 149 |

### 4.2.2 Ionization

All analytes were ionized in the positive ion mode by nanoelectrospray ionization. Briefly, 1.5 kV was applied to a nanospray electrode emitter (glass size 1.5 mm), which was purchased from Warner Instruments (Hamden, CT, USA) and fitted with 0.127 mm diameter silver wire, part number 00303 (Alfa Aesar, Ward Hill, MA), as the electrode. Borosilicate glass capillaries (1.5 mm O.D., 0.86 mm I.D.) from Sutter Instrument Co. (Novato, CA, USA) were pulled to 2 μm tip diameters using a Flaming/Brown micropipette puller (model P-97, Sutter Instrument Co.).

### 4.2.3 Instrumentation

A Finnigan LTQ linear ion trap (San Jose, CA, USA) was used for all experiments.10 The internal dimensions of the three-section trap are as follows: $x_0 = 4.75$ mm, $y_0 = 4$ mm, axial sections of length 12, 37, and 12 mm. The rf frequency was tuned to 1.166 MHz and the rf amplitude was held constant throughout the ionization, cooling, and mass scan periods by substituting the rf modulation signal usually supplied by the instrument with a ~600 ms DC pulse (90% duty cycle) of amplitude between 160 mV and 280 mV (corresponding to approximate low-mass cutoffs of 76 Th and 159 Th, respectively, scaling linearly with the DC pulse amplitude) supplied from an external function generator. Nitrogen was used as bath gas at an ion gauge reading of $1.3 \times 10^{-5}$ Torr. Helium was not used because it yielded poor fragmentation efficiency in the LTQ in the scan modes demonstrated here. Note, though, that the data in Table 4.1 was collected using helium since it is the standard bath gas in the LTQ.

The LTQ rf coil was modified as described previously[39–41] to allow low voltage ac signals from external function generators to be coupled onto the main rf on the x and y rods. The rf is applied in a quadrupolar fashion while each pair of ac signals is dipolar. Low voltage ac waveforms were applied by two Keysight 33612A (Newark element14, Chicago, IL, USA) function generators with 64 megasample memory upgrades for each channel. All waveforms (aside from single frequencies) were calculated in Matlab (Mathworks, Natick, MA) and imported to the function generators as .csv column vectors. For ion excitation, the ac amplitude was between 100 mV$_{pp}$ and 200 mV$_{pp}$ for single frequencies and ~2 V$_{pp}$ for broadband (multi-frequency) waveforms. For ion ejection or artifact rejection, the ac amplitude was 500 mV$_{pp}$ for single frequency waveforms and 3.8 Vpp for broadband waveforms. Ion excitation waveforms and artifact rejection waveforms

were always applied to the y electrodes, while product ion ejection waveforms were always applied to the x electrodes for ejection of mass-selected ions into the detectors. Function generators were triggered during the ionization step using triggers in the LTQ Tune 'Diagnostics' menu, and their outputs were delayed so they applied waveforms during the mass scan segment, during which the data acquisition rate was approximately 28.7 kHz (the 'normal' scan mode with 'high' mass range chosen in the 'LTQ Tune' software).

### 4.2.4   Waveform calculation

Inverse Mathieu q scans were calculated via a program in Matlab as described previously.[31] The inverse Mathieu q scan is a nonlinear ac frequency sweep with approximately linear mass scale.[31,69] The starting frequency always corresponded to Mathieu q = 0.908, the end frequency corresponded to q = 0.15, and the scan time was set at 600 ms. Broadband ac waveforms were also calculated in Matlab and had general characteristics of a 5 MHz sampling rate, 1 kHz frequency spacing, and phases distributed quadratically with frequency in order to obtain a flat amplitude profile with respect to time. Broadband waveforms contained zero, one, or two notches, with each notch being 10 kHz wide. For broadband waveforms whose frequency components did not vary with time (e.g. in TRUE/FALSE scans), the waveform spanned 300 kHz (q = 0.654) to 50 kHz (q = 0.12) to prevent selected product ions from being ejected while precursors were excited. In cases where the inverse Mathieu q scan was used for ion excitation, the frequencies present in the broadband ejection waveform were varied with time so that at any given point in the broadband waveform the lower bound of the frequencies included in the waveform was 10 kHz higher than the corresponding frequency being applied in the inverse Mathieu q scan at the same point in time. This ensures that precursor ions are not ejected by the broadband waveform before they are excited by the inverse Mathieu q scan. For example, if the inverse Mathieu q scan was exciting an ion with secular frequency 300 kHz, then at that time point only frequencies above 310 kHz were represented in the sum of sines broadband waveform.

## 4.3   Results and discussion

### 4.3.1   What is a logical MS/MS operation?

Logical MS/MS is an extension of tandem mass spectrometry in which interrogation of the data domain is performed by simultaneous implementation of the precursor and neutral loss scans (or complementary NOT/NOR scans), conceptually illustrated as moving through the 2D MS/MS data domain along multiple scan lines simultaneously. This allows experiments which explore the 2D data domain of MS/MS to be couched in terms of logical operations, AND, NAND, OR, XOR, NOT, etc. We emphasize that such logical operations are a means to connect the MS/MS data to the structural properties of the set of constituent molecules. Logical operations are efficient ways of connecting the data to particular structural properties of interest, e.g. which of the compounds in the mixture is a fentanyl?

For the case of two selected product ions (or two selected neutral fragments, viz. neutral losses), there are sixteen possible logical operations which include: (1) FALSE, (2) AND, (3) BUT NOT, (4) LEFT PROJECTION, (5) NOT…BUT, (6) RIGHT PROJECTION, (7) XOR (exclusive OR), (8) OR (inclusive), (9) NEITHER…NOR (NOR for short), (10) IFF (if and only if), (11) RIGHT COMPLEMENTATION (which we refer to as NOT), (12) IF, (13) LEFT COMPLEMENTATION (also NOT), (14) IF…THEN, (15) NAND, and (16) TRUE. Precursor ions can be grouped on a Venn diagram (Figure 4.1a) according to whether they share one product ion (region 2 or 3), two product ions (region 4), or none (region 1). Precursor ions residing in the same region of the Venn diagram thus also occupy the same scan lines on the 2D MS/MS domain (Figure 4.1b). An AND (example AND neutral loss shown) scan, for example, would thus traverse two scan lines simultaneously and detect ions residing on both lines.
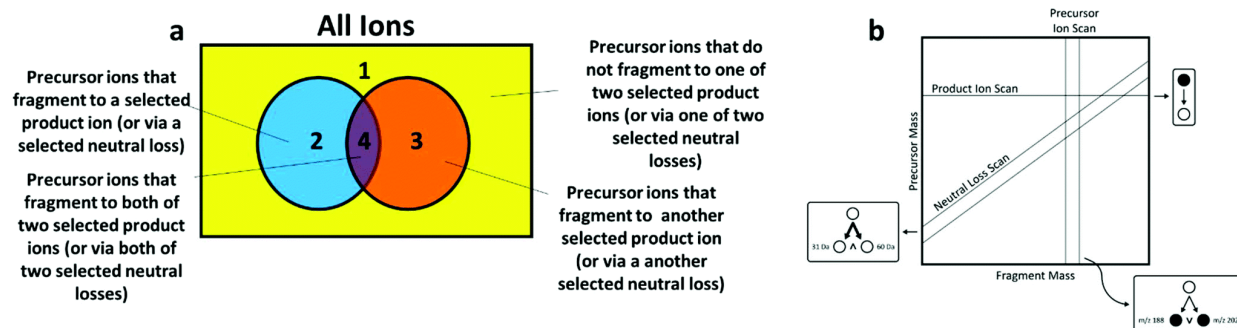
Figure 4.1. (a) Venn diagram representation of ion populations with respect to logical MS/MS experiments. Precursor ions may fragment to just two product ions and corresponding neutrals in the cases considered here. (b) 2D MS/MS domain with (i) single product ion scan, (ii) neutral loss scan of 31 Da AND 60 Da, and (iii) precursor ion scan of m/z 188 OR m/z 202.

In each of the following sections we describe the interpretation of each logical operation with respect to precursor and product ion relationships, using the symbolism shown in Table 4.2, and we also describe implementation of these scans using a linear quadrupole ion trap (Table 4.3). All ion trap implementations assume the rf voltage is constant during the scan events, which simplifies the experiments because the ions' secular frequencies remain constant throughout the scan. It is possible to perform these scans using the more common ion trap operation with varying rf voltage, but this implementation is much more difficult and is not recommended.

Table 4.2. Proposed logical MS/MS operations, terminology, symbolism, and interpretation. For logical operations, generally only the precursor ion symbolism is shown. For the neutral loss variants, closed circle product ions are replaced with open circles, the arrows are bolded, and any 'not' black bars are shown above the fixed neutral loss mass (as shown for NOT) instead of above the product ion circle (for fixed mass charged species)
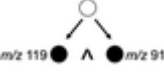
| | Operation | Symbol | Region in Figure 4.1 | Interpretation |
|---|---|---|---|---|
| Existing operations | Product ion scan |  ● m/z 188 | N/A | Detects product ions of a mass-selected precursor ion |
| | Precursor ion scan |  ● m/z 188 | 2 or 3 | Detects precursor ions of a mass-selected product ion |
| | Neutral loss scan |  148 Da | 2 or 3 | Detects precursor ions that fragment to product ions with a selected (fixed) mass offset from the precursor ions; a subset of the functional relationship scans |
| | Functional relationship scan |  | N/A | Detects precursor ions whose product ions satisfy a given mathematical relationship with respect to the precursors, *e.g.* product ions whose $m/z$ is half the precursor ion $m/z$ |
| | Single/multiple reaction monitoring | ● m/z 337 ● m/z 188 | N/A | Detects ions that satisfy the specified transition from a fixed precursor $m/z$ to a fixed product $m/z$ |
| New logical operations | TRUE/FALSE | □ ● m/z 188 | 2, 4 or 3, 4 (TRUE) | Detects whether any ion in the mass analyzer fragments to a mass-selected product ion; precursor ion $m/z$ values are not obtained |
| | | | None (FALSE) | |
| | AND | m/z 119 ● ∧ ● m/z 91 | 4 | Detects precursor ions that fragment to both of two mass-selected product ions |
| | BUT NOT | | 2 (BUT NOT) | Detects precursor ions that fragment exclusively to one of two mass-selected product ions but not the other |
| | NOT…BUT | m/z 119 ● ∧ ● m/z 91 | 3 (NOT…BUT) | |
| | LEFT/RIGHT PROJECTION | See 'Precursor Ion Scan' | 2, 4 (LEFT) | A precursor ion scan |
| | | | 3, 4 (RIGHT) | |

Table 4.2 continued
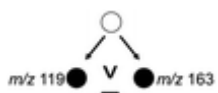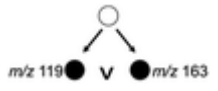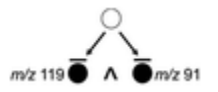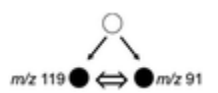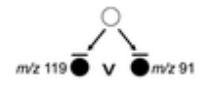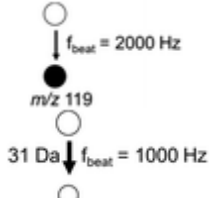
| | | | | |
|---|---|---|---|---|
| | XOR (exclusive OR) | $m/z$ 119 ● $\underline{\lor}$ ● $m/z$ 163 | 2, 3 | Detects precursor ions that fragment to either of two mass-selected product ions but not both |
| | OR (inclusive) | $m/z$ 119 ● $\lor$ ● $m/z$ 163 | 2, 3, 4 | Detects precursor ions that fragment to either of two mass-selected product ions or both |
| | NOT (also called LEFT/RIGHT COMPLEMENT ATION for binary systems) | $\overline{●}$ $m/z$ 188 | 1, 3 (LEFT) | Detects precursor ions that do not fragment to a particular product ion |
| | | $\downarrow$ $14\overline{8}$ Da | 1, 2 (RIGHT) | |
| | NOR | $m/z$ 119 ● $\land$ ● $m/z$ 91 | 1 | Detects precursor ions that do not fragment to either of two selected product ions |
| | IFF (if and only if) | $m/z$ 119 ● $\Leftrightarrow$ ● $m/z$ 91 | 1, 4 | Detects precursor ions that fragment to both of two mass-selected products ions or that fragment to neither |
| | IF | | 1, 2, 4 (IF) | Detects precursor ions that do not fragment to one of two particular product ions or that fragment to one of those ions |
| | IF…THEN | $m/z$ 119 $\overline{●}$ $\lor$ ● $m/z$ 91 | 1, 3, 4 (IF…THEN) | |
| | NAND | $m/z$ 119 ● $\lor$ $\overline{●}$ $m/z$ 91 | 1, 2, 3 | Detects precursor ions that do not fragment to both of two particular product ions |
| Ion trap scans | Frequency tagging | $f_{beat}$ = 2000 Hz ● $m/z$ 119 ○ 31 Da $\downarrow$ $f_{beat}$ = 1000 Hz | N/A | Resonance ejection of ions modulated at a particular beat frequency, $f_{beat}$; uses two closely spaced frequencies to form the beat frequency; useful for distinguishing resonantly ejected ions from boundary ejected ions and for distinguishing different resonance ejection processes |

Table 4.3 Proposed implementation of logical MS/MS on linear quadrupole ion traps

| | Operation | Ion trap implementation |
|---|---|---|
| Existing operations | Product ion scan | Resonance excitation followed by a full mass scan |
| | Precursor ion scan | Resonance excitation of precursors with simultaneous ejection of a selected product ion with a fixed ac frequency |
| | Neutral loss scan | Three simultaneous frequency sweeps with constant mass (time) offset |
| | Functional relationship scan | Three simultaneous frequency scans with variable mass offset |
| New logical operations | TRUE/FALSE | (Pre) Broadband excitation of precursors followed by ejection of fixed $m/z$ *via* single frequency; (NL) none, unless precursor ion $m/z$ values are known beforehand |
| | AND | Double precursor ion scan or double neutral loss scan using two different beat frequencies; peaks must correspond to both beats |
| | NOT…BUT, BUT NOT | Double precursor ion scan or neutral loss scan using two different beat frequencies; peaks must correspond to one beat but not the other |
| | LEFT/RIGHT PROJECTION | See 'Precursor Ion Scan' above |
| | XOR (exclusive OR) | Double precursor ion scan or neutral loss scan using two different beat frequencies; peaks must correspond to either beat but not both |
| | OR (inclusive) | Double precursor ion or neutral loss scan; no beat frequency required although can be used to differentiate regions 2,3,4 |
| | NOT | (Pre) Single frequency sweep for precursor ion excitation with singly notched broadband waveform for product ion ejection; (NL) no notch in broadband waveform; reject NL products into *y* electrodes with frequency sweep |

Table 4.3 continued

|  | NOR | (Pre) Single frequency sweep for precursor ion excitation with doubly notched broadband waveform for product ion ejection |
|  |  | (NL) Single frequency sweep for precursor ion excitation; broadband waveform for product ion ejection; two additional frequency sweeps for neutralization of neutral loss product ions on $y$ rods |
|  | IFF (if and only if) | Not currently known; cannot differentiate regions 2,3,4 |
|  | IF, IF…THEN | Not currently known; cannot differentiate regions 2,3,4 |
|  | NAND | Not currently known; cannot differentiate regions 2,3,4 |

*Note: These implementations assume rf voltage is constant throughout the scan*

### 4.3.2 TRUE/FALSE operation

TRUE/FALSE operation determines whether any precursor ions of unknown mass-to-charge fragment to a selected product ion m/z. This scan is not a precursor ion scan or a neutral loss scan because the m/z values of the precursor ions are not obtained during the scan. Instead, only a true or false result is obtained. That is, either the sample contains ions of a particular molecular class associated with a product ion m/z or neutral mass (TRUE) or it does not (FALSE). The symbol for this scan is similar to the precursor scan symbolism except that the open circle used for the scanned precursor m/z is substituted with an open square. It is our interpretation that an open circle corresponds to a varied (but known, i.e. scanned) mass-to-charge value[51] whereas the newly proposed open square corresponds to a range of mass-to-charge values that is excited simultaneously. Because no instrumental parameter is scanned, the m/z values of the precursors are not obtained.

Using a linear ion trap system, a TRUE/FALSE scan can be performed by first ejecting precursor ions whose m/z values match the selected product ion m/z, subsequently exciting a range of precursor ions using a broadband ac waveform, and finally applying a single frequency ac waveform to eject the targeted product ion m/z. The broadband waveform used here has frequency representation from q = 0.654 to q = 0.12 (1 kHz frequency spacing) in order to excite precursor ions but not eject the targeted product ions, which are purposely placed at working points above q

= 0.654 so they are retained in the trap. Precursor ions with m/z matching the product ion were rejected using a single frequency applied for 10 ms, the broadband waveform was applied for 50 ms to fragment the precursor ions simultaneously, and finally the product ion's secular frequency was applied for 10 ms to eject and detect it.

We applied a TRUE/FALSE scan to a set of eight fentanyl analogues: acetyl fentanyl, acryl fentanyl, fentanyl, butyryl fentanyl, cis-3-methylfentanyl, furanyl fentanyl, sufentanil, and alfentanil. As shown in Table 1 and Scheme 1, five of these analogues (the fentanyls) share a product ion at m/z 188, the single methylated analogue has a product ion at m/z 202, and the two fentanils share a neutral loss of 148/149 Da. A TRUE/FALSE scan of m/z 188 (Figure 4.2a) gives the expected 'true' as an answer, whereas the corresponding scan for m/z 185 gives 'false' (Figure 4.2b), showing mass selectivity. A TRUE/FALSE scan of m/z 202 (Figure 4.2c) also gives 'true' because of cis-3-methylfentanyl.
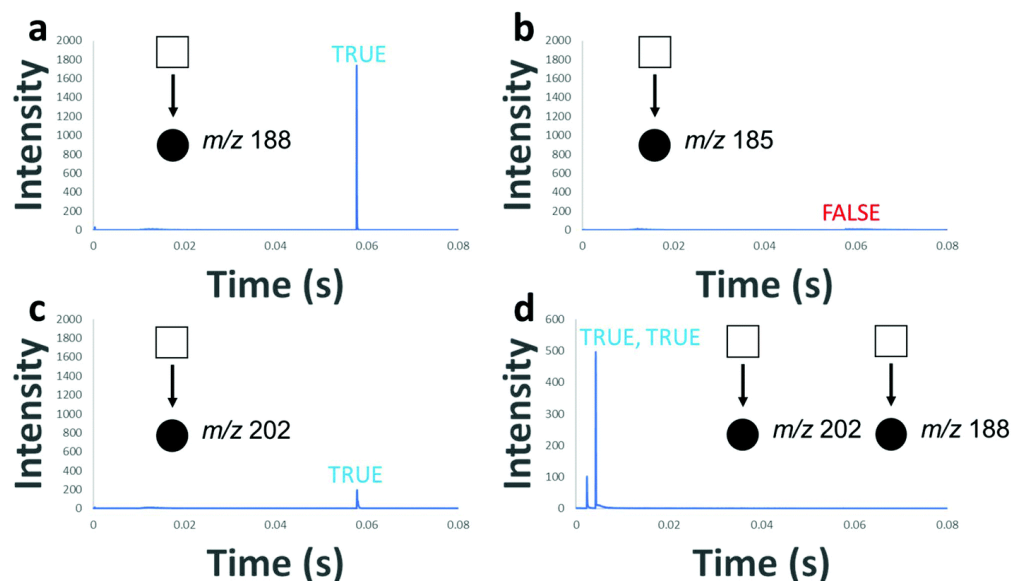


Figure 4.2. Logical TRUE/FALSE scans: (a) TRUE/FALSE scan performed on a set of eight fentanyl analogues (acetyl fentanyl, acryl fentanyl, fentanyl, butyryl fentanyl, cis-3-methylfentanyl, furanyl fentanyl, sufentanil, and alfentanil) wherein m/z 188 precursors were ejected for 10 ms, precursor ions were then excited with a broadband sum of sines for 50 ms, and finally m/z 188 product ions were ejected using a single frequency sine wave, resulting in TRUE, (b) the same set sequence but targeting m/z 185, resulting in FALSE, (c) the same sequence targeting m/z 202 for a result of TRUE (cis-3-methylfentanyl), and (d) optimized sequential TRUE/FALSE scans showing that precursor ions fragmenting to m/z 202 and/or m/z 188 are present in the sample (though their m/z values are not measured in this scan).

A TRUE/FALSE scan is useful because multiple 'scans' can be performed in rapid succession to target several different product ions. We performed two in succession (for product ions m/z 188 and m/z 202) in ~5 ms (Figure 4.2d), which is 240 times faster than the corresponding slow ion trap precursor scan which spans 600 ms for a single scan in our implementation. A TRUE/FALSE scan, in which no precursor m/z information is obtained, hence can be used to improve the efficiency of sample analysis so that a conventional precursor ion scan (which does retrieve the precursor ion m/z values) is only run when a value of 'true' is returned from a TRUE/FALSE scan, which should result in fewer wasted MS/MS survey scans.

### 4.3.3  OR operation

An inclusive OR operation determines which precursor ions either fragment to one of two selected product ions or fragment via one of two neutral losses without distinguishing the ions which fall on the particular scan lines. Ions thus can fall into either region 2, 3, or 4 in the Venn diagram. On the 2D MS/MS plot, an OR operation involves traversing two precursor ion (or neutral loss) scan lines simultaneously. Symbolically, we propose modifying the symbolism for a double precursor or neutral loss scan previously proposed in ref. 41 to include the downward facing carrot between the two product ion circles to represent logical 'or'.

Performing an inclusive OR operation on a linear ion trap simply requires excitation of precursor ions in one dimension (here the y dimension) via an ac frequency sweep with simultaneous ejection of two selected product ions in the x direction. For the precursor ion scan, two dipolar ac frequencies are used to eject two different product ions,[39,41] whereas for a double neutral loss scan, two swept ac frequencies are used to access the two different neutral losses (see ref. 40). Figure 4.3a shows a double precursor ion scan of m/z 119 and m/z 163 on a set of five amphetamines. The two lower molecular weight amphetamines fragment to m/z 119 and the other three fragment to m/z 163. As shown in the fast Fourier transforms of the peaks at m/z 150 and m/z 180 in Figure 4.3b, the two peaks are indistinguishable (despite resulting from resonance ejection of different m/z product ions), and hence it is ambiguous as to whether each peak is due to the ejection of m/z 119, m/z 163, or both. In the case of the inclusive OR operation, it does not matter because they need not be distinguished. For an exclusive or (XOR), described next, methodology is needed to differentiate product ions of different m/z observed at the detector.
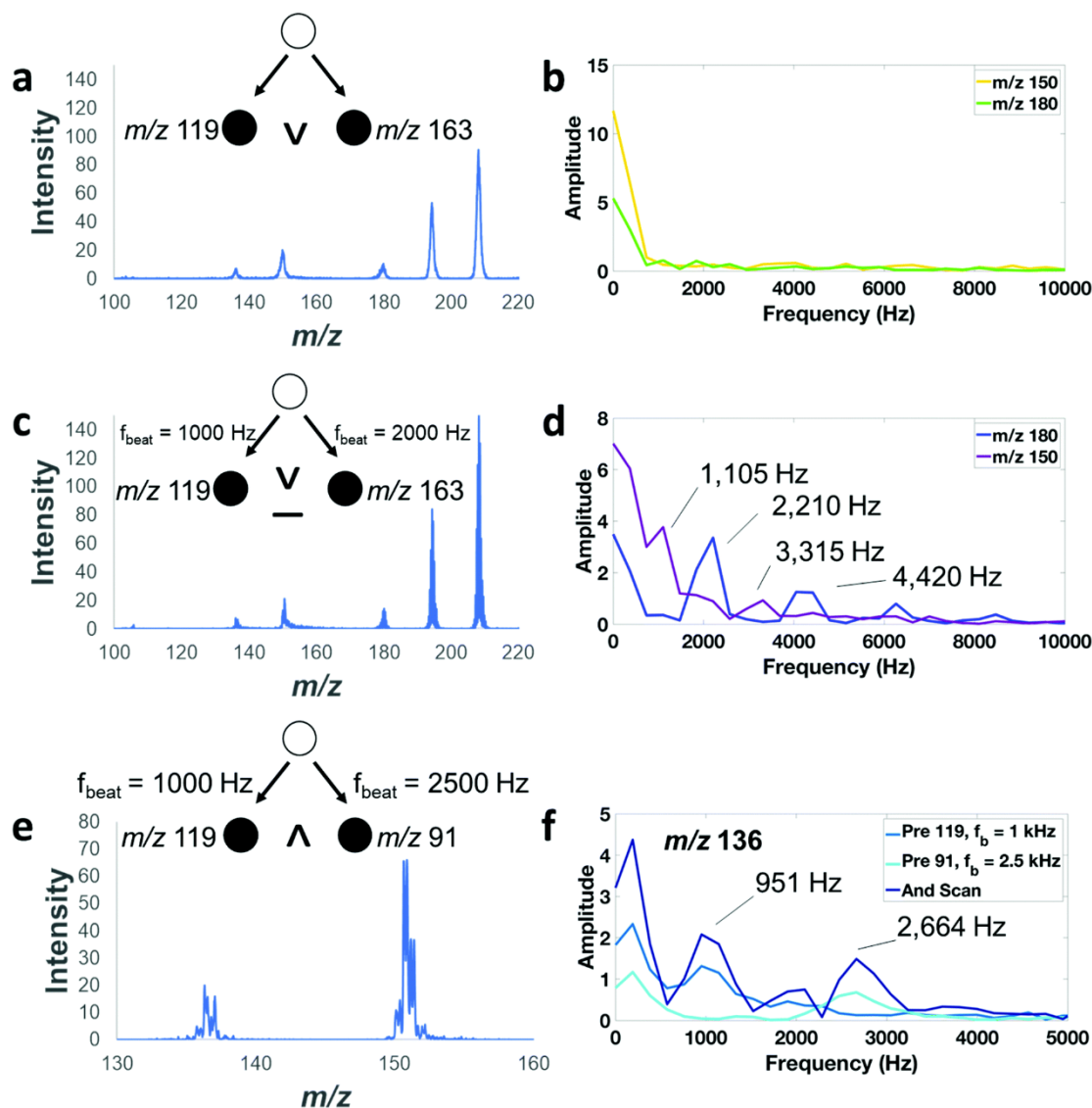
Figure 4.3. Logical OR/XOR/AND precursor ion scans: (a) conventional double precursor ion scan (OR scan) of m/z 119 and m/z 163 applied to a solution of five amphetamines, (c) XOR scan using two different beat frequencies for resonance ejection of m/z 119 and m/z 163, and (e) AND scan using two different beat frequencies for ejection of m/z 119 and m/z 91. No difference between the two resonance ejection processes is apparent in the fast Fourier transform (FFT) of the peaks in (a) in plot (b), but when using frequency tagging it becomes apparent in (d) that m/z 180 fragments to m/z 163 and m/z 150 fragments to m/z 119, and in (f) it is readily observed in the peak FFTs that m/z 136 and m/z 150 from plot (e) fragment to both targeted product ions and are thus AND peaks.

### 4.3.4   XOR operation

An XOR (exclusive or) operation, symbolically a downward-facing carrot with a bar underneath, determines the precursor ions that fragment exclusively to one of two mass-selected

product ions. That is, the ions must fall into region 2 or 3 of the Venn diagram but not into 4. Like the inclusive OR operation, an XOR operation traverses multiple precursor or neutral loss scan lines simultaneously, but in the XOR case we need a method of distinguishing different resonance ejection processes, assuming only a single scan is performed. (Otherwise one could perform two sequential scans targeting the two selected product ions.)

We recently developed frequency tagging as a method for distinguishing resonantly ejected product ions from those ejected due to boundary instability ('artifacts') in ion trap precursor and neutral loss scans (Snyder, Szalwinski, Cooks, ~~to be published~~). In this method, two closely spaced frequencies are used to resonantly eject product ions. The peak shapes of resonantly ejected ions are modulated according to the difference between the two frequencies (the beat frequency). For example, if an ion has a secular frequency at 200 kHz and a dual frequency waveform containing 200 kHz and 201 kHz is applied for resonance ejection, then the peak will have beats (maxima and minima) with frequency of 1 kHz. This method can also be used to distinguish resonantly ejected ions with different m/z values if two different beat frequencies are used for two different product ions, thus allowing us to distinguish peaks from regions 2, 3, and 4 of the Venn diagram. A fast Fourier transform of the peak in the mass spectrum can recover the beat frequency and thus determine on which of multiple simultaneously traversed scan lines a precursor/product ion pair resides. Note that ions in region 4 will have contributions from both beat frequencies whereas ions from regions 2 or 3 will have a single beat frequency.

Figure 4.3c shows an XOR precursor ion scan for a mixture of five amphetamines wherein product ions of m/z 119 were resonantly ejected with a beat frequency of 1 kHz while product ions of m/z 163 were ejected with a beat frequency of 2 kHz, all in a single scan. As shown in the peak FFTs in Figure 4.3d, m/z 150 (which fragments to m/z 119) and m/z 180 (which fragments to m/z 163) are now clearly distinct, with peak modulation frequencies that correspond to the appropriate beat frequency. Note that harmonics (e.g. twice the frequency tag) are also observed in the FFT spectrum, likely because the peak shapes are not perfectly sinusoidal.

A similar experiment can be performed with neutral losses as shown in Figure 4.4. The spectrum in (a) shows a full scan of a mixture of five fentanils whereas (b–d) show the results of single neutral losses of 31/32 Da (indistinguishable because of limited resolution in the ion trap neutral loss scan), 60 Da, and 148 Da using beat frequencies of 1 kHz, 1.5 kHz, and 1 kHz, respectively. An XOR neutral loss of 148 Da or 60 Da is shown in panel (e), and the peak shapes

and FFTs in panel (g) show unambiguously that sufentanil almost exclusively displays a neutral fragment of 148 Da (i.e. its peak has a beat frequency of 1 kHz as shown in panel g) while carfentanil has a neutral fragment of 60 Da (i.e. its peak has a beat frequency of 1.5 kHz in panel g).
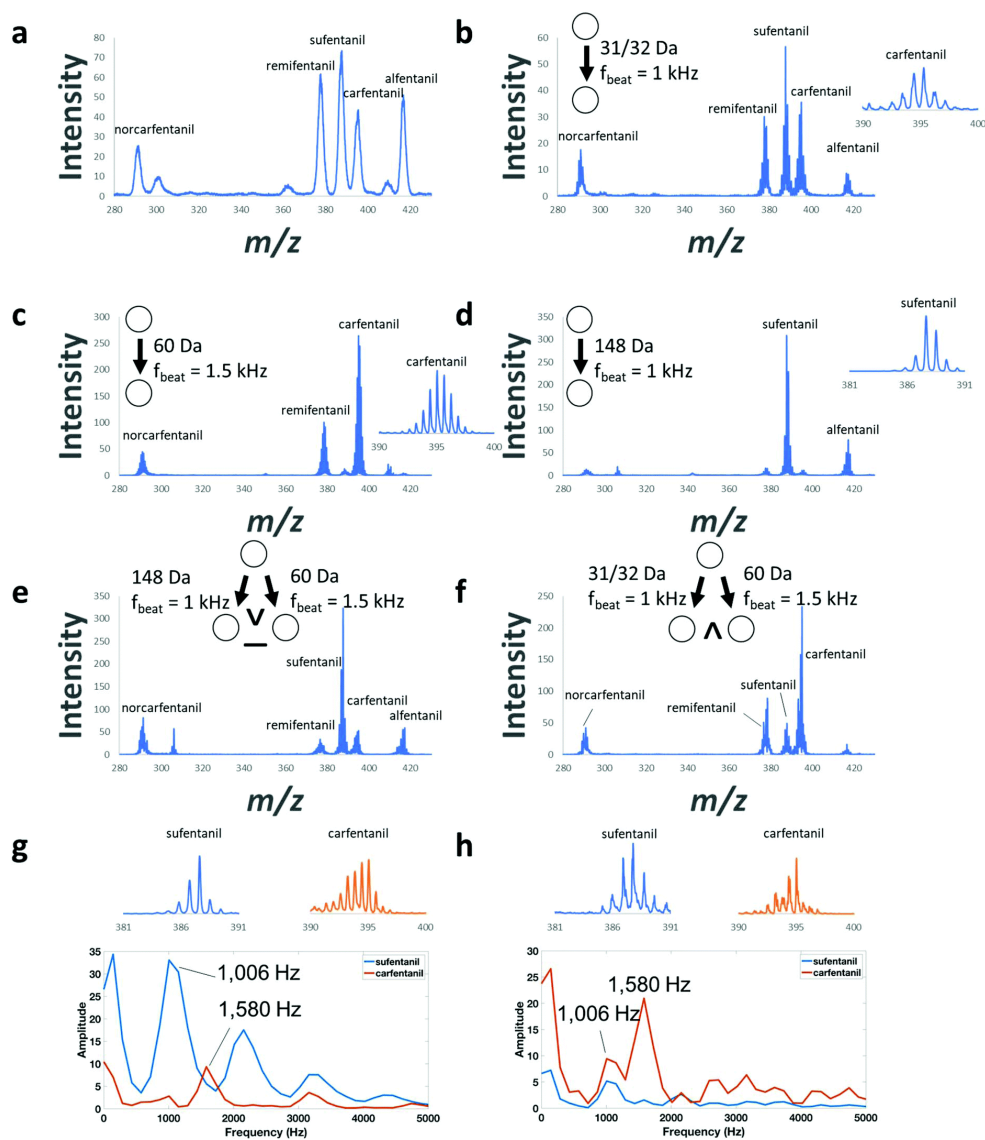


Figure 4.4. Logical XOR/AND neutral loss scans: (a) full scan of five fentanils, (b) neutral loss scan of 31/32 Da using a beat frequency of 1 kHz, (c) neutral loss scan of 60 Da using a beat frequency of 1.5 kHz, (d) neutral loss scan of 148 Da with beat frequency 1 kHz, (e) XOR neutral loss scan of 148 Da (1 kHz beat) or 60 Da (1.5 kHz beat), (f) AND neutral loss scan of 31 Da (1 kHz beat) and 60 Da (1.5 kHz beat), (g) peak shapes and FFTs for two peaks in (e), and (h) peak shapes and FFTs for two peaks in (f).

In what cases would an XOR operation be useful? The XOR scan allows precursor and neutral loss scans to be multiplexed via frequency tagging. Not only can two precursor or two neutral loss scans be performed simultaneously (while also differentiating the peaks from each scan line), but precursor and neutral loss scans can be performed together as a 'simultaneous combination'.[41] The capability to multiplex precursor and neutral loss scans therefore improves ion trap scan efficiency in terms of time, sample consumption, and instrument power.

### 4.3.5   AND operation

An AND operation detects ions that fragment to both of two selected product ions or to both of two neutral fragments (region 4). The upward carrot is used as a logical 'and' symbol. On the 2D MS/MS diagram, we must traverse two scan lines simultaneously and be able to determine which precursor ions lie on both lines. To accomplish the latter, frequency tagging is implemented once again.

Figure 4.3e gives an example of an AND scan using amphetamine ions. In a first experiment, a precursor ion scan of m/z 119 using a 1 kHz frequency tag yielded a peak at m/z 136 whose FFT yielded the medium blue curve in panel (f). Only a peak at 1 kHz is observed. Next, a precursor scan of m/z 91 using a 2.5 kHz frequency tag yielded a peak with FFT given by the light blue curve in panel (f). Again, only a 2.5 kHz frequency is observed. An AND scan combines both frequency tags on the x electrodes of the linear trap while simultaneously exciting the precursors in y using a frequency sweep. Note the presence of only one beat in the individual scans but both beats in the combined AND scan (panel (g), darkest blue), thus making it clear with a single scan that m/z 136 fragments to both m/z 119 and m/z 91. Note that m/z 150 also lies on both scan lines (FFT not shown to avoid congestion).

Figure 4.4f gives an example of a neutral loss AND operation, again using frequency tagging on the set of five fentanils. The AND scan in panel (f) can detect those ions which lose 31/32 Da and 60 Da. Peaks which lie on both scan lines will have beats corresponding to both 1 kHz and 1.5 kHz. Panel (h) clearly shows that sufentanil only has the neutral loss of 31 Da (1 kHz beat), whereas carfentanil has a neutral loss of both 32 Da (1 kHz) and 60 Da (1.5 kHz).

In what cases could an AND scan be useful? An AND scan clearly increases the selectivity of precursor and neutral loss scans. In Figure 4.4f and h, while the neutral loss scan of 31/32 Da could not differentiate the neutral fragments of sufentanil and carfentanil despite the neutral loss

originating from different molecular functionalities (see Scheme 4.1), the AND neutral loss of 31/32 Da and 60 Da does differentiate them because it targets a second neutral loss from the ester side chain of carfentanil. In contrast, sufentanil has a methoxy group that gives the neutral loss of 31 Da but does not yield other notable neutral losses.

### 4.3.6   NOT operation

A NOT operation detects precursor ions that do not produce a particular fragment ion or fragment neutral. The NOT operation is therefore the exact complement of the precursor or neutral loss scan. On the 2D MS/MS diagram, instead of traversing a single scan line or two scans lines, we must traverse an infinite number of scan lines but also exclude ions from one selected line. The NOR operation is an extension of this but excludes ions from more than one selected scan line.

NOT operations are denoted by horizontal bars either over the product ion circle (precursor scan) or over the neutral loss mass (neutral loss scan). When considering two circles in a Venn diagram, a NOT operation would detect ions which fall within regions 1 or 2 (NOT 3), or 1 or 3 (NOT 2). A simpler interpretation is a single-circle diagram. In this case a NOT operation would detect ions outside the circle, i.e. precursor ions which do not produce a selected product ion.

In the ion trap, a NOT precursor ion scan can be performed by sweeping an excitation frequency through precursor ion secular frequencies (to fragment the precursors) while simultaneously ejecting all product ions except the selected product m/z using a notched broadband waveform. Because we do not want to eject the precursor ions with the broadband waveform and because the product ion mass range varies with the excited precursor m/z, we constructed a specialized broadband sum of sines waveform whose frequency components are always higher than the excitation frequency. To keep the selected product ion in the trap (the NOT ion), a static notch is also implemented into the waveform. In our implementation, the notch is 10 kHz wide, and the lowest frequency at any given time in the broadband waveform is 10 kHz higher than the corresponding frequency of the excitation frequency sweep (again, this is to prevent the ejection of precursors before they are fragmented).

Figure 4.5a shows the full scan of the 8-component fentanyl mixture used in Figure 4.2. A precursor ion scan of m/z 188 (Figure 4.5b), the most abundant product ion of most of the fentanyl analogues, detects the fentanyls but not the methylated analogue and not the fentanils. The fentanils have a quaternary carbon which changes the primary route of fragmentation to a neutral

loss of either 31, 32, 60, or 148 Da, depending on the substituents. The complementary NOT scan of m/z 188, shown in panel (c), detects the remaining three fentanyl analogues. The other five fentanyls are still detected – but with significantly diminished intensity – because they have product ions other than m/z 188, although they are almost all <10% in abundance. Clearly the NOT scan is only useful for molecular classes which have a single high abundance product ion, or it should be used in comparison to a full scan mass spectrum. Without the full scan, it would be unclear which ion intensities were diminished by excluding particular product ions. For cases where molecular classes have two high abundance product ions, then the NOR operation may be useful.
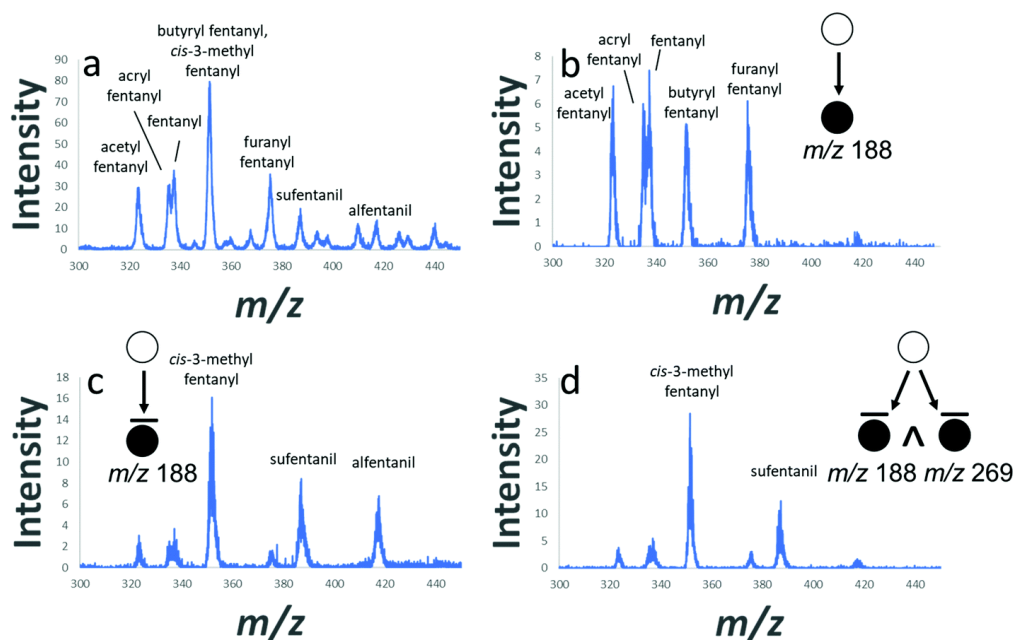
Figure 4.5. Logical NOT/NOR precursor ion scans: (a) full scan mass spectrum of eight fentanyl analogues (acetyl fentanyl, acryl fentanyl, fentanyl, butyryl fentanyl, cis-3-methylfentanyl, furanyl fentanyl, sufentanil, and alfentanil), (b) precursor ion scan of m/z 188, (c) NOT scan of m/z 188, showing ions that do not fragment to m/z 188, and (d) NOR scan of m/z 188 and m/z 269 showing ions that do not fragment to either selected product ion.

The neutral loss NOT scan is similar but has important procedural differences. It is not feasible to scan the notch in the broadband ejection waveform because as the notch is scanned, so too will all the neutral loss products be scanned out even though they were in the notch at one point during the scan, hence giving an artifact peak. That is, because the neutral loss product m/z is varied, it cannot always be in the static notch. A better way to do the experiment is to instead eject the neutral loss product ions into the y electrodes, preventing them from being ejected in x, where the LTQ detectors are. A neutral loss NOT scan thus requires the following waveforms: (1) an inverse Mathieu q scan for precursor ion excitation in the y dimension, (2) a broadband waveform with no notch for product ion ejection in x, and (3) an inverse Mathieu q scan for rejection of the selected neutral loss product ions into the y electrodes. Anecdotally, this neutralization implementation also works for a NOT precursor scan, though waveform 3 is replaced by a single frequency sine wave.

The spectrum in Figure 4.6a, which appears to be a full scan, is a NOT neutral loss scan without waveform 3. That is, precursor ions are mass-selectively excited via an inverse Mathieu q scan and all product ions of those precursor ions are ejected toward the detector via a broadband

waveform that has no notch. In other words, the scan detects precursor ions that form any product ion. Note that a square is once again used for the product ions because the product ion m/z is neither fixed nor scanned, i.e. not known. All product ions are ejected simultaneously.
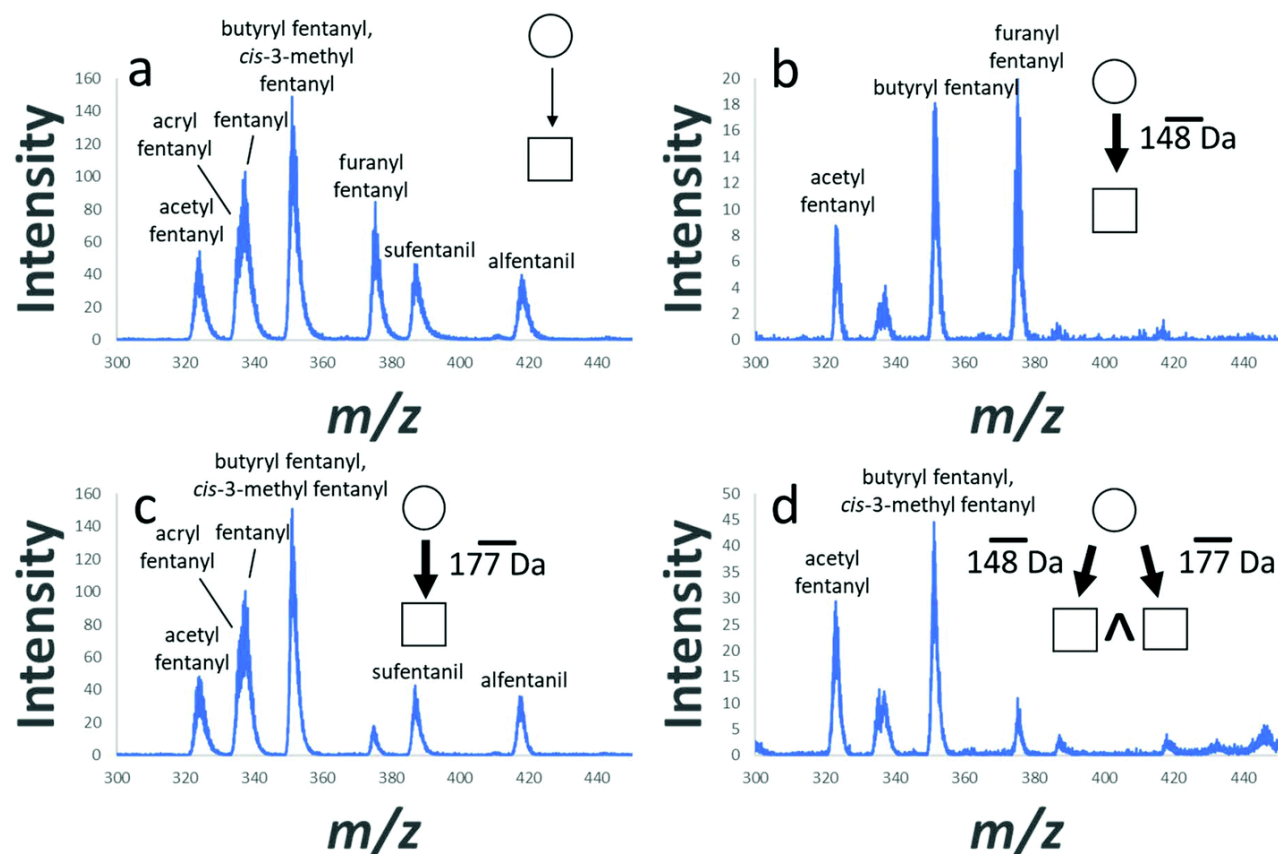


Figure 4.6. Logical NOT/NOR neutral loss scans: (a) arbitrary neutral loss scan detecting all precursor ions which fragment via any arbitrary neutral loss, (b) NOT neutral loss scan of 148 Da, detecting all precursor ions which give any neutral loss that is not 148 Da, (c) NOT neutral loss scan of 177 Da, and (d) NOR neutral loss scan of 148 Da and 177 Da.

If product ions that satisfy a neutral loss of 148 Da are neutralized on the y rods using a trigger-delayed inverse Mathieu q scan (recall that for the inverse Mathieu q scan, $t \propto m/z$, so that the trigger delay is proportional to the neutral loss mass), then their detection can be prevented, giving a NOT neutral loss scan as shown in Figure 4.6b. Again, it is worth noting that the diminished peaks (acryl fentanyl, fentanyl, cis-3-methylfentanyl, sufentanil, and alfentanil) still have some intensity because they have other neutral losses as well, but a neutral loss of 148 Da is by far the most abundant fragmentation pathway for these ions. Similarly, a NOT neutral loss of

177 Da (Figure 4.6c) decreases the abundance of furanyl fentanyl since it is the only precursor ion in the mixture that has such a loss. We again note that by themselves these scans are not easy to interpret, but with comparison to a full scan mass spectrum, logical conclusions about the precursor ions' fragmentation pathways can be made.

### 4.3.7  NOR operation

The final logical MS/MS operation demonstrated here is the NOR scan. The NOR scan, symbolically an upwards facing carrot with bars over both product ions (or neutral loss masses), detects precursor ions that do not produce either of two selected product ions or product neutrals, i.e. only ions in region 1 outside the circles. The NOR scan traverses an infinite number of scan lines, as did the NOT scan, and can be thought of as two (or more) simultaneous NOT scans.

In the ion trap, this can be accomplished by modifying the singly notched broadband waveform used in the NOT precursor scan to have two notches. For the NOR neutral loss scan, yet another trigger-delayed inverse Mathieu q scan must be used to reject product ions that satisfy the second selected neutral loss into the y electrodes, preventing their detection. Figure 4.5d shows a NOR precursor ion scan of m/z 188 and m/z 269. The former rejects acetyl fentanyl, acryl fentanyl, fentanyl, butyryl fentanyl, and furanyl fentanyl, and the latter rejects alfentanil, leaving cis-3-methylfentanyl and sufentanil. Similarly, Figure 4.6d shows a NOR neutral loss of 148 Da and 177 Da. The former largely rejects acryl fentanyl, fentanyl, sufentanil and alfentanil, and the latter largely rejects furanyl fentanyl. As stated previously, this scan should be particularly useful for classes of compounds which have two dominant product ions or product neutrals.

### 4.3.8  Other operations

Other logical MS/MS operations are proposed here but are not implemented. It may be possible to do these operations on other instruments or on the ion trap in the future, but currently the ion trap implementation is unknown. For example, a NAND scan would detect precursor ions that do not fragment to one selected product ion or do not fragment to a second selected ion. If for a NAND precursor ion scan two notches are implemented in the broadband ejection waveform, then the result will be a NOR scan, not a NAND. It is thus not possible to only reject precursor ions that fragment to both selected product ions without also rejecting those precursors which

fragment only to one. That is, ions from regions 2, 3, and 4 cannot be differentiated if they are not detected and frequency tagged. The IFF and IF/IF…THEN operations have similar complications on the ion trap.

## 4.4   Conclusion

A new set of logical MS/MS operations was described and demonstrated on a linear ion trap. Logical operations access, in a single scan, the logical connection between precursor ions and one or more product ions and may be useful for certain applications where precursor ions of a particular class share structural features that are expressed through common product ions or neutral losses, or in cases where dominant ions of similar molecular class are not of interest and can be excluded using a NOT or NOR operation. Additional selectivity and sensitivity as well as multiplexed capabilities can be gained through simultaneous acquisition of multiple fragmentation channels via frequency tagging. Although only the ion trap implementation was shown here, implementations on other mass spectrometer types – particular trapped ion analyzers – may be possible.

## 4.5   References

(1)     Paul, W., & Steinwedel, H. (1953). A new mass spectrometer without a magnetic field. *Z. Naturforsch. Sect. A*, *8*, 448-450.

(2)     Paul, W., Reinhard, H. P., & Vonzahn, U. (1958). Das Elektrische Massenfilter Als Massenspektrometer Und Isotopentrenner. *Zeitschrift Fur Physik*, *152*(2), 143-182.

(3)     Paul, W. (1990). Electromagnetic traps for charged and neutral particles. *Rev. Mod. Phys.*, *62*(3), 531.

(4)     Dawson, P. H. (2013). *Quadrupole mass spectrometry and its applications*. Elsevier.

(5)     March, R. E., & Todd, J. F. J. (2005). *Quadrupole Ion Trap Mass Spectrometry*. John Wiley & Sons.

(6)     Dehmelt, H. G. (1968). Radiofrequency spectroscopy of stored ions I: Storage. *Adv. At. Mol. Phys.*, *3*, 53-72.

(7)     Toschek, P. (2017). Hans Dehmelt (1922–2017). *Nature*, *545*, 290.

(8)     Fulford, J. E., & March, R. E. (1978). A new mode of operation for the three-dimensional quadrupole ion store (QUISTOR): The selective ion reactor. *Int. J. Mass Spectrom. Ion Phys.*, *26*(2), 155-162.

(9)     Stafford, G. C., Kelley, P. E., Syka, J. E. P., Reynolds, W. E., & Todd, J. F. J. (1984). Recent Improvements in and Analytical Applications of Advanced Ion Trap Technology. *Int. J. Mass Spectrom. Ion Processes*, *60*(Sep), 85-98.

(10)    Schwartz, J. C., Senko, M. W., & Syka, J. E. (2002). A two-dimensional quadrupole ion trap mass spectrometer. *J. Am. Soc. Mass Spectrom.*, *13*(6), 659-669.

(11)    Hager, J. W. (2002). A new linear ion trap mass spectrometer. *Rapid Commun Mass Sp*, *16*(6), 512-526.

(12)    Londry, F. A., & Hager, J. W. (2003). Mass selective axial ion ejection from a linear quadrupole ion trap. *J. Am. Soc. Mass Spectrom.*, *14*(10), 1130-1147.

(13)    Fulford, J. E. (1980). Radio-frequency mass selective excitation and resonant ejection of ions in a three-dimensional quadrupole ion trap. *J. Vac. Sci. Technol.*, *17*(4), 829.

(14)    Schwartz, J. C., Syka, J. E., & Jardine, I. (1991). High resolution on a quadrupole ion trap mass spectrometer. *J. Am. Soc. Mass Spectrom.*, *2*(3), 198-204.

(15)    Londry, F. A., Wells, G. J., & March, R. E. (1993). Enhanced mass resolution in a quadrupole ion trap. *Rapid Commun Mass Sp*, *7*(1), 43-45.

(16)    Goeringer, D. E., Whitten, W. B., Ramsey, J. M., Mcluckey, S. A., & Glish, G. L. (1992). Theory of High-Resolution Mass-Spectrometry Achieved Via Resonance Ejection in the Quadrupole Ion Trap. *Anal. Chem.*, *64*(13), 1434-1439.

(17)    Kaiser, R. E., Cooks, R. G., Stafford, G. C., Syka, J. E. P., & Hemberger, P. H. (1991). Operation of a Quadrupole Ion Trap Mass-Spectrometer to Achieve High Mass Charge Ratios. *Int. J. Mass Spectrom. Ion Processes*, *106*, 79-115.

(18)    Kaiser, R. E., Louris, J. N., Amy, J. W., & Cooks, R. G. (1989). Extending the mass range of the quadrupole ion trap using axial modulation. *Rapid Commun Mass Sp*, *7*(7), 225-229.

(19)    Landais, B., Beaugrand, C., Capron-Dukan, L., Sablier, M., Simonneau, G., & Rolando, C. (1998). Varying the radio frequency: a new scanning mode for quadrupole analyzers. *Rapid Commun Mass Sp*, *12*(6), 302-306.

(20)    Schlunegger, U. P., Stoeckli, M., & Caprioli, R. M. (1999). Frequency scan for the analysis of high mass ions generated by matrix-assisted laser desorption/ionization in a paul trap. *Rapid Commun Mass Sp*, *13*(18), 1792-1796.

(21)    Ding, L., Sudakov, M., & Kumashiro, S. (2002). A simulation study of the digital ion trap mass spectrometer. *Int. J. Mass Spectrom.*, *221*(2), 117-138.

(22)     Ding, L., Sudakov, M., Brancia, F. L., Giles, R., & Kumashiro, S. (2004). A digital ion trap mass spectrometer coupled with atmospheric pressure ion sources. *J. Mass Spectrom.*, *39*(5), 471-484.

(23)     Berton, A., Traldi, P., Ding, L., & Brancia, F. L. (2008). Mapping the stability diagram of a digital ion trap (DIT) mass spectrometer varying the duty cycle of the trapping rectangular waveform. *J. Am. Soc. Mass Spectrom.*, *19*(4), 620-625.

(24)     Wang, D., van Amerom, F. H., & Evans-Nguyen, T. (2013). High-speed digital frequency scanning ion trap mass spectrometry. *Anal. Chem.*, *85*(22), 10935-10940.

(25)     Todd, J., Penman, A., & Smith, R. (1991). Some alternative scanning methods for the ion trap mass spectrometer. *Int. J. Mass Spectrom. Ion Processes*, *106*, 117-135.

(26)     Welling, M., Schuessler, H. A., Thompson, R. I., & Walther, H. (1998). Ion/molecule reactions, mass spectrometry and optical spectroscopy in a linear ion trap. *Int. J. Mass Spectrom. Ion Processes*, *172*(1-2), 95-114.

(27)     Contreras, J. A., Murray, J. A., Tolley, S. E., Oliphant, J. L., Tolley, H. D., Lammert, S. A., Lee, E. D., Later, D. W., & Lee, M. L. (2008). Hand-portable gas chromatograph-toroidal ion trap mass spectrometer (GC-TMS) for detection of hazardous compounds. *J. Am. Soc. Mass Spectrom.*, *19*(10), 1425-1434.

(28)     Evans-Nguyen, T., Becker, L., Doroshenko, V., & Cotter, R. J. (2008). Development of a low power, high mass range mass spectrometer for Mars surface analysis. *Int. J. Mass Spectrom.*, *278*(2-3), 170-177.

(29)     Snyder, D. T., Pulliam, C. J., Wiley, J. S., Duncan, J., & Cooks, R. G. (2016). Experimental Characterization of Secular Frequency Scanning in Ion Trap Mass Spectrometers. *J. Am. Soc. Mass Spectrom.*, *27*(7), 1243-1255.

(30)     Snyder, D. T., Pulliam, C. J., & Cooks, R. G. (2016). Calibration procedure for secular frequency scanning in an ion trap. *Rapid Commun Mass Sp*, *30*, 1190-1196.

(31)     Snyder, D. T., Pulliam, C. J., & Cooks, R. G. (2016). Linear mass scans in quadrupole ion traps using the inverse Mathieu q scan. *Rapid Commun Mass Sp*, *30*(22), 2369-2378.

(32)     Li, G., Li, D., Cheng, Y., Pei, X., Zhang, H., Wang, Y., Sun, J., & Dong, M. (2017). Development of a low power miniature linear ion trap mass spectrometer with extended mass range. *Rev. Sci. Instrum.*, *88*(12), 123108.

(33)     Johnson, J. V., Yost, R. A., Kelley, P. E., & Bradford, D. C. (1990). Tandem-in-Space and Tandem-in-Time Mass-Spectrometry - Triple Quadrupoles and Quadrupole Ion Traps. *Anal. Chem.*, *62*(20), 2162-2172.

(34)     Yost, R. A., & Enke, C. G. (1979). Triple quadrupole mass spectrometry for direct mixture analysis and structure elucidation. *Anal. Chem.*, *51*(12), 1251-1264.

(35)     Louris, J. N., Cooks, R. G., Syka, J. E. P., Kelley, P. E., Stafford, G. C., & Todd, J. F. J. (1987). Instrumentation, applications, and energy deposition in quadrupole ion-trap tandem mass-spectrometry. *Anal. Chem.*, *59*(13), 1677-1685.

(36)     Louris, J. N., Brodbeltlustig, J. S., Cooks, R. G., Glish, G. L., Vanberkel, G. J., & Mcluckey, S. A. (1990). Ion isolation and sequential stages of mass-spectrometry in a quadrupole ion trap mass-spectrometer. *Int. J. Mass Spectrom. Ion Processes*, *96*(2), 117-137.

(37)     Johnson, J. V., Pedder, R. E., & Yost, R. A. (1991). Ms Ms parent scans on a quadrupole ion trap mass-spectrometer by simultaneous resonant excitation of multiple ions. *Int. J. Mass Spectrom. Ion Processes*, *106*, 197-212.

(38)     Snyder, D. T., Pulliam, C. J., & Cooks, R. G. (2016). Single analyzer precursor scans using an ion trap. *Rapid Commun Mass Sp*, *30*, 800-804.

(39)     Snyder, D. T., & Cooks, R. G. (2017). Single Analyzer Precursor Ion Scans in a Linear Quadrupole Ion Trap Using Orthogonal Double Resonance Excitation. *J. Am. Soc. Mass Spectrom.*, *28*(9), 1929-1938.

(40)     Snyder, D. T., & Cooks, R. G. (2017). Single Analyzer Neutral Loss Scans in a Linear Quadrupole Ion Trap Using Orthogonal Double Resonance Excitation. *Anal. Chem.*, *89*(15), 8148-8155.

(41)     Snyder, D. T., Szalwinski, L. J., & Cooks, R. G. (2017). Simultaneous and Sequential MS/MS Scan Combinations and Permutations in a Linear Quadrupole Ion Trap. *Anal. Chem.*, *89*(20), 11053-11060.

(42)     McClellan, J. E., Quarmby, S. T., & Yost, R. A. (2002). Parent and Neutral Loss Monitoring on a Quadrupole Ion Trap Mass Spectrometer:  Screening of Acylcarnitines in Complex Mixtures. *Anal. Chem.*, *74*(22), 5799-5806.

(43)     Olsen, J. V., Schwartz, J. C., Griep-Raming, J., Nielsen, M. L., Damoc, E., Denisov, E., Lange, O., Remes, P., Taylor, D., Splendore, M., Wouters, E. R., Senko, M., Makarov, A., Mann, M., & Horning, S. (2009). A Dual Pressure Linear Ion Trap Orbitrap Instrument with Very High Sequencing Speed. *Mol. Cell. Proteomics*, *8*(12), 2759-2769.

(44)     Beynon, J. H., Cooks, R.-G., Amy, J.-W., Baitinger, W., & Ridley, T. (1973). Design and performance of a mass-analyzed ion kinetic energy (MIKE) spectrometer. *Anal. Chem.*, *45*(12), 1023A-1031A.

(45)     Kruger, T. L., Litton, J. F., Kondrat, R. W., & Cooks, R. G. (1976). Mixture Analysis by Mass-Analyzed Ion Kinetic-Energy Spectrometry. *Anal. Chem.*, *48*(14), 2113-2119.

(46)     Schoen, A. E., Amy, J. W., Ciupek, J. D., Cooks, R. G., Dobberstein, P., & Jung, G. (1985). A Hybrid Beqq Mass-Spectrometer. *Int. J. Mass Spectrom. Ion Processes*, *65*(1-2), 125-140.

(47)    Louris, J. N., Wright, L. G., Cooks, R. G., & Schoen, A. E. (1985). New Scan Modes Accessed with a Hybrid Mass-Spectrometer. *Anal. Chem.*, *57*(14), 2918-2924.

(48)    Le Blanc, J. C., Hager, J. W., Ilisiu, A. M., Hunter, C., Zhong, F., & Chu, I. (2003). Unique scanning capabilities of a new hybrid linear ion trap mass spectrometer (Q TRAP) used for high sensitivity proteomics applications. *Proteomics*, *3*(6), 859-869.

(49)    Chernushevich, I. V., Loboda, A. V., & Thomson, B. A. (2001). An introduction to quadrupole-time-of-flight mass spectrometry. *J. Mass Spectrom.*, *36*(8), 849-865.

(50)    Cody, R., Burnier, R., & Freiser, B. (1982). Collision-induced dissociation with Fourier transform mass spectrometry. *Anal. Chem.*, *54*(1), 96-101.

(51)    Schwartz, J. C., Wade, A. P., Enke, C. G., & Cooks, R. G. (1990). Systematic delineation of scan modes in multidimensional mass spectrometry. *Anal. Chem.*, *62*(17), 1809-1818.

(52)    Vincenti, M., Schwartz, J., Cooks, R., Wade, A., & Enke, C. (1988). The functional relationship scan in tandem mass spectrometry. *J. Mass Spectrom.*, *23*(8), 579-584.

(53)    Chen, E. X., Gehm, M., Danell, R., Wells, M., Glass, J. T., & Brady, D. (2014). Compressive mass analysis on quadrupole ion trap systems. *J. Am. Soc. Mass Spectrom.*, *25*(7), 1295-1304.

(54)    Brock, A., Rodriguez, N., & Zare, R. N. (1998). Hadamard Transform Time-of-Flight Mass Spectrometry. *Anal. Chem.*, *70*, 3735-3741.

(55)    Zare, R. N., Fernandez, F. M., & Kimmel, J. R. (2003). Hadamard transform time-of-flight mass spectrometry: more signal, more of the time. *Angew Chem Int Ed Engl*, *42*(1), 30-35.

(56)    Gillet, L. C., Navarro, P., Tate, S., Röst, H., Selevsek, N., Reiter, L., Bonner, R., & Aebersold, R. (2012). Targeted data extraction of the MS/MS spectra generated by data-independent acquisition: a new concept for consistent and accurate proteome analysis. *Mol. Cell. Proteomics*, *11*(6), O111. 016717.

(57)    Collins, B. C., Hunter, C. L., Liu, Y., Schilling, B., Rosenberger, G., Bader, S. L., Chan, D. W., Gibson, B. W., Gingras, A.-C., & Held, J. M. (2017). Multi-laboratory assessment of reproducibility, qualitative and quantitative performance of SWATH-mass spectrometry. *Nat. Commun.*, *8*(1), 291.

(58)    Wilson, J., & Vachet, R. W. (2004). Multiplexed MS/MS in a Quadrupole Ion Trap Mass Spectrometer. *Anal. Chem.*, *76*(24), 7346-7353.

(59)    Pfändler, P., Bodenhausen, G., Rapin, J., Houriet, R., & Gäumann, T. (1987). Two-dimensional fourier transform ion cyclotron resonance mass spectrometry. *Chem. Phys. Lett.*, *138*(2), 195-200.

(60)    Pfandler, P., Bodenhausen, G., Rapin, J., Walser, M. E., & Gaumann, T. (1988). Broad-Band Two-Dimensional Fourier-Transform Ion-Cyclotron Resonance. *J. Am. Chem. Soc.*, *110*(17), 5625-5628.

(61)    van Agthoven, M. A., Barrow, M. P., Chiron, L., Coutouly, M. A., Kilgour, D., Wootton, C. A., Wei, J., Soulby, A., Delsuc, M. A., Rolando, C., & O'Connor, P. B. (2015). Differentiating Fragmentation Pathways of Cholesterol by Two-Dimensional Fourier Transform Ion Cyclotron Resonance Mass Spectrometry. *J. Am. Soc. Mass Spectrom.*, *26*(12), 2105-2114.

(62)    van Agthoven, M. A., Wootton, C. A., Chiron, L., Coutouly, M. A., Soulby, A., Wei, J., Barrow, M. P., Delsuc, M. A., Rolando, C., & O'Connor, P. B. (2016). Two-Dimensional Mass Spectrometry for Proteomics, a Comparative Study with Cytochrome c. *Anal. Chem.*, *88*(8), 4409-4417.

(63)    Floris, F., van Agthoven, M., Chiron, L., Soulby, A. J., Wootton, C. A., Lam, Y. P., Barrow, M. P., Delsuc, M. A., & O'Connor, P. B. (2016). 2D FT-ICR MS of Calmodulin: A Top-Down and Bottom-Up Approach. *J. Am. Soc. Mass Spectrom.*, *27*(9), 1531-1538.

(64)    Floris, F., Vallotto, C., Chiron, L., Lynch, A. M., Barrow, M. P., Delsuc, M. A., & O'Connor, P. B. (2017). Polymer Analysis in the Second Dimension: Preliminary Studies for the Characterization of Polymers with 2D MS. *Anal. Chem.*, *89*(18), 9892-9899.

(65)    Floris, F., van Agthoven, M. A., Chiron, L., Wootton, C. A., Lam, P. Y. Y., Barrow, M. P., Delsuc, M. A., & O'Connor, P. B. (2018). Bottom-Up Two-Dimensional Electron-Capture Dissociation Mass Spectrometry of Calmodulin. *J. Am. Soc. Mass Spectrom.*, *29*(1), 207-210.

(66)    van Agthoven, M. A., Lynch, A. M., Morgan, T. E., Wootton, C. A., Lam, Y. P. Y., Chiron, L., Barrow, M. P., Delsuc, M. A., & O'Connor, P. B. (2018). Can Two-Dimensional IR-ECD Mass Spectrometry Improve Peptide de Novo Sequencing? *Anal. Chem.*, *90*(5), 3496-3504.

(67)    Agthoven, M. A., & O'Connor, P. B. (2017). Two-dimensional mass spectrometry in a linear ion trap, an in silico model. *Rapid Commun Mass Sp*, *31*(8), 674-684.

(68)    Anders, L., Beauchamp, J., Dunbar, R., & Baldeschwieler, J. D. (1966). Ion-cyclotron double resonance. *J. Chem. Phys.*, *45*(3), 1062-1063.

(69)    Snyder, D. T., & Cooks, R. G. (2017). Improving mass assignments in quadrupole ion traps operated using ac scans: Theory and experimental validation. *Int. J. Mass Spectrom.*, *417*, 1-7.

# CHAPTER 5.    TWO-DIMENSIONAL TANDEM MASS SPECTROMETRY IN A SINGLE SCAN ON A LINEAR QUADRUPOLE ION TRAP

Portions of this work have been published in the journal *Analytical Chemistry* as the article: Snyder, D. T., Szalwinski, L. J., St. John, Z., & Cooks, R. G.. (2019). Two-Dimensional Tandem Mass Spectrometry in a Single Scan on a Linear Quadrupole Ion Trap. *Analytical Chemistry*, 91(21), 13752–13762.

## 5.1    Introduction

Two-dimensional mass spectrometry (2DMS) is a method for correlating precursor ions and product ions without isolation of the former.[1,2] Its origin can be traced to a 1987 paper by Pfändler *et al.* in which it was proposed to be useful for studying ion/molecule collisions via a series of rf pulses and delay/reaction times in a Fourier transform ion cyclotron resonance (FT-ICR) cell.[3] Subsequently, Guan and Jones described the theory of 2DMS in ICRs[4] and Pfändler provided the first experimental evidence correlating precursor and product ions without isolation.[5] Experimentally, 2DMS in ICRs requires an excitation pulse (a frequency sweep), a time delay which varies scan to scan, and an encoding pulse identical to the excitation pulse. This is followed by a conventional detection pulse, after which the induction current is measured and ion frequency (and hence *m/z*) obtained from the Fourier transform of the detected transient. As the time delay is varied between pulse sequences (each requiring a new ion injection), the abundance of fragment ions varies periodically according to the cyclotron frequency of the precursor ions because the encoding pulse will have a different phase relationship with respect to each precursor ion *m/z* and will thus excite some ions but de-excite others. This causes some precursor ions to fragment more than others if a radius-dependent activation mode is used (IRMPD, for example). Because each precursor ion *m/z* has a different cyclotron frequency, the periodicity of the product ion abundances (with respect to the time delay) generated from different precursor ions will also be unique. The product ion *m/z* values are obtained from fast Fourier transform (FFT) of the detected transients, whereas the precursor ion *m/z* values are determined from FFT of product ion abundance vs. delay time.

More recent 2D FT-ICR MS studies have investigated new pulse sequences using stored waveform inverse Fourier transform (SWIFT)[1,2] for ion radius modulation and denoising

algorithms for data analysis.[6,7] van Agthoven and coworkers have proposed an optimized pulse sequence in which two encoding pulses with optimized voltage amplitudes are separated by a delay time, and after the second pulse the ion signal is observed during the detection period.[8] In addition, others have demonstrated increased precursor ion resolution using nonuniform sampling.[9] Usually infrared multiphoton dissociation is used for fragmentation[10] but several implementations have used electron capture dissociation.[11,12] After decades of development and largely as a result of increased computational power, 2D MS in FT-ICRs is being applied to a wide variety of cases, e.g. for analysis of small molecule biologics (cholesterol),[13] peptides and glycopeptides,[12,14] proteins,[11,15,16] and polymers.[17] Even so, 2D MS in ICRs still faces multiple challenges including high instrument runtime, high sample consumption (one injection per time delay increment because fragmentation is irreversible), and loss of resolution during collision-induced dissociation in the ICR cell (hence, laser- and electron-based methods are prominent).[9]

To date, 2D MS has only been experimentally demonstrated on FT-ICR instruments; it has yet to garner much theoretical or experimental interest in the similar quadrupole ion trap (QIT). This is an odd omission given that many waveform methods (e.g. SWIFT, frequency 'chirps') that originated on ICRs were successfully translated to rf traps.[18,19] After all, both ICRs and QITs are ion frequency analyzers with MS/MS capabilities, although the QIT is indirectly so (the ions' frequencies are indirectly measured via resonance ejection at a fixed frequency, whereas in the ICR the frequencies are measured directly via ion excitation and charge detection). Simulated evidence that 2D MS is possible in a linear ion trap has been published by O'Connor's group.[20] In these simulations, SWIFT was used to radially excite ions as a laser pulse fragmented non-excited ions at the center. According to the work, the intensities of product ions were modulated corresponding to the secular frequency of the excited precursors, as is the case for the similar ICR experiments. Despite this simulated evidence, no experimental data of 2DMS on linear ion traps has emerged. Furthermore, the requirement of a laser for dissociation and a second mass analyzer (the ICR) for determination of product ion *m/z* limits the overall applicability of this method. Moreover, such a method would not be reasonable to implement on portable ion traps (because of speed concerns) which are of interest to us and which would benefit most from the efficiency of acquiring the entire 2D MS/MS domain with, in the most desirable case, a single scan.

Herein we propose two methods for *2D MS/MS* (*two-dimensional tandem mass spectrometry*) on quadrupole ion traps using collision-induced dissociation for precursor ion

activation and show experimental evidence that *the 2D MS/MS data domain can be obtained in a single scan*. In this work we use a nonlinear frequency sweep for time-dependent fragmentation of precursor ions from low to high *m/z* in one dimension of the linear trap while simultaneously ejecting all product ions of those precursor ions by using a broadband waveform applied in the orthogonal dimension. In a first implementation ('frequency tagging'), the broadband waveform is encoded with beat frequencies proportional to the product ion secular frequencies, thus modulating peak shapes according to those beat frequencies. By taking the FFT of each peak, the beat frequencies of the ejected product ions – hence, the product ions' secular frequencies – can be recovered and correlated to every precursor ion without isolation. Product ion secular frequency can then be converted to ion *m/z* using the Mathieu parameters, thereby yielding a product ion mass spectrum for every precursor ion. The precursor *m/z* domain can be calibrated (correlated with time) using known standards, and because product ion ejection occurs simultaneously with precursor ion activation, precursor->product relations are also conserved in time. In a second implementation, the frequency spacing in the broadband waveform is even and instead the product ion micropackets are observed at the detector and Fourier transformed to recover the product ions' secular frequencies and hence *m/z* values.

This work follows our recent experimental demonstration of precursor and neutral loss scans on a single linear ion trap in which orthogonal double resonance was used for mass analysis.[21-24] The 2D MS/MS scan similarly utilizes orthogonal double resonance excitation and can be thought of as conducting every possible precursor ion scan at once (or, correspondingly, every possible neutral loss or product ion scan). The data collection efficiency in 2D MS/MS will be most useful for miniature or portable instruments[23,25-28] with low acquisition rates (e.g. DAPI systems[29]). On such instruments data-dependent product ion scans are less favorable than on commercial benchtop systems due to acquisition rate constraints. It thus may be important to be able to acquire as much data as possible in each scan, i.e. utilize 2D MS/MS scans.

## 5.2   Experimental

### 5.2.1   Chemicals

All drug standards were purchased from Cerilliant (Round Rock, TX, USA) and were either used as provided or diluted in 50:50 methanol/water with 0.1% formic acid. Typical concentrations

were 1 to 10 ppm (μg/mL). All other standards were purchased from Sigma (St. Louis, MO, USA) and prepared similarly.

### 5.2.2 Ionization

Nanoelectrospray ionization was used for all experiments herein. In order to generate ions, 1.5 kV was applied to a nanospray electrode holder (glass size 1.5 mm), which was purchased from Warner Instruments (Hamden, CT, U.S.A.) and fitted with 0.127 mm diameter silver wire, part number 00303 (Alfa Aesar, Ward Hill, MA). Borosilicate glass capillaries (1.5 mm O.D., 0.86 mm I.D.) from Sutter Instrument Co. (Novato, CA, U.S.A.) were pulled to 2 μm tip diameters using a Flaming/Brown micropipette puller (model P-97, Sutter Instrument Co.).

### 5.2.3 Instrumentation

All data was generated on a Thermo LTQ linear quadrupole ion trap (San Jose, CA, USA). The LTQ ion trap has an rf frequency of 1.166 MHz and dimensions of $x_0 = 4.75$ mm, $y_0 = 4$ mm, and three axial sections of length 12, 37, and 12 mm.[30] In these experiments, the rf amplitude was constant throughout injection, cooling, and mass scan stages, as described previously.[22] Because the rf voltage was fixed, the ions' secular frequencies do not vary during the scan. The LTQ used in this work was previously modified to be able to apply low voltage auxiliary ac signals to both the x and y rods. The helium normally used in the LTQ was substituted with nitrogen with an ion gauge reading of $1.4 \times 10^{-5}$ torr. Nitrogen was used because it increases fragmentation efficiency (but also decreases resolution) compared to helium.[31]

### 5.2.4 Waveform Generation

Two waveforms were used in these experiments; both were calculated in Matlab (Mathworks, Natick, MA, USA), exported as .csv files and imported into one of two Keysight 33612A arbitrary waveform generators with 64 megasample memory upgrades (purchased from Newark element14, Chicago, IL, USA). One generator supplied the waveform for precursor ion excitation in the y dimension while the other supplied a broadband sum of sines for product ion ejection in the x dimension (where there are two electron multiplier detectors).

### 5.2.5  2D MS/MS Scan Table

A general scan table for the 2D MS/MS experiment is shown in Figure 5.1. Ions were first injected and cooled to the center of the trap through collisions with background gas molecules. The rf was set at a constant desired level for injection, cooling, and the 2D MS/MS scan because of electronic constraints; however, in principle one would leave the rf voltage low during injection/cooling and raise it for the 2D MS/MS scan as shown in Figure 5.1. After cooling, a dipolar inverse Mathieu q scan was applied to the y rods of the linear ion trap to mass-selectively fragment precursor ions such that $m/z \propto t$. The frequency sweep was an inverse Mathieu q scan[32] (nonlinear frequency sweep with linear mass scale with respect to time) from Mathieu q = 0.908 to q = 0.15 over 600 ms. This excitation sweep had a peak-to-peak amplitude of approximately 350 mVpp. Simultaneously, in the x dimension of the trap (where there are slits in the electrodes and two electron multiplier detectors) a broadband waveform was applied to eject all product ions of each precursor ion as they were formed. There are two types of broadband waveforms that were utilized, one for 'frequency tagging' 2D MS/MS and one for 'micropacket detection' 2D MS/MS.
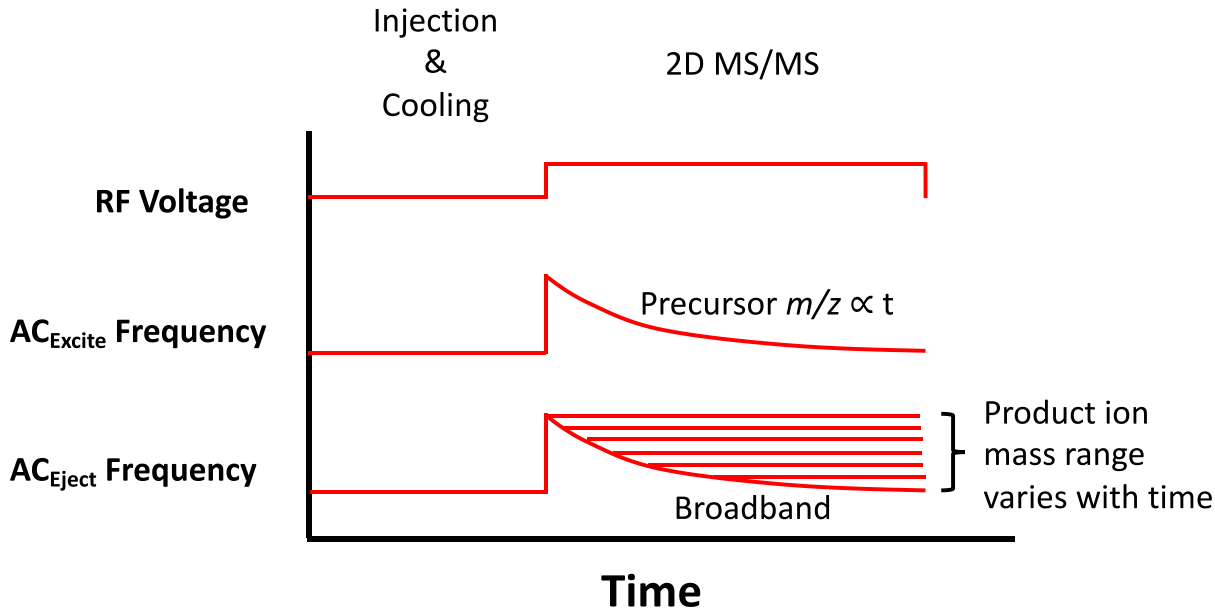
Figure 5.1 Scan table for 2D MS/MS in a linear ion trap. The rf voltage is held constant during the scan while a nonlinear ac frequency sweep, $AC_{Excite}$, fragments precursor ions selectively as a function of time in the y dimension of the ion trap. Simultaneously, a broadband $AC_{Eject}$ waveform is applied in the x dimension to eject product ions into the detectors.

### 5.2.6    Frequency Tagging for 2D MS/MS

For frequency tagging 2D MS/MS (Figure 5.2), the broadband waveform (Figure 5.1, $AC_{eject}$, 'Broadband'), constructed using the program in Figure S4.1, was a sum of sines; the product ions' *m/z* values were encoded in the beats in the waveform such that beat frequency and product ion secular frequency were directly proportional. A master array contained main frequencies that were spaced every 10 kHz from Mathieu q = 0.908 to q = 0.15, with the lowest frequency being 73 kHz. Beat frequencies were then encoded by adding a second frequency per 10 kHz, with a starting beat frequency of 500 Hz and subsequent spacings of 600 Hz, 700 Hz, 800 Hz, etc. The beat frequencies were therefore programmed to be proportional to ion secular frequency. The following is an example of frequencies that were included: 73 kHz and 73.5 kHz, 83 kHz and 83.6 kHz, 93 kHz and 93.7 kHz, and so on until half the rf frequency was met. Phase overmodulation using a quadratic function of phase vs. frequency[18,19,33] was used to maintain an approximately constant voltage amplitude (6 $V_{pp}$) as a function of time.
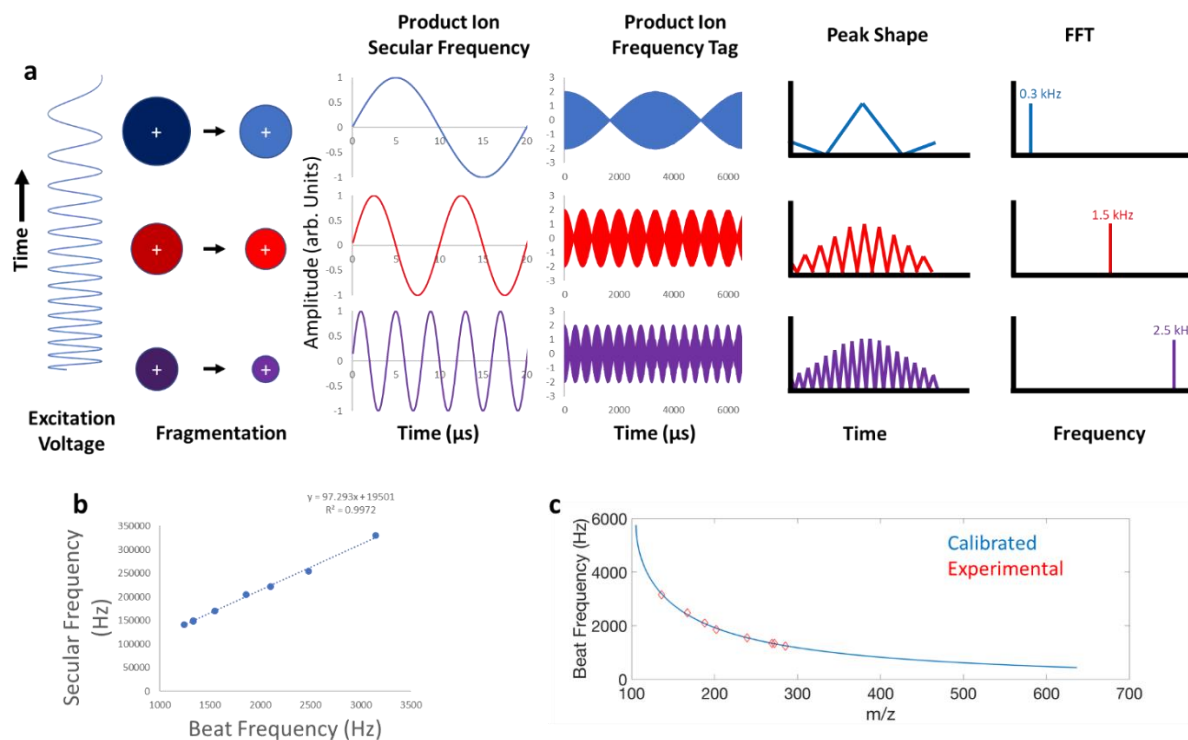
Figure 5.2. Frequency tagging mass spectrometry for 2D MS/MS. (a) Precursor ions are fragmented from low to high *m/z* via a frequency sweep ('Excitation Voltage'), forming product ions. Each product ion is 'tagged' with a secondary frequency by resonance excitation with two frequencies close to its secular frequency, the difference of which creates a beat frequency that modulates the mass spectral peak shapes. When product ions are generated they are immediately ejected and detected by a broadband sum of sines with encoded beat frequencies, but the ejection process follows the programmed beat pattern and hence the mass spectral peaks also show beats. (b) The beat frequencies, related linearly to product ion secular frequency, can be recovered by taking the fast Fourier transform of each peak. The beats can be plotted against the experimental secular frequencies for calibration. (c) Experimental vs. calibrated relationship between beat frequency and product ion *m/z*. Note that for the micropacket technique there is no frequency tag and instead the micropacket frequencies are observed and FFT'd.

The ejection waveform was built point-by-point, and, critically, *only frequencies at least 10 kHz above the precursor ion's frequency were included in each point (hence, this waveform implementation is only useful for singly charged ions).* In other words, each time point in the broadband waveform consisted of a different set of frequencies to coincide with a different product ion mass range. The excited precursor ion's frequency was known because it equaled the frequency applied by the excitation waveform (the inverse Mathieu q scan). For example, if at time 0.1 s the inverse Mathieu q scan was applying a frequency of 300 kHz to fragment a precursor ion, then at that time point the sum of sines waveform only included frequencies above 310 kHz.

The data collection rate in the LTQ's 'normal' scan rate mode with 'high' selected as the mass range was 28.732 kHz, which is fixed by the LTQ data system and cannot be changed. All mass and frequency spectra collected using frequency tagging are the result of an average of 10 scans. Fast Fourier transforms were calculated in Matlab using 301 points per peak and a sampling rate of 28.732 kHz. Images were constructed using the 'imagesc' function in Matlab.

### 5.2.7 Micropacket Detection for 2D MS/MS

For ion micropacket detection, the broadband was constructed similarly, but the frequencies of the waveform were equally spaced (1 kHz spacing) from 583 kHz to 62 kHz and their phases were distributed quadratically with frequency.[33] The broadband waveform was built point-by-point so that the frequency components included in each point were always at least 10 kHz above the corresponding frequency in the accompanying inverse Mathieu q scan. No extra beat frequencies were created for micropacket detection.

In order to observe the ion micropackets, data were obtained directly from the electron multipliers of the LTQ using a combination of a fast transimpedance (current) amplifier and either a Keysight MSOX3024T oscilloscope (Chicago, IL, USA) or a National Instruments USB-6343 DAQ device with BNC termination (Austin, TX, USA). The amplifier consisted of a current-to-voltage conversion followed by a two-stage current feedback operational amplifier (CFA) circuit. The CFAs allow the circuit to achieve a very high gain without the linear tradeoff in bandwidth, as with traditional voltage feedback operational amplifiers. The total gain of the circuit was around 200,000,000 V/A with a bandwidth of 225MHz. The oscilloscope was operated with a sampling rate between 50 and 100 MHz and acquired ~1.9 ms of data (but could only save 16,000 points of data), whereas the DAQ device had a fixed sampling rate of 2 MHz and could acquire and save

data over 600 ms (1.2 million points). FFTs of the oscilloscope data (16,000 points over 1.9 ms) were conducted in Matlab, whereas built-in Labview functions were used to calculate FFTs of DAQ data (using 10 ms windows containing 20,000 points each). All spectra acquired in this mode were an average of 20 scans. In order to observe the ion micropackets it was necessary to change the voltage on the electron multipliers from -1200 V to ~-2,000 V.

## 5.3 Results & Discussion

### 5.3.1 What is frequency tagging?

Frequency tagging[34,35] (Figure 5.2a) is a method of tagging ions resonantly ejected from a quadrupole ion trap with a secondary frequency observable at the detector. The primary frequency observed (if the detection electronics are fast and sensitive enough) is the ion's excitation/ejection frequency, which usually closely mirrors the ion's secular frequency, especially at low excitation amplitude.[36] However, if the detection electronics do not permit observation of the ion's so-called 'micropackets', then a secondary frequency tag may be used instead. Any ion in the trap can be frequency tagged by applying a dual frequency sine wave that is the sum of the ion's secular frequency and a second frequency very close to the secular frequency (Figure 5.2a, Product Ion Frequency Tag). For example, an ion whose secular frequency is 300 kHz can be tagged with a 2 kHz frequency if a dual frequency sine wave containing 300 kHz and 302 kHz is used for resonance excitation/ejection. The 2 kHz beat is observed in the mass spectral peak at the detector (Figure 5.2a, peak shape). A fast Fourier transform of the mass spectral peak results in recovery of the beat frequency, and if beat frequency and the secular frequency are related in some predetermined or pre-programmed fashion, then this relationship can be used to relate beat frequency to product ion *m/z*. In the work presented here, the beat frequency observed in the mass spectral peaks is directly proportional to the product ions' secular frequencies (Figure 5.2b). Note that the FFT in the illustration is a simplification; in reality harmonics and combinations of beat frequencies may be observed and can complicate spectral interpretation.

### 5.3.2 2D MS/MS Requisites

In this work we used frequency tagging to perform 2D MS/MS in a linear quadrupole ion trap. There are three key pieces of information obtained in a 2D MS/MS experiment: (1) precursor

ion $m/z$, (2) product ion $m/z$, and (3) the relationship between the precursor ions and the product ions (i.e. from which precursor ion did each product ion originate?).

In our implementation of 2D MS/MS, these three pieces of information are obtained as follows: (1) Precursor ion $m/z$ is linearly related to time because the precursor ions are fragmented from low to high $m/z$ using an inverse Mathieu q scan ('Excitation Voltage vs. Time' in Figure 5.2a). (2) Simultaneously, a broadband sum of sines is used to eject the product ions as they are being formed from fragmentation of the precursors. Product ion $m/z$ is recovered from fast Fourier transform of each mass spectral peak, where (for frequency tagging) beat frequency is linearly related to product ion secular frequency or (for micropacket detection) the product ion secular frequency is deduced from the micropackets. Figure 5.2b shows the experimentally observed relationship between secular frequency and beat frequency using frequency tagging, and converting secular frequency to $m/z$ via Mathieu parameters gives the plot in Figure 5.2c. The calibration is shown in blue and the experimentally observed values in red. (3) Lastly, product ions are ejected from the ion trap within hundreds of microseconds of their respective precursor ions being fragmented and hence their relationship is preserved in time, just as they were preserved in our implementation of precursor and neutral loss scans.[21-24,37]

### 5.3.3   2D MS/MS using frequency tagging

A simple mixture of 5 amphetamines (amphetamine, $m/z$ 136; methamphetamine, $m/z$ 150; 3,4-methylenedioxyamphetamine (mda), $m/z$ 180; 3,4-methylenedioxymethamphetamine (mdma), $m/z$ 194; and 3,4-methylenedioxyethylamphetamine (mdea), $m/z$ 208; all protonated) was analyzed using 2D MS/MS with nitrogen as the trap bath gas instead of the usual helium. The mass calibrated 2D MS/MS spectrum in Figure 5.3a gives the $m/z$ values of the precursor ions as a linear function of time. Note the unique beats in each peak which can be used to recover product ion $m/z$. It is also critical to remember that although the precursor ion $m/z$ correlates with time, *the vast majority of the ions detected are product ions*. Precursor ions are either ejected alongside their respective product ions in the x dimension (and can be observed at low frequency in the FFTs) or they collide with the y rods, preventing them from being observed at the electron multipliers. It is possible for unfragmented precursor ions to be observed as artifact peaks later in the scan, which can complicate data interpretation. This can be prevented by increasing the amplitude of the y dimension excitation so that unfragmented precursors are neutralized on the trap rods.

Figure 5.3. (a) 2D MS/MS spectrum of five amphetamines using the frequency tagging technique as observed at the detectors (precursor m/z values are labelled), (b) frequency spectrum of each peak, and (c) 2D representation of the spectrum. Known product ion m/z values are marked in (b).

Requirement #3, association between fragmented precursor ion *m/z* and generated product ion *m/z*, is simply inferred from time. That is, because fragment ions are ejected exactly after they are generated from fragmentation of their respective precursors (which are fragmented selectively), their relationship to each other is preserved.

In order to obtain the product ion mass spectrum for a particular precursor ion (requisite #2), we simply calculate the fast Fourier transform of each mass spectral peak and convert from observed beat frequency to secular frequency (using Figure 5.2b) and then to *m/z* using the Mathieu

parameters. Experimentally this can be done by taking FFTs of peaks of known standards and correlating beat frequency with the known product ion $m/z$. Because in our case beat frequency and secular frequency are directly proportional, we can calculate the calibrated relationship between beat frequency and product ion $m/z$, as shown in Figure 5.2**c** and compare it to experimental values, shown as red diamonds. This calibration can now be used to assign $m/z$ values in the frequency spectra.

Amphetamine and methamphetamine share product ions at $m/z$ 91 and 119, and this is evident in the FFTs (Figure 5.3b) of the peaks in the mass spectrum (Figure 5.3a). A peak at 3,400 Hz corresponds to $m/z$ 91 and 2,400 Hz corresponds to $m/z$ 119. Because beat frequency and secular frequency are proportional in our implementation, lower $m/z$ ions will have higher beat frequencies. Similarly, mda, mdma, and mdea fragment to $m/z$ 163 and $m/z$ 135/133 at 1,500 Hz and 2,000 Hz, respectively. Additional peaks in the frequency spectra correspond to harmonics (i.e. two and three times the beat frequency) as well as other beats and combination frequencies. Because of these additional peaks, frequency spectra are not converted into the mass domain in this paper. However, these peaks do serve to provide a unique pattern for each precursor ion and may be useful for distinguishing similar spectra. The complete 2D MS/MS domain can be constructed by using a moving FFT across the spectrum in Figure 5.3a (here, 300 data points per FFT spectrum), displayed as Figure 5.3c. The product ion spectra in panel (b) can be thought of as being 'extracted' from the total data domain in panel (c). Note the remarkable similarities between the structurally similar amphetamine and methamphetamine as well as mda, mdma, and mdea, even for frequencies which are difficult to assign to product ions (e.g. > 6 kHz).

Note that the precursor ion resolution is independent of the bin width used to calculate panel (c). The true precursor ion resolution is observed in the scan in panel (a). For reference, the full width at half maximum peak width of m/z 150 in panel (a) is ~1.8 Da, so the m/Δm is approximately 83.

### 5.3.4    2D MS/MS for analysis of fentanyls

We next applied 2D MS/MS to analysis of opioids of the fentanyl class, which have become a serious health risk due to their extreme potency and wide range of structurally diverse analogues.[38,39] When subject to CID in the ion trap, many of these compounds fragment almost exclusively to $m/z$ 188[40] and so their frequency spectra (i.e. product ion spectra) should be

markedly similar. A 2D MS/MS scan of a mixture of 16 fentanyl analogues is shown in Figure 5.4a. The precursor ion $m/z$ values are directly proportional to time, allowing for the spectrum to be mass calibrated. The beats in each peak are indicative of the product ion $m/z$ values and be recovered through FFTs. As shown in Figure 5.4b, 4-ANPP (a fentanyl precursor), acetyl fentanyl, 4-fluoroisobutyryl fentanyl, fentanyl, furanyl fentanyl, p-fluorofentanyl, isobutyryl fentanyl, butyryl fentanyl, valeryl fentanyl, and acryl fentanyl all fragment to $m/z$ 188 (2.1 kHz beat frequency, indicated by the white arrow) and hence have almost identical frequency spectra. *Cis*-3-methylfentanyl, $m/z$ 351, has a prominent product ion at $m/z$ 202 which is noticeably frequency shifted (about 240 Hz) from $m/z$ 188. Acetyl norfentanyl is a metabolite and hence fragments differently as well. Extracted product ion scans for each of these precursors can be found in Figure S4.2 and S4.3 of the supplemental information.
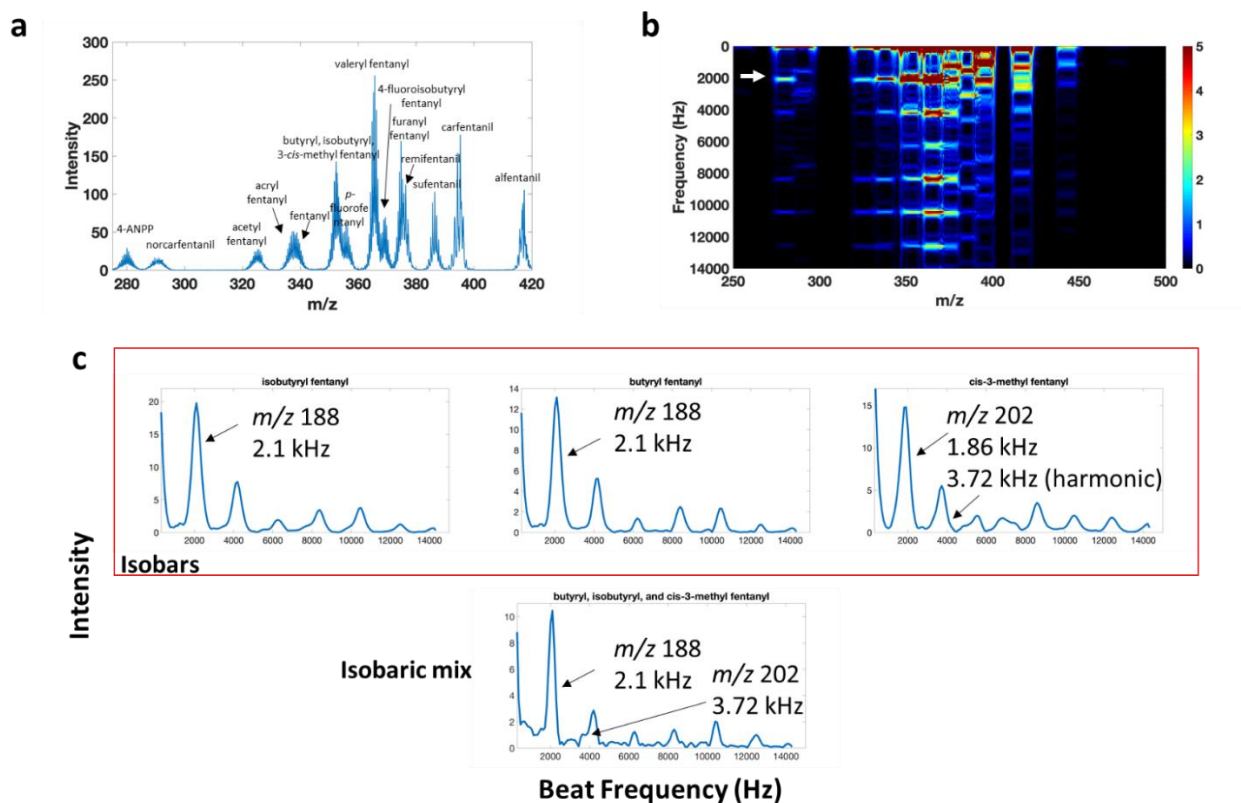
Figure 5.4. 2D MS/MS of a mixture of 16 fentanyl analogues using the frequency tagging technique. (a) Full scan mass spectrum of the mixture (note the beats in the spectra), (b) 2D tandem mass spectrum, (c) comparison of frequency spectra of three isobaric fentanyls and three-component mixture. Known product ions are marked in (c). The white arrow in (b) corresponds to a common product ion, m/z 188.

Notably, butyryl, isobutyryl, and *cis*-3-methylfentanyl are isobaric (*m/z* 351) and so their peaks overlap in the mass spectrum if they are in a mixture together. We tested whether we could observe all three components in a 1:1:1 mixture. The frequency spectrum in the isobaric mix, Figure 5.4c (bottom), indicates a primary product ion at *m/z* 188. Presumably, the peak at *m/z* 202 overlaps significantly and is not observed. However, the harmonic (1.86 kHz x 2 = 3.72 kHz) is observed, and thus it is umambiguous that methylated fentanyl is in the spectrum. Butyryl and isobutyryl fentanyl are nearly indistinguishable, though, since they almost exclusively fragment to *m/z* 188.

Quaternary fentanils (emphasis on the 'il') share neutral fragments – e.g. 31 Da, 32 Da, 60 Da, 148 Da are examples - instead of product ions. In the frequency domain the similarities are not obvious, which is a limitation of the current method. The frequency domain must be converted to

123

the mass-to-charge domain and then to neutral losses to make any reasonable conclusions about similarities between spectra. Figure S4.3 shows the frequency spectra of alfentanil and sufentanil (which share neutral losses of 31 Da and 148/149 Da) and norcarfentanil, carfentanil, and remifentanil (which share neutral losses of 32 Da, 60 Da, and 149 Da). Notable product ions are marked.

### 5.3.5   2D MS/MS for analysis of other molecular classes

Frequency tagging spectra of other molecular classes – focusing on classes that share product ions rather than neutral losses – are shown in Figure 4.4. Chemical warfare agent simulants cyclohexyl methylphosphonate, isopropyl methylphosphonate-d7, and pinacolyl methylphosphonate fragment exclusively to *m/z* 95 (*m/z* 96 for the deuterated analyte) in the negative ion mode and thus have very similar frequency spectra (Figure S4.4, green), including strong harmonics. Tetracyclic antidepressants amoxapine, loxapine, and clozapine share *m/z* 272 but otherwise have dissimilar spectra in both the mass and frequency domain (Figure S4.4, blue). Antihistamines pheniramine, chlorpheniramine, brompheniramine, and diphenhydramine share *m/z* 167 (or *m/z* 168), as noted on the spectra, but also have other dissimilar product ions (Figure S4.4, red).

### 5.3.6   Analysis of isobaric cathinones

A challenge in mass spectrometry is differentiating isobars, particularly if those isobars fragment similarly. Not only will their product ion spectra appear similar, but so will their 2D MS/MS frequency spectra. As shown in Figure S4.5, isobaric cathinones buphedrone and *N*-ethylcathinone (*m/z* 178) share product ions at *m/z* 160 and 132 and are nearly indistinguishable. However, three other cathinone isobars, namely pentedrone, 3,4-dimethylmethcathinone, and 4-methylethcathinone (*m/z* 192) are – remarkably – readily distinguished. Although they share water loss (*m/z* 174), they also have unique MS$^2$ ions *m/z* 132, *m/z* 161, and *m/z* 147.

### 5.3.7   Limitations of Frequency Tagging

Because the measured frequencies using frequency tagging are <10 kHz and are only measured for a few ms, the frequency resolution and hence mass resolution are limited. Next, we

describe an alternative approach to obtaining 2D MS/MS spectra through double resonance excitation combined with observation of micropacket frequencies which are on the order of 50-500 kHz. This approach measures higher frequencies and therefore achieves higher frequency and mass resolution for the product ions. Moreover, there is less spectral overlap from harmonics and combination frequencies.

### 5.3.8   What is an Ion Micropacket?

Ions can only be ejected from a quadrupole ion trap during certain 'allowed' periods when operated in the resonance ejection mode.[41] This has been observed through both simulation[41,42] and experiment[43] by several groups using a variety of ion trap configurations. As ions are resonantly excited for ejection through application of an auxiliary frequency, they oscillate coherently and are ejected such that the rate of appearance of the micropackets at the detector corresponds to the excitation frequency (*not* the ion secular frequency). If detectors are placed on both sides of the ion trap, then the micropackets are observed at a frequency corresponding to *twice* the auxiliary frequency since the ions are ejected twice per secular frequency cycle.[41,44]   The frequency of ejection can be determined through Fourier transform of each mass spectral peak, assuming the detection electronics are fast and sensitive enough to observe the micropackets.  In the experiments performed here, the LTQ electrometer board could not observe the micropackets, so we bypassed it and used a custom current amplifier and DAQ system operated at a 2 MHz sampling rate.

### 5.3.9   2D MS/MS Using Ion Micropackets

Ion micropackets can be used for two-dimensional tandem mass spectrometry scans in a quadrupole ion trap. Experimentally, this 2D MS/MS scan is identical to the frequency tagging 2D MS/MS scan in that precursor ions are excited in the y dimension using an ac frequency sweep (with constant rf voltage) while the product ions are ejected toward the detectors in the x dimension through application of a broadband auxiliary waveform. For these micropacket experiments, the frequency spacing of the waveform was a constant 1 kHz from low frequency 62 kHz to high frequency 583 kHz.

Figure 5.5a shows the two-dimensional tandem mass spectrum – using micropacket detection - of the same set of five amphetamines as was described previously. As before, precursor ion *m/z* and time are directly proportional. Note the beats in the peaks which are caused by the broadband waveform frequency spacing. The ion micropackets are also present within these patterns and can be determined via Fourier transform of the individual peaks (Figure 5.5b). Peak widths of 5-10 ms containing 10,000-20,000 points were used for the FFTs. Amphetamine and methamphetamine fragment to *m/z* 91 and *m/z* 119, and these peaks are noted. The shared product ions of mda, mdma, and mdea are also labeled. All labeled peaks are the second harmonic of the secular frequency. We can calibrate the secular frequency to *m/z* conversion through Mathieu parameters using the known product ion *m/z* values and experimentally observed micropacket frequencies. Based on these data, mass calibrated product ion spectra in Figure 5.5c were generated. Clearly the resolution at low *m/z* (high Mathieu q) is best (approaching unit resolution for *m/z* 91), which is expected and discussed later. The full 2D MS/MS data domain was calculated as described for the frequency tagging technique and is shown in Figure 5.5c. Note the remarkable similarities not only between spectra containing similar product ions (e.g. mda, mdma, and mdea), but also between the frequency tagging technique (Figure 5.3) and this micropacket technique (Figure 5.5). Mass errors for this experiment are as follows: (precursor ion domain) *m/z* 136, 0.09 Da; *m/z* 150, 0.21 Da; *m/z* 180, 0.03 Da; *m/z* 194, 0.09 Da; *m/z* 0.21 Da; (product ion domain) *m/z* 91, 0.26 Da; *m/z* 119, 0.51 Da; *m/z* 163, 0.22 Da. Given that every spectrum in this paper was calibrated separately and that the rf voltage of the LTQ was operated without feedback (allowing it to drift slightly from scan to scan and from experiment to experiment) due to electronic limitations, these mass errors should be judged with a great deal of caution.
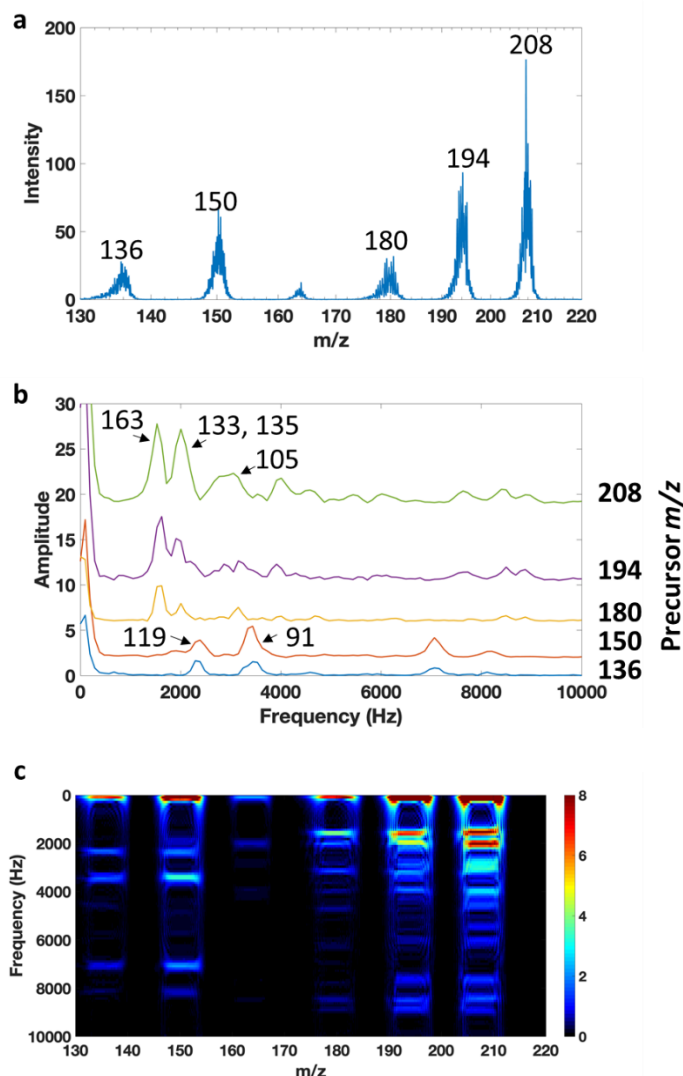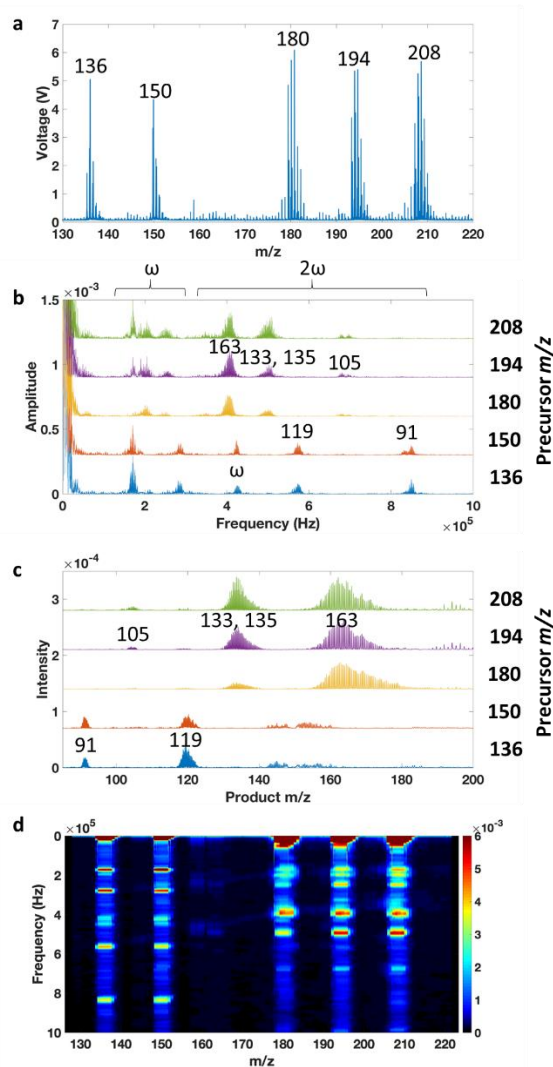
Figure 5.5. (a) 2D MS/MS spectrum of five amphetamines using the micropacket technique as observed at the detectors (precursor *m/z* values are labelled), (b) frequency spectrum of each peak, (c) mass calibrated product ion spectra, and (d) 2D representation of the spectrum. Known product ion *m/z* values are marked in (b) and (c).

Figure 5.6a is a 2D MS/MS spectrum of a set of 16 fentanyl analogues and metabolites, and the 2D data domain is illustrated as an image in Figure 5.6b. The similarities between many of the analytes are notable, with *m/z* 188 – the second harmonic of which is indicated by the white arrow in panel (b) - being the primary fragment. Selected product ion spectra are shown in panel (c) and indicate the structural similarities between 4-ANPP (a fentanyl precursor), acetyl fentanyl, and acryl fentanyl. Product ion spectra in the frequency domain for all the other fentanyl analogues are shown in Figure S4.6/S7 for reference.

127
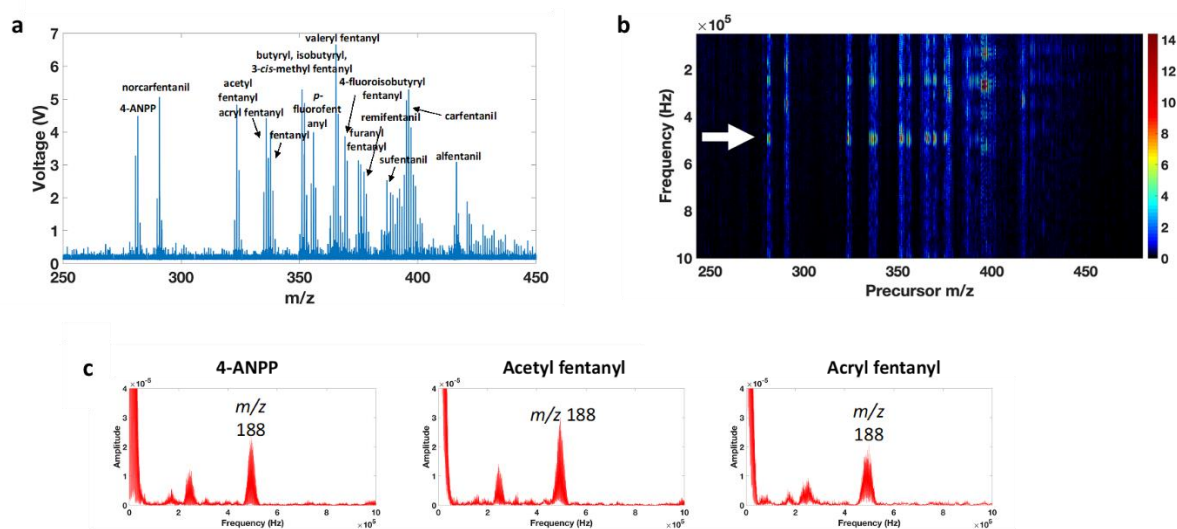
Figure 5.6. 2D MS/MS spectrum of fentanyl analogues using the micropacket technique. (a) mass calibrated spectrum of sixteen fentanyl analogues as observed at the detector, (b) image representing the 2D MS/MS domain reconstructed from (a), and (c) frequency spectra (i.e. product ion spectra) of selected peaks. Known product ion *m/z* values are marked in (c). The white arrow in (b) corresponds to the second harmonic of *m/z* 188's ejection frequency.

### 5.3.10  Application to Planetary Exploration

So far, only forensic applications have been demonstrated. However, planetary science is perhaps a more appropriate application of 2D MS/MS. A central objective of NASA's Planetary Sciences Division is to explore prebiotic chemistry on other worlds, that is, to elucidate possible chemical origins of life and determine if other habitable bodies do contain (or have contained) prebiotic molecules and the means to assemble those organics into more complex species. Within this framework, worlds containing (or suspected to contain) subsurface lakes – notably Mars and the icy moons of Saturn and Jupiter – are the most promising candidates for exploration and study. Mass spectrometry has played a critical role in several corresponding missions (Mars Curiosity - a quadrupole mass spectrometer;[45-48] Cassini-Huygens – time-of-flight and quadrupole mass spectrometers;[49-51] ExoMars Mars Organic Molecule Analyzer, planned launch in 2020 – linear ion trap[52,53]), with quadrupole ion trap technologies recently taking center stage because of their high sensitivity, MS/MS capabilities, and ease of miniaturization.[28]

A key difference between the Mars missions and those targeting Enceladus, Titan, and Europa is in the sampling methodology. Whereas Curiosity and ExoMars are *rovers* which drill into the Martian surface for sampling and use laser desorption/ionization or thermal desorption

electron impact ionization to produce gas-phase ions for mass spectrometric analysis, the icy moon missions are notably different. For example, Cassini-Huygens was a *flyby* mission wherein high-velocity (relative to the spacecraft) ice grains were collected and fragmented via impact with the spacecraft's rhodium sample collector and analyzed with a time-of-flight mass spectrometer. Other small molecular ions or their impact fragments were analyzed by a quadrupole mass spectrometer. Unfortunately, because MS/MS capabilities were not implemented, no structural information could be garnered from this data, only molecular weight information. Moreover, in these missions sampling opportunities and sample availability are extraordinarily limited, even more so than rover missions. For this reason, it is imperative that the mass spectrometer collect as much *m/z* information as possible in the least possible number of scans. This can be accomplished through 2D MS/MS.

Figure 5.7 shows the 2D MS/MS spectrum of four amino acids, serine, valine, isoleucine, and methionine, using the frequency tagging technique and the micropacket technique, respectively. Known product ions from conventional product ion scanning are noted in the table in Figure 5.7 and are evident in the (b) frequency tagging product ion spectra as well as the (d) micropacket product ion spectra. Again, it is remarkable that two different encoding schemes returned almost identical product ion spectra.

| Compound (m/z) | Product Ion m/z |
|---|---|
| Serine (m/z 106) | 88, 60 |
| Valine (m/z 118) | 72 |
| Isoleucine (m/z 132) | 86 |
| Methionine (m/z 150) | 133, 104 |
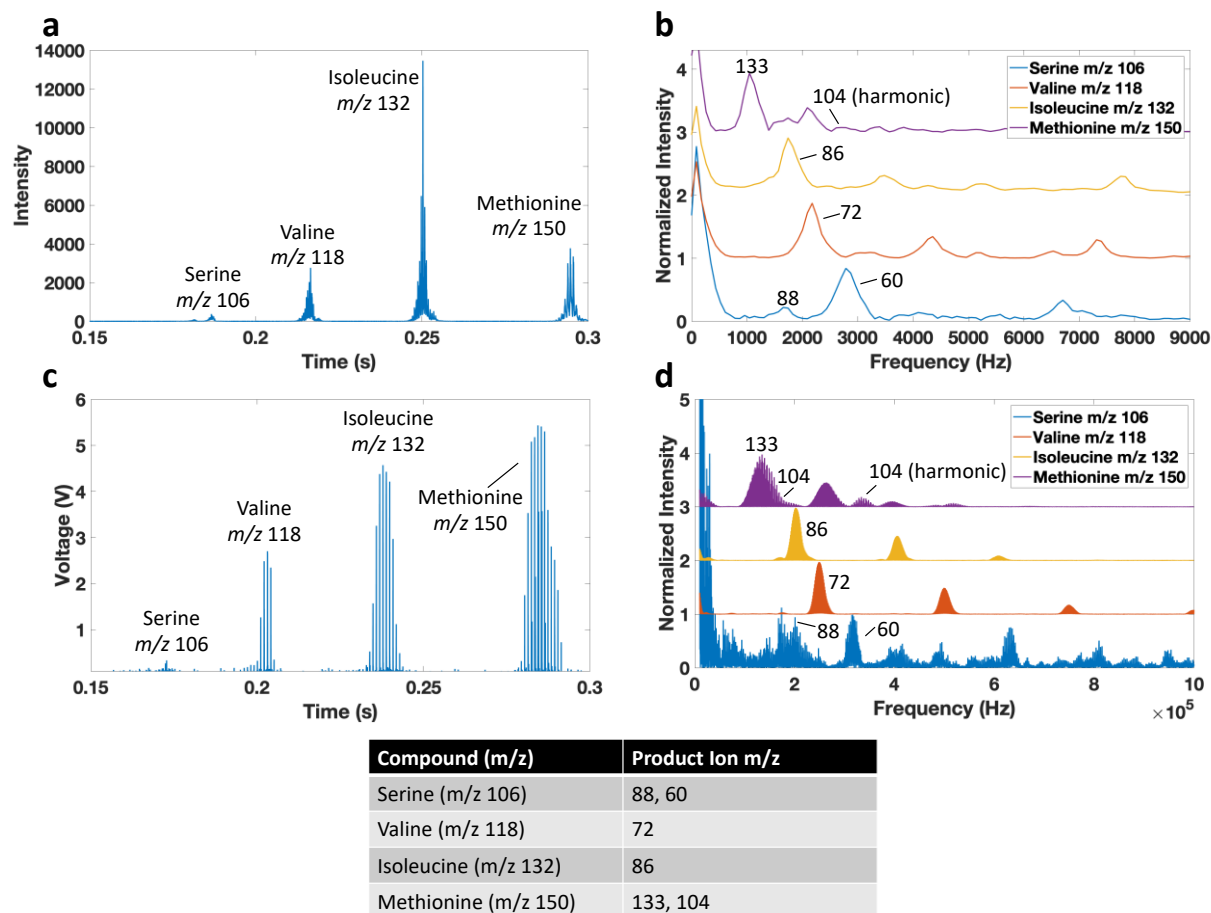
Figure 5.7. Two-dimensional tandem mass spectrometry of four amino acids on an LTQ linear ion trap. (a) Two-dimensional tandem mass spectrum as recorded at the electron multiplier detector using the 'frequency tagging' technique, (b) extracted product ion scans (in the frequency domain) obtained through FFT of each peak in panel a, (c) two-dimensional tandem mass spectrum recorded using the alternative micropacket technique, and (d) extracted product ion scans from panel c. Expected precursor and product ions are indicated in the table.  Note that all spectra in panels (c) and (d) were normalized.

## 5.3.11  Improved Product Ion Resolution

One of the primary motivations for measuring the ejection frequency of the product ions at the detector is to improve the resolution of 2D MS/MS compared to the 'frequency tagging' method. In 'frequency tagging' low kHz beat frequencies were observed in the mass spectral peaks at the detector, with mass resolutions (m/$\Delta$m) of 15 and 13 for *m/z* 91 and *m/z* 119 of amphetamine and 10 for *m/z* 163 of mdma (Figure 5.8). For *m/z* 91 and *m/z* 119 of amphetamine, much improved mass resolutions of 120 and 48 were obtained for the micropacket method, and for mdma the resolution of *m/z* 163 was increased to ~20. Because the product ions are distributed over a range

of Mathieu q values, higher mass resolution will always be obtained for the lower *m/z* product ions which have greater frequency dispersions in the ion trap than higher *m/z* ions.
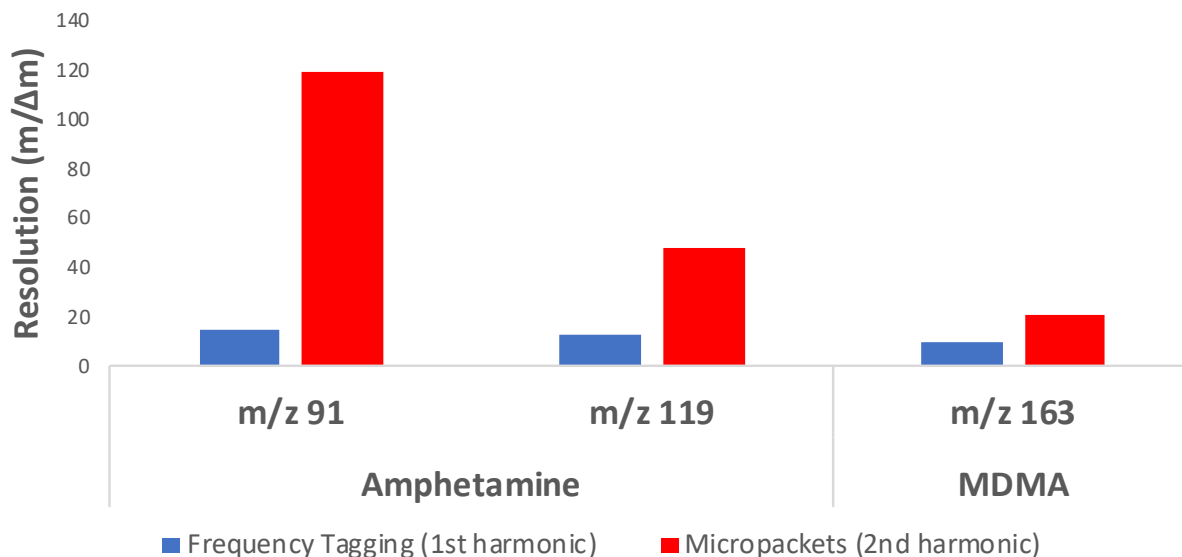


Figure 5.8. Product ion resolution comparison between 2D MS/MS using frequency tagging (blue, 1st harmonic) and the ion micropacket method (red, 2nd harmonic).

### 5.3.12 Conclusion

We have demonstrated a method of performing two-dimensional tandem mass spectrometry (2D MS/MS) in a linear quadrupole ion trap using orthogonal double resonance excitation. One method utilizes beat frequencies to modulate mass spectral peaks while the other utilizes the frequency information contained in the product ion micropackets to obtain product ion spectra. The method should be especially promising for ion traps with low acquisition rates or for cases where sample or instrument power is precious, as a single scan can be used to obtain a remarkable amount of information. These scans can then be followed by targeted data-dependent product ion scans to improve the resolution of the product ion spectra if needed.

Of course, improvements to this technology should be sought. These include minimizing the contribution of harmonics (or mitigating them during data analysis), increasing product ion resolution and mass accuracy, and seeking refinements to waveform construction, data acquisition, and analysis.

## 5.4 Supplementary Figures

Figure S5.1. Matlab program for building a frequency tagged broadband waveform for 2D MS/MS.

```
% Program for building a frequency tagged broadband waveform for use with the %
corresponding inverse Mathieu q scan

% Define variables
scan_time = .6;          % scan time in seconds
begin_q = 0.908;          % Starting Mathieu q value of the inverse q scan
end_q = 0.15;            % Ending Mathieu q value of the inverse q scan
sampling_rate = 5000000;   % sampling rate of waveform generator
rf_frequency = 1166000;     % tuned rf frequency in Hz
num_points = ceil(sampling_rate * scan_time); % number of points in waveform
time = linspace(0, num_points-1, num_points)*scan_time/num_points;
                                    % time variable
frequency_resolution = 10000; % spacing between main frequencies (Hz)
first_beat_freq_Hz = 500;    % smallest beat frequency
beat_freq_spacing_Hz = 100;    % spacing between beat frequencies
distance_from_lower_bound = 10000; % space between lower frequency bound and
                    % lowest frequency in broadband signal
                    % (Hz)
phase_fudge_factor = 0.0001;     % used for phase overmodulation to keep
                    % amplitude of waveform
                    % approximately constant with time

% Calculate Mathieu q values as a function of time
% assume sweep according to q = k / (t-j)
% The array 'q_values' tells us which precursor ion is being fragmented at
% any given time. We need to know this because the product ions of this
% precursor ion will always have frequencies higher than the precursor,
% assuming the ions are singly charged.
j = end_q*scan_time / (end_q - begin_q);
k = -begin_q*j;
q_values = k ./ (time - j);

% Calculate the frequency lower bound (i.e. the frequency of the excited
% precursor ions) as a function of time from Mathieu q
% values and rf frequency.
% We need the frequencies in the broadband waveform to always be above the
% lower bound because the product ion mass range – and thus frequency range –
% varies as a function of time (because the precursor ions are fragmented
% from low to high m/z) and thus the frequencies in the broadband
% waveform must also vary with time.
lower_bound_frequencies = zeros(num_points,1);
```

```matlab
betas = zeros(num_points,1);
for i = 1:num_points
    betas(i) = beta_calculator(q_values(i));
    lower_bound_frequencies(i) = betas(i)*rf_frequency/2;
end


% Build frequencies array
num_frequencies = floor(abs(rf_frequency/2-
lower_bound_frequencies(end))/frequency_resolution);
                % total number of frequencies in waveform
main_frequencies = linspace(rf_frequency/2,rf_frequency/2-
num_frequencies*frequency_resolution+frequency_resolution,num_frequencies);
main_frequencies = fliplr(main_frequencies);

% Add in beat frequencies to encode product ion m/z
for i=1:num_frequencies
    frequencies(2*i-1) = main_frequencies(i);
    frequencies(2*i) = main_frequencies(i) + first_beat_freq_Hz + (i-1)*beat_freq_spacing_Hz;
end
frequencies = fliplr(frequencies);

% Distribute phases so that master waveform has flat amplitude profile
phases = zeros(length(frequencies),1);
for i=1:length(frequencies)
    phases(i) = (frequencies(i)-frequencies(1))^2*scan_time/(2*(frequencies(num_frequencies)-
frequencies(1))*phase_fudge_factor);
end

% Build final waveform point by point, making sure to exclude frequencies
% below the precursor ion frequency
waveform = zeros(num_points,1);
for i=1:num_points
    for n=1:length(frequencies)
        if (frequencies(n) > lower_bound_frequencies(i) +
                              distance_from_lower_bound)
            waveform(i) = waveform(i)+sin(2*pi*frequencies(n)*time(i)+phases(n));
        else
            break;
        end
    end
end
```
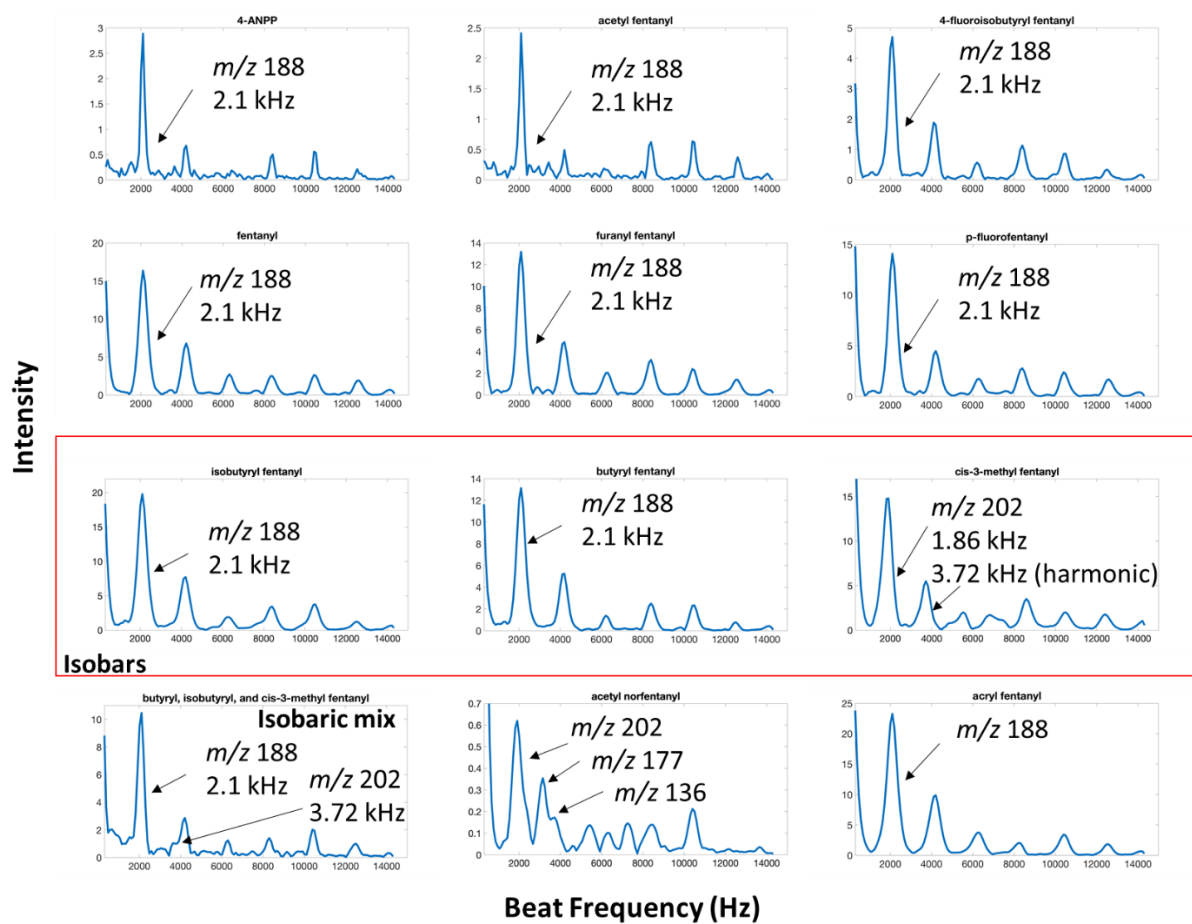
Figure S5.2. Frequency tagging spectra of various fentanyls. Peak assignments are as follows: *m/z* 136, 3.72 kHz; *m/z* 177, 3.15 kHz; *m/z* 188, 2.10 kHz; *m/z* 202, 1.86 kHz.
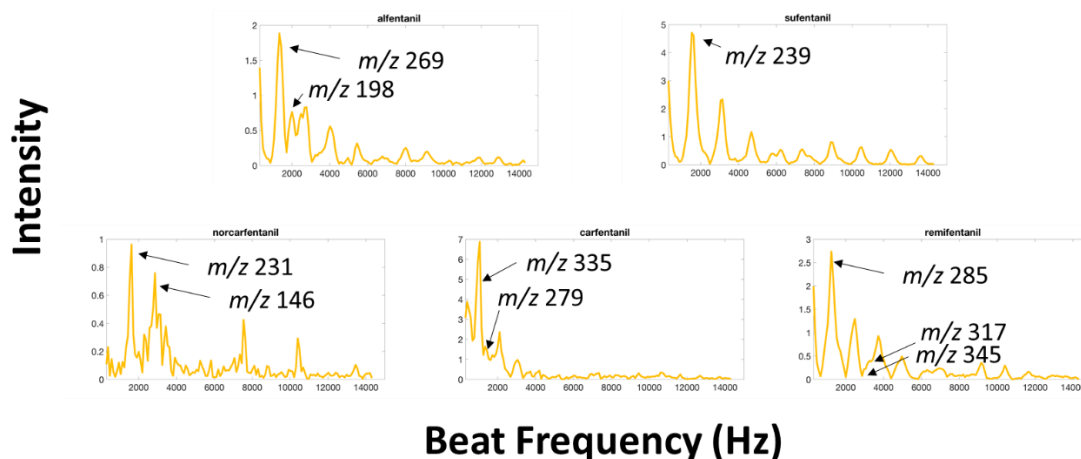
Figure S 5.3. Frequency tagging spectra of five fentanils. Peak assignments are as follows: m/z 146, 2.86 kHz; m/z 198, 2.01 kHz; m/z 231, 1.62 kHz; m/z 239, 1.53 kHz; m/z 269, 1.34 kHz; m/z 279, 1.34 kHz; m/z 285, 1.24 kHz; m/z 317, 3.25 kHz (third harmonic); m/z 335, 1.05 kHz; m/z 345, 2.96 kHz (third harmonic).
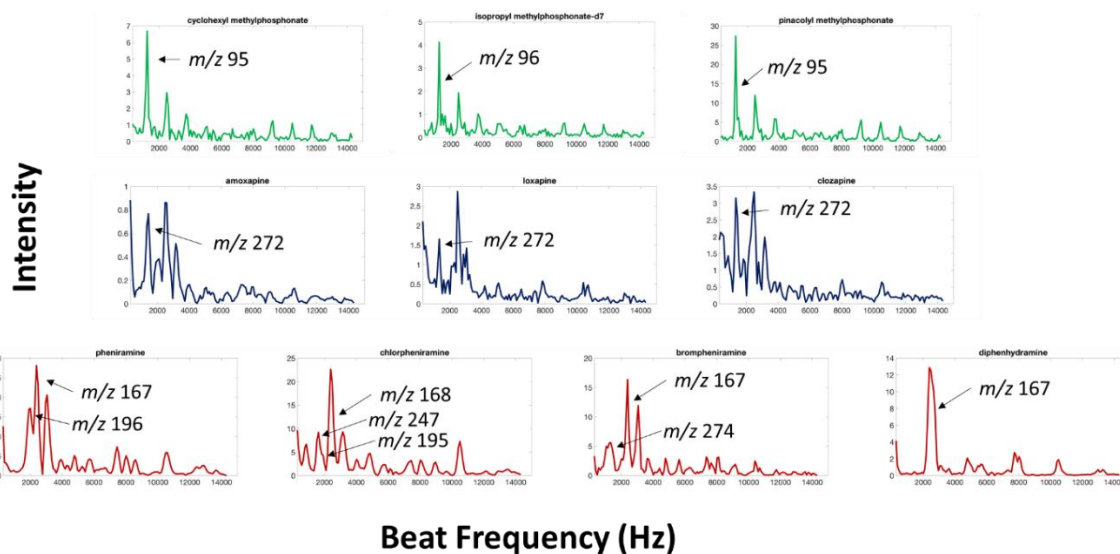


Figure S5.4. Frequency tagging spectra for (top, green) three chemical warfare agent simulants, (middle, dark blue) three tetracyclic antidepressants, and (bottom, red) four antihistamines. The chemical warfare agent spectra were obtained at a LMCO of 65 Th; other data was obtained with LMCO 100 Th. Peak assignments are as follows: m/z 95, 1.24 kHz; m/z 167 & 168, 2.39 kHz; m/z 195 & 196, 2.01 kHz; m/z 247, 1.62 kHz; m/z 272 & 274, 1.34 kHz.
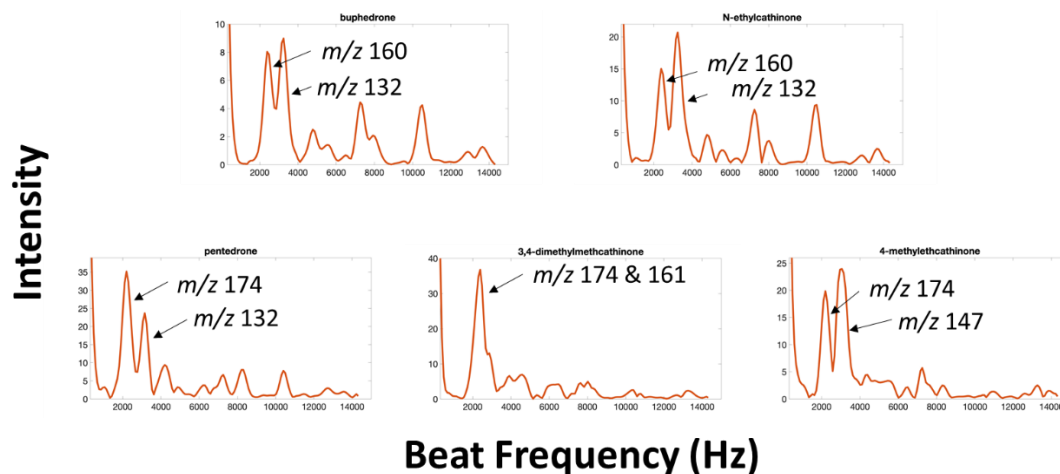
Figure S5.5. Frequency tagging spectra of sets of cathinone isobars: m/z 178 isobars (a) buphedrone and (b) N-ethylcathinone; m/z 192 isobars (c) pentedrone, (d) 3,4-dimethylcathinone, and (e) 4-methylethcathinone. Data was acquired with LMCO = 100 Th. Peak assignments are as follows: m/z 132, 3.25 kHz; m/z 147, 3.06 kHz; m/z 160 & 161, 2.386 kHz; m/z 174, 2.195 kHz.
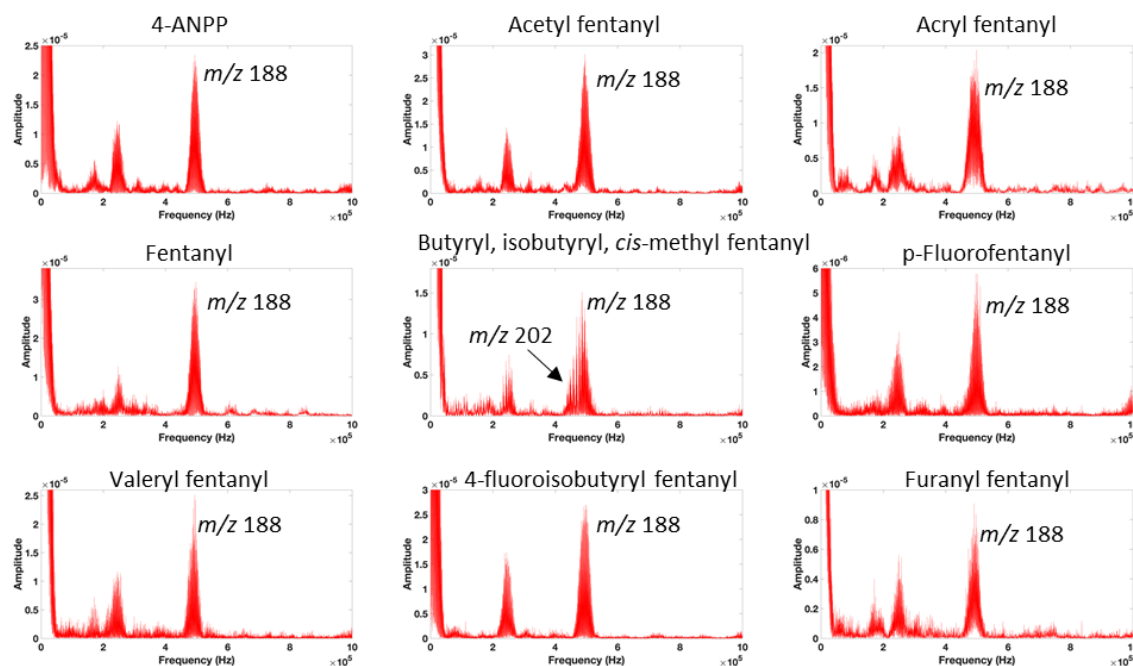


Figure S5.6. Product ion spectra (in the frequency domain) of various fentanyls using the micropacket method. Peak assignments are as follows: m/z 188, 496 kHz; m/z 202, 458 kHz.
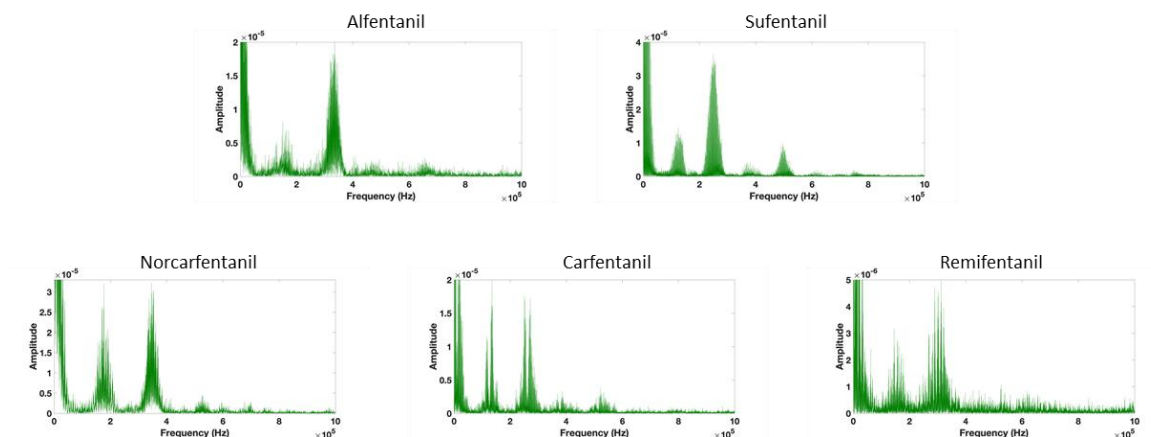
Figure S5.7. Product ion spectra (in the frequency domain) of various fentanils using the micropacket method.

## 5.5    References

(1)    Ross III, C. W., Guan, S., Grosshans, P. B., Ricca, T. L., & Marshall, A. G. (1993). Two-Dimensional Fourier Transform Ion Cyclotron Resonance Mass Spectrometry/Mass Spectrometry with Stored-Waveform Ion Radius Modulation. J. Am. Chem. Soc., 115, 7854-7861.

(2)    van der Rest, G., & Marshall, A. G. (2001). Noise analysis for 2D tandem Fourier transform ion cyclotron resonance mass spectrometry. Int. J. Mass Spectrom., 210(1-3), 101-111.

(3)    Pfändler, P., Bodenhausen, G., Rapin, J., Houriet, R., & Gäumann, T. (1987). Two-dimensional fourier transform ion cyclotron resonance mass spectrometry. Chem. Phys. Lett., 138(2), 195-200.

(4)    Guan, S., & Jones, P. R. (1989). A theory for two-dimensional Fourier-transform ion cyclotron resonance mass spectrometry. J. Chem. Phys., 91, 5291-5295.

(5)    Pfandler, P., Bodenhausen, G., Rapin, J., Walser, M. E., & Gaumann, T. (1988). Broad-Band Two-Dimensional Fourier-Transform Ion-Cyclotron Resonance. J. Am. Chem. Soc., 110(17), 5625-5628.

(6)    Agthoven, M. A., Coutouly, M. A., Rolando, C., & Delsuc, M. A. (2011). Two-dimensional Fourier transform ion cyclotron resonance mass spectrometry: reduction of scintillation noise using Cadzow data processing. Rapid Commun Mass Sp, 25(11), 1609-1616.

(7)    Chiron, L., van Agthoven, M. A., Kieffer, B., Rolando, C., & Delsuc, M. A. (2014). Efficient denoising algorithms for large experimental datasets and their applications in Fourier transform ion cyclotron resonance mass spectrometry. Proc. Natl. Acad. Sci. USA, 111(4), 1385-1390.

(8)     van Agthoven, M. A., Chiron, L., Coutouly, M.-A., Sehgal, A. A., Pelupessy, P., Delsuc, M.-A., & Rolando, C. (2014). Optimization of the discrete pulse sequence for two-dimensional FT-ICR mass spectrometry using infrared multiphoton dissociation. Int. J. Mass Spectrom., 370, 114-124.

(9)     Bray, F., Bouclon, J., Chiron, L., Witt, M., Delsuc, M. A., & Rolando, C. (2017). Nonuniform Sampling Acquisition of Two-Dimensional Fourier Transform Ion Cyclotron Resonance Mass Spectrometry for Increased Mass Resolution of Tandem Mass Spectrometry Precursor Ions. Anal. Chem., 89(17), 8589-8593.

(10)    Bensimon, M., Zhao, G., & Gäumann, T. (1989). A method to generate phase continuity in two-dimensional Fourier transform ion cyclotron resonance mass spectrometry. Chem. Phys. Lett., 157(1), 97-100.

(11)    Floris, F., van Agthoven, M. A., Chiron, L., Wootton, C. A., Lam, P. Y. Y., Barrow, M. P., Delsuc, M. A., & O'Connor, P. B. (2018). Bottom-Up Two-Dimensional Electron-Capture Dissociation Mass Spectrometry of Calmodulin. J. Am. Soc. Mass Spectrom., 29(1), 207-210.

(12)    van Agthoven, M. A., Lynch, A. M., Morgan, T. E., Wootton, C. A., Lam, Y. P. Y., Chiron, L., Barrow, M. P., Delsuc, M. A., & O'Connor, P. B. (2018). Can Two-Dimensional IR-ECD Mass Spectrometry Improve Peptide de Novo Sequencing? Anal. Chem., 90(5), 3496-3504.

(13)    van Agthoven, M. A., Barrow, M. P., Chiron, L., Coutouly, M. A., Kilgour, D., Wootton, C. A., Wei, J., Soulby, A., Delsuc, M. A., Rolando, C., & O'Connor, P. B. (2015). Differentiating Fragmentation Pathways of Cholesterol by Two-Dimensional Fourier Transform Ion Cyclotron Resonance Mass Spectrometry. J. Am. Soc. Mass Spectrom., 26(12), 2105-2114.

(14)    van Agthoven, M. A., Chiron, L., Coutouly, M. A., Delsuc, M. A., & Rolando, C. (2012). Two-dimensional ECD FT-ICR mass spectrometry of peptides and glycopeptides. Anal. Chem., 84(13), 5589-5595.

(15)    Floris, F., van Agthoven, M., Chiron, L., Soulby, A. J., Wootton, C. A., Lam, Y. P., Barrow, M. P., Delsuc, M. A., & O'Connor, P. B. (2016). 2D FT-ICR MS of Calmodulin: A Top-Down and Bottom-Up Approach. J. Am. Soc. Mass Spectrom., 27(9), 1531-1538.

(16)    van Agthoven, M. A., Wootton, C. A., Chiron, L., Coutouly, M. A., Soulby, A., Wei, J., Barrow, M. P., Delsuc, M. A., Rolando, C., & O'Connor, P. B. (2016). Two-Dimensional Mass Spectrometry for Proteomics, a Comparative Study with Cytochrome c. Anal. Chem., 88(8), 4409-4417.

(17)    Floris, F., Vallotto, C., Chiron, L., Lynch, A. M., Barrow, M. P., Delsuc, M. A., & O'Connor, P. B. (2017). Polymer Analysis in the Second Dimension: Preliminary Studies for the Characterization of Polymers with 2D MS. Anal. Chem., 89(18), 9892-9899.

(18)    Guan, S., & Marshall, A. G. (1993). Stored waveform inverse Fourier transform axial excitation/ejection for quadrupole ion trap mass spectrometry. Anal. Chem., 65(9), 1288-1294.

(19)    Guan, S., & Marshall, A. G. (1996). Stored waveform inverse Fourier transform (SWIFT) ion excitation in trapped-ion mass spectometry - theory and applications. Int. J. Mass Spectrom. Ion Processes, 157/158, 5-37.

(20)    Agthoven, M. A., & O'Connor, P. B. (2017). Two-dimensional mass spectrometry in a linear ion trap, an in silico model. Rapid Commun Mass Sp, 31(8), 674-684.

(21)    Snyder, D. T., & Cooks, R. G. (2017). Single Analyzer Precursor Ion Scans in a Linear Quadrupole Ion Trap Using Orthogonal Double Resonance Excitation. J. Am. Soc. Mass Spectrom., 28(9), 1929-1938.

(22)    Snyder, D. T., & Cooks, R. G. (2017). Single Analyzer Neutral Loss Scans in a Linear Quadrupole Ion Trap Using Orthogonal Double Resonance Excitation. Anal. Chem., 89(15), 8148-8155.

(23)    Snyder, D. T., Szalwinski, L. J., Hilger, R. T., & Cooks, R. G. (2018). Implementation of precursor and neutral loss scans on a miniature ion trap mass spectrometers and performance comparison to a benchtop linear ion trap. J. Am. Soc. Mass Spectrom., 29(7), 1355-1364.

(24)    Snyder, D. T., Szalwinski, L. J., Schrader, R., Pirro, V., Hilger, R. T., & Cooks, R. G. (2018). Precursor and neutral loss scans in an rf scanning linear quadrupole ion trap. J. Am. Soc. Mass Spectrom., 29(7), 1345-1354.

(25)    Badman, E. R., & Graham Cooks, R. (2000). Miniature mass analyzers. J. Mass Spectrom., 35(6), 659-671.

(26)    Ouyang, Z., & Cooks, R. G. (2009). Miniature mass spectrometers. Annu. Rev. Anal. Chem., 2, 187-214.

(27)    Xu, W., Manicke, N. E., Cooks, G. R., & Ouyang, Z. (2010). Miniaturization of Mass Spectrometry Analysis Systems. JALA Charlottesv Va, 15(6), 433-439.

(28)    Snyder, D. T., Pulliam, C. J., Ouyang, Z., & Cooks, R. G. (2016). Miniature and fieldable mass spectrometers: Recent advances. Anal. Chem., 88, 2-29.

(29)    Gao, L., Cooks, R. G., & Ouyang, Z. (2008). Breaking the pumping speed barrier in mass spectrometry: discontinuous atmospheric pressure interface. Anal. Chem., 80(11), 4026-4032.

(30)    Schwartz, J. C., Senko, M. W., & Syka, J. E. (2002). A two-dimensional quadrupole ion trap mass spectrometer. J. Am. Soc. Mass Spectrom., 13(6), 659-669.

(31)     Danell, R. M., Danell, A. S., Glish, G. L., & Vachet, R. W. (2003). The use of static pressures of heavy gases within a quadrupole ion trap. J. Am. Soc. Mass Spectrom., 14(10), 1099-1109.

(32)     Snyder, D. T., Pulliam, C. J., & Cooks, R. G. (2016). Linear mass scans in quadrupole ion traps using the inverse Mathieu q scan. Rapid Commun Mass Sp, 30(22), 2369-2378.

(33)     Guan, S. (1989). General phase modulation method for stored waveform inverse Fourier transform excitation for Fourier transform ion cyclotron resonance mass spectrometry. J. Chem. Phys., 91(2), 775-777.

(34)     Snyder, D. T., Szalwinski, L. J., Wells, M., & Cooks, R. G. (2018). Triple resonance excitation methods for improving the performance of ion trap precursor and neutral loss scans.

(35)     Snyder, D. T., Szalwinski, L. J., Wells, M., & Cooks, R. G. (2018). Logical MS/MS Scans: A New Set of Operations for Tandem Mass Spectrometry. Analyst.

(36)     Carette, M., Perrier, P., Zerega, Y., Brincourt, G., Payan, J. C., & Andre, J. (1997). Probing radial and axial secular frequencies in a quadrupole ion trap. Int. J. Mass Spectrom., 171(1-3), 253-261.

(37)     Snyder, D. T., Pulliam, C. J., & Cooks, R. G. (2016). Single analyzer precursor scans using an ion trap. Rapid Commun Mass Sp, 30, 800-804.

(38)     Bebinger, M. (2018). Fentanyl-laced cocaine becoming a deadly problem among drug users. NPR. Retrieved 11 April 2018, from https://www.npr.org/sections/health-shots/2018/03/29/597717402/fentanyl-laced-cocaine-becoming-a-deadly-problem-among-drug-users

(39)     Armenian, P., Vo, K. T., Barr-Walker, J., & Lynch, K. L. (2017). Fentanyl, fentanyl analogs and novel synthetic opioids: A comprehensive review. Neuropharmacology.

(40)     McBride, E. M., Keller, R. E., & Verbeck, G. F. (2018). Direct-infusion electrospray ionization-mass spectrometry profiling of fentanyl and acetylfentanyl reaction mixtures. Int. J. Mass Spectrom., 428, 55-61.

(41)     Remes, P. M., Syka, J. E. P., Kovtoun, V. V., & Schwartz, J. C. (2015). Re-print of "Insight into the Resonance Ejection Process during Mass Analysis through Simulations for Improved Linear Quadrupole Ion Trap Mass Spectrometer Performance". Int. J. Mass Spectrom., 377, 368-384.

(42)     Julian, R. K., Reiser, H. P., & Cooks, R. G. (1993). Large-Scale Simulation of Mass-Spectra Recorded with a Quadrupole Ion Trap Mass-Spectrometer. Int. J. Mass Spectrom. Ion Processes, 123(2), 85-96.

(43)     Hager, J. W. (2009). Off-resonance excitation in a linear ion trap. J. Am. Soc. Mass Spectrom., 20(3), 443-450.

(44)    Schwartz, J. C., & Louris, J. N. (1994). Method of detecting ions in an ion trap mass spectrometer (United States Patent No. 5,285,063).

(45)    Mahaffy, P. R., Webster, C. R., Atreya, S. K., Franz, H., Wong, M., Conrad, P. G., Harpold, D., Jones, J. J., Leshin, L. A., Manning, H., Owen, T., Pepin, R. O., Squyres, S., Trainer, M., & Team, M. S. L. S. (2013). Abundance and isotopic composition of gases in the martian atmosphere from the Curiosity rover. Science, 341(6143), 263-266.

(46)    Leshin, L. A., Mahaffy, P. R., Webster, C. R., Cabane, M., Coll, P., Conrad, P. G., Archer, P. D., Jr., Atreya, S. K., Brunner, A. E., Buch, A., Eigenbrode, J. L., Flesch, G. J., Franz, H. B., Freissinet, C., Glavin, D. P., McAdam, A. C., Miller, K. E., Ming, D. W., Morris, R. V., . . . Team, M. S. L. S. (2013). Volatile, isotope, and organic analysis of martian fines with the Mars Curiosity rover. Science, 341(6153), 1238937.

(47)    Vasavada, A. R., Grotzinger, J. P., Arvidson, R. E., Calef, F. J., Crisp, J. A., Gupta, S., Hurowitz, J., Mangold, N., Maurice, S., Schmidt, M. E., Wiens, R. C., Williams, R. M. E., & Yingst, R. A. (2014). Overview of the Mars Science Laboratory mission: Bradbury Landing to Yellowknife Bay and beyond. J. Geophys. Res.-Planet, 119(6), 1134-1161.

(48)    Freissinet, C., Glavin, D. P., Mahaffy, P. R., Miller, K. E., Eigenbrode, J. L., Summons, R. E., Brunner, A. E., Buch, A., Szopa, C., Archer, P. D., Franz, H. B., Atreya, S. K., Brinckerhoff, W. B., Cabane, M., Coll, P., Conrad, P. G., Des Marais, D. J., Dworkin, J. P., Fairen, A. G., . . . Team, M. S. (2015). Organic molecules in the Sheepbed Mudstone, Gale Crater, Mars. J. Geophys. Res.-Planet, 120(3), 495-514.

(49)    Waite, J. H., Lewis, S., Kasprzak, W. T., Anicich, V. G., Block, B. P., Cravens, T. E., Fletcher, G. G., Ip, W. H., Luhmann, J. G., McNutt, R. L., Niemann, H. B., Parejko, J. K., Richards, J. E., Thorpe, R. L., Walter, E. M., & Yelle, R. V. (2004). The Cassini ion and neutral mass spectrometer (INMS) investigation. Space Science Reviews, 114(1-4), 113-231.

(50)    Waite, J. H., Niemann, H., Yelle, R. V., Kasprzak, W. T., Cravens, T. E., Luhmann, J. G., McNutt, R. L., Ip, W.-H., Gell, D., De La Haye, V., Müller-Wordag, I., Magee, B., Borggren, N., Ledvina, S., Fletcher, G., Walter, E., Miller, R., Scherer, S., Thorpe, R., . . . Arnett, K. (2005). Ion Neutral Mass Spectrometer Results from the First Flyby of Titan. Science, 308, 982-986.

(51)    Postberg, F., Khawaja, N., Abel, B., Choblet, G., Glein, C. R., Gudipati, M. S., Henderson, B. L., Hsu, H. W., Kempf, S., Klenner, F., Moragas-Klostermeyer, G., Magee, B., Nolle, L., Perry, M., Reviol, R., Schmidt, J., Srama, R., Stolz, F., Tobie, G., . . . Waite, J. H. (2018). Macromolecular organic compounds from the depths of Enceladus. Nature, 558(7711), 564-568.

(52)    Brinckerhoff, W. B., Pinnick, V. T., van Amerom, F. H. W., Danell, R. M., Arevalo, R. D., Atanassova, M. S., Li, X., Mahaffy, P. R., Cotter, R. J., Goesmann, F., Steininger, H., & Team, M. (2013). Mars Organic Molecule Analyzer (MOMA) Mass Spectrometer for ExoMars 2018 and Beyond. Aerosp Conf Proc.

(53)  Li, X., Danell, R. M., Pinnick, V. T., Grubisic, A., van Amerom, F., Arevalo, R. D., Getty, S. A., Brinckerhoff, W. B., Southard, A. E., Gonnsen, Z. D., & Adachi, T. (2017). Mars Organic Molecule Analyzer (MOMA) laser desorption/ionization source design and performance characterization. Int. J. Mass Spectrom., 422, 177-187.

# CHAPTER 6.     2D MS/MS SPECTRA RECORDED IN THE TIME DOMAIN USING REPETITIVE FREQUENCY SWEEPS IN LINEAR QUADRUPOLE ION TRAPS

## 6.1    Introduction

The use of tandem mass spectrometry (MS/MS) is often central to complex mixture analysis, especially for *in situ* measurements where chromatographic separations are not practicable.[1–3] The ideal portable instrument for characterization of complex mixtures would have a single mass analyzer and would use ambient ionization for little-to-no sample preparation.[4,5] Advances in ambient ionization methods are routinely transferred from benchtop instrument to portable instruments.[6,7] By contrast, most advances in mass analyzers moved in the direction of increased instrumental complexity towards devices that cannot be easily miniaturized.[8,9] Two-dimensional tandem mass spectrometry is an experiment that has been adapted for use in high performance instruments but it is also transferable to smaller systems. Figure 6.1 summarizes the three-dimensional data domain (two dimensions of mass/charge, one dimension of ion abundance) of 2D MS/MS. It includes recording the entire 2D domain (green) as well as several common one-dimensional *m/z* experiments (neutral loss, precursor and product ion scans) and the zero-dimensional multiple ion monitoring (MRM) experiment. Acquisition of the full 2D MS/MS data domain as opposed to its sub-parts, has the potential to provide comprehensive chemical characterization of a sample in a single scan.
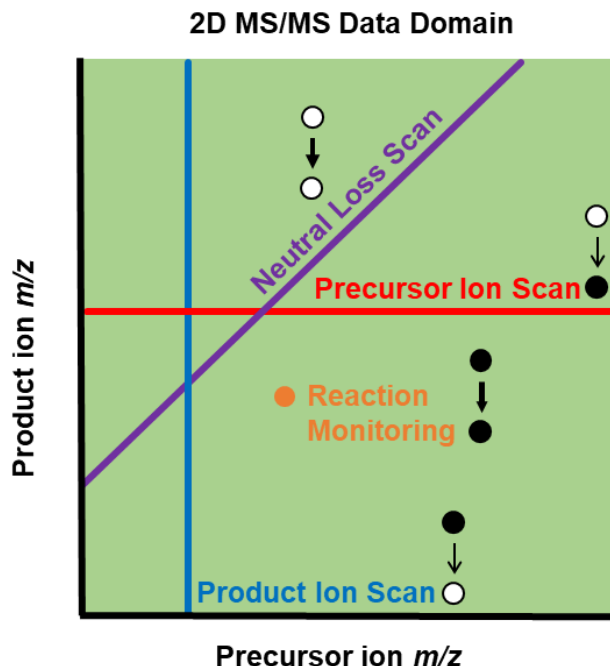
**2D MS/MS Data Domain**

Figure 6.1. Summary of MS/MS scan modes represented in the 2D MS/MS data domain. Open circles indicate variable mass while closed circle represents fixed mass. Narrow arrow indicates variable mass transition while block arrow indicates fixed or defined mass transition.

Two-dimensional tandem mass spectrometry was first demonstrated by Pfändler working with an FT-ICR instrument and using a series of timed rf pulses to excite and de-excite ions to achieve 2D FT ICR data.[10] More recent FT-ICR-based improvements in 2D-MS/MS include coupling radius dependent fragmentation methods,[11] phase correction of the signal output,[12] and rf pulse sequence optimization.[13] Recently, our group demonstrated the experimental implementation of two-dimensional tandem mass spectrometry (2D MS/MS) in a single scan of a linear quadrupole ion trap.[14,15] The FT-ICR experiment provides high resolution on a wide range of precursor ions; however, this method requires ultrahigh vacuum instrumentation, a superconducting magnet, and lengthy acquisition times.[16,17] By contrast, the quadrupole ion trap method has modest vacuum requirements and short acquisition times, albeit with reduced mass range and resolution; as such it should be best suited to implementation in the form of a miniature mass spectrometer for on-site analysis.[18,19]

The first experimental implementation of 2D MS/MS in a quadrupole ion trap used a non-linear frequency (inverse $q$ ) sweep[20] to dissociate precursor ions while a broadband signal was used to eject all fragment ions.[14] The precursor ion $m/z$ was determined from the time at which

product ions were detected and the product ion *m/z* values were determined by analyzing the frequencies present in the detected signal. The resulting signal showed distinct product ion peaks with spacings corresponding to the secular period of motion of an individual product ion (Figure 6.2a). This motion,[21] termed– "micropacket"[22] or "micromotion",[23] serves for mass analysis in the micropacket method of 2D MS/MS. Taking short fast Fourier transforms of the signal, the secular frequency of the ejected product ions can be determined and then translated to a mass/charge ratio (*m/z*) through calculation of the Mathieu $\beta$ value, hence the Mathieu *q*-value, and so by solving the Mathieu equation, to the value of *m/z*.[24,25]
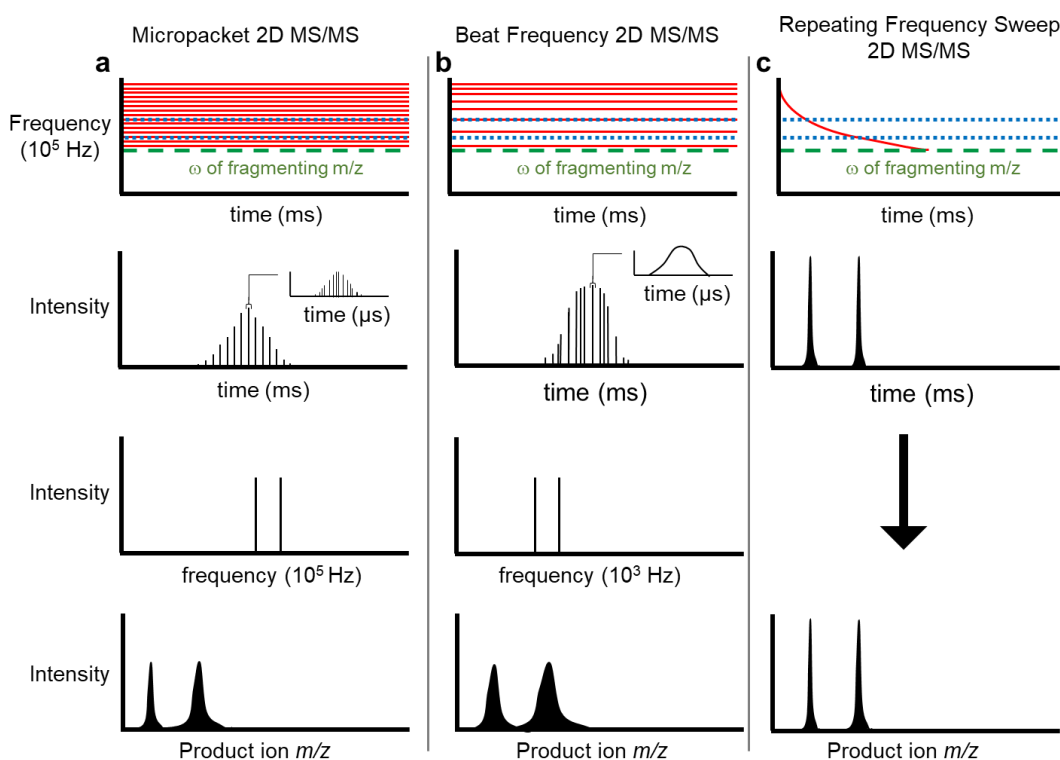


Figure 6.2. Comparison of the product ion ejection process for (a) micropacket, (b) beat frequency, and (c) repetitive frequency sweep methods of 2D MS/MS in a linear quadrupole ion trap. First row: waveform (red) and secular frequencies of product ions being analyzed (blue). Second row: signal obtained at the detector. Third row: fast Fourier transform of the detected signal. Fourth row: product ion spectra calibrated for m/z.

Most commercial ion trap detection circuits are too slow to detect ion micromotion, so a second method, frequency tagging, was implemented (Figure 6.2b).[14] In this method, each secular frequency was modulated by a unique low frequency beat. The detection circuitry was insensitive

to the high frequency signal allowing only the detected beat frequency to be observed, converted to secular frequency, and hence to *m/z* in the same fashion as in the micropacket method.

The performance of the initial micropacket method was far superior to that of the frequency tagging method of 2D MS/MS because the frequencies being measured were much higher. The measurement of higher frequencies over the same time period provided higher frequency resolution, which in turn improved mass resolution. One major disadvantage of both these methods is that the transients used for the Fourier transforms last only for hundreds of microseconds, thus limiting frequency resolution. The trade-off between frequency and time resolution is well known. This limitation can be circumvented by avoiding frequency-based methods and the associated Fourier transforms when short analysis times are desired using micropacket techniques.[26] Furthermore, difficulties in discriminating frequency harmonics, as well as the non-linear calibration, makes converting frequency to *m/z* challenging by this method. The new method presented in Figure 6.2c, avoids the need to use Fourier transforms by ejecting product ions using a non-linear frequency sweep during which the time of product ion detection is linearly correlated to its *m/z*. This allows simple *m/z* calibration as well as improving product ion mass range and resolution.

## 6.2    Experimental

### 6.2.1    Chemicals

All drugs of abuse were bought from Sigma Aldrich (St. Louis, MO) and diluted in 50:50 methanol/water containing 0.1% formic acid. The drug target mixture was diluted to 1000, 500, 400, 300, 200, 100, 50, and 25 ppb while the internal standard, methamphetamine-d5, was held at 300 ppb when determining limits of detection (LOD). Two peptides, Gly-His-Gly and Ala-Gly, were purchased from Sigma Aldrich while all others were from Bachem (Torrance, CA). The combined peptide mixture was diluted in acetonitrile to 5 ppm of each compound. The fentanyl analog mixture was diluted in methanol to a concentration of 5 ppm for each compound.

### 6.2.2    Ionization

Nanoelectrospray (nESI) was used for all experiments. Borosilicate glass capillaries (1.5mm o.d., 0.86 mm i.d.) from Sutter Instruments (Novato, CA) were pulled to 5 μm tip

diameters using a Flaming/Brown micropipette puller (model P-97, Sutter Instrument Co.). Solutions were pipetted into the capillary. An electrode holder (Warner Instruments, Hamden, CT) was used to place the tip of the capillary within 2 cm of the mass spectrometer inlet. A 1.5 kV potential was applied to generate the electrospray.

### 6.2.3   Instrumentation

A modified Thermo Finnigan LTQ mass spectrometer (San Jose, CA) was used for all experiments. This instrument was previously modified so the rf trapping voltage could be controlled externally.[27]  This allowed the rf voltage to be kept constant throughout the analytical scan to maintain the motion of trapped ions at a constant secular frequency. Additional modifications were made to apply externally controlled low voltage auxiliary waveforms individually to both the x- and y-rod pairs.[28]  Nitrogen was used instead of helium as bath gas in order to improve sensitivity.[29]  An uncalibrated ion gauge reading of $1.5 \times 10^{-5}$ torr was used in the experiments.

### 6.2.4   Waveform Generation

Two Keysight 33612A arbitrary waveform generators with 64 megasample memory upgrades (Newark element14, Chicago, IL) were separately coupled to the x- and y-electrode pairs. The waveforms were calculated in Matlab (MathWorks, Natick, MA), exported as .csv files and imported into the waveform generator software.

### 6.2.5   Time-Domain 2D MS/MS Scan Methodology

The experiment is illustrated in Figure 6.3. Two simultaneous waveforms are applied orthogonally to fragment precursor ions and eject product ions. The waveform applied to fragment the precursor ions is swept non-linearly through the ion secular frequencies in order to linearize the choice of *m/z* fragmented over time.  The second waveform, applied to the x-rod pair to eject product ions, is composed of repeating non-linear frequency sweeps. These repeated sweeps are identical in their frequency components, but the amplitude is dropped to zero during times when the applied frequency corresponds to *m/z* values higher than that of the ion being fragmented with the assumption that only singly-charged ions are being interrogated. This modulation is used to

avoid ejecting precursors before fragmentation occurs. The product ion scan rate is conserved throughout the scan while maintaining the linear time vs. *m/z* correlation in the product ion spectrum. The two-dimensional spectra are produced by splitting the signal output into segments of the same length as the product ion sweep. The product ion *m/z* is determined by the signal location within each of these segments while the precursor ion *m/z* is determined by the location of that segment within the entire scan.
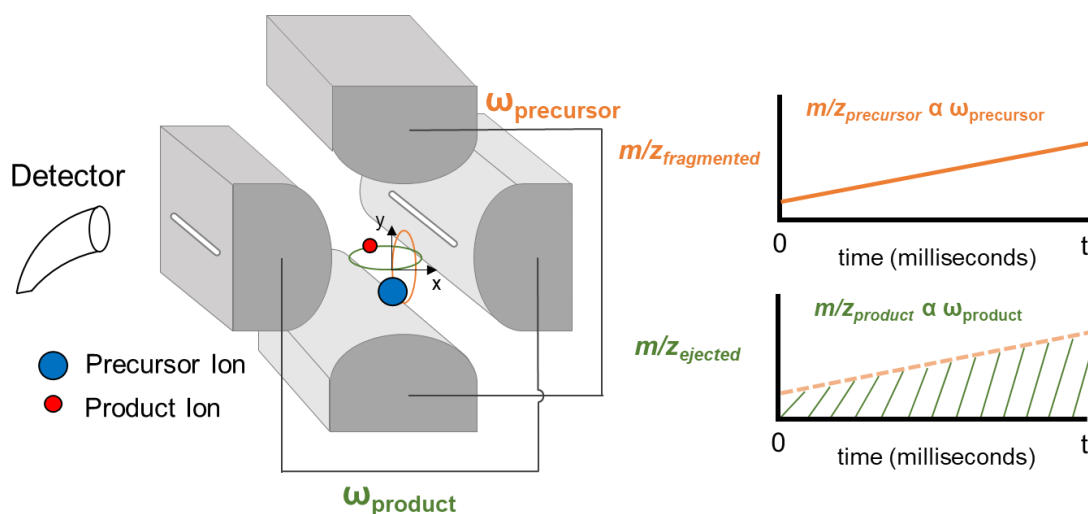


Figure 6.3. Methodology for performing time domain 2D MS/MS in a quadrupole ion trap. Precursor ions are fragmented by an auxiliary ac frequency applied to the rod pair used to create the field in the y-coordinate. The orthogonal rod pair provides a field in the x-coordinate that quickly sweeps ions into the detector as it passes through secular frequencies of the possible product ions. Product ion ejection is repeated multiple times over a single precursor m/z value in order to preserve precursor ion m/z information.

### 6.2.6   Scan and Trapping Experimental Parameters

The *m/z* range analyzed was the same for both precursor and product ions. However, the LMCO was different for each experiment. The drugs of abuse, peptides, and fentanyl analogs had LMCO values of 80, 85 and 120 Th (*m/z* units), respectively. In each experiment, ion injection times were optimized to avoid space charging while providing adequate signal. The injection times for all the above experiments were between 0.5 and 2 milliseconds and they were held constant for each experiment. For the drug and peptide mixtures, the scan time was 900 milliseconds with the product ion ejection waveform being repeated every 1.5 milliseconds. The fentanyl mixture scan time was 1200 milliseconds with the product ion ejection waveform also

being repeated every 1.5 milliseconds. The scan time for tetraalkylammonium mixture was 600 milliseconds with a product ion ejection sweep occurring every 1 millisecond. The precursor ion activation and product ion ejection time ranges were selected to provide a sufficient number of data points across each peak in both precursor and product ion dimensions. It would be assumed that slower scanning rates would improve both mass accuracy and resolution. However, both scan rates are limited to the fragmentation time of the precursor ion population. Better analytical performance would be expected if using fragmentation methods that fragments precursor ions faster. Additional time, typically 10's of milliseconds duration, was added between consecutive 2D MS/MS scans to avoid possible overlap of scans.

## 6.3 Results

This new repetitive frequency sweep version of 2D MS/MS was explored in three cases involving complex mixture analysis and to which MS/MS has been applied previously. The first two examples concern detection and identification of known analyte(s)in a complex mixture. In one case there is an emphasis on *detection* of the analytes and in the other the emphasis is on *identification* of the analytes, operating on the assumption that the requirements for detection are less stringent than those for identification. In the context of MS/MS*, detection* of a compound might be accomplished using one or two transitions (precursor to product ions) whereas compound *identification* might require four or five such transitions. The first example consists in the determination of 12 drugs of abuse in a single scan in which a single precursor/product ion transition is used to go beyond detection and identification to *quantification* of the analyte at ppb levels. The second example compares the 2D MS/MS data with data previously collected using product ion scans to identify unknown peptides in a complex mixture. Lastly, fentanyl analogs are interrogated in a single scan to identify fragmentation patterns that could be used to identify unknown analogs for which no data are currently available.

### 6.3.1 Determination of 12 drugs of abuse

The ability to determine known drugs of abuse from a complex mixture is exemplified in Figure 6.4. The drugs of interest were determined by monitoring the abundance of a single precursor/product ion transition against a precursor/product ion transition for an internal standard.

This represents the conventional method for quantitation of drugs of abuse, multiple reaction monitoring (MRM, ●➡● ) in which two or more transitions are monitored.[30] A few precursor/product ion transitions can be used to confirm the detected analyte while a single transition is used as quantifier. This "scan" is rarely used in instruments other than triple quadrupoles; however, pseudo-MRM methods have been implemented in other instruments where the single transition of interest can be extracted from a product ion scan.[31] The same method in which single transitions are extracted out of a higher dimensional spectrum is also useful for targeted drug quantification in 2D MS/MS. Acceptable quantitative performance was obtained for most of the drugs of abuse analyzed using methamphetamine-d5 as internal standard. With the single exception of 6-MAM, LOD's were 50 ng/mL or less and correlation coefficients were 0.94 or better (see Figure S6.3 for additional detail).

| # - Compound | Quantifier | LOD (ppb) |
|---|---|---|
| 1 - Amphetamine | $136 \to 91$ | $13.5 \pm 6.9$ |
| 2 - Methamphetamine | $150 \to 91$ | $15.8 \pm 4.5$ |
| 3 - MDMA | $194 \to 163$ | $5.7 \pm 1.6$ |
| 4 - MDEA | $208 \to 163$ | $5.7 \pm 1.6$ |
| 5 - Acetyl Norfentanyl | $219 \to 84$ | $20.7 \pm 25.0$ |
| 6 - Amitriptyline | $278 \to 233$ | $15.1 \pm 7.4$ |
| 7 - Hydrocodone | $300 \to 199$ | $24.3 \pm 21.2$ |
| 8 - Acetyl Fentanyl | $323 \to 188$ | $4.1 \pm 1.4$ |
| 9 - 6-MAM | $328 \to 211$ | $96.7 \pm 54.3$ |
| 10 - Fentanyl | $337 \to 188$ | $27.2 \pm 8.7$ |
| 11 - Isobutryl Fentanyl | $351 \to 188$ | $4.9 \pm 1.5$ |
| 12 - Furanyl Fentanyl | $375 \to 188$ | $30.7 \pm 12.0$ |



Figure 6.4. 2D MS/MS scan of 12 drugs of abuse quantified by a single internal standard, methamphetamine-d5 (transition m/z $155 \to 91$). The signal intensity for each transition was determined as the integrated volume of signal divided by integrated volume of the internal standard signal. Limits of detection were estimated as the analyte concentrations that would provide signal/noise ratios of 3. All samples and blanks were run in triplicate.

Note that a single transition might be sufficient for detection, but several different transitions are needed to confirm the identification of a particular analyte. Figure 6.5a shows the extracted product ion scan for precursor *m/z* 278, amitriptyline, in the 2D MS/MS scan. The similarity to the product ion scan obtained on a commercial ion trap instrument (Thermo LTQ, Figure 6.5b) demonstrates how the same fragments can be used for confirmation in the 2D MS/MS scan. The differences in relative abundances of the product ions are attributed to the use of nitrogen as a bath gas which causes additional fragmentation of the primary product ion, *m/z* 233, and to the instrumental differences that affect energy transfer and ion transmission.
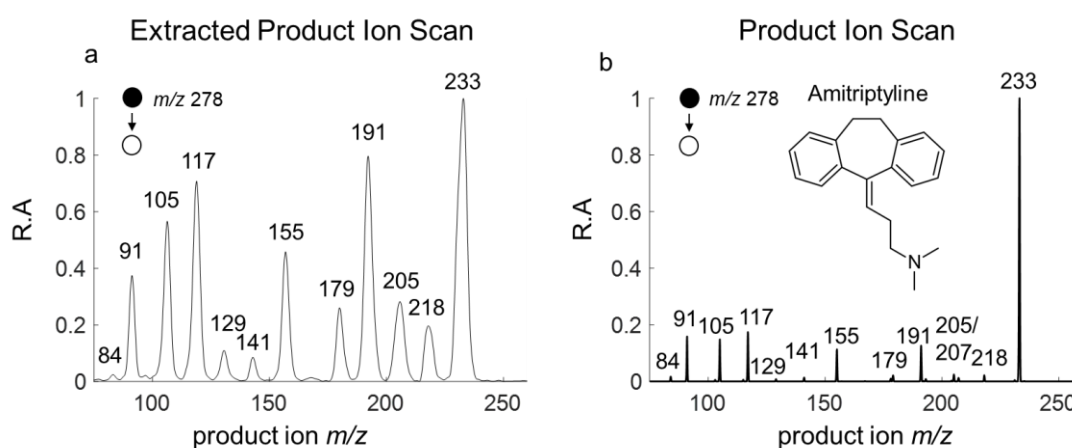


Figure 6.5. (a) Product ion scan of amitriptyline (m/z 278) extracted from the 2D MS/MS scan (b) authentic product ion scan of amitriptyline (m/z 278). Note the similarity in products but the difference in resolution. The data in (b) were recorded in 0.1 s while the data in (a) were extracted from a larger data set collected over a period of 1 second with several hundred other product ion spectra being acquired at the same time.

### 6.3.2    2D MS/MS for identification of peptides

Although Figure 6.5a shows the potential for compound identification, the canonical method for confirming the identity of an analyte is to compare the fragmentation data of the unknown to that for an authentic sample. A simple example of the application of this methodology using 2D MS/MS data is shown in Figure 6.6b where each peptide in a mixture was identified by matching its fragmentation data (extracted product ion scan) to data obtained in directly recorded product ion MS/MS scans after isolating the ionized peptide. *In silico* generation of fragment ion data could become an alternative to annotate newly acquired mass spectra quickly.[32] The comparison can be done quickly regardless of whether the data were acquired *in silico* or *in situ*,

so the main limitation is how quickly experimental MS/MS data can be obtained. Figure 6.6 demonstrates the quality of the information generated in a 2D MS/MS scan in less than a second.
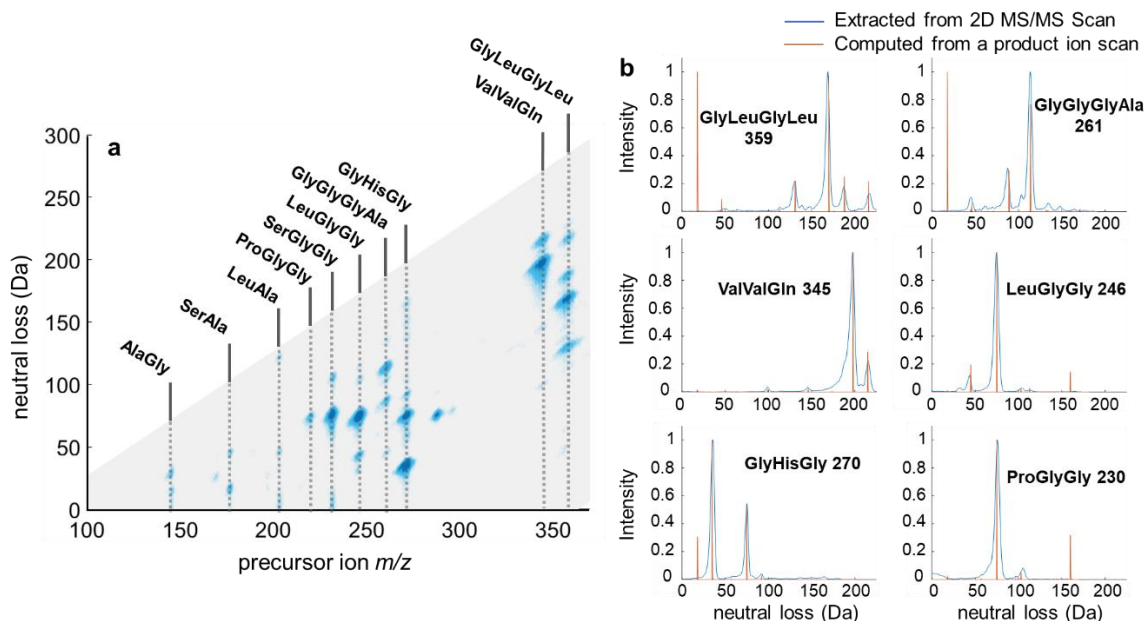


Figure 6.6. (a) 2D mass spectra of 10 small peptides showing precursor ion m/z plotted against neutral loss (instead of the more usual product ion axis) by subtracting a given product ion by its precursor ion m/z (b) comparison of the neutral losses calculated from a 2D MS/MS scan (blue) with those derived from an authentic product ion scans (orange).

This figure shows data for a mixture of 10 peptides analyzed to determine how the extracted information obtained in a 2D MS/MS scan compares to conventional ion trap product ion spectra. Peptide identification typically is achieved by sequential fragmentation along the peptide backbone. The charge is typically retained along the backbone, so identification of the amino acid sequence can be based on neutral losses observed in the spectra. For this reason, it is sometimes more convenient to observe the neutral losses for each precursor ion rather than the more usual direct observation of product ions. This is readily accomplished by subtracting the product ion *m/z* from the precursor ion *m/z* at every point in the precursor/product ion plane and replacing the normal product ion axis with a neutral loss axis. It seen in Figure 6.6a**,** peptides with N-terminal glycine all undergo a neutral loss of 75 Da (neutral glycine) and peptides with N-terminal alanine undergo a neutral loss of 46 Da (CO + H$_2$O). Furthermore, the extracted data from the 2D MS/MS scan compare favorably with ion trap product ion scans, shown in Figure 6.6b. The notable differences

being in the loss of water and the neutral loss of 160. The expected neutral loss of 160 gives a product ion, *m/z* 86 for precursor ion *m/z* 246, which lies near the low mass cut off, while a loss of water falls within the bandwidth of the frequency applied for fragmentation. This means the primary product of dehydration will be further fragmented. Figure 6.6b demonstrates that the 2D MS/MS scan captures the same depth of information obtained as the individual product ion scans. The decrease in resolution also is clear, however it does not severely limit successful matching of fragmentation patterns. This point is demonstrated in Figure S6.2 where all nine of the fragments observed in the extracted product ion scans were found also in the 2D MS/MS data with an average mass/charge error of 1.3 Th. An important point not yet considered is the efficiency with which the 2D data can be collected. A *single* product ion scan (180 milliseconds) can be recorded faster than the whole 2D MS/MS scan (900 milliseconds); however, the product ion scan acquisition time scales directly with the number of mixture components of interest, while the 2D MS/MS acquisition time is independent of that number. In the case shown in Fig S2, the 10-analyte mixture requires more than twice the time to analyze even if only the specified ten analytes are targeted. Furthermore, to generate the whole 2D MS/MS spectrum from product ion scans across the whole precursor mass range, 250 product ion scans from precursors separated by 1 Th would take 45 seconds compared to the constant 900 milliseconds for the 2D MS/MS scan.

### 6.3.3   2D MS/MS for the untargeted detection of fentanyl analogs

The detection and subsequent identification of novel fentanyl analogs is representative of a larger challenge in analytical chemistry where the *desired* list of identifiable compounds is always larger than the *known* list of identifiable compounds. Data independent acquisition (DIA) methods are well suited to identifying truly unknown analytes. Among these methods is SWATH-MS on AB Sciex instruments where multiple precursor ion isolation windows allow for "shotgun CID" in which the precursor ion is replaced by retention time and the product ion/retention time relationship allows for improved detection coverage.[33] These methods have seen widespread use due to the ability to provide extensive amounts of fragmentation data for very complex samples. There are two offsetting features to these "shotgun CID" methods of DIA. First, these methods are used in practice to identify compounds already present in libraries, they do not expand the library. Secondly, the requirement for LC is not amenable to portable instruments. A non-LC-

153

based DIA method on a portable mass spectrometer would allow *de novo* on-site identification of compounds in complex samples.

The strength of DIA using 2D MS/MS is demonstrated for the case of a complex mixture of 16 fentanyl analogs (Figure 6.7). Those analogs with names ending in -yl have a conserved phenylpiperidine moiety while those ending in -il have a conserved *N*-phenylpropanamide moiety. These conserved moieties can be detected by monitoring the charged product, *m/z* 188, for -yls and the neutral product, loss of 149 Da, in the -ils. The parent compound, fentanyl contains both functionalities and thus lies on the intersection of the neutral loss and precursor ion scan lines is this rapid class differentiation experiment. All other compounds are detected on either the neutral loss or precursor ion scan line. It would be sufficient to detect either of these transitions to signal a potential fentanyl analog but, by obtaining the full 2D data, further identification can be obtained by simply extracting the product ion spectrum from the existing data. The coupling of a method of detecting known transitions to the identification of unknown analytes is an attractive feature of 2D MS/MS. Certainly this feature will facilitate library expansion and thus forensic analysis.
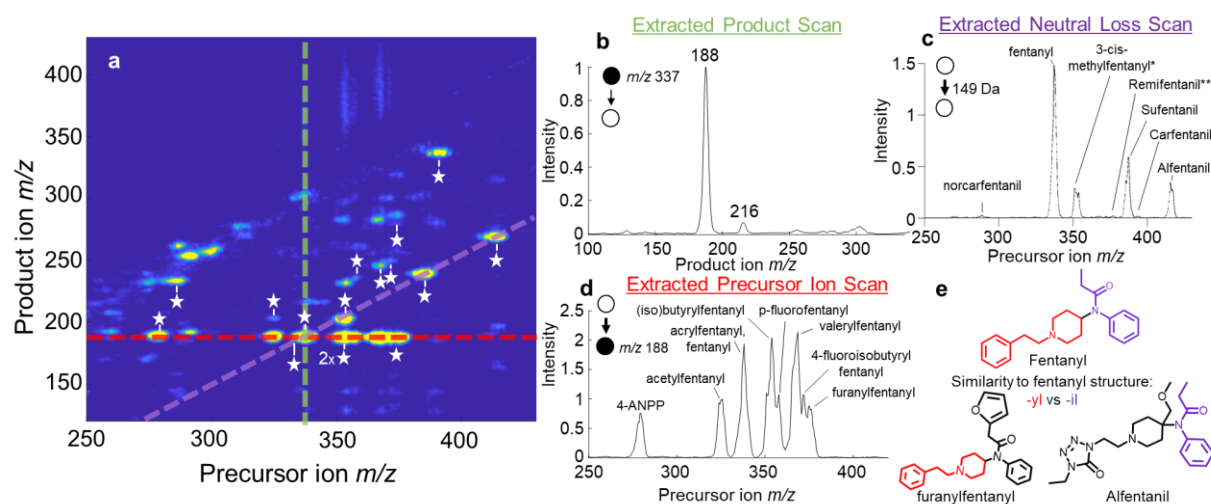


Figure 6.7. (a) 2D MS/MS scan of 16 fentanyl analogs in a mixture with extracted scans overlaid (b) extracted product ion scan of fentanyl (c) extracted neutral loss scan of 149 Da (d) extracted precursor ion scan of m/z 188 (e) structural comparison of the -yl vs -il fentanyl analogs. White stars indicate a known transition of each precursor ion analyzed. 3-Cis-methylfentanyl possesses the same conserved structural feature as the -il variants. The neutral loss of 149 Da for remifentanil is observed with a signal/noise ratio of 8 in the extracted product ion scan.

### 6.3.4    Identification of non-linear precursor/product ion relationships

The two one-dimensional $MS^2$ scans in which the product, whether charged or neutral, is conserved and these can be used to identify the corresponding precursors as belonging to a particular chemical class.  The precursor ion scan implies that the transition will produce common charged product ions for precursors of the same or similar class.  The neutral loss scan implies that the transition will produce a common neutral product molecule for precursors of the same or similar class. Both of these statements implicitly assume that addition or subtraction to the precursor molecule will produce the same addition or subtraction even in the products. Additions conserved on the charged product are expected to yield a common neutral loss while additions conserved on the neutral product yield constant product ions. This will indeed produce a linear relationship between increase of mass of the precursor and increase in mass of the product. However, this analysis does not cover all possibilities.  For example, if a precursor is modified in more than one way (besides simple addition of a functional group), then the precursor would not be seen in the 1D MS/MS scans.  An example of a chemical system not able to be related through a single 1D MS/MS scan is shown in Figure S6.4. The six tetraalkylammonium ions differ in the lengths of the four alkyl chains attached to the nitrogen center.  No conserved neutral losses or product ions are observed; however, it can be seen that these analytes do share a common functional relationship. The identification of these complex relationships in mixtures could prove useful in situations where the chemical modifications are not limited to simple additions or subtractions.

### 6.3.5    Frequency vs. Time Measurements for Product Ion Analysis in 2D MS/MS

Previous 2D MS/MS experiments using a linear quadrupole ion trap were performed using the same fragmentation waveform as done in this study but by ejecting the product ions using a sum of sines broadband waveform.[14]  The product ion information was determined from iterative fast Fourier transforms across the mass spectrum. This produced a two-dimensional mass spectrum where the product ion *m/z* was determined by the frequency components found in each FFT and the precursor ion *m/z* was determined by the time at which the FFT was recorded. This previous micropacket method[14] demonstrated the power of acquiring MS/MS data across a range of masses. This was shown specifically by identifying fentanyls in a mixture.

However, there are two main shortcomings when performing the 2D MS/MS experiment by this method and both stem from the decreased frequency dispersion at lower q-values (higher *m/z*). The first shortcoming relates to the decreased product ion mass resolution in the higher *m/z* range covered, which is caused by decreased frequency dispersion in two ways. Firstly, the product ion ejection broadband waveform will lose specificity in product ion selection with increasing *m/z*, as is the case for any ion trap method that uses ion secular frequencies for activation. This is mitigated by performing frequency scans in such a way that the frequency scan rate is varied across the mass range to make the mass scan rate constant.[20] However, applying this methodology to broadband ejection methods is not trivial. The second factor affecting resolution lies in the *m/z* calibration from frequency, as peaks of similar frequency widths will necessarily have decreased mass resolution as mass increases. These two effects result in wider peaks in frequency that are widened even further during the mass calibration.

The second shortcoming in the previous micropacket method using a broadband method for product ion analysis is that the mass range over which precursor ions can be detected in the 2D MS/MS scan is limited. Earlier, it was argued that there is a loss of resolution at higher product ion *m/z*; however, the loss in frequency dispersion also affects precursor ion measurements. The broadband waveform in the micropacket method was continuously updated during the scan to include product ions of higher mass. The highest mass product ion included in the broadband waveform in these experiments had a secular frequency not much greater (just 10 kHz) than frequencies present in the fragmentation waveform. This was done so that the product ion ejection waveform would not eject precursor ions. However, at higher precursor ion mass, the 10 kHz difference was insufficient, and precursors were ejected before fragmentation. The simple solution is to increase the separation between the two frequencies, but this results in loss of product ion mass range. A comparison between the micropacket method and this new repetitive frequency sweep is demonstrated in Figure S1. The improvement in product ion information comprehensiveness is presented in the product ion spectra extracted from this new repetitive frequency sweep (Figure S1b) and is comparable to the conventional product ion spectra (Figure S1c), whereas the extracted product ion spectra obtained by the micropacket method (Figure S1a) contains only one or two fragment ions.

## 6.4    Conclusions

A new method of performing a 2D MS/MS scan using a single mass analyzer is demonstrated. This method directly provides product ion *m/z* values from the ejection time during a product ion sweep.  This avoids the frequency/time trade-off typical of the Fourier analysis inherent in the micropacket method of 2D MS/MS.  The new method is contextualized using chemical analytes including mixtures of drugs of abuse and peptides. These examples outline the method's capability to obtain large amounts of MS/MS in very short analysis times (typically 1 second per scan). Comparisons to existing MS/MS scan modes are made by reducing the dimensionality of the 2D data *after* mass analysis to compare the data obtained by conventional methods. This data treatment is favorable to the conventional product ion scan as 100% of the data collected in that scan is shown, whereas less than 1% of the data acquired in the 2D MS/MS scans is included (since all other precursor ions are being analyzed simultaneously in this experiment).  The difference between reducing dimensionality *after* analysis versus reducing the dimensionality *before* should not be underestimated, especially in the context of *in situ* analysis of complex mixtures of unknowns.   These capabilities are expected to be most valuable in resource constrained environments. This new 2D MS/MS method provides combined detection/identification of the constituents of a complex mixture in a mass analyzer which has the potential to be miniaturized.

## 6.5 Supplementary Figures
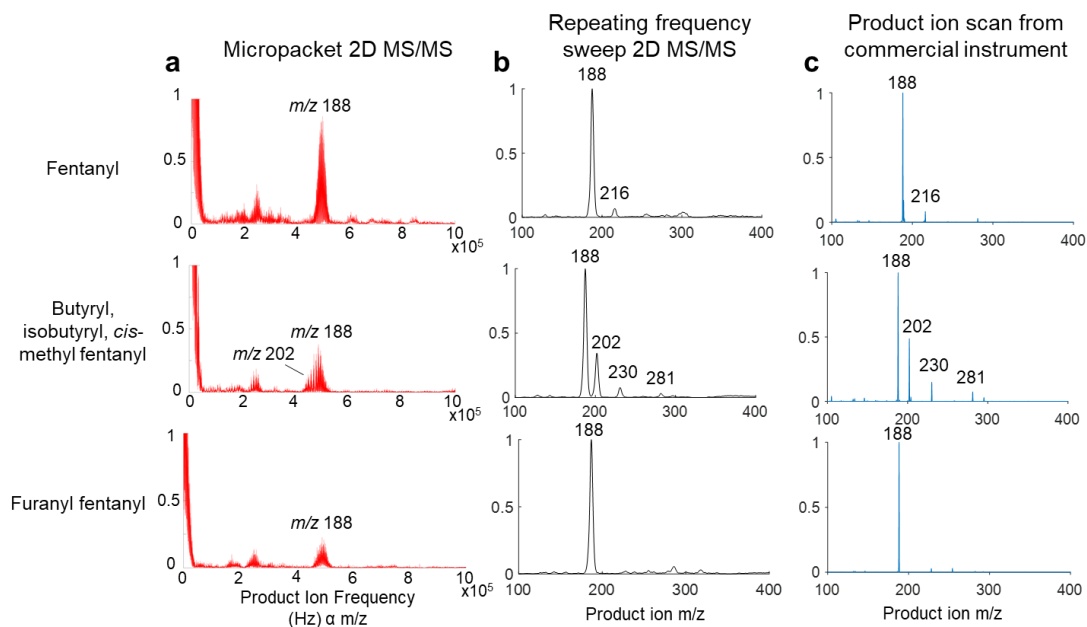


Figure S6.1. Comparison between product ion scans extracted from (a) micropacket method of 2D MS/MS, (b) repeating frequency sweep 2D MS/MS, compared to (c) a conventional product ion scan. The improvement in resolution using frequency sweeps is most apparent in the (iso)butyryl, cis-methyl fentanyl extracted spectra where m/z 202 and 188 are hardly separated in the micropacket method but are clearly separated in the repeating frequency sweep method.
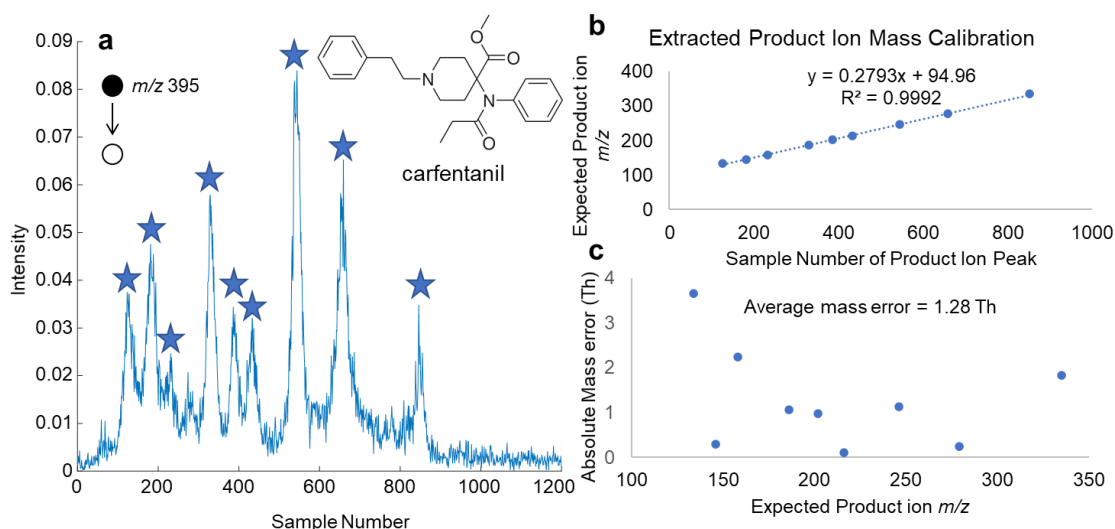


Figure S6.2. (a) Unfiltered signal detected in a single product ion sweep. (b) Calibration of sample number and product ion m/z. (c) Absolute mass error for a given product ion.
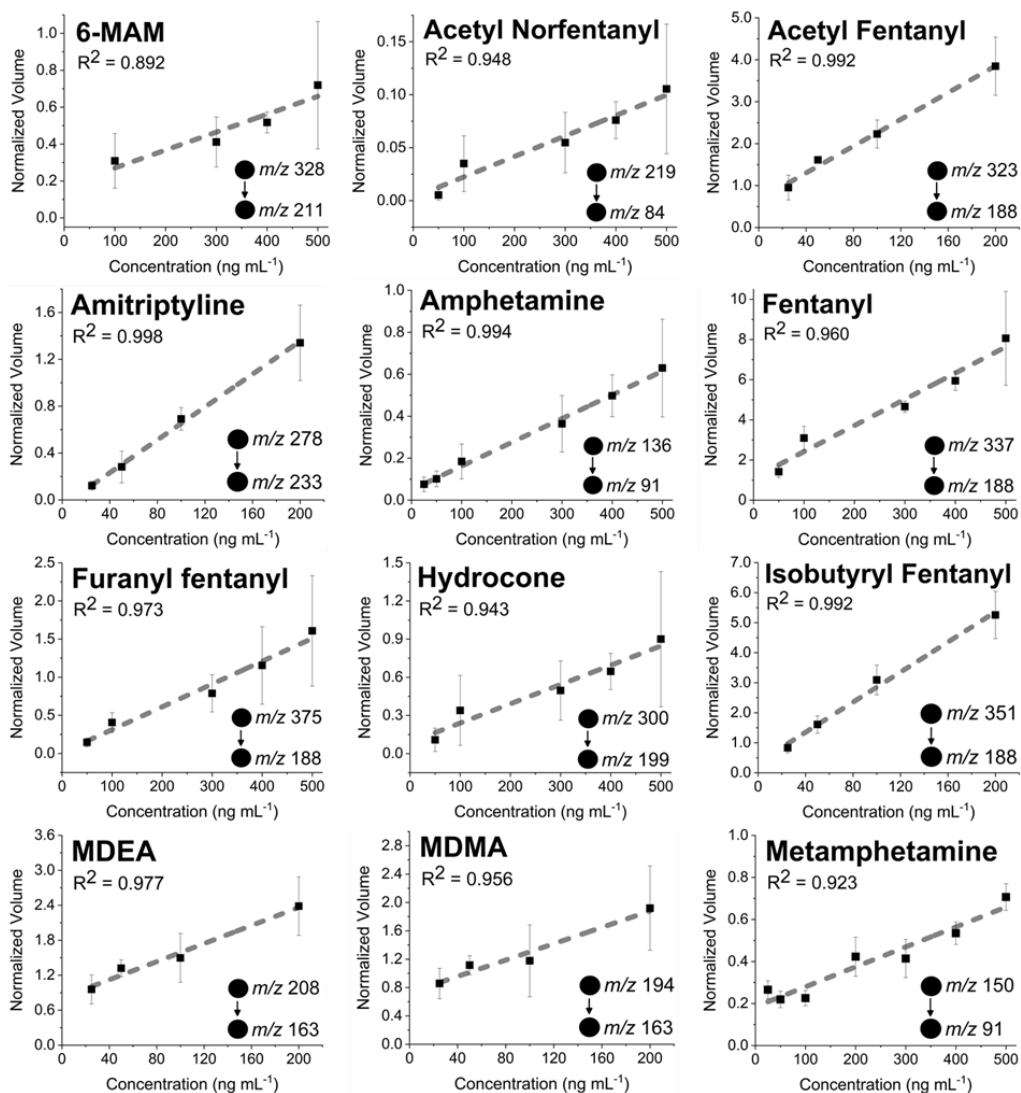
Figure S6.3. Quantification of 12 drugs of abuse. Intensities were normalized using a single internal standard, methamphetamine-d5. The signal for each transition was determined by taking the area under the surface in the 2D MS/MS spectrum. The ion injection time was the same for all concentrations which decreased quantitative performance. The product ions used for quantitation were chosen to maximize sensitivity. When peak overlap is expected, other less intense transitions can be used to prioritize selectivity, as is the case for methamphetamine.
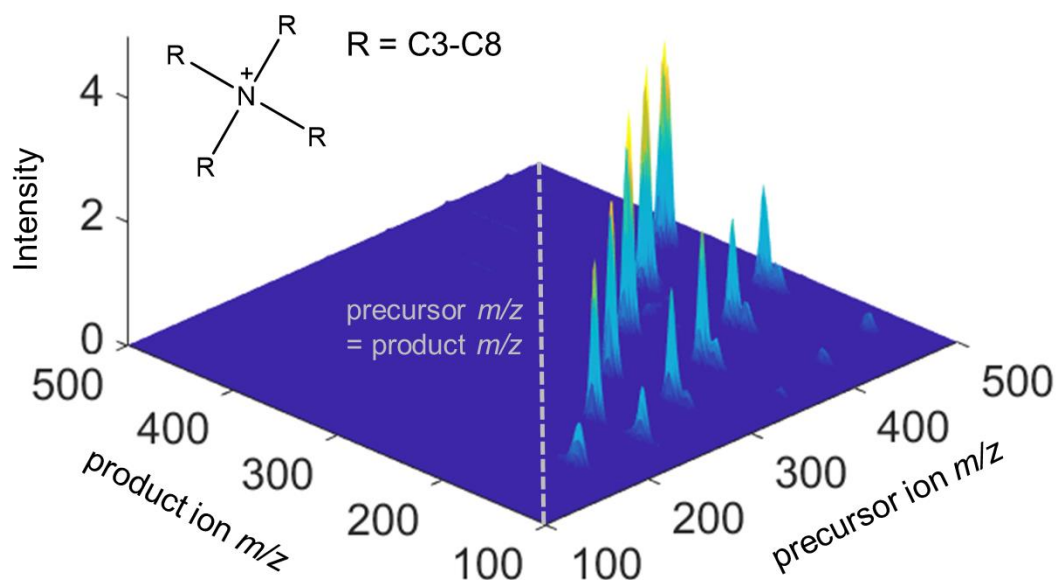
Figure S6.4. 2D MS/MS scan of 6 tetraalkylammonium cations. The six precursor ions have differing chain lengths, but since only one chain is fragmented the neutral loss is not constant for the six precursor ions.

## 6.6 References

(1)    Dowling, S.; McBride, E. M.; McKenna, J.; Glaros, T.; Manicke, N. E. Direct soil analysis by paper spray mass spectrometry: Detection of drug sand chemical warfare agent hydrolysis products. Forensic Chemistry 2020, 17, 100206.

(2)    Morato, N. M.; Pirro, V.; Fedick, P. W.; Cooks, R. G. Quantitative Swab Touch Spray Mass Spectrometry for Oral Fluid Drug Testing. Anal. Chem. 2019, 91 (11), 7450–7457.

(3)    Kerpel dos Santos, M.; Gleco, E.; Davidson, J. T.; Jackson, G. P.; Pereira Limberger, R.; Arroyo, L. E. DART-MS/MS screening for the determination of 1,3- dimethylamylamine and undeclared stimulants in seized dietary supplements from Brazil. Forensic Chemistry 2018, 8, 134–145.

(4)    Silva, L. C. da; Pereira, I.; Carvalho, T. C. de; Allochio Filho, J. F.; Romão, W.; Gontijo Vaz, B. Paper spray ionization and portable mass spectrometers: a review. Anal. Methods 2019, 11 (8), 999–1013.

(5)    Ma, X.; Ouyang, Z. Ambient ionization and miniature mass spectrometry system for chemical and biological analysis. TrAC Trends in Analytical Chemistry 2016, 85, 10–19.

(6)    Wickramasekara, S.; Kaushal, R.; Li, H.; Patwardhan, D. Paper spray portable mass spectrometry for screening of phorbol ester contamination in glycerol-based medical products. Anal Bioanal Chem 2019, 411 (12), 2707–2714.

(7)     Fedick, P. W.; Pu, F.; Morato, N. M.; Cooks, R. G. Identification and Confirmation of Fentanyls on Paper using Portable Surface Enhanced Raman Spectroscopy and Paper Spray Ionization Mass Spectrometry. J. Am. Soc. Mass Spectrom. 2020, 31 (3), 735–741.

(8)     Wilkinson, S. D.; Martin, S.; Orton, A. L.; Markandu, R.; Jones, B. C. Drug metabolite identification using ultrahigh-performance liquid chromatography–ultraviolet spectroscopy and parallelized scans on a tribrid Orbitrap mass spectrometer. Rapid Commun. Mass Spectrom. 2020, 34 (10), e8735.

(9)     Smith, D. F.; Podgorski, D. C.; Rodgers, R. P.; Blakney, G. T.; Hendrickson, C. L. 21 Tesla FT-ICR Mass Spectrometer for Ultrahigh-Resolution Analysis of Complex Organic Mixtures. Anal. Chem. 2018, 90 (3), 2041–2047.

(10)    Pfändler, P.; Bodenhausen, G.; Rapin, J.; Houriet, R.; Gäumann, T. Two-dimensional fourier transform ion cyclotron resonance mass spectrometry. Chem. Physi. Lett. 1987, 138 (2), 195–200.

(11)    van Agthoven, M. A.; Delsuc, M.-A.; Rolando, C. Two-dimensional FT-ICR/MS with IRMPD as fragmentation mode. Int. J Mass Spectrom. 2011, 306 (2), 196–203.

(12)    van Agthoven, M. A.; Kilgour, D. P. A.; Lynch, A. M.; Barrow, M. P.; Morgan, T. E.; Wootton, C. A.; Chiron, L.; Delsuc, M.-A.; O'Connor, P. B. Phase relationships in two-dimensional mass spectrometry. J. Am. Soc. Mass Spectrom. 2019, 30 (12), 2594–2607.

(13)    van Agthoven, M. A.; Chiron, L.; Coutouly, M.-A.; Sehgal, A. A.; Pelupessy, P.; Delsuc, M.-A.; Rolando, C. Optimization of the discrete pulse sequence for two-dimensional FT-ICR mass spectrometry using infrared multiphoton dissociation. Int. J Mass Spectrom. 2014, 370, 114–124.

(14)    Snyder, D. T.; Szalwinski, L. J.; St. John, Z.; Cooks, R. G. Two-Dimensional Tandem Mass Spectrometry in a Single Scan on a Linear Quadrupole Ion Trap. Anal. Chem. 2019, 91 (21), 13752–13762.

(15)    Snyder, D. T.; Demond, P. S.; Szalwinski, L. J.; Dhummakupt, E. S.; McBride, E. M.; Cooks, R. G.; Glaros, T.; Mach, P. M. Two-dimensional MS/MS scans on a linear ion trap mass analyzer: Identification of V-series chemical warfare agents. Int. J Mass Spectrom. 2019, 444, 116171.

(16)    Chiu, C. K. C.; Lam, Y. P. Y.; Wootton, C. A.; Barrow, M. P.; Sadler, P. J.; O'Connor, P. B. Metallocomplex–Peptide Interactions Studied by Ultrahigh Resolution Mass Spectrometry. J. Am. Soc. Mass Spectrom. 2020, 31 (3), 594–601.

(17)    Floris, F.; van Agthoven, M. A.; Chiron, L.; Wootton, C. A.; Lam, P. Y. Y.; Barrow, M. P.; Delsuc, M.-A.; O'Connor, P. B. Bottom-Up Two-Dimensional Electron-Capture Dissociation Mass Spectrometry of Calmodulin. J. Am. Soc. Mass Spectrom. 2018, 29 (1), 207–210.

(18)     Tang, Y.; Xu, Q.; Li, D.; Xu, W. A mini mass spectrometer with a low noise Faraday detector. Analyst 2020, 145 (11), 3892–3898.

(19)     Li, A.; Hansen, B. J.; Powell, A. T.; Hawkins, A. R.; Austin, D. E. Miniaturization of a planar-electrode linear ion trap mass spectrometer. Rapid Commun. Mass Spectrom. 2014, 28 (12), 1338–1344.

(20)     Snyder, D. T.; Pulliam, C. J.; Cooks, R. G. Linear mass scans in quadrupole ion traps using the inverse Mathieu q scan. Rapid Commun. Mass Spectrom. 2016, 30 (22), 2369–2378.

(21)     Julian, R. K.; Reiser, H.-P.; Graham Cooks, R. Large scale simulation of mass spectra recorded with a quadrupole ion trap mass spectrometer. Int. J. Mass Spectrom. Ion Processes. 1993, 123 (2), 85–96.

(22)     Remes, P. M.; Syka, J. E. P.; Kovtoun, V. V.; Schwartz, J. C. Insight into the resonance ejection process during mass analysis through simulations for improved linear quadrupole ion trap mass spectrometer performance. Int. J Mass Spectrom. 2014, 370, 44–57.

(23)     Hager, J. W. Off-Resonance Excitation in a Linear Ion Trap. J. Am. Soc. Mass Spectrom. 2009, 20 (3), 443–450.

(24)     Snyder, D. T.; Pulliam, C. J.; Cooks, R. G. Calibration Procedure for Secular Frequency Scanning in Ion Trap Mass Spectrometers. Rapid Commun. Mass Spectrom. 2016, 30 (10), 1190–1196.

(25)     March, R. E.; Todd, J. F. J. Theory of Quadrupole Instruments. In Quadrupole Ion Trap Mass Spectrometry; John Wiley & Sons, Inc. Hoboken, New Jersey. 2005; pp 34–72. https://doi.org/10.1002/0471717983.ch2.

(26)     Dziekonski, E. T.; Johnson, J. T.; Lee, K. W.; McLuckey, S. A. Fourier-Transform MS and Closed-Path Multireflection Time-of-Flight MS Using an Electrostatic Linear Ion Trap. Anal. Chem. 2017, 89 (20), 10965–10972.

(27)     Snyder, D. T.; Cooks, R. G. Single Analyzer Neutral Loss Scans in a Linear Quadrupole Ion Trap Using Orthogonal Double Resonance Excitation. Anal. Chem. 2017, 89 (15), 8148–8155.

(28)     Snyder, D. T.; Pulliam, C. J.; Cooks, R. G. Single analyzer precursor scans using an ion trap. Rapid Commun. Mass Spectrom. 2016, 30 (7), 800–804.

(29)     Snyder, D. T.; Szalwinski, L. J.; Hilger, R.; Cooks, R. G. Implementation of Precursor and Neutral Loss Scans on a Miniature Ion Trap Mass Spectrometer and Performance Comparison to a Benchtop Linear Ion Trap. J. Am. Soc. Mass Spectrom. 2018, 1–10.

(30)     Kontostathi, G.; Makridakis, M.; Bitsika, V.; Tsolakos, N.; Vlahou, A.; Zoidakis, J. Development and Validation of Multiple Reaction Monitoring (MRM) Assays for Clinical Applications. In Proteomics for Biomarker Discovery: Methods and Protocols; Brun, V., Couté, Y., Eds.; Springer New York: New York, NY, 2019; pp 205–223. https://doi.org/10.1007/978-1-4939-9164-8_14.

(31)     Xu, Z.; Jiang, T.; Xu, Q.; Zhai, Y.; Li, D.; Xu, W. Pseudo-Multiple Reaction Monitoring (Pseudo-MRM) Mode on the "Brick" Mass Spectrometer, Using the Grid-SWIFT Waveform. Anal. Chem. 2019, 91 (21), 13838–13846.

(32)     Allen, F.; Greiner, R.; Wishart, D. Competitive fragmentation modeling of ESI-MS/MS spectra for putative metabolite identification. Metabolomics 2015, 11 (1), 98–110.

(33)     Gillet, L. C.; Navarro, P.; Tate, S.; Röst, H.; Selevsek, N.; Reiter, L.; Bonner, R.; Aebersold, R. Targeted Data Extraction of the MS/MS Spectra Generated by Data-independent Acquisition: A New Concept for Consistent and Accurate Proteome Analysis. Mol Cell Proteomics 2012, 11 (6), O111.016717.

# CHAPTER 7.    NOVEL ION TRAP SCAN MODES TO DEVELOP CRITERIA FOR ON-SITE DETECTION OF SULFONAMIDE ANTIBIOTICS

## 7.1    Introduction

The rapid emergence of antibiotic-resistant pathogens has developed into a global health crisis.[1] A major contributor to the development of resistant strains is the misuse or overuse of antibiotics in agriculture and food industry. Such overuse of antibiotics in the livestock industry has resulted in strict regulations requiring the monitoring of antibiotic use. For example, the European Union has set the maximum residue limit (MRL) for sulfonamides in all food products at 100 μg/kg.[2] However, adequate food safety testing is a complex logistic operation, where samples are collected on-site, and then brought to a central laboratory for analysis. Since the great majority of those samples, fortunately, tests negative for contamination, time and resources could be saved by eliminating them at the sampling site – thus only collecting the suspect samples for further confirmatory analysis in the lab. The standard method of quantifying antibiotics in food products is extraction followed by liquid chromatography.[3,4] However, this is a time-consuming process that is not well suited to on-site measurements with portable instrumentation. In order to overcome such limitations, appropriate techniques for direct sampling of analytes with minimal sample cleanup[5] have been developed and these methods have been used on a variety of samples and have also been demonstrated on portable instrumentation.[6] However, the majority of such efforts have focused on the front side, namely ambient ionization, rather than investigating the possibilities of optimizing the subsequent mass analyzer (scan operations). Dedicated development in the scan operations is needed in order to further characterize the species generated from (ambient) ionization methods.

Ambient ionization comprises a family of methods which allow *in situ* analysis to be performed using mass spectrometers of a range of sizes.[7] Much research has been done on various ionization techniques optimizing performance for specific analyses.[8,9] The flexibility afforded by

changing many physical or chemical parameters while performing ambient ionization has given practitioners many options to tailor the ion source to maximize performance. Examples of ionization methods for antibiotic detection in complex matrixes include: electrospray ionization (ESI) for milk samples[10–12], nano-electrospray ionization (nESI) for infant formula[13], paper spray for biofluids[14], microwave plasma torch (MPT) for honey[15], and extractive electrospray ionization (EESI) for viscous cosmetic products[16], with sample preconcentration and cleanup methods, such as solid-phase microextraction (SPME)[10,11,13], solid-phase extraction (SPE)[12], or simplified extraction[14] often being necessary to compensate for the lack of chromatographic separation. Requiring minimal sample preparation and time, ambient ionization is most impactful when coupled to mass spectrometers that can be operated outside an analytical lab.

While ambient ionization is advantageous in the effort to move the analysis to the sample, it suffers from several limitations as well. The lack of sample pretreatment and separation before ionization results in a complex set of ions entering the MS all at once, reducing the selectivity of an analysis, and necessitating tandem mass spectrometry (MS/MS) operations. Moreover, in the absence of sample cleanup, ion suppression, which is known to especially influence electrospray processes can become a serious limitation.[17] While selective enrichment in ambient ionization methods can be employed to partially overcome such issues, selectivity remains a major challenge, which cannot be so easily overcome by ambient ionization alone. Therefore, it is imperative that tandem mass spectrometry be performed on-site as well. Especially valuable are scan modes that allow the analysis of a class of compounds, based on a shared product ion or common neutral loss when screening for larger families of molecules, such as the sulfonamides. Simply put, the mass spectrometer must be able to quickly determine what ionic species are of interest, based on specific fragmentation patterns. However, this poses another dilemma, which is that traditionally space-dependent tandem mass spectrometers, quadrupole mass filters, allow the most flexibility in the types of MS/MS scans available, whereas time-dependent tandem mass spectrometers, quadrupole ion traps, are best suited for miniaturization due to mild vacuum requirements and requiring only a single mass analyzer.

Previously we have demonstrated that data-independent MS/MS scans, first implemented using benchtop ion traps, can be used with miniature mass spectrometers to optimize sample use and analysis time.[18,19] These MS/MS scans are most readily coupled to miniature mass spectrometers by utilizing a discontinuous atmospheric pressure interface (DAPI) which

introduces both ions and neutrals over a small time interval in order to reduce vacuum pump requirements.[20] Instruments utilizing DAPI require significant pump-down time after sample introduction before mass analysis thereby increasing the total scan-to-scan time. Remarkably, a single low-resolution quadrupole ion trap allows implementation of precursor ion, neutral loss, and two-dimensional scans. The data-independent one- and two-dimensional scans are more time-efficient than is the traditional ion trap product ion scan when examining multiple precursor ions containing the same functional group, because product ion scans require ion isolation for each precursor ion interrogated, thereby requiring multiple ion injections. The precursor ion and neutral loss scans only require one ion injection per fragment (ionic or neutral) interrogated, as no isolation is required.

These novel ion trap scans are useful in the case of sulfonamide antibiotics, as there are two substituents that vary in this compound class. The sulfur-bonded substituent is typically a *para*-aniline functional group, while the nitrogen substituent varies depending on the specific biological activity, with the most common moieties being nitrogen containing heteroaromatics. All 17 sulfonamide antibiotics studied here contain a *para*-aniline moiety. This conserved moiety is the basis for the untargeted detection of this class of compound using MS/MS scan modes, which is therefore very suited to demonstrate the value of optimizing the MS/MS transitions for on-site detection of classes of food contaminants. The conserved moiety and how the molecules containing this moiety fall into the two-dimensional MS/MS data space are shown in Figure 7.1. It should be noted that combinations of one-dimensional MS/MS scans are also useful, as demonstrated previously.[21] Logical operations can be performed by combining scans, in particular, the AND/OR operation can be performed by simultaneously performing two scans.[22] These simultaneous scans can be tailored for certain analytes and in this study, we show how combinations of scans, specifically (i) two precursor scans and (ii) a precursor and a neutral loss scan can be tailored to prioritize quantitative precision or detection limits, respectively. The latter combination scan, because of its lower detection limit using benchtop instrumentation, was then implemented on a miniature mass spectrometer to demonstrate the feasibility of detection such antibiotics on-site at concentrations of practical significance.
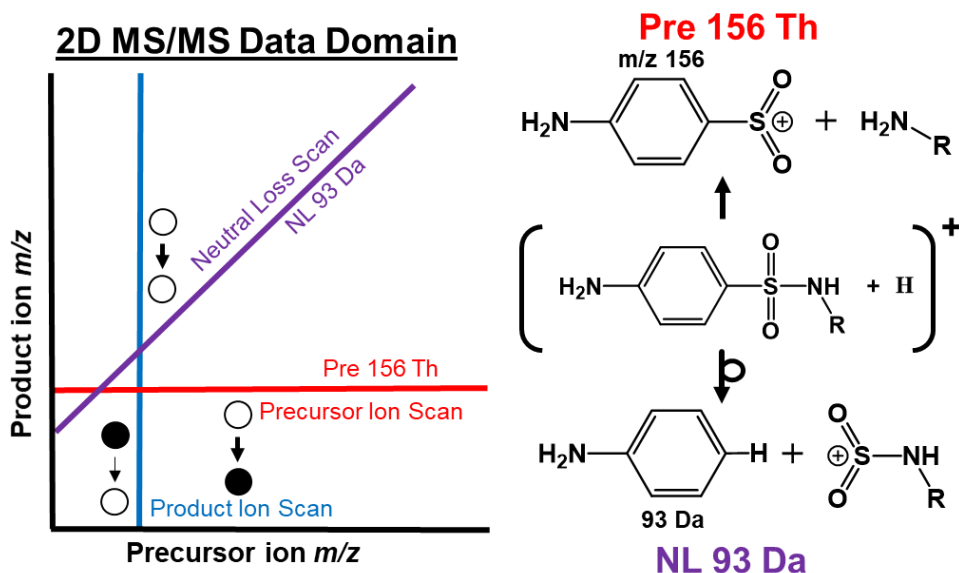
Figure 7.1. 2D MS/MS data domain with one-dimensional scan lines depicted. Also shown are the routes to two common fragments of p-aniline sulfonamides: neutral loss (NL) 93 Da or formation of product ion m/z 156.

## 7.2 Experimental

### 7.2.1 Chemicals

Sulfadiazine, sulfamerazine, sulfamethizole, sulfamethoxazole, sulfamethoxypyridazine, sulfapyridine, sulfaquinoxaline, sulfathiazole, dapsone, sulfisoxazole, sulfamonomethoxine, sulfadimethoxine, sulfamoxole, sulfacetamide, sulfaphenazole, trimethoprim, sulfadimidine and sulfachlorpyridazine were provided by Riedel de Haen (Seelze, Germany), the isotope labeled sulfadimethoxine-d6 were purchased from Sigma-Aldrich (St. Louis, US), the isotope labelled dapsone-d8 from Toronto Research (Toronto, ON, Canada) sulfapyridine-$^{13}$C6, sulfamerazine-$^{13}$C6, sulfamethizole-$^{13}$C6, sulfamethoxypyridazine-d3, sulfachlorpyridazine-$^{13}$C6, sulfisoxazole-$^{13}$C6, and sulfaquinoxaline-$^{13}$C6 were purchased from Witega (Berlin, Germany). Each sulfonamide was diluted in methanol to create stock solutions at 1 mg/mL. For the 2D MS/MS scan, three mixtures containing ten sulfonamides each, whose light-isotope structures and precursor m/z values can be found in the Supporting information (SI, Figure S7.1 and Table S7.1, respectively), were diluted to 1 μg/mL in 1:1 MeOH:$H_2O$ and 0.1% formic acid. For quantitation by simultaneous precursor ion scans, five sulfonamides, sulfapyridine, sulfamerazine, sulfadimidine, sulfaquinoxaline, and sulfadimethoxine, were combined and diluted to 1000, 800,

600, 400, 200, 100, and 50 ng/mL in a 1:1 MeOH:H$_2$O and 0.1% formic acid solution containing the corresponding isotopically labeled internal standards at 400 ng/mL. A significant degradation of the analytes, identified by a strong decrease in ion signal, was observed over the course of a day, so further experiments were performed using acetonitrile as solvent (i.e. the five sulfonamides were diluted to working concentrations by diluting stock solutions of the mixtures in acetonitrile). Fresh solutions were prepared daily.

### 7.2.2 Instrumentation

The modified Finnigan LTQ mass spectrometer (San Jose, CA) and modified Mini 12 mass spectrometer capable of performing single-analyzer MS/MS scans have been described previously.[18,23] The precursor ion and neutral loss scan mode have been previously implemented in one of two possible configurations in a quadrupole ion trap where the radio frequency (RF) trapping voltage is either constant[24,25] or varied[26,27]. For the scan modes demonstrated here, the RF trapping voltage must be kept constant so that ions maintain a constant secular frequency throughout the scan. This is accomplished in the benchtop LTQ instrument by substituting the instrument's RF voltage control with an external waveform generator. This implementation does not have any feedback and results in a slight drift in the output RF voltage. The voltage drift results in an ion having slightly different secular frequencies throughout the experiment. Frequent calibration and re-optimization therefore is required for optimal performance. The miniature mass spectrometer has active RF voltage feedback resulting in far less drift, so no re-optimization was required. Both instruments have been previously modified so that external waveform generators can be inductively coupled to the x- and y-rod pairs of the ion trap. The bath gas in the modified LTQ was nitrogen while the miniature instrument used the air introduced during ion introduction when the DAPI valve was open.

Nano-electrospray ionization was accomplished by pipetting a liquid sample into a borosilicate glass capillary (1.5 mm o.d., 0.86 mm i.d.) from Sutter Instrument Co. pulled to a 5 μm tip diameter by a Flaming/Brown micropipette puller (model P-97, Sutter Instrument Co.). The loaded tip is then placed in a nano-spray electrode holder (model ESW-M15P Warner instruments, Hamden, CT). A 1.5 kV potential is applied to the electrode holder with the tip of capillary placed ~1 cm away from the mass spectrometer inlet to generate nano-electrospray. Paper spray mass spectrometry was accomplished by applying 5 μL of diluted solutions in the center of a Whatman

1 (Fisher Scientific) paper substrate with an isosceles triangle geometry with a width of 1.5 cm and 2 cm long. The paper substrate was held 5 mm away from the mass spectrometer inlet by stainless-steel alligator clip (CAL-HAWK) and allowed to dry. Electrospray was generated by the application of 45 μL of 9:1 ACN:$H_2O$ to the back of the paper substrate and a potential of 3.5 kV to the attached alligator clip. Copper alligator clips were avoided as the presence of copper/acetonitrile adducts were observed in the mass spectrum.

### 7.2.3 Scan Modes

In order to perform single analyzer MS/MS scans, the ion trap was operated at constant RF voltage to allow ions to maintain a constant secular frequency.[28] The ions can be resonantly excited in either x- or y- dimension by applying an auxiliary waveform containing their particular secular frequencies. The resonant ions can be ejected or fragmented by increasing or decreasing the applied amplitude of the applied ac waveform, respectively. A fragmentation waveform that results in a linear mass/time calibration was created in a previously described MATLAB program.[28] This waveform is applied across the y-electrode pair (Figure 7.2) and it slowly fragments precursor ions of increasing *m/z* over the entire scan. The resulting product ions can then be rapidly ejected for detection by applying another waveform to the orthogonal rod pair (Figure 7.2). The combination of precursor and product ion fragmentation/ejection waveforms determines which of the MS/MS scans is being performed. A precursor ion scan uses a fixed ejection frequency resulting in a single product ion being continuously ejected throughout the scan.[25] Ions are detected when a precursor ion is fragmented to produce an ion whose secular frequency matches the applied ejection frequency. Neutral loss scans are performed by applying the same waveform for ejection as that used for fragmentation but with a fixed time offset so that a fixed mass offset is established.[29] An additional waveform is applied in the time between the fragmentation and ejection waveform so that unfragmented precursors are not detected. The 2D MS/MS scan is done by rapidly sweeping through all possible product ion frequencies and iterating this sweep continuously to preserve precursor/product ion relationships.[23] The observed output is spliced into individual product ion sweeps and those individual sweeps are combined into a single matrix in MATLAB. The simultaneous combinations of scans were accomplished by applying product ion ejection waveforms at the same time as those corresponding to the individual MS/MS scans.[21]
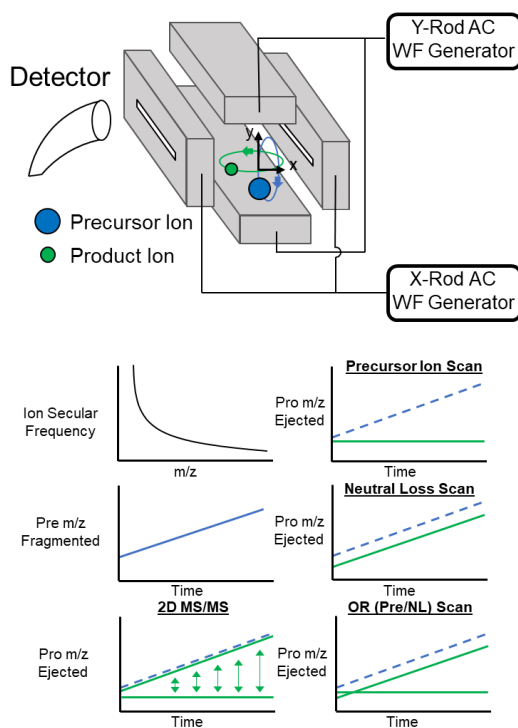
Figure 7.2. Orthogonal double resonance performed using a rectilinear ion trap. The y-rod waveform generator is used to successively fragment precursor ions of increasing m/z value while the x-rod continuously ejects either a constant m/z (precursor ion scan) or constant mass offset (neutral loss scan). To record the 2D MS/MS spectrum the waveform applied to the x-rod pair was continuously swept over the possible product ion mass range while that applied to the y-rods was incremented. The OR scan is performed by combining individual precursor ion / neutral loss waveforms.

## 7.3    Results and Discussion

### 7.3.1    Discovery of diagnostic transitions by 2D MS/MS

Data-independent MS/MS scan modes require a characteristic fragment that can be used to identify a particular functional group. If the characteristic fragment retains a charge, it can be observed with a scan of a single product ion. If instead the charge resides within the non-specific fragment, the characteristic neutral fragment can be observed in the neutral loss scan (constant mass difference between the detected product ion and the fragmented precursor ion). The location of the charge site for an ionized analyte with many functional groups is dependent on thermochemical properties of the various charge sites.[30,31] The charge site location can influence the fragmentation pattern determining if the characteristic fragment is charged or neutral.[32] Rearrangements during fragmentation can further complicate assessing where charge is retained.[33]

170

In order to determine the nature and distribution of characteristic fragment ions for various antibiotics, three mixtures of sulfonamides, and their corresponding isotope labeled standards, were interrogated using the 2D MS/MS scan in which all precursor ions and their subsequent product ions are detected. The three 2D MS/MS spectra obtained are shown in Figure 7.3. The characteristic fragments for the sulfonamides are seen in the 2D MS/MS spectrum are aligned horizontally and diagonally, representing conserved charged and neutral fragments, respectively. The fragment that was obtained for all sulfonamides, and thus has the highest diagnostic value, was that due to cleavage of the sulfur-nitrogen bond to form product ions $m/z$ 156 (Figure 1) for light-isotope sulfonamides, and larger product ions for heavy-isotope standards depending on the location of the heavy isotopes. The second most commonly occurring fragment was due to the neutral loss of 93 Da, which corresponds to dissociation at the sulfur-carbon bond. This fragmentation pathway involves a rearrangement requiring a proton transfer to form neutral aniline (93 Da). The appearance of this neutral loss competes with other previously observed rearrangements such as the neutral loss of 66, $H_2SO_2$, and the formation of product ion $m/z$ 108, which requires breaking a sulfur-oxygen bond and the formation of a carbon-oxygen bond.[34] Interestingly, for three pyrimidine sulfonamides, each addition of a methyl group increases the likelihood of fragmenting to form neutral aniline over p-aniline sulfonyl cation, viz. the fragment resulting from neutral loss of 93 Da versus the product ion $m/z$ 156 (Figure S7.2).
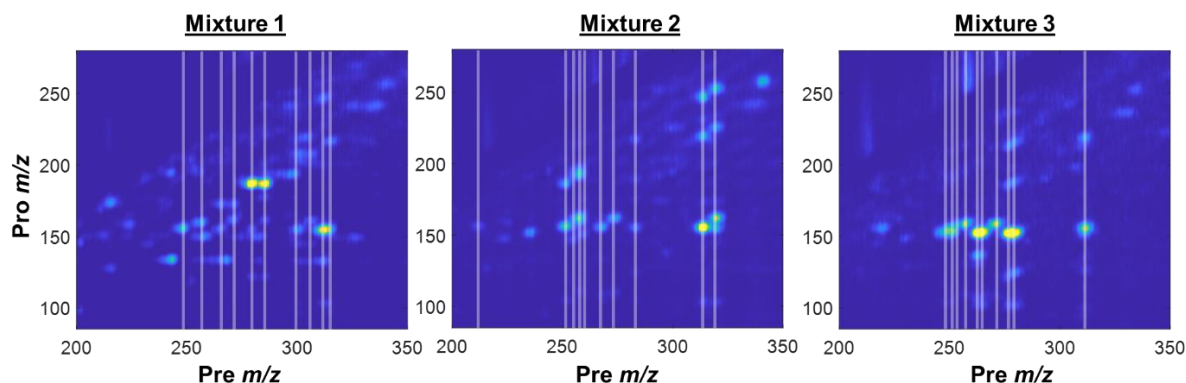


Figure 7.3. 2D MS/MS scan recorded using the benchtop instrument for three 10-component sulfonamide mixtures, each at 1 µg/mL. The spots are aligned to form horizontal and diagonal lines which correspond to precursor ion scan lines (constant product (Pro) values) and neutral loss scan lines, respectively. Vertical lines added to the figure indicate predicted m/z values for [M+H]+ product ion scans (constant precursor (Pre) values) of each of the ten components. The composition of each mixture can be found in SI, Table S7.1.

### 7.3.2 Two-dimensional scan performance

The 2D MS/MS scan provides a comprehensive view of the ionic landscape, but the data suffers from poorer mass resolution compared to traditional ion trap product ion scans. The composition of the mixtures shown in Figure 3 was chosen to decrease spectral overlap of sulfonamide precursor ions. In real samples, higher resolution may be required in order to improve specificity. In order to improve mass selectivity, the mass scan rate can be decreased by reducing the mass range, while keeping the scan time constant, or by acquiring the same mass range over a longer time period. The extreme case of this is by reducing the mass range so that a single $m/z$ is being monitored, in other words, a reduction in mass dimensionality.

In order to assess the tradeoff between mass dimensionality and mass resolution, a comparison between an extracted precursor ion scan and the equivalent single-analyzer precursor ion scan is shown in Figure 7.4b. The peaks obtained in the one-dimensional scan are better resolved than the equivalent peaks extracted from the 2D MS/MS scan. Specifically, the full width at half-maximum (FWHM) of precursor ion $m/z$ 250 is 4.5 in the 2D MS/MS scan and 1.6 in the precursor ion scan. The difference in mass resolution is due to the fact that the 2D MS/MS scan must be performed in on approximately 250 possible product ion $m/z$ values in 1.5 milliseconds whereas the precursor ion scan devotes that time on a single $m/z$ value. In certain analyses, the greater mass resolution of the precursor ion scan would be more useful even at the cost of loss of additional MS/MS information. The sulfonamide analytes being monitored are expected to be found in many different food products which contain very different chemical interferents. The difference in chemical complexity dictates that a mass spectrometer be able to operate in multiple configurations.
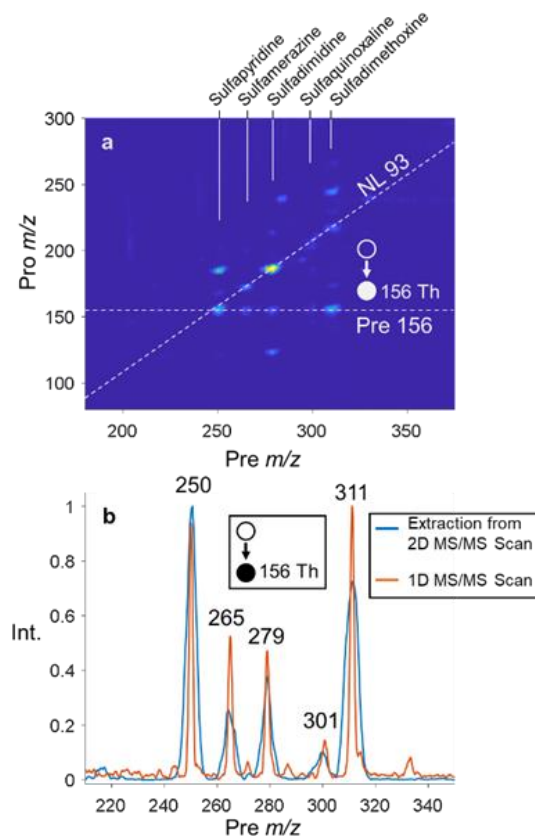
Figure 7.4. (a) 2D MS/MS spectrum of five sulfonamides with Pre and NL scan lines overlaid. (b) Comparison of the extracted precursor ion scan (blue) and 1D precursor ion scan (orange) for product ion m/z 156. Both (a) and (b) were acquired from a benchtop ion trap mass spectrometer.

### 7.3.3 Simultaneous one-dimensional scan modes

The combination of multiple MS/MS scans provides flexibility in detecting multiple product ions belonging to the same chemical class. The detection of all the sulfonamides is accomplished using the characteristic *m/z* 156 product ion. However, the carbon-13 labeled standards used to quantify the sulfonamides do not fragment to the same product ion *m/z* as the light-isotopologues. Instead, these labeled standards fragment to product ion *m/z* 162. Traditional analysis would require an additional scan to record the internal standard thereby doubling the analysis time. Furthermore, by detecting the standard and analyte in separate ion injections, fluctuations in ion current can decrease quantitative precision which are common in ambient ionization. By combining two precursor ion scans for the common product ions of both the analyte and internal standard, better quantitative performance would be expected.

173

The quantification of five sulfonamides by the simultaneous precursor scan for *m/z* 156 and 162 is shown in Figure 7.5. The analyte signal is normalized using the intensity of the internal standard to correct for deviations in the spray current. After normalization to the internal standard intensity, the R-squared coefficients of the linear regression models improved on average 12% for the five analytes (Table S7.2). However, large sample-to-sample variation was observed across the three calibration sets evaluated. This was reflected in an adequate linear response within each calibration set, but significant variation in the signal intensity for both analytes and internal standards across different sets. The variation was attributed to a drift over time in the amplitude of the voltage used to trap ions. This drift results in ions having slightly different secular frequencies and not being completely in resonance with the frequency used to eject product ions, thereby decreasing ejection efficiency, and lowering sensitivity. One solution to this problem is to further improve the modified instrument's electronics to minimize the error in the output voltage. A more immediately accessible approach is to normalize each measurement to the average response of the internal standard across each of the three replicates. As expected, this second normalization has no significant effect on the linearity of the response, but it does decrease the relative standard deviation calculated across replicates by 15% (in average for the five analytes and all the calibration standards), compared to non-normalized data (Table S7.2). It should be noted that by detecting an additional product ion, it is possible to detect interferents that would otherwise not be detected, thus decreasing specificity. This operation is considered a simultaneous OR scan because the intensity observed for each m/z can come from one product ion *or* the other product ion. If the intensities attributed from either product ion can be obtained, it is possible to include more sophisticated logical operations such as the AND, XOR (exclusive OR), and BUT NOT scans.
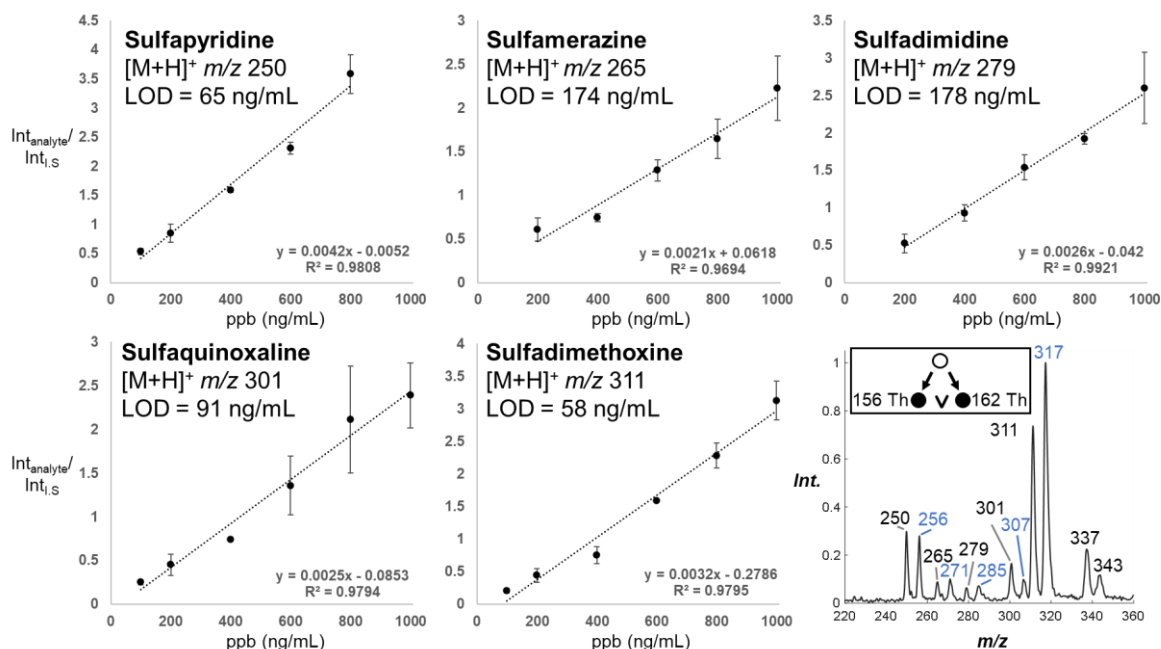
Figure 7.5. Quantification of five sulfonamides using internal standard normalization from simultaneous precursor ion scans acquired from a benchtop mass spectrometer. Bottom right: Example of simultaneous OR precursor ion scan for m/z 156 (analyte, black) and 162 (IS, blue) at 200 ng/mL.

Although the combination of precursor ion scans improves quantitative precision, many on-site chemical detection experiments prioritize sensitivity and selectivity over quantitative accuracy as suspect samples are sent to labs for confirmatory analysis. It can be seen that two of the sulfonamides, sulfamerazine (*m/z* 265) and sulfadimidine (*m/z* 279), have notably high limit of detections, 174 ng/mL and 178 ng/mL respectively, compared to the other analytes. To improve sensitivity, the supplemental waveform used to eject the product ions of *m/z* 162 (the product ion used for detecting the internal standard) is exchanged for one that ejects the product ions that result from a neutral loss scan for 93 Da from the fragmenting precursor ion. Note that the integration of two product ions into one detection channel (i.e. the combination precursor/neutral loss scan) results in greater signal than each of the individual scans, as demonstrated in Figure 7.6. It is expected, however, that as the overall signal is increased by adding two channels together, the overall noise should increase as well. Nonetheless, this increase in noise is minor compared to the increase in signal and an improvement in signal/noise ratio is observed for all the analytes at 100 ng/mL (Figure S7.3). As all signal/noise ratios are greater than 3, it is assumed that these analytes would be detected at concentrations below the MRL in matrices when combined with an

175

appropriate ion source. It is noteworthy that all three spectra show the same peaks, consistent with the fact that the simultaneous scan used here is an OR function, but also indicating that these precursor ion (for product ion *m/z* 156) and neutral loss (of 93 Da) scans are highly diagnostic for all the sulfonamides in this set.
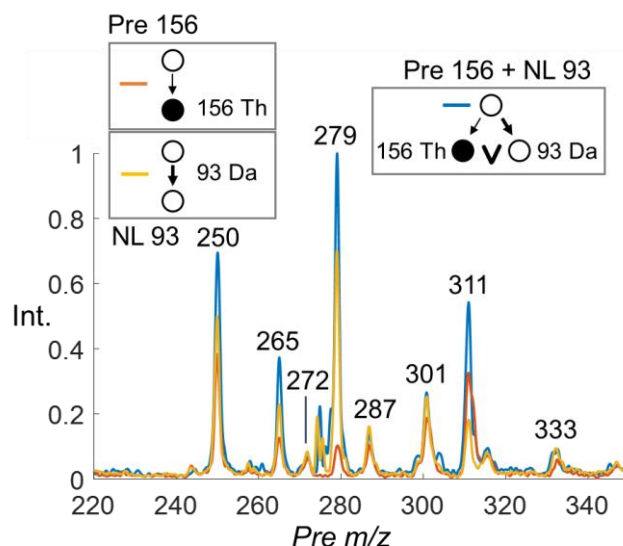


Figure 7.6. Comparison of individual precursor ion (orange), neutral loss (yellow) scan, and simultaneous OR precursor/neutral loss scan (blue) of a solution containing five sulfonamides at 200 ng/mL acquired from a benchtop mass spectrometer. The peaks at m/z 272, 287, and 333 correspond to sodiated sulfonamide species.

### 7.3.4   Detection of sulfonamides using a miniature mass spectrometer

The benchtop performance of the combination scans has allowed flexibility in prioritizing either quantitative performance or improved detection limits. The utilization of these scan modes for the on-site detection of sulfonamides should be tailored specifically to the analytical demands. For example, the *ambient* detection of these antibiotics would require direct analysis from a sample, such as milk, without separation. Despite the typical decrease in quantitative performance of these ambient ionization techniques when compared to traditional analytical workflows (i.e. extraction, separation and then ionization), there are many situations in which rapid on-site analysis using only relative intensities between multiple analytes is preferred if a choice must be made with high quality  quantitation.[35,36]

For the on-site detection of antibiotics in food products, it is likely that improved detection limits would be more important than quantitative precision. For this reason, the simultaneous precursor/neutral loss scan was implemented on a homebuilt miniature mass spectrometer to prioritize detection limits. A comparison of the performance of the homebuilt mass spectrometer to the benchtop mass spectrometer can be found in Figure 7.7. For four of the five analytes, an improvement of signal/noise was observed across three replicates at the 100 ng/mL level. This is expected as previous comparisons between the two instruments using similar scans showed greater sensitivity on the miniature instrument,[18,19] a phenomenon mostly attributed to the miniature instrument operating at higher pressure thereby increasing fragmentation efficiency due to greater momentum transfer into the ion.
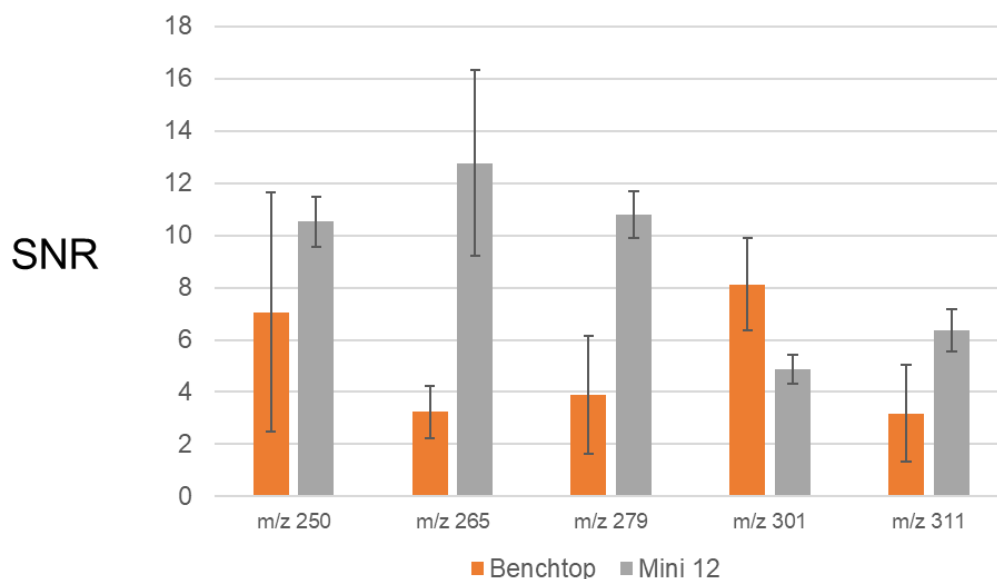


Figure 7.7. Comparison of signal/noise (SNR) for the simultaneous precursor/neutral loss scan on the benchtop mass spectrometer (orange) and miniature mass spectrometer (gray) for the mixture of five sulfonamides. Note that m/z 301 contains contributions from both protonated and sodiated species.

Nano-electrospray was used in previous experiments as it was able to generate stable ion currents for longer periods than paper spray ionization. This was done to better characterize the performance of the MS/MS scan modes. To demonstrate the feasibility of detecting antibiotic sulfonamides in a miniature instrument, the five analytes were detected at various amounts by paper spray ionization. This was accomplished by pipetting 5 μL of solutions containing the

analytes at 1000, 500, and 100 ng/mL on a triangular paper substrate. In one successful experiment, the five analytes were detected at each concentration (SI, Figure S7.4). However, the results presented in Figure S7.4represent the only successful attempt and even at the highest concentration, multiple replicates were unsuccessful. Similar difficulties in consistency were observed when using a commercial benchtop instrument. To a lesser extent, difficulties with spray consistency were also observed in nano-electrospray. Earlier experiments demonstrated that the ionization of the protonated analytes is drastically affected by nano-electrospray capillary geometry (SI, Figure S7.5). The difficulty of ionizing these analytes emphasizes the need for continued development in ambient ionization ion sources.

## 7.4 Conclusions

This work establishes a framework for interrogating (new) classes of molecules by data-independent MS/MS with respect to analytical metrics. First, representative molecules are chosen and detected by a 2D MS/MS scan which identifies all precursor/product ion relationships. From the 2D MS/MS spectrum, the most informative 1D MS/MS scan lines can be identified. By spending the entire scan time on the identified 1D MS/MS scan line (Pre 156), greater mass resolution is obtained (FWHM 4.5 for the 2D MS/MS scan and 1.6 for the precursor ion scan). Furthermore, individual 1D MS/MS scan lines can be combined simultaneously in order to prioritize either detection limits or quantitative precision. These 1D MS/MS combinatory scans are most important when combined with ambient ionization and miniature mass spectrometers to make measurements on-site with minimal sample preparation. The simultaneous OR precursor/neutral loss scan was shown to have the best detection limit (<100 ng/mL) and was used to detect representative sulfonamides on a miniature mass spectrometer. Further improvements on the reproducibility and direct interfacing capability of ambient ionization sources, such as paper spray, will complement the approach reported here, to allow robust and reliable on-site analysis with miniature mass spectrometry.

## 7.5 Supplementary Figures
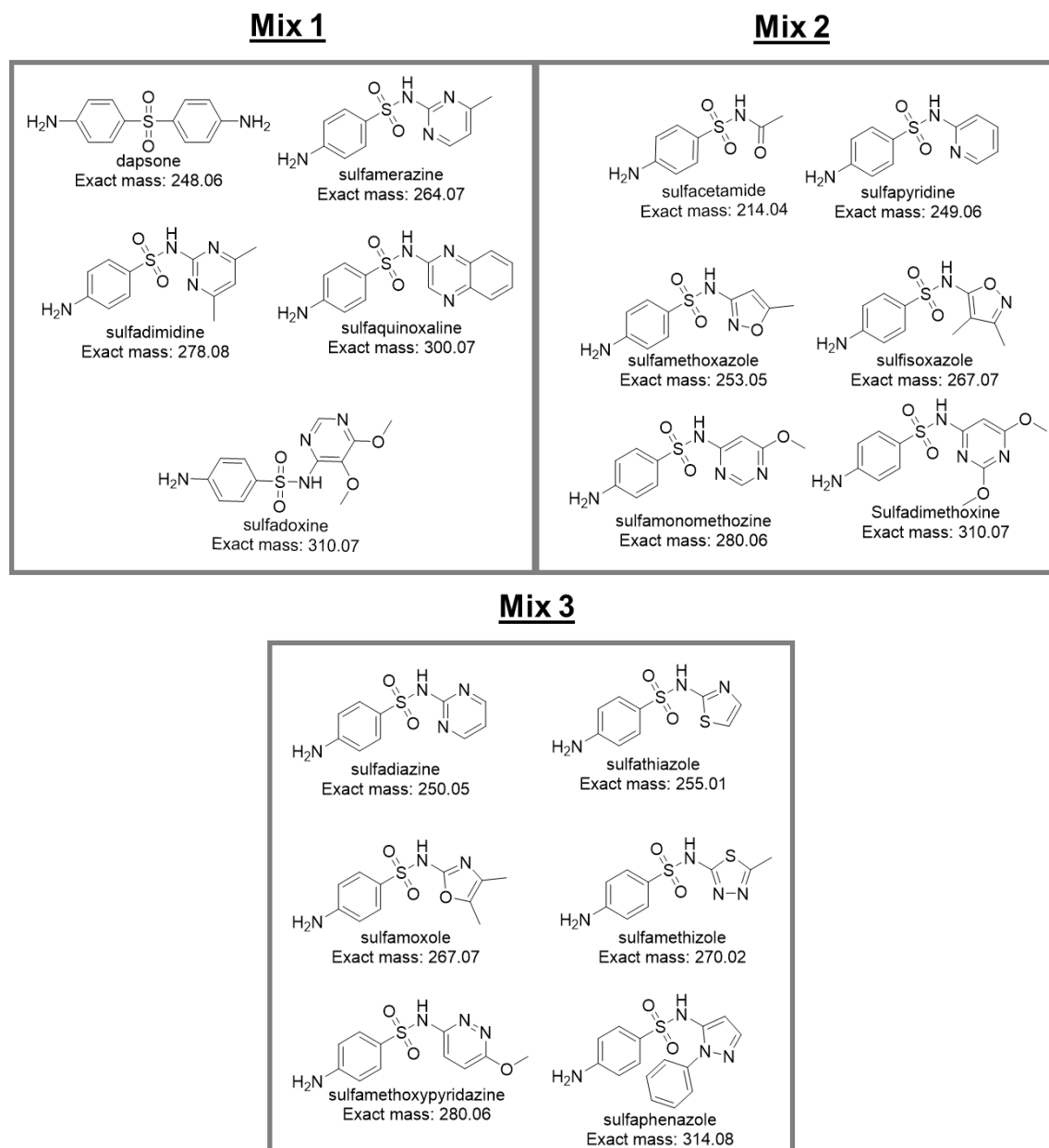


Figure S7.1. Structures of the sulfonamides in the three mixtures analyzed in Figure 7.3.

| Name | Side Group Composition | Intensity of $\dfrac{NL93}{Pre156}$ |
|---|---|---|
| Sulfadiazine | $R_1$=H, $R_2$=H | 0.093 |
| sulfamerazine | $R_1$=CH$_3$, $R_2$=H | 1.03 |
| sulfadimidine | $R_1$=CH$_3$, $R_2$=CH$_3$ | 10.6 |
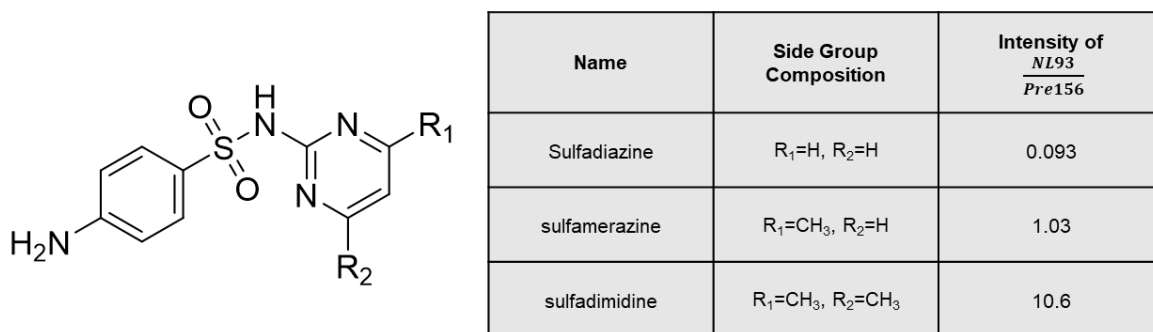
Figure S7.2. Structure of pyrimidine sulfonamides with intensity ratio of neutral loss 93 Da and product ion m/z 156.
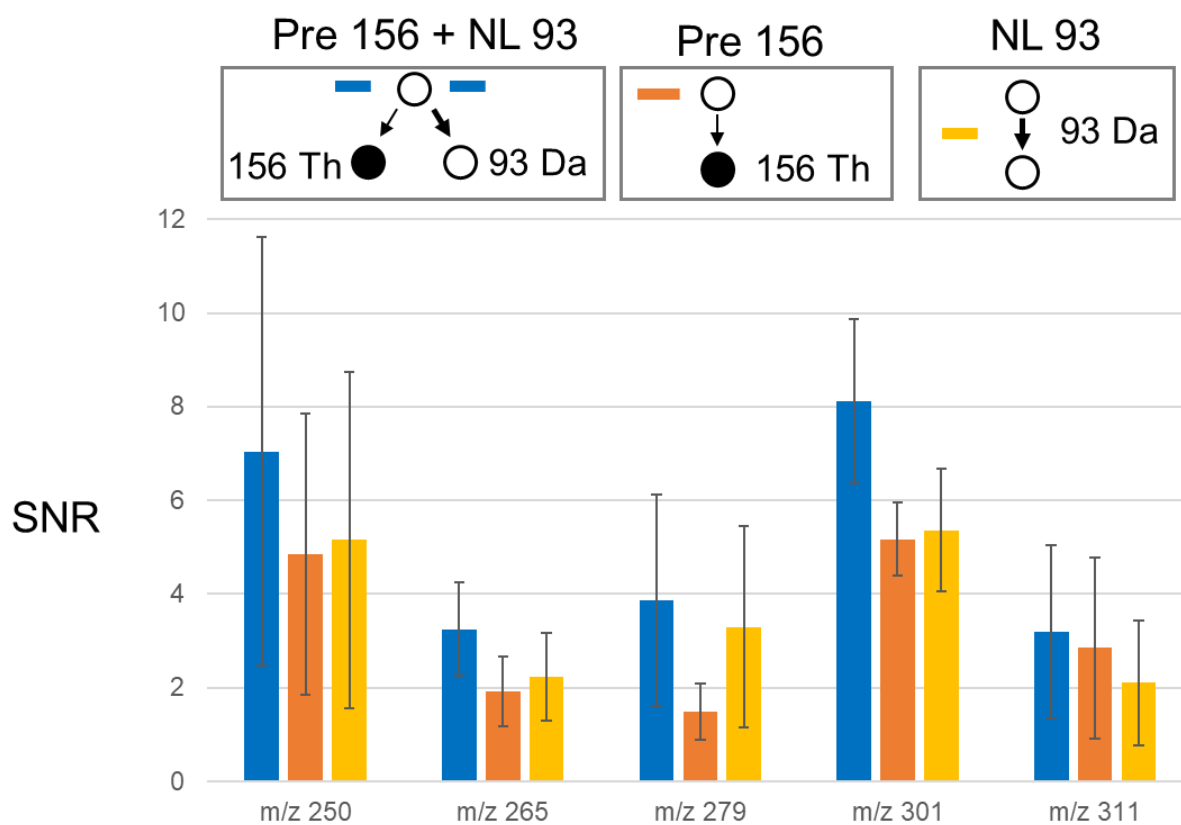


Figure S7.3. Comparison of signal/noise (SNR) for the simultaneous precursor/neutral loss scan (blue), precursor ion scan (orange), and neutral loss scan (yellow) at 100 ng/mL. Three replicates were obtained for each scan mode.
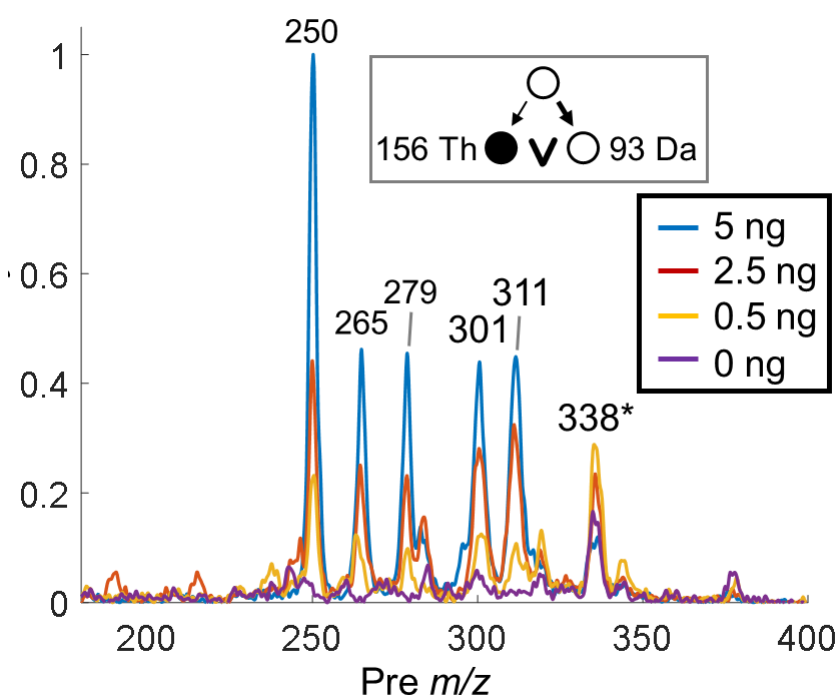
Figure S7.4. Paper spray ionization of five sulfonamides detected by simultaneous OR precursor/neutral loss scan on a miniature mass spectrometer in various amounts.
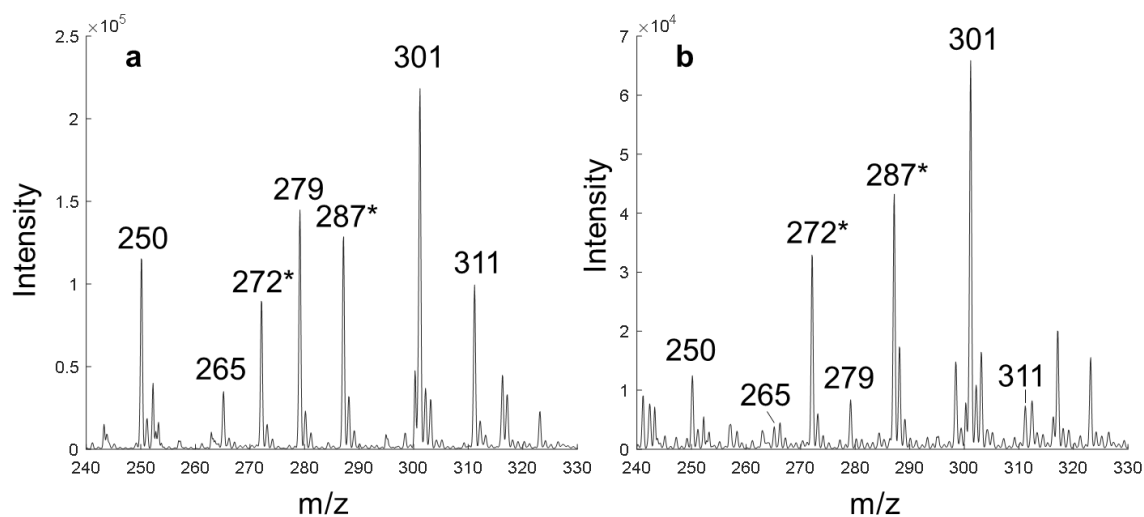
Figure S7.5. (a) Mass spectrum obtained by nESI of a 1 µg/mL solution of five sulfonamides using a capillary with filament. (b) Mass spectrum obtained by nESI of the same solution using a capillary without filament. Note that peaks at m/z 272 and 287 are sodiated peaks for sulfapyridine (M+H)+, m/z 250 and sulfamerazine (M+H)+, m/z 265. The peak at m/z 301 is due to both protonated sulfaquinoxaline and sodiated sulfadimidine.

Table S7.1 Table of sulfonamides in the three mixtures analyzed in Figure 7.3 with *m/z* values for the light and heavy isotopologues

| Mixture 1: | [M+H]⁺ *m/z* | [I.S. + H]⁺ *m/z* |
|---|---|---|
| Dapsone | 249 | 257 |
| Sulfamerazine | 265 | 271 |
| Sulfadimidine | 279 | 285 |
| Sulfaquinoxaline | 301 | 307 |
| Sulfadoxine | 311 | 314 |
| **Mixture 2:** | | |
| Sulfacetamide | 215 | - |
| Sulfapyridine | 250 | 256 |
| Sulfamethoxazole | 254 | 258 |
| Sulfisoxazole | 268 | 274 |
| Sulfamonomethozine | 281 | - |
| Sulfadimethoxine | 311 | 317 |
| **Mixture 3:** | | |
| Sulfadiazine | 251 | 255 |
| Sulfathiazole | 256 | 262 |
| Sulfamoxole | 268 | - |
| Sulfamethizole | 271 | 277 |
| Sulfamethoxypyridazine | 281 | 284 |
| Sulfaphenazole | 315 | - |

Table S7.2. R-squared and coefficient of variation for the calibration curves without normalization, with normalization to only internal standards, and with normalization to the internal standards and response factors.

|  | Analyte | No Normalization | Normalization to Internal Standard | Normalization to Internal Standard and Response Factor |
|---|---|---|---|---|
| **R²** | Sulfapyridine | 0.95 | 0.98 | 0.98 |
|  | Sulfamerazine | 0.85 | 0.97 | 0.97 |
|  | Sulfadimidine | 0.82 | 0.99 | 0.99 |
|  | Sulfaquinolaxine | 0.79 | 0.98 | 0.98 |
|  | Sulfadimethoxine | 0.95 | 0.98 | 0.98 |
|  | Average | 0.87 | 0.98 | 0.98 |
|  | Average Change† | **0.00** | **+0.11** | **+0.11** |
|  | Average % Change† | **0.0%** | **+12.1%** | **+12.2%** |
| **CV\*** | Sulfapyridine | 25.7% | 38.6% | 15.9% |
|  | Sulfamerazine | 26.1% | 31.3% | 13.5% |
|  | Sulfadimidine | 23.9% | 21.3% | 13.7% |
|  | Sulfaquinolaxine | 36.7% | 43.6% | 20.8% |
|  | Sulfadimethoxine | 27.7% | 20.8% | 12.7% |
|  | Average | 28.0% | 31.1% | 15.3% |
|  | Average Change† | **0.0%** | **+3.1%** | **-12.7%** |
|  | Average % Change† | **0.0%** | **+11.1%** | **-45.4%** |

\* Average coefficient of variance (CV) across all the concentrations within the calibration curve

† Average changes (absolute and percentages) are calculated respect to the "No Normalization" case

## 7.6 References

(1)    Yadav, S.; Kapley, A. Antibiotic Resistance: Global Health Crisis and Metagenomics. Biotechnol. Rep. 2021, 29, e00604. https://doi.org/10.1016/j.btre.2021.e00604.

(2)    Commission Regulation (EU) No 37/2010 of 22 December 2009 on pharmacologically active substances and their classification regarding maximum residue limits in foodstuffs of animal origin (2010) Official Journal L 015. Commission Regulation (EU) No 37/2010 of 22 December 2009 on Pharmacologically Active Substances and Their Classification Regarding Maximum Residue Limits in Foodstuffs of Animal Origin (2010) Official Journal L 015.

(3)    Wu, J.; Li, Y.; Li, W.; Gong, Z.; Huang, X. Preparation of a Novel Monolith-Based Adsorbent for Solid-Phase Microextraction of Sulfonamides in Complex Samples Prior to HPLC-MS/MS Analysis. Anal. Chim. Acta 2020, 1118, 9–17. https://doi.org/10.1016/j.aca.2020.04.035.

(4)     Choi, S. Y.; Kang, H.-S. Multi-Residue Determination of Sulfonamides, Dapsone, Ormethoprim, and Trimethoprim in Fish and Shrimp Using Dispersive Solid Phase Extraction with LC–MS/MS. Food Anal. Methods 2021. https://doi.org/10.1007/s12161-021-01965-x.

(5)     Lawton, Z. E.; Traub, A.; Fatigante, W. L.; Mancias, J.; O'Leary, A. E.; Hall, S. E.; Wieland, J. R.; Oberacher, H.; Gizzi, M. C.; Mulligan, C. C. Analytical Validation of a Portable Mass Spectrometer Featuring Interchangeable, Ambient Ionization Sources for High Throughput Forensic Evidence Screening. J. Am. Soc. Mass Spectrom. 2017, 28 (6), 1048–1059. https://doi.org/10.1007/s13361-016-1562-2.

(6)     Jager, J.; Gerssen, A.; Pawliszyn, J.; Sterk, S. S.; Nielen, M. W. F.; Blokland, M. H. USB-Powered Coated Blade Spray Ion Source for On-Site Testing Using Transportable Mass Spectrometry. J. Am. Soc. Mass Spectrom. 2020, 31 (11), 2243–2249. https://doi.org/10.1021/jasms.0c00307.

(7)     Huang, M.-Z.; Yuan, C.-H.; Cheng, S.-C.; Cho, Y.-T.; Shiea, J. Ambient Ionization Mass Spectrometry. Annu. Rev. Anal. Chem. 2010, 3 (1), 43–65. https://doi.org/10.1146/annurev.anchem.111808.073702.

(8)     Marić, M.; Marano, J.; Cody, R. B.; Bridge, C. DART-MS: A New Analytical Technique for Forensic Paint Analysis. Anal. Chem. 2018, 90 (11), 6877–6884. https://doi.org/10.1021/acs.analchem.8b01067.

(9)     Tillner, J.; Wu, V.; Jones, E. A.; Pringle, S. D.; Karancsi, T.; Dannhorn, A.; Veselkov, K.; McKenzie, J. S.; Takats, Z. Faster, More Reproducible DESI-MS for Biological Tissue Imaging. J. Am. Soc. Mass Spectrom. 2017, 28 (10), 2090–2098. https://doi.org/10.1007/s13361-017-1714-z.

(10)    Tian, H.; Liu, T.; Mu, G.; Chen, F.; He, M.; You, S.; Yang, M.; Li, Y.; Zhang, F. Rapid and Sensitive Determination of Trace Fluoroquinolone Antibiotics in Milk by Molecularly Imprinted Polymer-Coated Stainless Steel Sheet Electrospray Ionization Mass Spectrometry. Talanta 2020, 219, 121282.

(11)    Liu, Y.; Yang, Q.; Chen, X.; Song, Y.; Wu, Q.; Yang, Y.; He, L. Sensitive Analysis of Trace Macrolide Antibiotics in Complex Food Samples by Ambient Mass Spectrometry with Molecularly Imprinted Polymer-Coated Wooden Tips. Talanta 2019, 204, 238–247.

(12)    Zhang, H.; Kou, W.; Bibi, A.; Jia, Q.; Su, R.; Chen, H.; Huang, K. Internal Extractive Electrospray Ionization Mass Spectrometry for Quantitative Determination of Fluoroquinolones Captured by Magnetic Molecularly Imprinted Polymers from Raw Milk. Sci. Rep. 2017, 7 (1), 1–11.

(13)    Guo, X.; Bai, H.; Ma, X.; Li, J.; Ren, Y.; Ouyang, Z.; Ma, Q. Online Coupling of an Electrochemically Fabricated Solid-Phase Microextraction Probe and a Miniature Mass Spectrometer for Enrichment and Analysis of Chemical Contaminants in Infant Drinks. Anal. Chim. Acta 2020, 1098, 66–74.

(14)     Suraritdechachai, S.; Charoenpakdee, C.; Young, I.; Maher, S.; Vilaivan, T.; Praneenararat, T. Rapid Detection of the Antibiotic Sulfamethazine in Pig Body Fluids by Paper Spray Mass Spectrometry. J. Agric. Food Chem. 2019, 67 (10), 3055–3061.

(15)     Jiang, T.; Peng, Z.; Xie, M.; Fang, X.; Hong, Y.; Huang, Z.; Gao, W.; Zhou, Z.; Li, L.; Zhu, Z. Rapid Analysis of Tetracycline in Honey by Microwave Plasma Torch Mass Spectrometry with Ablation Samples. Anal. Methods 2020, 12 (4), 535–543.

(16)     Liu, Y.; Zhang, X.; Ouyang, Y.; Hu, Z.; Ma, L.; Zhang, J.; Lin, J.; Chen, H. Trace Detection of Hormones and Sulfonamides in Viscous Cosmetic Products by Neutral Desorption Extractive Electrospray Ionization Tandem Mass Spectrometry. J. Mass Spectrom. 2011, 46 (8), 794–803.

(17)     Annesley, T. M. Ion Suppression in Mass Spectrometry. Clin. Chem. 2003, 49 (7), 1041–1044. https://doi.org/10.1373/49.7.1041.

(18)     Snyder, D. T.; Szalwinski, L. J.; Hilger, R.; Cooks, R. G. Implementation of Precursor and Neutral Loss Scans on a Miniature Ion Trap Mass Spectrometer and Performance Comparison to a Benchtop Linear Ion Trap. J. Am. Soc. Mass Spectrom. 2018, 1–10. https://doi.org/10.1007/s13361-018-1922-1.

(19)     Szalwinski, L. J.; Cooks, R. G. Complex Mixture Analysis by Two-Dimensional Mass Spectrometry Using a Miniature Ion Trap. Talanta Open 2021, 3, 100028. https://doi.org/10.1016/j.talo.2020.100028.

(20)     Gao, L.; Cooks, R. G.; Ouyang, Z. Breaking the Pumping Speed Barrier in Mass Spectrometry: Discontinuous Atmospheric Pressure Interface. Anal. Chem. 2008, 80 (11), 4026–4032. https://doi.org/10.1021/ac800014v.

(21)     Snyder, D. T.; Szalwinski, L. J.; Cooks, R. G. Simultaneous and Sequential MS/MS Scan Combinations and Permutations in a Linear Quadrupole Ion Trap. Anal. Chem. 2017, 89 (20), 11053–11060. https://doi.org/10.1021/acs.analchem.7b03064.

(22)     Snyder, D. T.; Szalwinski, L. J.; Wells, J. M.; Cooks, R. G. Logical MS/MS Scans: A New Set of Operations for Tandem Mass Spectrometry. Analyst 2018, 143 (22), 5438–5452. https://doi.org/10.1039/C8AN01661E.

(23)     Szalwinski, L. J.; Holden, D. T.; Morato, N. M.; Cooks, R. G. 2D MS/MS Spectra Recorded in the Time Domain Using Repetitive Frequency Sweeps in Linear Quadrupole Ion Traps. Anal. Chem. 2020, 92 (14), 10016–10023. https://doi.org/10.1021/acs.analchem.0c01719.

(24)     Johnson, J. V.; Pedder, R. E.; Yost, R. A. MS-MS Parent Scans on a Quadrupole Ion Trap Mass Spectrometer by Simultaneous Resonant Excitation of Multiple Ions. Int. J. Mass Spectrom. Ion Process. 1991, 106, 197–212. https://doi.org/10.1016/0168-1176(91)85019-I.

(25) Snyder, D. T.; Cooks, R. G. Single Analyzer Precursor Ion Scans in a Linear Quadrupole Ion Trap Using Orthogonal Double Resonance Excitation. J. Am. Soc. Mass Spectrom. 2017, 28 (9), 1929–1938. https://doi.org/10.1021/jasms.8b05645.

(26) McClellan, J. E.; Quarmby, S. T.; Yost, R. A. Parent and Neutral Loss Monitoring on a Quadrupole Ion Trap Mass Spectrometer: Screening of Acylcarnitines in Complex Mixtures. Anal. Chem. 2002, 74 (22), 5799–5806. https://doi.org/10.1021/ac026073d.

(27) Snyder, D. T.; Szalwinski, L. J.; Schrader, R. L.; Pirro, V.; Hilger, R.; Cooks, R. G. Precursor and Neutral Loss Scans in an RF Scanning Linear Quadrupole Ion Trap. J. Am. Soc. Mass Spectrom. 2018, 1–10. https://doi.org/10.1007/s13361-018-1920-3.

(28) Snyder, D. T.; Pulliam, C. J.; Cooks, R. G. Calibration Procedure for Secular Frequency Scanning in Ion Trap Mass Spectrometers. Rapid Commun. Mass Spectrom. 2016, 30 (10), 1190–1196. https://doi.org/10.1002/rcm.7550.

(29) Snyder, D. T.; Cooks, R. G. Single Analyzer Neutral Loss Scans in a Linear Quadrupole Ion Trap Using Orthogonal Double Resonance Excitation. Anal. Chem. 2017, 89 (15), 8148–8155. https://doi.org/10.1021/acs.analchem.7b01963.

(30) Tian, Z.; Wang, X.-B.; Wang, L.-S.; Kass, S. R. Are Carboxyl Groups the Most Acidic Sites in Amino Acids? Gas-Phase Acidities, Photoelectron Spectra, and Computations on Tyrosine, p-Hydroxybenzoic Acid, and Their Conjugate Bases. J. Am. Chem. Soc. 2009, 131 (3), 1174–1181. https://doi.org/10.1021/ja807982k.

(31) Warnke, S.; Seo, J.; Boschmans, J.; Sobott, F.; Scrivens, J. H.; Bleiholder, C.; Bowers, M. T.; Gewinner, S.; Schöllkopf, W.; Pagel, K.; von Helden, G. Protomers of Benzocaine: Solvent and Permittivity Dependence. J. Am. Chem. Soc. 2015, 137 (12), 4236–4242. https://doi.org/10.1021/jacs.5b01338.

(32) Lermyte, F.; Theisen, A.; O'Connor, P. B. Solution Condition-Dependent Formation of Gas-Phase Protomers of Alpha-Synuclein in Electrospray Ionization. J. Am. Soc. Mass Spectrom. 2021, 32 (1), 364–372. https://doi.org/10.1021/jasms.0c00373.

(33) Demarque, D. P.; Crotti, A. E. M.; Vessecchi, R.; Lopes, J. L. C.; Lopes, N. P. Fragmentation Reactions Using Electrospray Ionization Mass Spectrometry: An Important Tool for the Structural Elucidation and Characterization of Synthetic and Natural Products. Nat. Prod. Rep. 2016, 33 (3), 432–455. https://doi.org/10.1039/C5NP00073D.

(34) Klagkou, K.; Pullen, F.; Harrison, M.; Organ, A.; Firth, A.; Langley, G. J. Fragmentation Pathways of Sulphonamides under Electrospray Tandem Mass Spectrometric Conditions. Rapid Commun. Mass Spectrom. 2003, 17 (21), 2373–2379. https://doi.org/10.1002/rcm.1201.

(35) Jarmusch, A. K.; Pirro, V.; Baird, Z.; Hattab, E. M.; Cohen-Gadol, A. A.; Cooks, R. G. Lipid and Metabolite Profiles of Human Brain Tumors by Desorption Electrospray Ionization-MS. Proc. Natl. Acad. Sci. 2016, 113 (6), 1486. https://doi.org/10.1073/pnas.1523306113.

(36)    Brown, H. M.; Pu, F.; Dey, M.; Miller, J.; Shah, M. V.; Shapiro, S. A.; Ouyang, Z.; Cohen-Gadol, A. A.; Cooks, R. G. Intraoperative Detection of Isocitrate Dehydrogenase Mutations in Human Gliomas Using a Miniature Mass Spectrometer. Anal. Bioanal. Chem. 2019, 411 (30), 7929–7933. https://doi.org/10.1007/s00216-019-02198-y.

# CHAPTER 8.    COMPLEX MIXTURE ANALYSIS BY TWO-DIMENSIONAL MASS SPECTROMETRY USING A MINIATURE ION TRAP

## 8.1    Introduction

Mass spectrometers have become indispensable in analytical research labs. In order to cater to many different application areas, commercial mass spectrometer development has centered around combining different instrumental components to create integrated platforms.[1,2] These innovations prioritize mass resolution and sensitivity over instrument simplicity, speed, and size. On the other hand, miniature mass spectrometers are typically built for a specific type of analytical problem.[3–6] The size requirements are stringent, only allowing for relatively simple instrumentation.  The instruments are designed to have sensitivity and selectivity appropriate for designated problems.   Because of the design requirements, innovations demonstrated in commercial or modified commercial benchtop mass spectrometers are typically achieved with significant performance loss when transferred to miniature mass spectrometers. For example, high-resolution ($R > 10^5$) benchtop instruments have become commonplace in part due to improvements in both time-of-flight and orbitrap mass analyzers.[7,8] Neither of these mass analyzers transfers well to miniature instruments due to their high vacuum requirements.

Quadrupole ion traps do not require precise machining tolerances or high vacuum, making them an attractive option for miniature mass spectrometers.[9–12] Another feature that has made miniature quadrupole ion traps popular is their ability to perform tandem mass spectrometry (MS/MS).  Traditionally, quadrupole ion traps require ion isolation in order to acquire interpretable MS/MS data. The efficiency in terms of both sample and time in which MS/MS data is obtained by this method is relatively poor because a new ion population must be introduced for each scan. Previously, our group demonstrated a method of avoiding ion isolation yet obtaining MS/MS data, so allowing for the implementation of precursor and neutral loss scan modes.[13,14] MS/MS was performed by mass selectively fragmenting precursor ions while simultaneously ejecting the product ions orthogonally into the detector. The improved efficiency, and thus speed, of these scan

modes was due to the ability to interrogate many different precursor ions after their trapping in a single ion injection event. This improvement was expected to be particularly valuable when using miniature instruments that utilize a discontinuous atmospheric pressure interface (DAPI)[15] because of the long dwell time required to achieve operating vacuum after each ion injection. Remarkably, the miniature instrument implementation of precursor and neutral loss scans showed improved sensitivity over that of commercial benchtop instruments.[16]

Although the implementation of precursor and neutral loss scans marked a substantial improvement of MS/MS efficiency, recently our group demonstrated that the entire 2D MS/MS data domain, containing two dimensions of mass and one of intensity, can be recorded in a single ion introduction event.[17–19] The 2D MS/MS scan is the most efficient way to obtain MS/MS data on a complex sample because of the high mass scan rate and avoiding ion isolation. In this study, the 2D MS/MS scan was implemented in a miniature quadrupole ion trap and the performance was compared to its benchtop counterpart for the detection of fentanyl and related fentanyl analogs (fentalogs). Then, the 2D MS/MS scan on the miniature mass spectrometer was used to interrogate a sample containing a high concentration of matrix. Finally, a sample containing many lipids was interrogated to determine the method's feasibility for providing a miniature lipidomics platform capable of determining lipid profiles.

## 8.2   Experimental

### 8.2.1   Chemicals

Fentanyl analogs and other pharmaceuticals were purchased from Sigma Aldrich (St. Louis, MO) and diluted in methanol. For the fentanyl quantitation and resolution comparison, fentanyl was diluted to 1000, 500, 300, 100, 50, 25 ppb (ng/mL) with acetyl fentanyl as an internal standard held at 250 ppb. The 13 fentalog mixture was made by diluting each fentalog from a standard solution so that each fentalog had a final concentration of 100 ppb. A 100 µL solution of Differential Ion Mobility System Suitability Lipidomix (Avanti Polar Lipids, Inc, Alabaster, Alabama) was dried and redissolved in 400 µL of acetonitrile/methanol/300 mM ammonium acetate (3:6.65:0.35, v/v/v) so that each lipid, besides 14:1 PI, had a final concentration of 250 ppm (PI was at 62.5 ppm).

### 8.2.2  Instrumentation

A previously modified Finnigan LTQ mass spectrometer (San Jose, CA) utilizing the 2D MS/MS scan was used for all benchtop mass spectrometry experiments.[17,18] A modified Mini 12 mass spectrometer developed at Purdue University was used for all miniature mass spectrometry experiments.[16,20] The 2D MS/MS scan utilizes a constant trapping RF voltage as well as the capability to apply auxiliary waveforms individually to the x- and y-rod pairs. The RF trapping voltage of the modified LTQ mass spectrometer was controlled using an external waveform generator as described previously.[14] The Mini 12 has user-controlled RF voltages accessible within the user interface, so no modification was needed. In both instruments, auxiliary waveforms were applied to the x-rod pair without any other modification; however, both instruments required modification in order to apply auxiliary waveforms to the y-rod pair.[16] The Mini 12 was improved by further optimization of the secondary transform.[16] This included using a new iron core toroidal transformer (Laird Technologies LFB180100-000, Earth City, MO, USA) and wrapping the transformer in glass wool to avoid discharge across the toroid. This resulted in a change in the resonant frequency from 1 MHz to 1.1 MHz. Figure 8.1a details how the trapping RF and auxiliary AC were inductively coupled to the x- and y- rod pairs.

### 8.2.3  Scan Time

Figure 8.1b depicts the difference in scan time between the benchtop and miniature mass spectrometers. The scan table for the 2D MS/MS scan on the modified benchtop instrument has been described previously.[17] The scan table used in the Mini 12 is similar except for one key difference. The Mini 12 requires approximately one second after sample introduction before mass analysis can be performed in order to remove neutral molecules to achieve appropriate vacuum.[21] A period of 100 milliseconds was added to the end of each scan on both instruments in order to ensure all electronics are ready for the next scan. However, additional time is added to the Mini 12 scan to ensure that the vacuum is at steady state. This time was made sufficiently long during optimization of scan parameters and no further changes are required once optimization is complete. The additional time allocated for achieving appropriate pressures during the scan is the main reason for the decreased duty cycle of miniature instruments utilizing DAPI interfaces. The decrease in duty cycle is most felt when performing product ion scans as each additional scan requires re-

191

introduction of a new precursor ion population as most precursors are removed during ion isolation in order to correlate product ions to a single precursor ion *m/z*. The 2D MS/MS scan avoids ion isolation and re-introduction of analytes by fragmenting each precursor ion sequentially while continuously monitoring for product ions. The decrease in duty cycle is one motivation for implementing the 2D MS/MS scan as it provides more MS/MS data per ion introduction event than other MS/MS scans. Another improvement is that no precursor ions are wasted during ion isolation as all precursor ions are fragmented or detected in each 2D MS/MS scan.
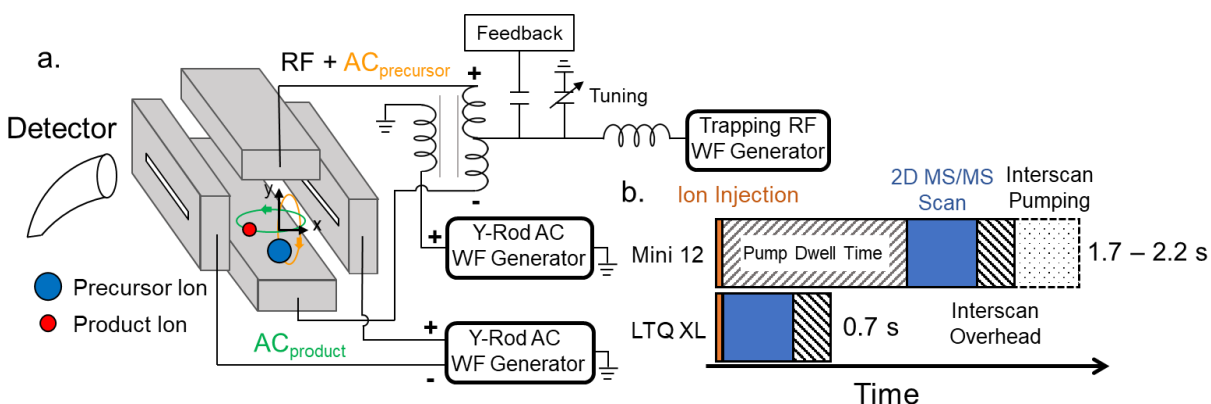


Figure 8.1. (a) Schematic of applied waveforms on the Mini 12 mass spectrometer. (b) Typical 2D MS/MS scan table for both the Mini 12 and LTQ XL mass spectrometers.

## 8.3    Results and Discussion

### 8.3.1    Comparison of performance for the detection of fentanyl

In order to characterize sensitivity and resolution, fentanyl was interrogated using a 2D MS/MS scan on the miniature and modified commercial instruments. In both instruments, the trapped precursor ion was held at the same *q*-value, 0.357, and because *m/z* and *q*-values are proportional, the product ions for both instruments occur at the same *q*-value. Both the miniature and benchtop 2D MS/MS scan covered the same range of *q*-values over the same scan time in order to minimize differences caused by different scan rates. The resulting three-dimensional data for fentanyl collected by the 2D MS/MS scan in both instruments is shown in Figure 8.2. The peak widths at half of the maximum amplitude (FWHM) for the benchtop are 5.9 and 5.4 Thomson (Th) in the precursor (337 Th) and product ion (188 Th) dimensions, respectively. Surprisingly, the miniature instrument shows the better resolution with the FWHM decreasing to 3.5 and 3.0 Th for

the precursor (337 Th) and product ion (188 Th), respectively. The improved miniature system resolution is likely due to contributions from higher order fields and the higher operating pressure. The miniature instrument is operated at a higher pressure and has more significant contributions from higher order fields.[22,23] The effect of higher order fields on resonance ejection for mass analysis has been extensively studied using numerical simulations.[24,25] However, the current study combines the fragmentation and ejection processes so comparison to previously explored systems is difficult.
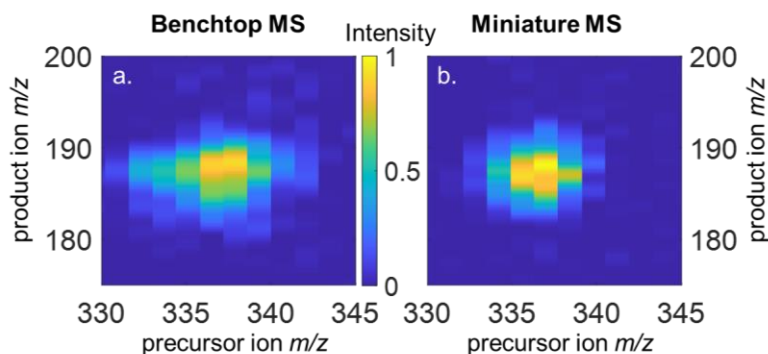


Figure 8.2. Comparison of the 2D MS/MS data for fentanyl showing the characteristic precursor/product ion (Pre/Pro, 337/188 Th) using 2D MS/MS scans in a modified (a) benchtop LTQ XL mass spectrometer and (b) Mini 12 mass spectrometer.

Evaluation of the sensitivity of each system was performed by constructing calibration curves for each instrument. These calibration curves (Figure S8.1) showed adequate quantitative performance across the ppb range for fentanyl. The limit of detection for fentanyl was determined as the concentration that would give S/N of 3. The miniature instrument yielded a limit of detection of 3 ppb compared to 37 ppb for the LTQ benchtop instrument. A similar more favorable performance of the miniature instrument was previously demonstrated for neutral loss/precursor ion scans on the same systems.[16] Previously, it was shown that moving from helium to nitrogen/air was a major factor for improved sensitivity in that experiment. However, it is unlikely that the difference in bath gas composition is the only factor affecting sensitivity; the greater contribution from octopolar fields in the Mini in improving the fragmentation efficiency is also involved.

### 8.3.2 Identification of Fentalogs by Mini 2D MS/MS

To better compare the performance of both systems, a mixture of 13 fentalogs (Figure S8.5) was analyzed. The 2D MS/MS spectrum for each system is shown in Figure 8.3. The first notable difference between the two spectra is that the systems have different mass-dependent transmissions. The miniature instrument performs better in detecting low mass product ions from low mass precursor ions while the benchtop instrument has a higher transmission of higher mass product ions arising from higher mass precursor ions. This result can be explained by the intra-scan pressure changes within in each instrument. The pressure in the benchtop instrument is constant throughout the whole scan. The pressure in the miniature instrument decreases throughout the scan due to pumping following discontinuous sample introduction. The decrease in collisional cooling with decreasing pressure affects the 2D MS/MS experiment in two major ways. The precursor ions are more likely to be ejected before they fragment, and the fragment ions produced are not sufficiently cooled to the center of the trap thereby increasing the chance of off-resonant excitation from the auxiliary waveform used for fragmentation opposed to the ejection waveform.
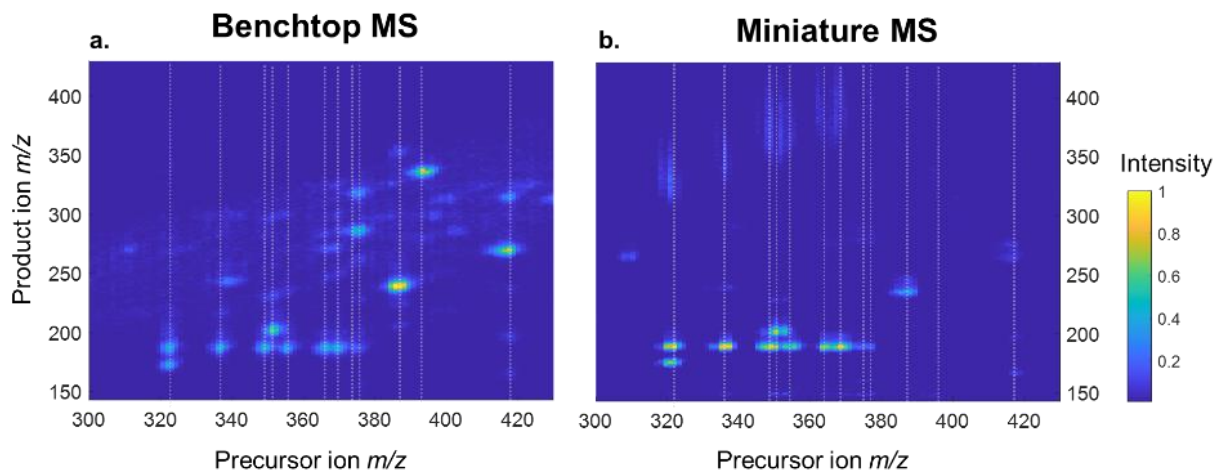


Figure 8.3. Mixture of 13 fentanyl analogs analyzed by 2D MS/MS using modified (a) benchtop LTQ XL mass spectrometer and (b) Mini 12 mass spectrometer. White dotted lines indicate expected precursor ion *m/z* for each analyte. There are two isomeric fentalogs at *m/z* 323. Each spectrum was normalized relative to the highest peak.

This latter effect is present as the second notable difference in Figure 8.3 where peaks at precursor ion *m/z* 377 and 395, corresponding to remifentanil and carfentanil respectively, are

absent in the mini 2D MS/MS spectrum. It would appear that the ejection of the precursor before sufficient fragmentation is the cause of the absence of these peaks as indicated by the fact that even low mass product ions are not observed in either of the extracted product ion scans (data not shown). The presence of low mass product ions for alfentanil, precursor ion *m/z* 417, indicates that product ions generated at sufficient well-depth can be trapped and ejected at the reduced pressure reached near the end of the scan. This off-resonance excitation of the precursor ions could be mitigated by reducing the amplitude of the fragmentation waveform. The fragmentation waveform amplitude is limited by the amplitude required in the ejection waveform. This ejection waveform must perform mass analysis on the millisecond time scale. This fact, in combination with higher operating pressure and the use of nitrogen as the bath gas, increases the amplitude required for product ion ejection

In many cases it becomes convenient to extract slices of the 2D MS/MS spectrum into a 1D MS/MS spectrum to facilitate comparisons, e.g. study of a conserved functional group. For example, previous work has divided the fentalogs into two categories separated by whether or not the conserved moiety in the analog was phenylpiperidine or N-phenylpropanamide.[17] Any analog with the unmodified phenylpiperidine should produce a charged fragment at *m/z* 188 whereas any analog with an unmodified N-phenylpropamide should produce a neutral fragment with a mass of 149 Da. The absolute abundance of these fragments is analyte dependent, but this general trend allows analogs to be identified by using only these two scans. An advantage of the 2D MS/MS scan is that in addition to identifying which of the analytes is a potential fentalog, the product ion scan for every potential analog has already been captured. Extracted precursor and product ion scans obtained from the 2D MS/MS spectra for both instruments are shown in Figure 8.4. Figure 8.4a demonstrates that all fentalogs containing phenylpiperidine produce a fragment ion at *m/z* 188. Figure 8.4b shows that an extracted product ion scan for precursor ion *m/z* 323 indicates the presence of two isomeric fentalogs. Benzylfentanyl and acetylfentanyl differ by the location of a methyl group and are separated by their fragmentation behavior in both instruments. Examples of extracted neutral loss spectra can be found in SI Figure S8.2 where 5 fentalogs are identified by the neutral loss of phenylpropamide.
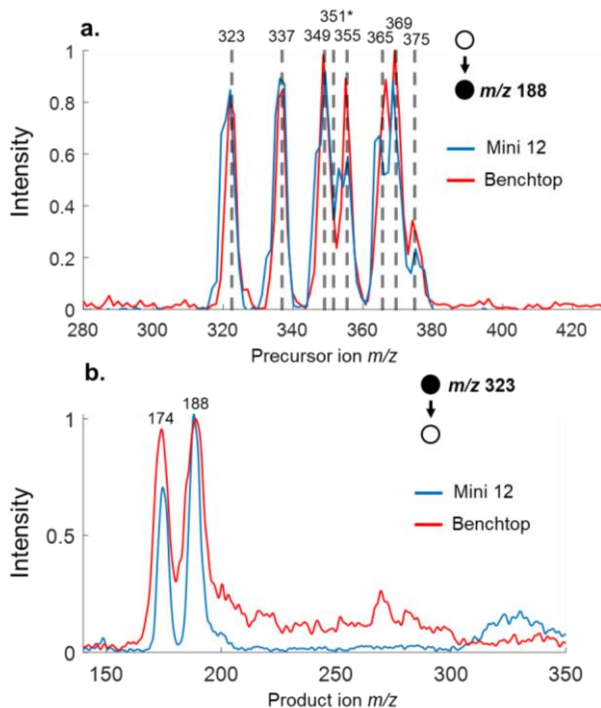
Figure 8.4. Comparison of extracted (a) precursor ion scan and (b) product ion scan on both miniature and benchtop ion trap mass spectrometers. Ion intensity is relative to largest peak in each individual spectrum.

### 8.3.3 Mixture Analysis for a Heroin Matrix

An important aspect of mixture analysis by mass spectrometry is the ability to detect particular analytes in the presence of substantial matrix. Matrix effects can affect the ionization of the analyte by either sequestering charge away from the analyte or by forming adducts with the charged analyte thereby changing its *m/z* value. These effects are traditionally mitigated by relying on separation before ionization or by using ionization methods that are matrix independent. The matrix can also generate background ions that are isobaric with the analyte ion, resulting in a false positive. This is mitigated in an MS/MS experiment by choosing product ions that are unique to the analyte. In order to determine how miniature 2D MS/MS performs when a substantial amount of matrix is present, heroin was chosen as the matrix to determine how the detection of seven drugs would be affected. First, the analytes were analyzed as a mixture without heroin. The resulting 2D MS/MS spectrum is shown in Figure 8.5. The same analytes were then examined with heroin at 100 and 1000 times the concentration of the analytes. The analytes' concentrations were held

196

at 100 ppb and from the resulting data a limit of detection was calculated for the concentration that gives a S/N of 3. The decision to express the results as a LOD instead of S/N at a given concentration was made to emphasize the relatively low concentrations detectable using the miniature instrument.
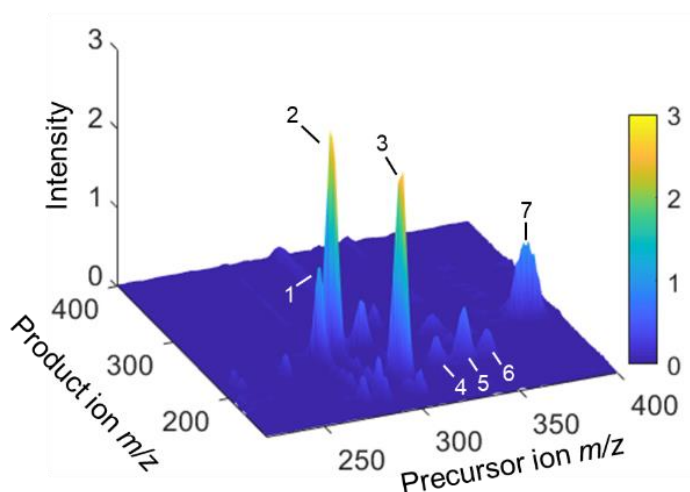


Figure 8.5. 2D MS/MS mass spectrum of seven analytes at 100 ppb. The indicated peaks are the most intense product ions observed for each expected preucrsor ion *m/z*. The identities of each analyte can be found in Table 1.

The limit of detection of an analyte encompasses effects due to both the reduction of signal caused by ion suppression as well as increased signal in the blank caused by interfering peaks overlapping with the analyte peak. In a traditional ion trap MS/MS experiment, ion suppression can be partially compensated for by altering the injection time so that the number of trapped analyte ions is kept constant. This solution is not feasible in the 2D MS/MS scan as all precursor ions are interrogated simultaneously, so the total precursor ion population limits the ion storage capacity for any particular analyte. This is not the case in the traditional ion trap methodology because the number of trapped ions is reduced during the precursor ion isolation step so that only the analyte ion population's charge is present during mass analysis. Finally, if background peak overlap is expected, which would result in a false positive, a more unique transition can be chosen, or additional qualifier transitions can be measured.

The limits of detection determined in Table 8.1 show interesting trends. The most notable is how different the fentalogs' responses are to the matrix. Fentanyl's limit of detection increases from 6 ppb to 18 ppb whereas acetyl fentanyl goes from 10 pbb to 95 ppb in the presence of 1000x heroin. The difference could be attributed to an interfering peak overlapping with the transition used to detect acetylfentanyl and not to decreased fentanyl signal. Without peak overlap, the difference in LOD trends could either be caused by differences in ionization or fragmentation efficiencies. It can be seen from Figure S8.3 that neither the fentanyl or acetyl fentanyl suffers from peak overlap at the transition used for detection, so the change must be caused by either fragmentation or ionization differences between the molecules. Since fragmentation efficiency should be independent of the matrix, the ratio between the product ion peaks with and without the matrix demonstrates how the matrix affects the ionization of the molecule. The advantage of this technique is that all of the analytes are sampled from the source at the exact same time. This is possible because the whole ion population is utilized in the 2D MS/MS scan whereas traditional product ion scans would require different ion injections for each analyte and thus be susceptible to drift in the ion source for changes in sample.

Table 8.1. Detection of seven analytes at 100 ppb in the precence of $10^3$ and $10^4$ times greater concentration of heroin.

| Analyte # - Name | Quantifier Transition (Pre → Pro) | LOD Analytes only (ppb) | LOD with 100x Heroin (ppb) | LOD with 1000x Heroin (ppb) |
|---|---|---|---|---|
| 1 - Amitriptyline | 278 → 233 | 8 | 10 | 30 |
| 2 - Morphine | 286 → 155 | 15 | 20 | 81 |
| 3 - Cocaine | 304 → 185 | 4 | 5 | 13 |
| 4 - Acetyl Fentanyl | 323 → 188 | 10 | 34 | 95 |
| 5 - Fentanyl | 337 → 188 | 6 | 16 | 18 |
| 6 - Cyclopropyl Fentanyl | 349 → 188 | 9 | 39 | 52 |
| 7 - Sufentanil | 387 → 238 | 12 | 35 | 30 |

It can be seen that none of the analytes or heroin ionizes to give isobaric ions. However, the introduction of ions into the miniature ion trap, using air as a bath gas, can cause the protonated molecules to fragment. These ions are still considered precursor ions because they are not fragmented mass selectively. The charged fragments of heroin can be isobaric with one of these analyte ions. The overlap of interfering background fragment ions with analyte precursor ions does not significantly affect any of the analytes tested besides morphine. Morphine and heroin are very similar in structure except that the former's two alcohol groups have been acetylated to produce the latter. Fragmentation by deacetylation (loss of neutral ketene) from protonated heroin is seen at high concentrations of heroin. The extracted product ion spectra of $m/z$ 286 from protonated morphine, deacetylated protonated heroin, and a mixture of the two drugs is shown in Figure S8.4. There is a product ion at $m/z$ 155 seen in the mixture and the morphine sample, but not in the heroin spectrum. The differences in the product ion spectra indicate a difference in ion structure. It might be assumed that neutral morphine and the neutral product of a deacetylated heroin would be the same neutral structure and thus ionize in a similarly. The difference in ion structure is due to how the precursor ions are generated. The ability to differentiate ionic species is a hallmark of MS/MS. This difference could also be observed by traditional product ion scans; however, the data shown is just a sliver of that obtained in a single 2D MS/MS scan. By being sensitive to all possible precursor/product ion relationships, it is possible to detect analytes affected by the confounding matrix. The 2D MS/MS scan is the only scan that is sensitive to changes during ionization thereby either altering precursor ion identity or abundance as well as the fragmentation of the individual precursor ion $m/z$ thus producing different product ions from a single precursor ion $m/z$ as shown above.

### 8.3.4  Future Potential Use for Lipid Profiling

The detection of individual analytes is a key aspect of mixture analysis as discussed above. For many practical applications, it is only important to identify the complex sample as such rather than identifying the individual analytes within the complex sample. In rare cases a single biomarker can identify the sample type even if it contains a complex mixture, and then the experiment can be simplified to only detect that marker. This was shown where genomic and immunohistological analysis were replaced by analysis using a miniature mass spectrometer when the determination of isocitrate dehydrogenase (IDH) mutation status was enabled by the

199

measurement of a single biomarker, 2-hydroxyglutarate.[26]  However, a single biomarker is typically less reliable in identifying a sample than a combination of biomarkers.  It has previously been demonstrated that many different biological systems can be identified by their lipid profile.[27–29]  Specifically, by observing the relative abundance of many lipids, different samples can be characterized by type, e.g. heathy or diseased.  A lipid profile is then a more robust identification technique than is the monitoring of absolute abundances of individual analytes.  This can be done without chromatographic separation as ion suppression affects the lipids similarly.  Lipid profile information has been commonly obtained by 1D MS (full scan), 1D MS/MS (precursor/product/neutral loss scan), and dimensionless MS/MS (multiple reaction monitoring). These methods increase in their specificity per scan. An ideal 2D MS/MS scan lies at the extreme of specificity per scan as all lipids are identified in a single scan (although the sensitivity falls relative to the more specific scans).   In order to determine the feasibility of the 2D MS/MS scan in lipid profiling, a mixture of known lipids was analyzed using the miniature instrument.  Figure 6 demonstrates that many lipid classes can be detected using the 2D MS/MS scan.  A specific example of how this could be used to identify a particular class is seen for lipids containing a choline group. A few common product ions are seen for the three different lipid headgroups containing the same acyl chain length.  Although the analytes are individually identified in this experiment, this is only done to demonstrate that many different lipid class are detected in a single scan.  In the profiling experiment, the exact identity of these lipids would not be required in order to identify a difference of the lipid profile between two samples.
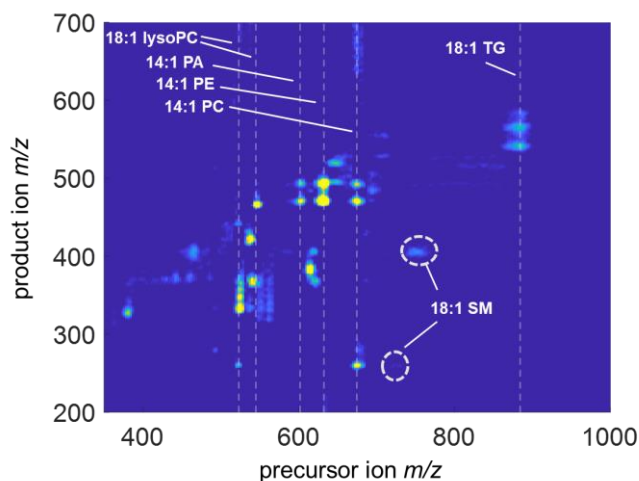
Figure 8.6. 2D MS/MS scan of a mixture of lipids. The two precursor lines related to 18:1 PC and 18:1 SM are from the $[M+H]^+$ and $[M+Na]^+$

## 8.4 Conclusions

The 2D MS/MS experiment was successfully implemented using a miniature rectilinear ion trap. The scan demonstrated here is particularly useful for experiments where time and/or sample is limited because both are utilized efficiently. The miniature instrument outperformed a commercial benchtop ion trap instrument in terms of sensitivity and resolution for a single analyte. This was not true when analyzing a wide range of analytes as the miniature instrument's performance degraded at high precursor ion $m/z$. This is potentially due to the time-varying pressure profile, an effect that might be mitigated in future modifications to the instrumentation. Importantly, the capability of using a miniature mass spectrometer utilizing the 2D MS/MS scan on mixtures was demonstrated on mixtures including fentalogs, drugs of abuse, and phospholipids.

## 8.5 Supplementary Figures
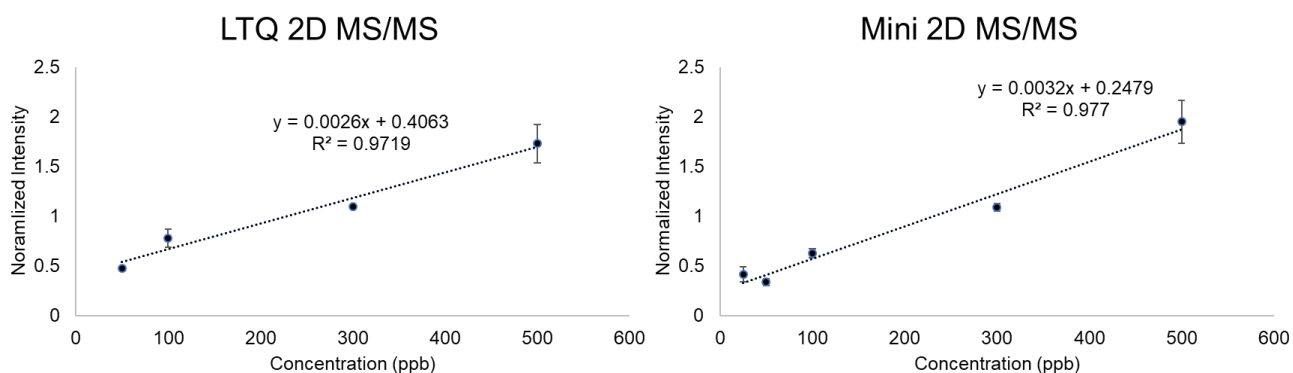


Figure S8.1. Calibration curve for fentanyl (precursor ion $m/z$ 337, product ion $m/z$ 188) for (left) benchtop and (right) miniature mass spectrometer using acetyl fentanyl as an internal standard.
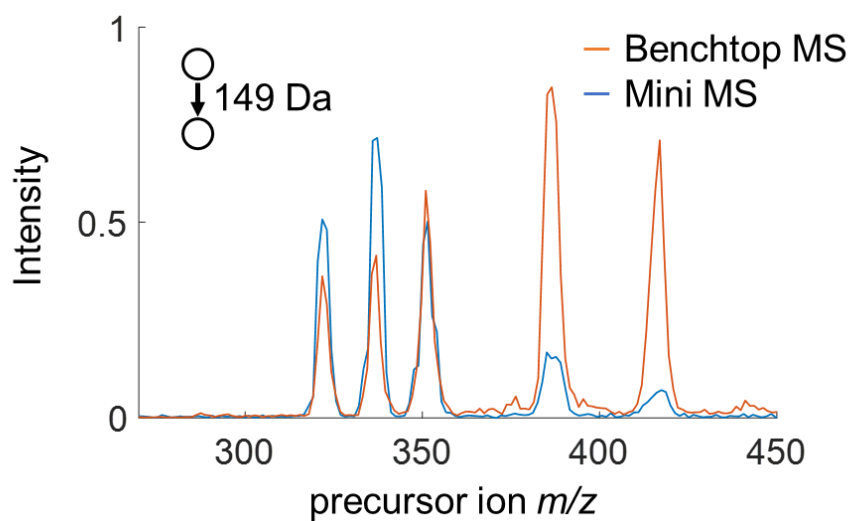
Figure S8.2. Extracted neutral loss scan of 149 Da from the 2D MS/MS scan shown in Figure 3 detecting -il fentalogs using (orange) benchtop and (blue) miniature mass spectrometer.
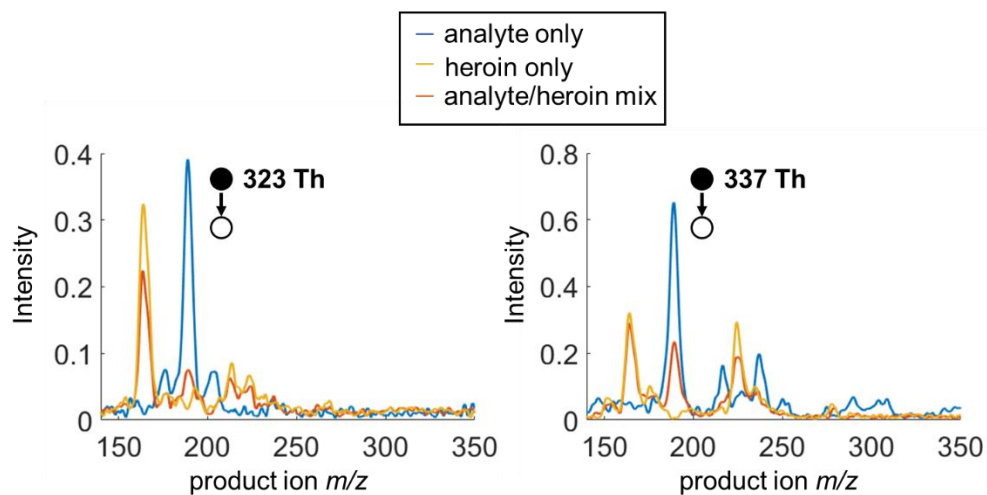


Figure S8.3. Extracted product ion scan of precursor ion (left) *m/z* 323 and (right) *m/z* 337 taken from the 2D MS/MS spectrum of the three samples
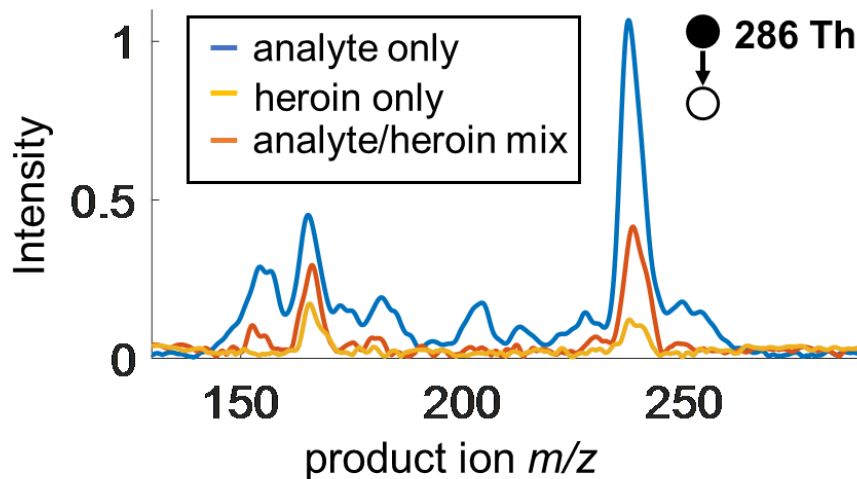
Figure S8.4. Extracted product ion scan of precursor ion *m/z* 286 extracted from the 2D MS/MS spectrum of the three samples. Product ion *m/z* 237 comes from stearamide which is centered at the precursor ion *m/z* 284.
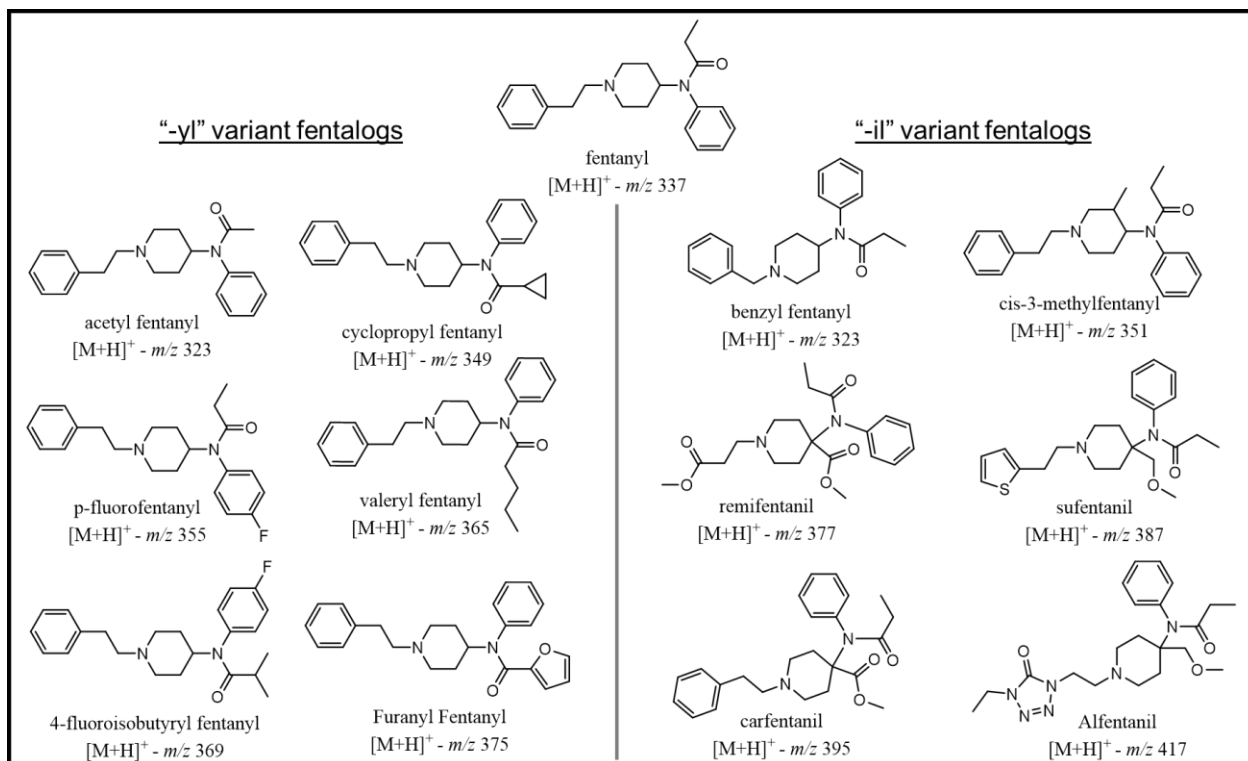


Figure S8.5. Structures of fentalogs used in the 2D MS/MS experiment. The analogs can be separated by the conservation of either phenylpiperidine or N-phenylpropamide. The nomenclature loosely coincides that "-yl" variants conserve the phenylpiperidine moiety while "il" variants conserve the N-phenylpropamide.

203

## 8.6   References

(1)     Senko, M. W.; Remes, P. M.; Canterbury, J. D.; Mathur, R.; Song, Q.; Eliuk, S. M.; Mullen, C.; Earley, L.; Hardman, M.; Blethrow, J. D.; Bui, H.; Specht, A.; Lange, O.; Denisov, E.; Makarov, A.; Horning, S.; Zabrouskov, V. Novel Parallelized Quadrupole/Linear Ion Trap/Orbitrap Tribrid Mass Spectrometer Improving Proteome Coverage and Peptide Identification Rates. Anal. Chem. 2013, 85 (24), 11710–11714. https://doi.org/10.1021/ac403115c.

(2)     Meier, F.; Brunner, A.-D.; Koch, S.; Koch, H.; Lubeck, M.; Krause, M.; Goedecke, N.; Decker, J.; Kosinski, T.; Park, M. A.; Bache, N.; Hoerning, O.; Cox, J.; Räther, O.; Mann, M. Online Parallel Accumulation–Serial Fragmentation (PASEF) with a Novel Trapped Ion Mobility Mass Spectrometer. Mol Cell Proteomics 2018, 17 (12), 2534. https://doi.org/10.1074/mcp.TIR118.000900.

(3)     Mielczarek, P.; Silberring, J.; Smoluch, M. MINIATURIZATION IN MASS SPECTROMETRY. Mass Spectrometry Reviews 2020, 39 (5–6), 453–470. https://doi.org/10.1002/mas.21614.

(4)     Brown, H. M.; Pu, F.; Dey, M.; Miller, J.; Shah, M. V.; Shapiro, S. A.; Ouyang, Z.; Cohen-Gadol, A. A.; Cooks, R. G. Intraoperative Detection of Isocitrate Dehydrogenase Mutations in Human Gliomas Using a Miniature Mass Spectrometer. Analytical and Bioanalytical Chemistry 2019, 411 (30), 7929–7933. https://doi.org/10.1007/s00216-019-02198-y.

(5)     Meng, X.; Tang, C.; Zhang, C.; Li, D.; Xu, W.; Zhai, Y. A "Brick" Mass Spectrometer with Photoionization for Direct Analysis of Trace Volatile Compounds. J. Am. Soc. Mass Spectrom. 2020, 31 (4), 961–968. https://doi.org/10.1021/jasms.0c00019.

(6)     Zhang, M.; Kruse, N. A.; Bowman, J. R.; Jackson, G. P. Field Analysis of Polychlorinated Biphenyls (PCBs) in Soil Using Solid-Phase Microextraction (SPME) and a Portable Gas Chromatography–Mass Spectrometry System. Appl Spectrosc 2016, 70 (5), 785–793. https://doi.org/10.1177/0003702816638268.

(7)     Alvarez-Rivera, G.; Ballesteros-Vivas, D.; Parada-Alfonso, F.; Ibañez, E.; Cifuentes, A. Recent Applications of High Resolution Mass Spectrometry for the Characterization of Plant Natural Products. TrAC Trends in Analytical Chemistry 2019, 112, 87–101. https://doi.org/10.1016/j.trac.2019.01.002.

(8)     Liu, Y.; D'Agostino, L. A.; Qu, G.; Jiang, G.; Martin, J. W. High-Resolution Mass Spectrometry (HRMS) Methods for Nontarget Discovery and Characterization of Poly- and per-Fluoroalkyl Substances (PFASs) in Environmental and Human Samples. TrAC Trends in Analytical Chemistry 2019, 121, 115420. https://doi.org/10.1016/j.trac.2019.02.021.

(9)     Snyder, D. T.; Pulliam, C. J.; Ouyang, Z.; Cooks, R. G. Miniature and Fieldable Mass Spectrometers: Recent Advances. Anal. Chem. 2016, 88 (1), 2–29. https://doi.org/10.1021/acs.analchem.5b03070.

(10) Decker, T. K.; Zheng, Y.; Ruben, A. J.; Wang, X.; Lammert, S. A.; Austin, D. E.; Hawkins, A. R. A Microscale Planar Linear Ion Trap Mass Spectrometer. J. Am. Soc. Mass Spectrom. 2019, 30 (3), 482–488. https://doi.org/10.1007/s13361-018-2104-x.

(11) Zhai, Y.; Feng, Y.; Wei, Y.; Wang, Y.; Xu, W. Development of a Miniature Mass Spectrometer with Continuous Atmospheric Pressure Interface. Analyst 2015, 140 (10), 3406–3414. https://doi.org/10.1039/C5AN00462D.

(12) Janulyte, A.; Zerega, Y.; Brkić, B.; Taylor, S.; Andre, J. Accurate Modelling of Small-Scale Linear Ion Trap Operating Mode Using He Buffer Gas to Improve Sensitivity and Resolution for in-the-Field Mass Spectrometry. J. Anal. At. Spectrom. 2019, 34 (8), 1672–1682. https://doi.org/10.1039/C9JA00017H.

(13) Snyder, D. T.; Cooks, R. G. Single Analyzer Precursor Ion Scans in a Linear Quadrupole Ion Trap Using Orthogonal Double Resonance Excitation. J. Am. Soc. Mass Spectrom. 2017, 28 (9), 1929–1938. https://doi.org/10.1021/jasms.8b05645.

(14) Snyder, D. T.; Cooks, R. G. Single Analyzer Neutral Loss Scans in a Linear Quadrupole Ion Trap Using Orthogonal Double Resonance Excitation. Analytical Chemistry 2017, 89 (15), 8148–8155. https://doi.org/10.1021/acs.analchem.7b01963.

(15) Gao, L.; Cooks, R. G.; Ouyang, Z. Breaking the Pumping Speed Barrier in Mass Spectrometry: Discontinuous Atmospheric Pressure Interface. Anal. Chem. 2008, 80 (11), 4026–4032. https://doi.org/10.1021/ac800014v.

(16) Snyder, D. T.; Szalwinski, L. J.; Hilger, R.; Cooks, R. G. Implementation of Precursor and Neutral Loss Scans on a Miniature Ion Trap Mass Spectrometer and Performance Comparison to a Benchtop Linear Ion Trap. J. Am. Soc. Mass Spectrom. 2018, 1–10. https://doi.org/10.1007/s13361-018-1922-1.

(17) Szalwinski, L. J.; Holden, D. T.; Morato, N. M.; Cooks, R. G. 2D MS/MS Spectra Recorded in the Time Domain Using Repetitive Frequency Sweeps in Linear Quadrupole Ion Traps. Anal. Chem. 2020, 92 (14), 10016–10023. https://doi.org/10.1021/acs.analchem.0c01719.

(18) Snyder, D. T.; Szalwinski, L. J.; St. John, Z.; Cooks, R. G. Two-Dimensional Tandem Mass Spectrometry in a Single Scan on a Linear Quadrupole Ion Trap. Anal. Chem. 2019, 91 (21), 13752–13762. https://doi.org/10.1021/acs.analchem.9b03123.

(19) Snyder, D. T.; Demond, P. S.; Szalwinski, L. J.; Dhummakupt, E. S.; McBride, E. M.; Cooks, R. G.; Glaros, T.; Mach, P. M. Two-Dimensional MS/MS Scans on a Linear Ion Trap Mass Analyzer: Identification of V-Series Chemical Warfare Agents. International Journal of Mass Spectrometry 2019, 444, 116171. https://doi.org/10.1016/j.ijms.2019.06.007.

(20) Li, L.; Chen, T.-C.; Ren, Y.; Hendricks, P. I.; Cooks, R. G.; Ouyang, Z. Mini 12, Miniature Mass Spectrometer for Clinical and Other Applications—Introduction and Characterization. Anal. Chem. 2014, 86 (6), 2909–2916. https://doi.org/10.1021/ac403766c.

(21) Pulliam, C. J.; Bain, R. M.; Wiley, J. S.; Ouyang, Z.; Cooks, R. G. Mass Spectrometry in the Home and Garden. Journal of The American Society for Mass Spectrometry 2015, 26 (2), 224–230. https://doi.org/10.1007/s13361-014-1056-z.

(22) Franzen, J. The Non-Linear Ion Trap. Part 4. Mass Selective Instability Scan with Multipole Superposition. International Journal of Mass Spectrometry and Ion Processes 1993, 125 (2), 165–170. https://doi.org/10.1016/0168-1176(93)80039-H.

(23) Franzen, J. The Non-Linear Ion Trap. Part 5. Nature of Non-Linear Resonances and Resonant Ion Ejection. International Journal of Mass Spectrometry and Ion Processes 1994, 130 (1), 15–40. https://doi.org/10.1016/0168-1176(93)03907-4.

(24) Remes, P. M.; Syka, J. E. P.; Kovtoun, V. V.; Schwartz, J. C. Insight into the Resonance Ejection Process during Mass Analysis through Simulations for Improved Linear Quadrupole Ion Trap Mass Spectrometer Performance. International Journal of Mass Spectrometry 2014, 370, 44–57. https://doi.org/10.1016/j.ijms.2014.06.015.

(25) Wu, Q.; Tian, Y.; Li, A.; Austin, D. E. Simulations of Electrode Misalignment Effects in Two-Plate Linear Ion Traps. International Journal of Mass Spectrometry 2015, 393, 52–57. https://doi.org/10.1016/j.ijms.2015.10.011.

(26) Pu, F.; Alfaro, C. M.; Pirro, V.; Xie, Z.; Ouyang, Z.; Cooks, R. G. Rapid Determination of Isocitrate Dehydrogenase Mutation Status of Human Gliomas by Extraction Nanoelectrospray Using a Miniature Mass Spectrometer. Analytical and Bioanalytical Chemistry 2019, 411 (8), 1503–1508. https://doi.org/10.1007/s00216-019-01632-5.

(27) Lellman, S. E.; Cramer, R. Bacterial Identification by Lipid Profiling Using Liquid Atmospheric Pressure Matrix-Assisted Laser Desorption/Ionization Mass Spectrometry. Clinical Chemistry and Laboratory Medicine (CCLM) 2020, 58 (6), 930–938. https://doi.org/10.1515/cclm-2019-0908.

(28) Xie, Z.; Gonzalez, L. E.; Ferreira, C. R.; Vorsilak, A.; Frabutt, D.; Sobreira, T. J. P.; Pugia, M.; Cooks, R. G. Multiple Reaction Monitoring Profiling (MRM-Profiling) of Lipids To Distinguish Strain-Level Differences in Microbial Resistance in Escherichia Coli. Anal. Chem. 2019, 91 (17), 11349–11354. https://doi.org/10.1021/acs.analchem.9b02465.

(29) Yannell, K. E.; Ferreira, C. R.; Tichy, S. E.; Cooks, R. G. Multiple Reaction Monitoring (MRM)-Profiling with Biomarker Identification by LC-QTOF to Characterize Coronary Artery Disease. Analyst 2018, 143 (20), 5014–5022. https://doi.org/10.1039/C8AN01017J.

# CHAPTER 9.     BACTERIAL GROWTH MONITORED BY TWO-DIMENSIONAL TANDEM MASS SPECTROMETRY

## 9.1    Introduction

A molecular understanding of biological systems is a fundamental driver in bioanalytical chemistry, particularly when temporal information is also sought. Several choices need to be made to obtain such information: first there is the choice of a signifying class of molecules, as comprehensive analysis is beyond reach.  If the biological system is taken to be a bacterial colony, then lipids might be chosen for their chemical diversity and their many roles in the cellular functions of bacteria.[1–3] The high dimensionality of phospholipids - in the sense of a large number of closely related molecular structures - is a key advantage of this choice is that different states of the biological system can be expressed in great detail in such a complex array of molecules.[4–6] The potential of this approach is clear from that fact that answers to simple questions – diseased/healthy – are readily read out from the lipid profiles of higher organisms, as in brain cancer diagnostics from phospholipid profiles.[7] With the organism and target class now selected, the read-out method must be chosen. The usual numerical criteria of chemical analysis, expressed as analytical sensitivity and specificity and dynamic range and quantitative accuracy and precision, all apply.  But having chosen lipids and the scale of the experiment, as well as the need to measure many related molecules, only methods based on mass spectrometry (MS) need be considered further. Spectroscopic measurements can broadly detect lipid composition, and in some cases follow individual molecular species in 3D[8] and in vivo[9–11] and they have naturally excellent time resolution[12,13], but they fall short in their broad applicability in specific molecular recognition. The most widely used MS method of assessing the lipid content of a cell is by liquid chromatography tandem mass spectrometry (LC-MS/MS).[14,15] This method typically requires sample preparation followed by a chromatographic run where the elute is monitored over time by a mass spectrometer. The sample preparation required by this method is not strictly necessary for the analysis of bacterial lipids by desorption electrospray ionization (DESI).[16,17] The LC-MS/MS method is often

acceptable except when a molecular understanding of an organism or cell requires rapid time-dependent information on the molecular composition, i.e. where rapid temporal changes in lipid distributions are needed to signal the biological state.[18–20]

Direct mass spectrometry of a complex sample is most commonly performed using data-dependent acquisition where only the most abundant ions in the single stage MS are fragmented to provide structural information. Low-abundance ions are ignored in this approach. Data-independent acquisition methods[21,22] avoid this issue by analyzing all precursor ions. In this experiment individual precursor ions are mass-selected in turn and fragmented. The precursor ion *m/z* is correlated to chromatographic retention time. The result is a set of MS/MS spectra acquired relatively slowly due to the requisite chromatographic separation prior to the mass spectrometer.

An alternative is to record, in a single scan, all products of all precursors (the full 2D MS/MS data domain) by utilizing the special properties of ion traps. Such an experiment was first demonstrated for a Fourier transform ion cyclotron resonance spectrometer (FT-ICR).[23,24] We have used a quadrupole ion trap for the same purpose, activating a set of trapped precursor ions with a dipolar set of ramped frequencies while rapidly scanning product ions to the detector in an orthogonal direction with a second dipolar frequency ramp. Using this approach, we identified the components of mixtures of proscribed drugs.[25] Such experiments have two further advantages for the problem at hand: (i) the MS scan can be performed on the 1 Hz time scale and (ii) with appropriate ionization methods no sample preparation is needed.

In this study we seek to demonstrate a modest version of the general problem laid out in this Introduction: we seek to demonstrate the ability to monitor the changing lipid profile of *E. coli as a function of growth time*. The degree of chemical detail in glycerophospholipids is remarkable as there are isomers associated with differences in the fatty acid chain lengths, double bond position, and substitution position on the glycerol for ions at a single *m/z* value.[26] New methods have been developed to distinguish lipids at this very high degree of chemical detail.[27–29] Without seeking to utilize this extra dimension of information, we demonstrate the potential to solve the larger problem by showing direct analysis by DESI using a repetition time of under 10 seconds to acquire the full 2D MS/MS data domain.

## 9.2 Experimental

### 9.2.1 E. Coli Culture Conditions and Optical Density Measurements

*Escherichia coli* was provided by bioMérieux, Inc. (Hazelwood, MO). The initial cell concentration at the point of inoculation was $4.3 \times 10^7$ cells/mL and the culture was incubated at 37 ˚C, aerobically, in 200 mL of LB broth. To monitor the growth of *E. coli*, aliquots were taken at various times over an 8-hour period. The $OD_{600}$ of the aliquots were measured with a UV-vis spectrophotometer. Two time-intervals were used while making measurements over the 8h growth period; 3 – 30 min intervals during the lag and during the stationary phases, and 22 – 15 min intervals in the time range in which we suspected the exponential phase to occur. Duplicate $OD_{600}$ measurements were taken for each point. The MS measurements were made using nano electrospray ionization (nESI).

A subsequent set of experiments used DESI-MS to analyze lipids in *E. coli*, initial concentration of $3.35 \times 10^8$ cells/mL in a culture incubated at 37 ˚C aerobically in 50 mL of LB broth. Aliquots were taken every 30 minutes until 20 samples had been collected. This was done for three biological replicates. Aliquots were transferred into a 96-well plate and their absorbances were measured in triplicate by a BioTek Synergy 2 microplate reader (Winooski, Vermont USA). Each biological replicate absorbance measurement was taken in triplicate.

### 9.2.2 2D MS/MS Measurements

For nano-electrospray (nESI) measurements, aliquots of suspended *E. coli* were taken from the same stocks used for the optical density measurements to monitor the growth curve. The cell concentration of the first and last time point were determined by hemocytometry to correlate optical density and cell concentration. A constant number of cells were profiled ($9 \times 10^7$ cells or ~100 µg dry weight of cells) for each time point. The cell aliquots were taken directly from the cell culture and centrifuged to separate the cells from the growth medium. Ethanol was then added to the cell pellet to lyse the cells and the corresponding lysate was sprayed without prior workup to record nESI mass spectra.

The nESI 2D MS/MS scans were performed by trapping precursor ions in a modified LTQ mass spectrometer (Thermo Fisher) with an externally controlled RF trapping voltage.[30] The 2D MS/MS scan was performed in 900 milliseconds with precursor ions of *m/z* 600 – 900 being

fragmented by one waveform while the resulting fragment (product) ions were continuously ejected using a second waveform as described previously.[31] Twenty-five averages were recorded for each replicate and three replicates were performed for each time point. The raw data (.txt files) were processed in MATLAB and the data requires no computationally intensive pre-processing meaning the 2D MS/MS spectra can be plotted nearly instantaneously.

### 9.2.3   DESI-2D MS/MS measurements

Cell concentrations were determined by the same method as described above. An equivalent number of cells ($1.6 \times 10^8$) were taken from each aliquot and lipids were extracted using the Bligh and Dyer method.[32]  From each extract, 10 µL of solution (equivalent to $4 \times 10^7$ cells) was deposited onto an individual well of a Teflon-coated 12-well glass microscope slide and allowed to dry. This was done manually for each biological replicate for a total of 60 samples. Samples were analyzed by DESI using a Prosolia DESI 2D system (Indianapolis, IN). Methanol Chromasolv LC-MS grade (Riedel-de Haën - Honeywell, Muskegon, MI) was used as spray solvent for all experiments. The DESI spray voltage was set to -5 kV.  Nitrogen (150 psi) was used as nebulizing gas. The emitter distance and DESI spray angle were fixed at ~1 mm and 55°, respectively. Secondary ions formed by DESI were injected into the ion trap for 200 milliseconds, followed by a 300-millisecond 2D MS/MS scan focused on the lipid mass region. Each 2D MS/MS mass spectrum consisted of 25 averages for a total analysis time of 12.5 seconds/sample. Each biological replicate was run in triplicate resulting in 180 2D MS/MS mass spectra acquired in under 40 minutes.

### 9.2.4   Automated DESI-2D MS/MS measurements

Aliquots of *E. coli* after 48 hours of growth were centrifuged, the supernatant was removed, and the resulting pellet was dissolved in ethanol. The cell lysate was deposited on four wells within a Teflon-coated 12-well glass microscope slide. Each well was analyzed automatically for approximately 5 seconds. Automated DESI was carried out using identical analysis conditions as described above but by controlling the stage motion using the Omni Spray 2D Ion Source Automation software (Prosolia, Indianapolis, IN). The microscope slide was located on the slide holder of the DESI stage, and the positions of the wells were calibrated prior to analysis. An

automated *point-to-point oscillatory* motion profile centered in turn on each of the wells was used to define the stage motion. The screening rate and the number of oscillations were manually adjusted to cover the spot diameter in ca. 5 seconds. The slide was located on the stage the analysis proceeded automatically.

## 9.3    Results and Discussion

### 9.3.1    Bacterial Growth Monitored by Optical Density
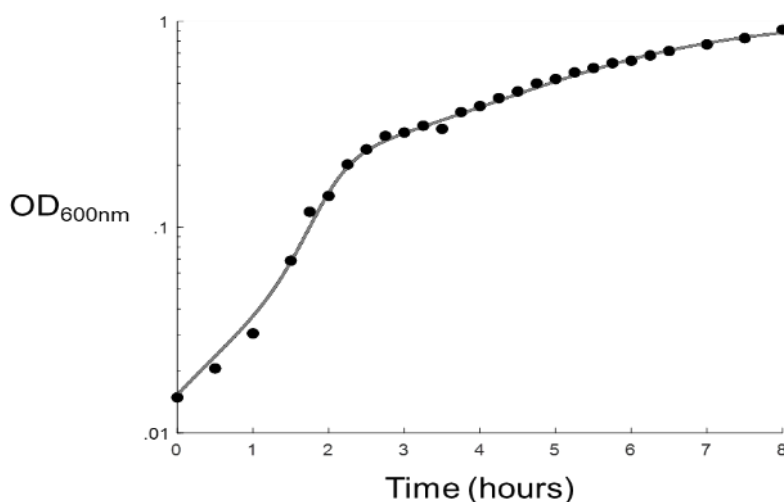


Figure 9.1. Optically measured growth curve of E. coli in LB medium at 37 °C

The biological system (bacteria), target molecular class (lipids), and read-out system (2D MS/MS) have been chosen. A demonstration of the capabilities laid out in the Introduction requires that the bacterial samples have rich lipidomic features that change over time. A simple version of this experiment is to simply allow the bacteria to grow under favorable conditions and extract aliquots over time. Because bacterial growth is slow the fast-analytical response available in 2D MS/MS is not strictly required. The E. coli growth curve is shown in Figure 9.1.

Examination of the growth curve shows three distinct phases. The lag phase, in which slow initial growth is observed, occurs within the first hour. The exponential phase occurs from roughly the first hour to three hours while the stationary phase continues until the end of the monitoring. A similar growth curve[33] has been reported using similar culturing conditions. Because it was expected that the greatest changes observed 2D MS/MS data domain would occur during the

exponential and lag phases, sampling was conducted every 30 minutes from 0 to 1.5 hours, 15 minutes from 1.5 hours to 3.5 hours, and intermittingly from 3.5 hours to 8 hours.

### 9.3.2   E. coli Lipid Profile over Time Monitored by nano-electrospray-2D MS/MS

Representative 2D MS/MS data for the three growth phases are shown in Figure 9.2. The 2D MS/MS data domain has three axes, a precursor $m/z$ axis, a product $m/z$ axis, and an intensity axis. The precursor $m/z$ axis value gives the $m/z$ of the precursor ion which is then fragmented, while the product ion $m/z$ axis value gives the $m/z$ values of the fragments of the precursor ions. Negatively-charged phosphatidyl ethanolamine (PE) and phosphatidylglycerol (PG) ions (the most abundant ions observed) primarily produce fragments of their constituent fatty acid chains ($m/z$ 200 - 400). Such information, which is required for structural identification, cannot be obtained in a single-stage MS experiment, while conventional MS/MS product ion scans would need to be performed individually.  The 2D MS/MS scan provides this information with a 1 second scan.  In the discussion of 2D MS/MS data which follows, the coordinates for 2D MS/MS points will be given as (precursor $m/z$, product $m/z$), meaning that the $m/z$ 255 product ion associated with precursor $m/z$ 688, written in the text as (688, 255).
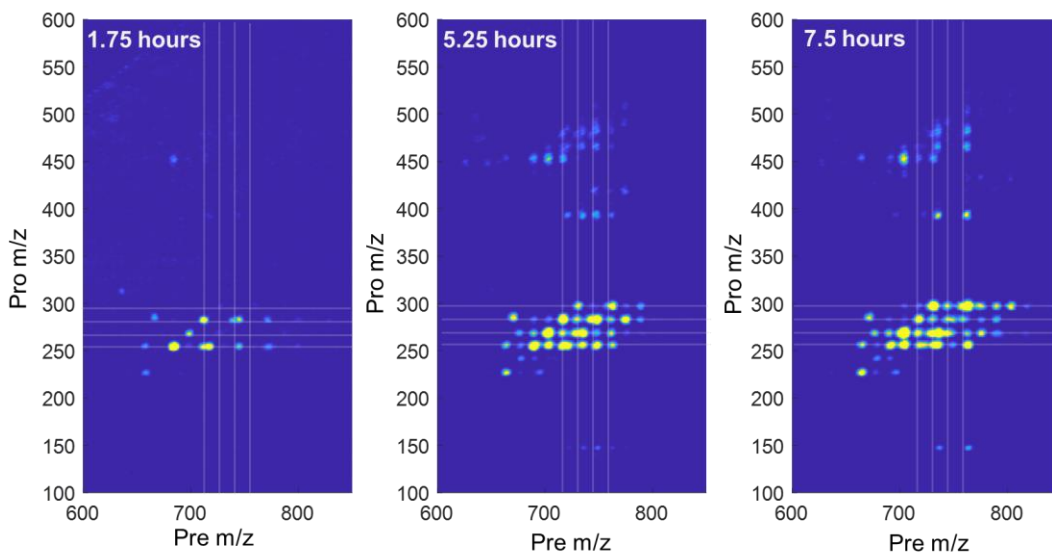
Figure 9.2. Lipid region of three 2D MS/MS spectra obtained from E. coli lysate over (left to right) at 1.75, 5.25, and 7.5 hours of growth. Product ions that fall on the same horizontal or diagonal lines are related by a common structural feature: they correspond to conventional MS/MS precursor and constant neutral loss scans. White vertical and horizontal lines are equally spaced approximately 14 mass units apart.

Examination of the 2D MS/MS data domains reveals, as its most prominent feature, the increasing intensity and complexity in the lipid region going from 1.75 hour to 5.25 hour. The strongest features in the early exponential phase are observed at (688, 255), (719, 255), (719, 283), (747, 255) and (747, 283). These combinations of precursor and product ions, which reveal the fatty acid chain composition, correspond to PE 16:0_16:1 (precursor $m/z$ 688), PG 16:0_16:1 (precursor $m/z$ 719), and PG 16:0_18:1 (precursor $m/z$ 747). A lower intensity feature is observed at (702, 267), corresponding to a PE lipid with a $C_{17}$ fatty acid chain. A second feature is observed at (660, 283), potentially corresponding to PE 18:0_12:1, although the second fatty acid lipid is not observed elsewhere in the 2D MS/MS domain. At 5.25 hours, which is near the end of the exponential phase, increased intensity is observed at (702, 255) and (702, 267), corresponding to PE 16:0_17:1. Finally, at longer times, during the stationary phase, the shift to cyclopropyl PE's and PG's continues, resulting in a distribution favoring odd-carbon number lipids over even-carbon lipids. Individual 2D MS/MS mass spectra can be found in the time-lapse video in Figure S2.

The 2D MS/MS data domains can be simplified by manipulating the 2D data. Extraction of individual 1D lines from the 2D domain results in spectra identical to those obtained by the

213

commonly used MS/MS scan modes: product ion, precursor ion, and neutral loss scan. A much less common operation is to project the data onto either the precursor or product ion axis so producing the anterior and posterior mass spectrum, respectively.[34] Whereas extraction of data removes data in order to observe specific functional groups, the projection of data allows all data to be observed in a simpler form. By projecting all observed ions to the precursor ion axis, the spectrum obtained (anterior mass spectrum) has axes which are equivalent to those of a simple single-stage mass spectrum. The data in this form allows for gross interpretation of molecular changes in the bacterium. The 2D MS/MS data domains shown in Figure 2, is converted into the anterior mass spectra are shown in Figure 9.3. Note that the data observed in these spectra are composed of ions detected after the activation of the precursor ion, viz. to product ions or unfragmented precursor ions. A few key trends are observed. At early growth times the mass spectrum is largely comprised of signals in the lower mass region, whilst phospholipids are in low abundance. As growth progresses, the phospholipid region (*m/z* 650-850) shows increasing intensity. Furthermore, the dominant phospholipid peaks shift over time towards higher *m/z* values. Such behavior is consistent with the known *E. coli* lipid metabolic pathways, in which free fatty acids are phosphorylated and then incorporated into phospholipids in a multi-step process.[35]
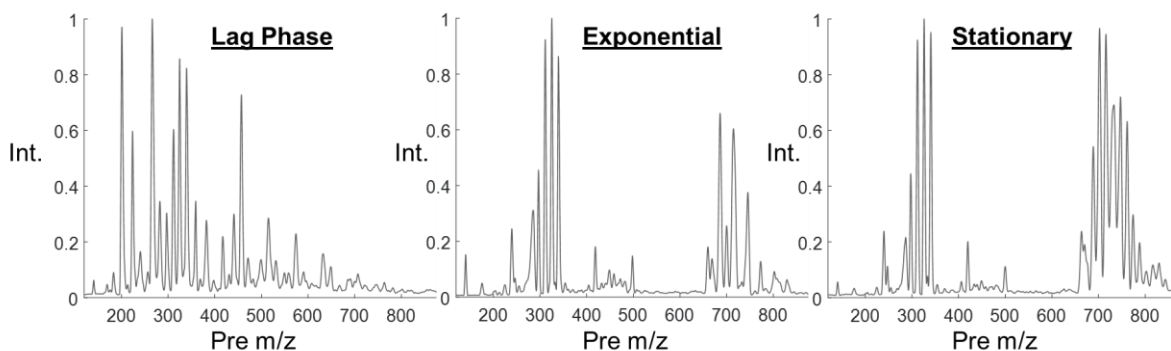


Figure 9.3. Anterior mass spectrum (projected from 2D MS/MS mass spectrum) from E. coli lysate at log, exponential and stationary stages of growth where fragments and residual precursor ions are observed at their respective precursor ion m/z

In the phospholipid region, the most intense features at early times are at *m/z* 688, *m/z* 719, and *m/z* 747. Analysis of these peaks, simply based upon their masses, gives putative assignments of PE 32:1, PG 32:1, and PG 34:1, respectively.[36] At longer times, particularly towards the end of the exponential growth period, ions of *m/z* 702 and *m/z* 733 peaks increase in intensity relative to

the other three peaks. These peaks have masses consistent with PE 33:1 and PG 33:1, respectively. At longer times, the $m/z$ 702 and $m/z$ 733 become the dominant spectral features, along with a new feature at $m/z$ 761 (putatively assigned as PG 35:1). While the full scan MS provides some information about the lipids present, this data lacks the detailed structural information about the side chain composition which is crucial for phospholipid identification. For this information, the full 2D MS/MS data domain provides detailed structural information. Since the major molecular change appears to be the conversion of alkenes into cyclopropyl groups, this conversion can be monitored by extracting information pertaining to those two functional groups. Specifically, the shift in distribution between even carbon number to odd carbon number fatty acids can be simplified so that only lipids fatty acids with 16, 17, 18, or 19 carbons are detected. The lipid data corresponding to the product ions of fatty acids of each chain length were obtained from the 2D MS/MS scan and fitted to a curve and is shown in Figure 9.4. It can be seen that the even carbon-number fatty acids ($FA_{16}/FA_{18}$)) have intensities that follow optical density measurements through the exponential phase. The odd-carbon number fatty acids ($FA_{17}/FA_{19}$)) lag behind and begin at the late exponential phase and continue into the stationary phase.
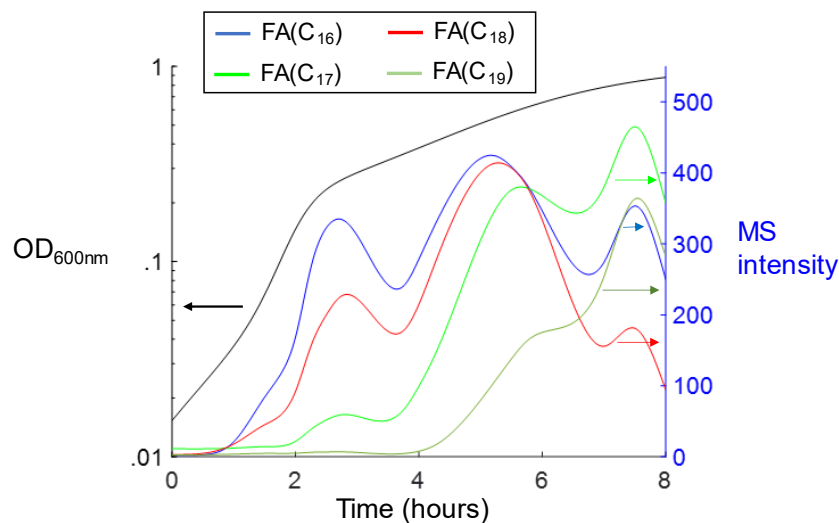
Figure 9.4. Fatty acid composition monitored over time detected by summing the product ion intensities corresponding to different fatty acid chain lengths from the lipid mass region. The OD600nm measurements are shown for comparison.

### 9.3.3   DESI-2D MS/MS of Bacterial Extracts

The nESI experiments just described are mainly limited by the time required for bacterial growth (hours). However, this feature is specific to this experiment and many other analyses involving bacteria will not be so constrained. The 2D MS/MS approach can be made even faster by using DESI instead of nano-electrospray experiments. In the latter, the analysis time per sample is 25 seconds, but significant time is spent moving from one sample to the next. In order to improve throughput, DESI was implemented so that the samples could be placed directly on a microscope slide and the time between samples could be reduced to under a second. This allowed a full 2D MS/MS scan (m/z 100 – m/z 900), both axes) to be recorded three times as fast as taken to record only the lipid region in the nESI experiment.

To demonstrate performance of the automated DESI-2D MS/MS system, cell lysate of *E. coli* was deposited onto four wells of a microscope slide and interrogated by DESI-2D MS/MS. Figure 9.5a shows the 2D MS/MS mass spectrum obtained from one of the wells containing the cell lysate acquired over approximately 5 seconds. The cell lysate analyzed in this experiment is from the stationary phase where most of the double bonds are converted to cyclopropyl groups resulting in a higher abundance of odd-carbon number lipids (PE/PG(33:1)).  The ion chronogram

216

acquired while moving the DESI sprayer over all four wells is shown in Figure 9.5b where the extracted ion signal relates to a particular lipid present in *E. coli.* A time-lapse graphic displaying multiple 2D MS/MS spectra acquired by DESI can be found in Figure S3 where *E. coli* and *Pseudomonas aeruginosa* are analyzed in duplicate in a single run.
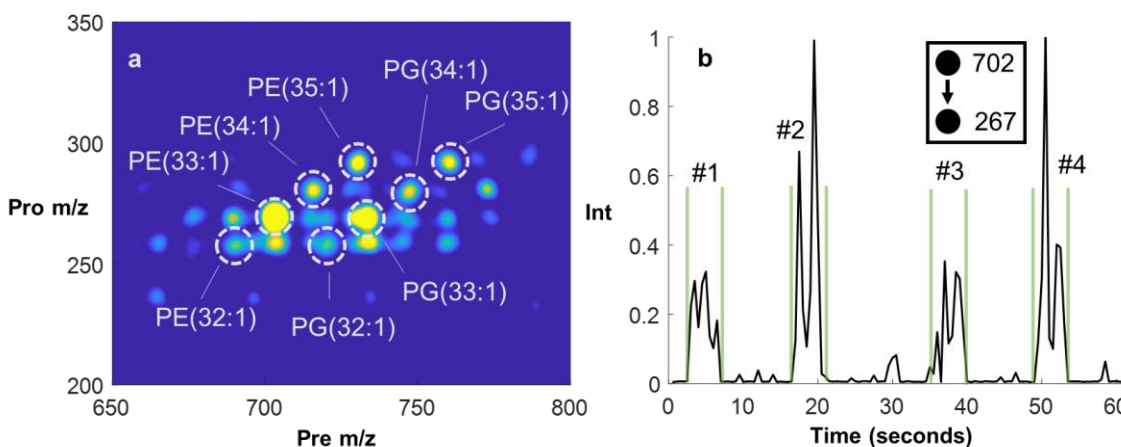


Figure 9.5. (a) 2D MS/MS mass spectrum obtained from automated DESI-2D MS/MS system. (b) Extracted ion signal corresponding to PE(33:1) recorded over time as four bacteria samples placed on a microscope slide are examined by DESI-MS.

To further illustrate how the DESI-2D MS/MS system can be used to interrogate a large number of samples, the bacterial growth of *E. coli* was again investigated. Figure 9.6a shows the resulting growth curve and extracted lipidomic information. Each of the twenty timepoints shown in Figure 9.6a contains 3 biological replicates with 3 scan replicates resulting in 180 unique spectra acquired in under 38 minutes (12.5 seconds a sample). It can be seen that the growth curve barely reaches the stationary phase resulting in smaller differences than observed in Figure 9.4. This can most likely be attributed to the differences in growth conditions although exact correlations cannot be made. The 2D MS/MS mass spectrum of the last time point (570 minutes) is shown in Figure 9.6b. The conversion of $C_{16}$ to $C_{17}$ fatty acids is lower than what has been previously observed after the same time further confirming the reduced growth rate.

These DESI-MS data showcase two key advantages of the 2D MS/MS methodology, namely: i) the technique allows for data independent acquisition (DIA) by sampling all ions which fragment in a sample and ii) the short scan time to acquire all MS/MS data without chromatography allows for relatively high sample throughput. Furthermore, the extraction used for the growth curve

monitored by DESI-2D MS/MS was not required in order to observe lipids. The spectrum acquired in Figure 9.5a was acquired from a bacterial sample without sample extraction. This experiment allows detailed insights into the changing lipidome. Lipids can have many structural isomers due to the possible combinations of fatty acid chains; this means that these structural isomers can be readily observed and identified although additional information in terms of double bond and sn-positional isomers is not acquired.
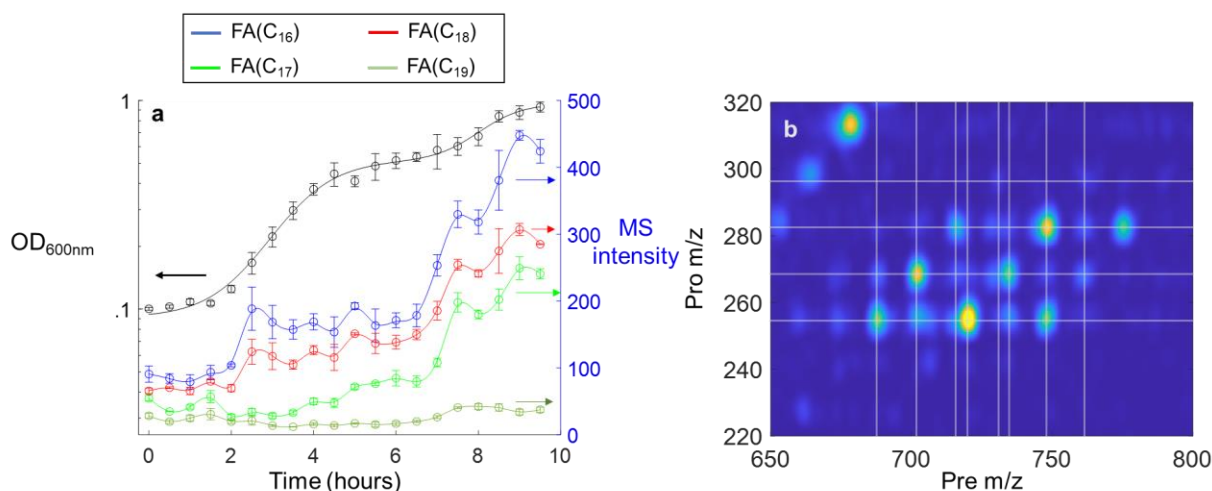


Figure 9.6. (a) Fatty acid composition monitored over time for three biological replicates under the same conditions. OD600nm measurements are also shown. (b) DESI 2D MS/MS mass spectrum of lipid extract after 570 minutes of growth.

It can be seen that the mass resolution in the 2D MS/MS mass spectrum is poor (>5 Th in both axes) compared to more conventional MS/MS methods. This is due to the incredibly fast scan rate and the use of nitrogen as bath gas. Slower 2D MS/MS scans are possible with increased mass resolution and accuracy, but a quicker scan was chosen to emphasize speed. The major changes observed in this experiment, conversion of a double bond into a cyclopropyl group, do not necessitate higher mass resolution. However, the poor mass resolution does not allow distinction between different degrees of unsaturation for fatty acids with the same carbon number. Additionally, the more conventionally used helium could be substituted for the nitrogen bath gas to achieve higher mass resolution but at the cost of sensitivity. Another drawback of this method is the low dynamic range of the current detection circuitry (~2 orders of magnitude) caused by an exceptionally high electronic noise floor. With proper detection electronics now being constructed,

the dynamic range is expected to be four orders of magnitude. The current instrument is still being improved so metrics such as resolving power and accuracy are not final values.

## 9.4    Conclusions

The work presented here demonstrates a technique which leverages 2D MS/MS to make powerful molecular measurements on biological mixtures without the need of chromatographic separation. The use of ambient ionization provides high sample throughput as demonstrated by monitoring the growth of *E. coli* by 2D MS/MS using two ionization methods, nano-electrospray ionization, and DESI. The lipid profile of *E. coli* was monitored to observe a major lipidomic change, the conversion of double bond fatty acids into cyclopropyl fatty acids. Importantly, this lipid profile shift was also monitored using high throughput instrumentation where an entire 20-point growth curve with 9 replicates interrogated in under 38 minutes by DESI-2D MS/MS. The method gives insight into lipid modifications, specifically lipid fatty acid chain modifications of unsaturated to cyclopropyl groups, with unprecedented speed

## 9.5    References

(1)     Henderson, J. C.; Zimmerman, S. M.; Crofts, A. A.; Boll, J. M.; Kuhns, L. G.; Herrera, C. M.; Trent, M. S. The Power of Asymmetry: Architecture and Assembly of the Gram-Negative Outer Membrane Lipid Bilayer. *Annu. Rev. Microbiol.* **2016**, *70* (1), 255–278. https://doi.org/10.1146/annurev-micro-102215-095308.

(2)     Lin, T.-Y.; Weibel, D. B. Organization and Function of Anionic Phospholipids in Bacteria. *Appl. Microbiol. Biotechnol.* **2016**, *100* (10), 4255–4267. https://doi.org/10.1007/s00253-016-7468-x.

(3)     Barák, I.; Muchová, K. The Role of Lipid Domains in Bacterial Cell Processes. *Int. J. Mol. Sci.* **2013**, *14* (2), 4050–4065. https://doi.org/10.3390/ijms14024050.

(4)     Magnuson K; Jackowski S; Rock C O; Cronan J E. Regulation of Fatty Acid Biosynthesis in Escherichia Coli. *Microbiol. Rev.* **1993**, *57* (3), 522–542. https://doi.org/10.1128/mr.57.3.522-542.1993.

(5)     Jeucken, A.; Molenaar, M. R.; van de Lest, C. H. A.; Jansen, J. W. A.; Helms, J. B.; Brouwers, J. F. A Comprehensive Functional Characterization of Escherichia Coli Lipid Genes. *Cell Rep.* **2019**, *27* (5), 1597-1606.e2. https://doi.org/10.1016/j.celrep.2019.04.018.

(6)     Furse, S.; Wienk, H.; Boelens, R.; de Kroon, A. I. P. M.; Killian, J. A. E. Coli MG1655 Modulates Its Phospholipid Composition through the Cell Cycle. *FEBS Lett.* **2015**, *589* (19, Part B), 2726–2730. https://doi.org/10.1016/j.febslet.2015.07.043.

(7)     Jarmusch, A. K.; Pirro, V.; Baird, Z.; Hattab, E. M.; Cohen-Gadol, A. A.; Cooks, R. G. Lipid and Metabolite Profiles of Human Brain Tumors by Desorption Electrospray Ionization-MS. *Proc. Natl. Acad. Sci.* **2016**, *113* (6), 1486. https://doi.org/10.1073/pnas.1523306113.

(8)     Czamara, K.; Majzner, K.; Selmi, A.; Baranska, M.; Ozaki, Y.; Kaczor, A. Unsaturated Lipid Bodies as a Hallmark of Inflammation Studied by Raman 2D and 3D Microscopy. *Sci. Rep.* **2017**, *7* (1), 40889. https://doi.org/10.1038/srep40889.

(9)     Minamikawa, T.; Ichimura-Shimizu, M.; Takanari, H.; Morimoto, Y.; Shiomi, R.; Tanioka, H.; Hase, E.; Yasui, T.; Tsuneyama, K. Molecular Imaging Analysis of Microvesicular and Macrovesicular Lipid Droplets in Non-Alcoholic Fatty Liver Disease by Raman Microscopy. *Sci. Rep.* **2020**, *10* (1), 18548. https://doi.org/10.1038/s41598-020-75604-6.

(10)    Zhang, C.; Boppart, S. A. Dynamic Signatures of Lipid Droplets as New Markers to Quantify Cellular Metabolic Changes. *Anal. Chem.* **2020**, *92* (24), 15943–15952. https://doi.org/10.1021/acs.analchem.0c03366.

(11)    Fu, D.; Yu, Y.; Folick, A.; Currie, E.; Farese, R. V.; Tsai, T.-H.; Xie, X. S.; Wang, M. C. In Vivo Metabolic Fingerprinting of Neutral Lipids with Hyperspectral Stimulated Raman Scattering Microscopy. *J. Am. Chem. Soc.* **2014**, *136* (24), 8820–8828. https://doi.org/10.1021/ja504199s.

(12)    Lin, H.; Lee, H. J.; Tague, N.; Lugagne, J.-B.; Zong, C.; Deng, F.; Shin, J.; Tian, L.; Wong, W.; Dunlop, M. J.; Cheng, J.-X. Microsecond Fingerprint Stimulated Raman Spectroscopic Imaging by Ultrafast Tuning and Spatial-Spectral Learning. *Nat. Commun.* **2021**, *12* (1), 3052. https://doi.org/10.1038/s41467-021-23202-z.

(13)    Zhu, C.; Shi, W.; Daleke, D. L.; Baker, L. A. Monitoring Dynamic Spiculation in Red Blood Cells with Scanning Ion Conductance Microscopy. *Analyst* **2018**, *143* (5), 1087–1093. https://doi.org/10.1039/C7AN01986F.

(14)    Cajka, T.; Fiehn, O. Comprehensive Analysis of Lipids in Biological Systems by Liquid Chromatography-Mass Spectrometry. *TrAC Trends Anal. Chem.* **2014**, *61*, 192–206. https://doi.org/10.1016/j.trac.2014.04.017.

(15)    Vasilopoulou, C. G.; Sulek, K.; Brunner, A.-D.; Meitei, N. S.; Schweiger-Hufnagel, U.; Meyer, S. W.; Barsch, A.; Mann, M.; Meier, F. Trapped Ion Mobility Spectrometry and PASEF Enable In-Depth Lipidomics from Minimal Sample Amounts. *Nat. Commun.* **2020**, *11* (1), 331. https://doi.org/10.1038/s41467-019-14044-x.

(16)    Song, Y.; Talaty, N.; Tao, W. A.; Pan, Z.; Cooks, R. G. Rapid Ambient Mass Spectrometric Profiling of Intact, Untreated Bacteria Using Desorption Electrospray Ionization. *Chem. Commun.* **2007**, No. 1, 61–63. https://doi.org/10.1039/B615724F.

(17)     Meetani, M. A.; Shin, Y.-S.; Zhang, S.; Mayer, R.; Basile, F. Desorption Electrospray Ionization Mass Spectrometry of Intact Bacteria. *J. Mass Spectrom.* **2007**, *42* (9), 1186–1193. https://doi.org/10.1002/jms.1250.

(18)     Cronan, J. E., Jr. Phospholipid Alterations during Growth of Escherichia Coli. *J. Bacteriol.* **1968**, *95* (6), 2054–2061. https://doi.org/10.1128/jb.95.6.2054-2061.1968.

(19)     Arneborg, N.; Salskov-Iversen, A. S.; Mathiasen, T. E. The Effect of Growth Rate and Other Growth Conditions on the Lipid Composition of Escherichia Coli. *Appl. Microbiol. Biotechnol.* **1993**, *39* (3), 353–357. https://doi.org/10.1007/BF00192091.

(20)     Gidden, J.; Denson, J.; Liyanage, R.; Ivey, D. M.; Lay, J. O. Lipid Compositions in Escherichia Coli and Bacillus Subtilis During Growth as Determined by MALDI-TOF and TOF/TOF Mass Spectrometry. *Int. J. Mass Spectrom.* **2009**, *283* (1–3), 178–184. https://doi.org/10.1016/j.ijms.2009.03.005.

(21)     Gillet, L. C.; Navarro, P.; Tate, S.; Röst, H.; Selevsek, N.; Reiter, L.; Bonner, R.; Aebersold, R. Targeted Data Extraction of the MS/MS Spectra Generated by Data-Independent Acquisition: A New Concept for Consistent and Accurate Proteome Analysis. *Mol. Amp Cell. Proteomics* **2012**, *11* (6), O111.016717. https://doi.org/10.1074/mcp.O111.016717.

(22)     Bateman, K. P.; Castro-Perez, J.; Wrona, M.; Shockcor, J. P.; Yu, K.; Oballa, R.; Nicoll-Griffith, D. A. MSE with Mass Defect Filtering for in Vitro and in Vivo Metabolite Identification. *Rapid Commun. Mass Spectrom.* **2007**, *21* (9), 1485–1496. https://doi.org/10.1002/rcm.2996.

(23)     Pfändler, P.; Bodenhausen, G.; Rapin, J.; Houriet, R.; Gäumann, T. Two-Dimensional Fourier Transform Ion Cyclotron Resonance Mass Spectrometry. *Chem. Phys. Lett.* **1987**, *138* (2), 195–200. https://doi.org/10.1016/0009-2614(87)80367-6.

(24)     Paris, J.; Morgan, T. E.; Marzullo, B. P.; Wootton, C. A.; Barrow, M. P.; O'Hara, J.; O'Connor, P. B. Two-Dimensional Mass Spectrometry Analysis of IgG1 Antibodies. *J. Am. Soc. Mass Spectrom.* **2021**, *32* (7), 1716–1724. https://doi.org/10.1021/jasms.1c00096.

(25)     Szalwinski, L. J.; Cooks, R. G. Complex Mixture Analysis by Two-Dimensional Mass Spectrometry Using a Miniature Ion Trap. *Talanta Open* **2021**, *3*, 100028. https://doi.org/10.1016/j.talo.2020.100028.

(26)     Blevins, M. S.; James, V. K.; Herrera, C. M.; Purcell, A. B.; Trent, M. S.; Brodbelt, J. S. Unsaturation Elements and Other Modifications of Phospholipids in Bacteria: New Insight from Ultraviolet Photodissociation Mass Spectrometry. *Anal. Chem.* **2020**, *92* (13), 9146–9155. https://doi.org/10.1021/acs.analchem.0c01449.

(27)     Li, Z.; Cheng, S.; Lin, Q.; Cao, W.; Yang, J.; Zhang, M.; Shen, A.; Zhang, W.; Xia, Y.; Ma, X.; Ouyang, Z. Single-Cell Lipidomics with High Structural Specificity by Mass Spectrometry. *Nat. Commun.* **2021**, *12* (1), 2869. https://doi.org/10.1038/s41467-021-23161-5.

(28) Zhang, X.; Ren, X.; Chingin, K.; Xu, J.; Yan, X.; Chen, H. Mass Spectrometry Distinguishing C=C Location and Cis/Trans Isomers: A Strategy Initiated by Water Radical Cations. *Anal. Chim. Acta* **2020**, *1139*, 146–154. https://doi.org/10.1016/j.aca.2020.09.027.

(29) Claes, B. S. R.; Bowman, A. P.; Poad, B. L. J.; Young, R. S. E.; Heeren, R. M. A.; Blanksby, S. J.; Ellis, S. R. Mass Spectrometry Imaging of Lipids with Isomer Resolution Using High-Pressure Ozone-Induced Dissociation. *Anal. Chem.* **2021**, *93* (28), 9826–9834. https://doi.org/10.1021/acs.analchem.1c01377.

(30) Snyder, D. T.; Cooks, R. G. Single Analyzer Precursor Ion Scans in a Linear Quadrupole Ion Trap Using Orthogonal Double Resonance Excitation. *J. Am. Soc. Mass Spectrom.* **2017**, *28* (9), 1929–1938. https://doi.org/10.1021/jasms.8b05645.

(31) Szalwinski, L. J.; Holden, D. T.; Morato, N. M.; Cooks, R. G. 2D MS/MS Spectra Recorded in the Time Domain Using Repetitive Frequency Sweeps in Linear Quadrupole Ion Traps. *Anal. Chem.* **2020**, *92* (14), 10016–10023. https://doi.org/10.1021/acs.analchem.0c01719.

(32) Sündermann, A.; Eggers, L. F.; Schwudke, D. Liquid Extraction: Bligh and Dyer. In *Encyclopedia of Lipidomics*; Wenk, M. R., Ed.; Springer Netherlands: Dordrecht, 2016; pp 1–4. https://doi.org/10.1007/978-94-007-7864-1_88-1.

(33) Wei, C.; Zhao, X. Induction of Viable but Nonculturable Escherichia Coli O157:H7 by Low Temperature and Its Resuscitation. *Front. Microbiol.* **2018**, *9*, 2728. https://doi.org/10.3389/fmicb.2018.02728.

(34) Schwartz, J. C.; Wade, A. P.; Enke, C. G.; Cooks, R. G. Systematic Delineation of Scan Modes in Multidimensional Mass Spectrometry. *Anal. Chem.* **1990**, *62* (17), 1809–1818. https://doi.org/10.1021/ac00216a016.

(35) Zhang, Y.-M.; Rock, C. O. Membrane Lipid Homeostasis in Bacteria. *Nat. Rev. Microbiol.* **2008**, *6* (3), 222–233. https://doi.org/10.1038/nrmicro1839.

(36) LMSD: LIPID MAPS® structure database. Sud M., Fahy E., Cotter D., Brown A., Dennis E., Glass C., Murphy R., Raetz C., Russell D., and Subramaniam S., Nucleic Acids Research 35, D527-32 (2006).